

Drivers of plant nutrient acquisition and allocation strategies and their influence
on plant responses to environmental change

by

Evan A. Perkowski, B.S.

A Dissertation

In

Biological Sciences

Submitted to the Graduate Faculty
of Texas Tech University in
Partial Fulfillment of
the Requirements for
the Degree of

Doctor of Philosophy

Approved

Nicholas G. Smith, Ph.D.
Chair of Committee

Aimée T. Classen, Ph.D.

Natasja van Gestel, Ph.D.

Lindsey C. Slaughter, Ph.D.

Dylan W. Schwilk, Ph.D.

Mark Sheridan, Ph.D.
Dean of the Graduate School

May 2023

Copyright 2023, Evan A. Perkowski

Acknowledgements

This dissertation was made possible by the mentorship, collaboration, and friendship of many people. I am so thankful to be surrounded by such supportive and helpful mentors, peers, and friends that have made navigating through graduate school and finishing this dissertation an enjoyable experience. Specifically, I am thankful for the incredible mentorship of my advisor and committee chair, Dr. Nick Smith, who provided invaluable insight and tools that have helped shape me into the plant ecophysiological I claim to be today. I am also indebted to my committee members, Drs. Aimée Classen, Natasja van Gestel, Dylan Schwilk, and Lindsey Slaughter, for useful feedback, invaluable support, and encouragement as I planned and implemented experiments.

I am also thankful for past and present members of the EcoHealth lab for encouragement, support, and extracurricular activities that made time inside and outside the lab enjoyable and memorable. Particular thanks go to Dr. Lizz Waring, Dr. Xiulin Gao, Helen Scott, and Risa McNellis, Billi Jean Petermann, and the late Dr. Kris Petterson, all of whom were invaluable to helping me navigate my first year. I am especially thankful for the mentorship and friendship of Dr. Lizz Waring, as our weekly coffee chats were instrumental for helping me feel welcome in Lubbock and acclimate to life as a graduate student. I am also grateful for the friendship of Billi Jean Petermann and the late Dr. Kris Petterson for their encouragement and willingness to discuss microbial symbioses over coffee on random Saturday mornings.

Additional thanks go out to Isa Beltran, Snehanjana Chatterjee, Jeff Chi-

eppa, Peter Eludini, Zinny Ezekannagha, Hannah German, Eve Gray, Monika Kelley, Azaj Mahmud, Jorge Ochoa, Brad Posch, Avery Schoenherr, and Jose Villeda for help with experiments or for lending an ear over puzzling results. I am also thankful for collaborators Dr. Christy Goodale and Dave Frey, who provided invaluable insight for the second experimental chapter.

I would like to thank my undergraduate advisor, Dr. Janice Krumm, for continued mentorship and friendship and for insightful advice about navigating graduate school, but most of all for helping me realize my career aspirations and pushing me to pursue this endeavor. Additional thanks go out to my family, particularly my parents, partner, and dog for continued support and distractions outside the lab. The experiments included here would not have been possible without their emotional and monetary support.

This work was made possible from funding by the NSF, USDA, Braun and Gresham, PLLC., and was a contribution to the LEMONTREE (Land Ecosystem Models based On New Theory, obseRvations and ExperimEnts) project. The LEMONTREE project is funded through the generosity of Eric and Wendy Schmidt by recommendation of the Schmidt Futures programme and the Imperial College initiative on Grand Challenges in Ecosystems and the Environment. This work was also funded by graduate student research awards from Texas Tech University and the Botanical Society of America.

I have inevitably missed mentioning folks that were instrumental to the completion of these experiments and contributed to my development as a plant physiological ecologist. Please know that I am grateful and appreciative of our interactions.

Table of Contents

Acknowledgements	ii
Abstract	ix
List of Tables	xi
List of Figures	xv
1. Introduction	1
2. Structural carbon costs to acquire nitrogen are determined by nitrogen and light availability in two species with different nitrogen acquisition strategies	7
2.1 Introduction	7
2.2 Methods	11
2.2.1 <i>Experiment setup</i>	11
2.2.2 <i>Plant measurements and calculations</i>	12
2.2.3 <i>Statistical analyses</i>	13
2.3 Results	15
2.3.1 <i>Carbon costs to acquire nitrogen</i>	15
2.3.2 <i>Whole plant nitrogen biomass</i>	18
2.3.3 <i>Root carbon biomass</i>	20
2.3.4 <i>Root nodule biomass</i>	22
2.4 Discussion	26
2.4.1 <i>Carbon costs to acquire nitrogen increase with light availability and decrease with fertilization</i>	26
2.4.2 <i>Modeling implications</i>	28
2.4.3 <i>Study limitations</i>	30
2.4.4 <i>Conclusions</i>	32
3. Soil nitrogen availability modifies leaf nitrogen economies in mature temperate deciduous forests: a direct test of photosynthetic least-cost theory	34
3.1 Introduction	34

3.2	Methods	38
3.2.1	<i>Study site description</i>	38
3.2.2	<i>Experimental design</i>	39
3.2.3	<i>Leaf gas exchange and trait measurements</i>	39
3.2.4	A_{net}/C_i curve-fitting and parameter estimation	42
3.2.5	<i>Proportion of leaf nitrogen allocated to photosynthesis and structure</i>	44
3.2.6	<i>Tradeoffs between nitrogen and water use</i>	45
3.2.7	<i>Soil nitrogen availability and pH</i>	46
3.2.8	<i>Statistical analyses</i>	48
3.3	Results	50
3.3.1	<i>Leaf nitrogen content</i>	50
3.3.2	<i>Net photosynthesis and leaf biochemistry</i>	53
3.3.3	<i>Leaf N allocation</i>	56
3.3.4	<i>Tradeoffs between nitrogen and water use</i>	59
3.4	Discussion	62
3.4.1	<i>Soil nitrogen availability modifies tradeoffs between nitrogen and water use</i>	63
3.4.2	<i>Soil pH did not modify tradeoffs between nitrogen and water usage</i>	65
3.4.3	<i>Species identity explains a large amount of variation in leaf and whole plant traits</i>	66
3.4.4	<i>Implications for photosynthetic least-cost theory model development</i>	67
3.4.5	<i>Conclusions</i>	69
4.	The relative cost of resource use for photosynthesis drives variance in leaf nitrogen content across a climate and soil resource availability gradient	70
4.1	Introduction	70
4.2	Methods	76
4.2.1	<i>Site descriptions and sampling methodology</i>	76

4.2.2	<i>Leaf trait measurements</i>	76
4.2.3	<i>Site climate data</i>	82
4.2.4	<i>Site edaphic characteristics</i>	82
4.2.5	<i>Plant functional group assignments</i>	84
4.2.6	<i>Data analysis</i>	85
4.3	Results	87
4.3.1	<i>Cost to acquire nitrogen relative to water</i>	87
4.3.2	$C_i:C_a$	91
4.3.3	<i>Leaf nitrogen content</i>	94
4.3.4	<i>Structural equation model</i>	98
4.4	Discussion	101
4.4.1	<i>Negative effects of leaf $C_i:C_a$ on N_{area} are driven by reductions in M_{area}, not N_{mass}</i>	101
4.4.2	<i>Soil nitrogen availability increases N_{area} through changes in the cost to acquire nitrogen</i>	103
4.4.3	<i>Soil moisture increases N_{area} by facilitating increases in soil nitrogen availability</i>	104
4.4.4	<i>Indirect effects of climate on N_{area} are mediated through changes in leaf $C_i:C_a$ and β</i>	105
4.4.5	<i>Species identity traits modify effects of the environment on β, leaf $C_i:C_a$, and N_{area}</i>	105
4.4.6	<i>Next steps for optimality model development</i>	107
4.4.7	<i>Conclusions</i>	108
5.	Optimal resource investment to photosynthetic capacity maximizes nutrient allocation to whole plant growth under elevated CO₂	109
5.1	Introduction	109
5.2	Methods	114
5.2.1	<i>Seed treatments and experimental design</i>	114
5.2.2	<i>Growth chamber conditions</i>	115
5.2.3	<i>Leaf gas exchange measurements</i>	117

5.2.4 <i>Leaf trait measurements</i>	118
5.2.5 <i>A/C_i curve fitting and parameter estimation</i>	120
5.2.6 Stomatal limitation	120
5.2.7 <i>Proportion of leaf nitrogen allocated to photosynthesis and structure</i>	121
5.2.8 <i>Whole plant traits</i>	123
5.2.9 <i>Statistical analyses</i>	125
5.3 Results	127
5.3.1 <i>Leaf nitrogen and chlorophyll content</i>	127
5.3.2 <i>Leaf biochemistry and stomatal conductance</i>	131
5.3.3 <i>Leaf nitrogen allocation</i>	135
5.3.4 <i>Whole plant traits</i>	139
5.3.5 <i>Nitrogen fixation</i>	143
5.4 Discussion	147
5.4.1 <i>Soil nitrogen fertilization has divergent effects on leaf and whole plant acclimation responses to CO₂</i>	148
5.4.2 <i>Implications for future model development</i>	152
5.4.3 <i>Study limitations and future directions</i>	153
5.4.4 <i>Conclusions</i>	155
6. Conclusions	157
References	168
Appendix A: Supplemental material for "Structural carbon costs to acquire nitrogen are determined by nitrogen and light availability in two species with different nitrogen acquisition strategies"	205
Appendix B: Supplemental material for "Soil nitrogen availability modifies leaf nitrogen economies in mature temperate deciduous forests: a direct test of photosynthetic least-cost theory"	209

Appendix C: Supplemental material for "The relative cost of resource use for photosynthesis drives variance in leaf nitrogen content across a climate and soil resource availability gradient"	214
Appendix D: Supplemental material for "Optimal resource investment to photosynthetic capacity maximizes nutrient allocation to whole plant growth under elevated CO₂" . . .	221

Abstract

Photosynthesis is the largest carbon flux between the atmosphere and is constrained by ecosystem carbon and nutrient cycle dynamics, which causes terrestrial biosphere models to be sensitive to the formulation of photosynthetic processes. Terrestrial biosphere models exhibit high divergence in simulated carbon and nitrogen fluxes under future environmental conditions, which may be due to uncertainty in the acclimation response of photosynthetic processes to environmental change. Photosynthetic least-cost theory provides a promising framework for understanding effects of climatic and edaphic factors on photosynthetic acclimation responses to changing environments. Yet, empirical tests of the theory are rare, limiting our ability to assess whether the theory is suitable for implementation in next-generation terrestrial biosphere models.

Here, I present four experiments designed to test assumptions of photosynthetic least-cost theory using a combination of greenhouse, growth chamber, field manipulation, and field gradient experiments. Experiment chapters are flanked by a general introduction chapter and conclusions chapter. The first experimental chapter quantifies structural carbon costs to acquire nitrogen in *Glycine max* and *Gossypium hirsutum* grown under four nitrogen fertilization levels and four light availability levels in a full factorial greenhouse experiment. I find that carbon costs to acquire nitrogen in both species increase with increasing light availability and decrease with increasing fertilization, though responses to fertilization in *G. max* were markedly less than *G. hirsutum*. The second experimental chapter quantifies leaf nitrogen and photosynthetic traits in upper canopy leaves of deciduous trees

growing in a 9-year nitrogen-by-sulfur field manipulation experiment. I find strong evidence for nitrogen-water use tradeoffs with increasing soil nitrogen availability, evidenced through a strong negative relationship between leaf nitrogen content and leaf $C_i:C_a$ and stronger increase in leaf nitrogen content with increasing soil nitrogen availability than leaf $C_i:C_a$. The third experiment investigates variance in leaf nitrogen content across a climate and soil resource availability gradient in Texan grasslands, showing that effects of soil resource availability and climate on leaf nitrogen content are driven by changes in leaf $C_i:C_a$. Finally, the fourth experiment quantifies leaf and whole plant acclimation responses in *G. max* grown under two atmospheric CO₂ levels, with and without inoculation with *Bradyrhizobium japonicum*, and across nine nitrogen fertilization treatments in a full factorial growth chamber experiment. I find that leaf acclimation responses to CO₂ were independent of soil nitrogen fertilization or inoculation treatment, though stimulations in whole plant growth under elevated CO₂ were enhanced with increasing soil nitrogen fertilization and in inoculated pots under low nitrogen fertilization.

Experiments included in this dissertation provide consistent support for patterns expected from photosynthetic least-cost theory. The use of multiple experimental approaches allowed me to examine mechanisms driving patterns expected from the theory and investigate whether these patterns occur naturally across environmental gradients. Findings from these chapters challenge common paradigms in plant ecophysiology, providing evidence that including photosynthetic least-cost frameworks in next-generation terrestrial biosphere models may improve the observed divergence in simulated outcomes across terrestrial biosphere model products.

List of Tables

2.1	Analysis of variance results exploring species-specific effects of light availability, nitrogen fertilization, and their interactions on carbon costs to acquire nitrogen, whole-plant nitrogen biomass, and root carbon biomass	16
2.2	Analysis of variance results exploring effects of light availability, nitrogen fertilization, and their interactions on <i>G. max</i> root nodule biomass and the ratio of root nodule biomass to root biomass	23
2.3	Slopes of the regression line describing the relationship between each dependent variable and nitrogen fertilization at each light level	24
3.1	Effects of soil N availability, soil pH, and species on leaf N content per unit leaf area (N_{area}), leaf N content per unit leaf mass (N_{mass}), and leaf mass per unit leaf area (M_{area})	51
3.2	Effects of soil N availability, soil pH, species, and N_{area} on leaf biochemistry	54
3.3	Effects of soil N availability, soil pH, and species on the proportion of leaf nitrogen content allocated to photosynthesis, Rubisco, bioenergetics, and structure	57
3.4	Effects of soil N availability, soil pH, species, and N_{area} on tradeoffs between nitrogen and water use	60

4.1	Site locality information, sampling year(s), 2006-2020 mean annual precipitation (MAP; mm), mean annual temperature (MAT; °C), and water holding capacity (WHC; mm)*	80
4.2	Effects of soil moisture, soil nitrogen availability, and plant functional group on β	89
4.3	Effects of soil moisture, soil nitrogen availability, and plant functional group on leaf $C_i:C_a^*$	92
4.4	Effects of soil nitrogen fertilization, inoculation, and CO ₂ treatments on N_{area} , N_{mass} , and M_{area}	96
4.5	Structural equation model results investigating direct effects of climatic and soil resource availability on N_{area} , N_{mass} , M_{area} , leaf $C_i:C_a$, and β	99
5.1	Effects of soil nitrogen fertilization, inoculation, and CO ₂ treatments on N_{area} , N_{mass} , M_{area} , and Chl_{area}	129
5.2	Effects of soil nitrogen fertilization, inoculation, and CO ₂ on leaf biochemistry	133
5.3	Effects of soil N availability, soil pH, species, and N_{area} on leaf nitrogen allocation	137
5.4	Effects of soil N availability, soil pH, species, and N_{area} on total leaf area, whole plant biomass, and carbon costs to acquire nitrogen . .	141
5.5	Effects of soil N availability, soil pH, species, and N_{area} on root nodule biomass and plant investments in symbiotic nitrogen fixation	145

A1	Summary table containing volumes of compounds used to create modified Hoagland's solutions for each soil nitrogen fertilization treatment. All volumes are expressed as milliliters per liter (mL/L)	205
A2	Analysis of variance results exploring species-specific effects of light availability, nitrogen fertilization, and their interactions on the ratio of whole plant biomass to pot volume	206
A3	Slopes of the regression line describing the relationship between each dependent variable and nitrogen fertilization at each light level* ²⁰⁷	207
B1	Sample sizes of each species, abbreviated by their USDA NRCS PLANTS database code, within each plot at each site	209
B2	Analysis of variance results exploring the linear effect of leaf temperature on net photosynthesis rate and stomatal conductance measured at 400 $\mu\text{mol mol}^{-1}$ CO ₂	210
B3	Second order log-polynomial regression coefficients that described the effect of leaf temperature on net photosynthesis and stomatal conductance measured at 400 $\mu\text{mol mol}^{-1}$ CO ₂	211
B4	Mean, standard error, and 95% confidence interval ranges of soil nitrogen availability estimates across all measured plots. All units are expressed as $\mu\text{g N g}^{-1}$ resin d ⁻¹	212
C1	List of sampled species and their plant functional group assignment	216
C2	List of sampled species and their plant functional group assignment (cont.)	217

C3	List of sampled species and their plant functional group assignment (cont.)	218
C4	Model selection results for soil moisture, air temperature, and vapor pressure deficit. Soil moisture was used in a bivariate regression against β , while vapor pressure deficit was used in bivariate regressions against leaf $C_i:C_a^*$	219
D1	Summary table containing volumes of compounds used to create modified Hoagland's solutions for each soil nitrogen fertilization treatment. All volumes are expressed as milliliters per liter (mL/L)	221
D2	Summary of the daily growth chamber growing condition program	222

List of Figures

2.1 Relationships between soil nitrogen fertilization and light availability on carbon costs to acquire nitrogen in <i>G. hirsutum</i> and <i>G. max</i>	17
2.2 Relationships between soil nitrogen fertilization and light availability on whole-plant nitrogen biomass in <i>G. hirsutum</i> and <i>G. max</i>	19
2.3 Relationships between soil nitrogen fertilization and light availability on root carbon biomass in <i>G. hirsutum</i> and <i>G. max</i>	21
2.4 Effects of shade cover and nitrogen fertilization on root nodule biomass and the ratio of root nodule biomass to root biomass in <i>G. max</i>	25
3.1 Effects of soil N availability and species on leaf N content per unit leaf area, leaf nitrogen content per unit leaf biomass, and leaf mass per leaf area	52
3.2 Effects of soil N availability, species, and leaf N content leaf biochemistry	55
3.3 Effects of soil N availability, species, and leaf N content on the fraction of leaf nitrogen allocated to photosynthesis and structure	58
3.4 Effects of soil N availability, species, and leaf N content on tradeoffs between nitrogen and water use	61
4.1 Maps that detail site locations along 2006-2020 mean annual precipitation and mean annual temperature gradients in Texas, USA.	81

4.2 Effects of soil nitrogen availability and soil moisture on the unit cost ratio β	90
4.3 Effects of 4-day mean vapor pressure deficit, 2-day soil moisture (per water holding capacity), and soil nitrogen availability on leaf $C_i:C_a$.	93
4.4 Effects of leaf $C_i:C_a$, soil nitrogen availability, and soil moisture on leaf nitrogen content per unit leaf area, leaf nitrogen content per unit leaf biomass, and leaf mass per area.	97
4.5 Structural equation model results exploring drivers of N_{area}	100
5.1 Effects of CO_2 , fertilization, and inoculation on leaf nitrogen per unit leaf area, leaf nitrogen content, leaf mass per unit leaf area, and chlorophyll content per unit leaf area.	130
5.2 Effects of CO_2 , fertilization, and inoculation on maximum rate of Rubisco carboxylation, the maximum rate of RuBP regeneration, and the ratio of the maximum rate of RuBP regeneration to the maximum rate of Rubisco carboxylation leaf mass per unit leaf area, dark respiration, stomatal conductance, and stomatal limitation.	134
5.3 Effects of CO_2 , fertilization, and inoculation on the relative fraction of leaf nitrogen allocated to photosynthesis and the fraction of leaf nitrogen allocated to structure.	138
5.4 Effects of CO_2 , fertilization, and inoculation on total leaf area, total biomass, and structural carbon costs to acquire nitrogen.	142

5.5 Effects of CO ₂ , fertilization, and inoculation on nodule biomass, nodule: root biomass, and percent nitrogen fixed from the atmosphere.	146
A1 Effects of shade cover and nitrogen fertilization on the ratio of plant biomass to rooting volume in <i>G. hirsutum</i> and <i>G. max</i>	208
B1 Effects of leaf temperature on net photosynthesis rate and stomatal conductance values when measured at 400 μmol mol ⁻¹ CO ₂	213
C2 Model selection results exploring relevant timescales for soil moisture and vapor pressure deficit	220
D1 Relationships between area-based leaf nitrogen content, mass-based leaf nitrogen content, and leaf mass per unit leaf area measured on the focal leaf used to generate A_{net}/C_i curves and leaf nitrogen content measured on the leaf used for chlorophyll extractions	223
D2 Effects of CO ₂ , fertilization, and inoculation on the ratio of whole plant biomass to pot volume	224

1 Chapter 1

2 Introduction

3 Photosynthesis represents the largest carbon flux between the atmosphere
4 and biosphere, and is regulated by complex ecosystem carbon and nutrient cy-
5 cles (Hungate et al. 2003; IPCC 2021). As a result, the inclusion of robust,
6 empirically tested representations of photosynthetic processes is critical in order
7 for terrestrial biosphere models to accurately and reliably simulate carbon and
8 nutrient fluxes between the atmosphere and terrestrial biosphere (Oreskes et al.
9 1994; Smith and Dukes 2013; Prentice et al. 2015; Wieder et al. 2015). Despite
10 evidence that the inclusion of coupled carbon and nutrient cycles can improve
11 model uncertainty, widespread divergence in predicted carbon and nutrient fluxes
12 is still apparent across model products (Friedlingstein et al. 2014; Arora et al.
13 2020; Davies-Barnard et al. 2020). Divergence in predicted carbon and nutrient
14 fluxes across terrestrial biosphere models may be due to an incomplete under-
15 standing of how plants acclimate to changing environments (Smith and Dukes
16 2013; Davies-Barnard et al. 2020), as terrestrial biosphere models are sensitive to
17 the formulation of photosynthetic processes (Bonan et al. 2011; Ziehn et al. 2011;
18 Booth et al. 2012; Smith et al. 2016; Smith et al. 2017; Rogers et al. 2017).

Many terrestrial biosphere models predict leaf-level photosynthesis through linear relationships between area-based leaf nitrogen content and the maximum rate of Ribulose-1,5-bisphosphate carboxylase/oxygenase ("Rubisco"), following the idea that large fractions of leaf nitrogen content are allocated to the construction and maintenance of Rubisco and other photosynthetic enzymes (Evans

24 1989). The inclusion of coupled carbon and nutrient cycles in terrestrial bio-
25 sphere models (Shi et al. 2016; Braghieri et al. 2022) allows for the prediction
26 of leaf nitrogen content through soil nitrogen availability, which causes models to
27 indirectly predict photosynthetic processes through shifts in soil nitrogen avail-
28 ability (Smith et al. 2014; Lawrence et al. 2019). While these patterns are
29 commonly observed in ecosystems globally (Brix 1971; Evans 1989; Firn et al.
30 2019; Liang et al. 2020), this formulation does not allow for the prediction of
31 leaf and whole plant acclimation responses to changing environments (Smith and
32 Dukes 2013; Rogers et al. 2017; Harrison et al. 2021), and suggests that constant
33 leaf nitrogen-photosynthesis relationships are ubiquitous across ecosystems.

34 Photosynthetic least-cost theory (Prentice et al. 2014; Wang et al. 2017;
35 Smith et al. 2019; Scott and Smith 2022; Harrison et al. 2021) provides a con-
36 temporary framework for predicting leaf and whole plant acclimation responses
37 to environmental change. The theory, which unifies photosynthetic optimal coor-
38 dination (Chen et al. 1993; Maire et al. 2012) and least-cost (Wright et al. 2003)
39 theories, posits that plants optimize photosynthetic processes by minimizing the
40 summed cost of nutrient and water use (referred to here and in the rest of this
41 dissertation as β). The summed cost of nutrient and water use is predicted to
42 be positively correlated with the ratio of intercellular CO₂ to atmospheric CO₂
43 (referred to here and in the rest of this dissertation as leaf $C_i:C_a$). Leaf $C_i:C_a$ is
44 determined by factors that influence leaf nutrient demand, such as CO₂, temper-
45 ature, vapor pressure deficit, and light availability (Prentice et al. 2014; Wang
46 et al. 2017; Smith et al. 2019; Stocker et al. 2020), and may change in response to
47 changing edaphic characteristics through changes in β . Photosynthetic processes

48 are optimized such that nutrients are allocated to photosynthetic enzymes to allow
49 net photosynthesis rates to be equally co-limited by the maximum rate of Rubisco
50 carboxylation and the maximum rate of Ribulose-1,5-bisphosphate (RuBP) regen-
51 eration (Chen et al. 1993; Maire et al. 2012). The theory indicates that costs
52 of nutrient and water use are substitutable such that, in a given environment,
53 optimal photosynthesis rates can be achieved by sacrificing inefficient use of a
54 relatively more abundant (and less costly to acquire) resource for more efficient
55 use of a relatively less abundant (and more costly to acquire) resource.

56 Optimality models leveraging patterns expected from photosynthetic least-
57 cost theory have been developed for both C₃ (Wang et al. 2017; Smith et al. 2019;
58 Stocker et al. 2020) and more recently for C₄ species (Scott and Smith 2022). Such
59 models show broad agreement with patterns observed across environmental gradi-
60 ents (Smith et al. 2019; Paillassa et al. 2020; Querejeta et al. 2022; Westerband
61 et al. 2023), and are capable of reconciling dynamic leaf nitrogen-photosynthesis
62 relationships and acclimation responses to elevated CO₂, temperature, light avail-
63 ability, and vapor pressure deficit (Dong et al. 2017; Dong et al. 2020; Smith
64 and Keenan 2020; Luo et al. 2021; Peng et al. 2021; Dong et al. 2022; Dong
65 et al. 2022; Querejeta et al. 2022; Westerband et al. 2023). Current versions of
66 optimality models that invoke patterns expected from photosynthetic least-cost
67 theory hold β constant across growing environments. As growing evidence sug-
68 gests that costs of nutrient use change across resource availability and climatic
69 gradients in species with different nutrient acquisition strategies (Fisher et al.
70 2010; Brzostek et al. 2014; Terrer et al. 2018; Allen et al. 2020), one might
71 expect that β should dynamically change across environments and in species with

72 different nutrient acquisition strategies.

73 Despite recent recognition that patterns expected from photosynthetic
74 least-cost theory occur across broad environmental gradients, no study has investi-
75 gated how β varies across edaphic and climatic gradients aside from a single study
76 investigating variance in β due to soil water stress (Lavergne et al. 2020). Further-
77 more, no previous study has investigated whether β varies in species with different
78 nutrient acquisition strategies, or if changes in β due to changes in edaphic char-
79 acteristics scale to influence leaf or whole plant acclimation responses to changing
80 environments. The lack of these studies provided motivation for the experimental
81 chapters included in this dissertation.

82 In this dissertation, I use a combination of greenhouse, field manipulation,
83 environmental gradient, and growth chamber experiments to quantify leaf and
84 whole plant acclimation responses across various climatic and edaphic conditions
85 and different nutrient acquisition strategies. Together, these experiments eval-
86 uate patterns expected from photosynthetic least-cost theory and test mechanisms
87 predicted to drive responses expected from theory. The empirical data collected
88 in these experiments will also provide important information needed to refine ex-
89 isting optimality models that include photosynthetic least-cost frameworks, and
90 could help determine whether such models are suitable for implementing in next-
91 generation terrestrial biosphere models. While theory suggests that plants accli-
92 mate across environments by minimizing the summed cost of nutrients relative
93 to water, I choose to isolate effects of soil nitrogen availability on costs of nitro-
94 gen acquisition relative to water for the sake of brevity. Though, I acknowledge
95 that patterns expected from theory may be modified by other nutrients (e.g.,

96 phosphorus) or edaphic characteristics, and, though not included here, should be
97 investigated.

98 In the first experimental chapter, I re-analyze data from a greenhouse ex-
99 periment that grew *Glycine max* and *Gossypium hirsutum* seedlings under full-
100 factorial combinations of four light treatments and four fertilization treatments
101 to examine effects of nitrogen and light availability on structural carbon costs to
102 acquire nitrogen. In the second experimental chapter, I measure leaf physiological
103 traits in the upper canopy of mature trees growing in a 9-year nitrogen-by-pH
104 field manipulation experiment to assess whether changes in soil nitrogen availabil-
105 ity or soil pH modify nitrogen-water use trade-offs expected from photosynthetic
106 least-cost theory. The third experimental chapter leverages a broad precipitation
107 and soil nutrient availability gradient in Texan grasslands to investigate primary
108 drivers of leaf nitrogen content. In the fourth experimental chapter, I use growth
109 chambers to quantify leaf and whole plant acclimation responses to CO₂ across
110 a soil nitrogen fertilization gradient, while also manipulating nutrient acquisition
111 strategy by controlling whether seedlings were able to form associations with sym-
112 biotic nitrogen-fixing bacteria.

113 Across experiments, I find strong and consistent support for patterns ex-
114 pected from photosynthetic least-cost theory, showing that shifts in edaphic char-
115 acteristics predictably alter β , and that shifts in β facilitate changes in leaf
116 nitrogen-water use tradeoffs and leaf nitrogen-photosynthesis relationships. I also
117 show that costs of nitrogen acquisition vary in species with different nitrogen
118 acquisition strategies. Finally, I show strong evidence suggesting that leaf accli-
119 mation responses to elevated CO₂ are decoupled from soil nitrogen availability and

120 inoculation with symbiotic nitrogen-fixing bacteria. It is my hope that these ex-
121 periments will encourage future iterations of optimality models that adopt photo-
122 synthetic least-cost frameworks to consider frameworks for implementing dynamic
123 β values across soil resource availability gradients and in species with different nu-
124 trient acquisition strategies.

125 Finally, the four experimental chapters presented in this dissertation are
126 presented either as previously published journal articles (copyright clearance avail-
127 able upon request) or as manuscript drafts currently in preparation for journal
128 submission. Specifically, the first experimental chapter was published in *Journal*
129 *of Experimental Botany* in 2021 and the second chapter is currently in review,
130 while the third and fourth chapters are each in preparation for journal submis-
131 sion. This dissertation concludes with a sixth chapter that summarizes experiment
132 findings and briefly synthesizes common themes observed across experiments.

133

Chapter 2

134

Structural carbon costs to acquire nitrogen are determined by
135 nitrogen and light availability in two species with different nitrogen
136 acquisition strategies

137 2.1 Introduction

138 Carbon and nitrogen cycles are tightly coupled in terrestrial ecosystems. This
139 tight coupling influences photosynthesis (Walker et al. 2014; Rogers et al. 2017),
140 net primary productivity (LeBauer and Treseder 2008; Thomas et al. 2013), de-
141 composition (Cornwell et al. 2008; Bonan et al. 2013; Sulman et al. 2019), and
142 plant resource competition (Gill and Finzi 2016; Xu-Ri and Prentice 2017). Ter-
143 restrial biosphere models are beginning to include connected carbon and nitrogen
144 cycles to improve the realism of their simulations (Fisher et al. 2010; Brzostek
145 et al. 2014; Wieder et al. 2015; Shi et al. 2016; Zhu et al. 2019). Simula-
146 tions from these models indicate that coupling carbon and nitrogen cycles can
147 drastically influence future biosphere-atmosphere feedbacks under global change,
148 such as elevated carbon dioxide or nitrogen deposition (Thornton et al. 2007;
149 Goll et al. 2012; Wieder et al. 2015; Wieder et al. 2019). Nonetheless, there
150 are still limitations in our quantitative understanding of connected carbon and
151 nitrogen dynamics (Thomas et al. 2015; Meyerholt et al. 2016; Rogers et al.
152 2017; Exbrayat et al. 2018; Shi et al. 2019), forcing models to make potentially
153 unreliable assumptions.

154

Plant nitrogen acquisition is a process in terrestrial ecosystems by which
155 carbon and nitrogen are tightly coupled (Vitousek and Howarth 1991; Delaire
156 et al. 2005; Brzostek et al. 2014). Plants must allocate photosynthetically de-

157 rived carbon belowground to produce and maintain root systems or exchange with
158 symbiotic soil microbes in order to acquire nitrogen (Högberg et al. 2008; Hög-
159 berg et al. 2010). Thus, plants have an inherent carbon cost associated with
160 acquiring nitrogen, which can include both direct energetic costs associated with
161 nitrogen acquisition and indirect costs associated with building structures that
162 support nitrogen acquisition (Gutschick 1981; Rastetter et al. 2001; Vitousek
163 et al. 2002; Menge et al. 2008). Model simulations (Fisher et al. 2010; Brzostek
164 et al. 2014; Shi et al. 2016; Allen et al. 2020) and meta-analyses (Terrer et al.
165 2018) suggest that these carbon costs vary between species, particularly those
166 with different nitrogen acquisition strategies. For example, simulations using iter-
167 ations of the Fixation and Uptake of Nitrogen (FUN) model indicate that species
168 that acquire nitrogen from non-symbiotic active uptake pathways (e.g. mass flow)
169 generally have larger carbon costs to acquire nitrogen than species that acquire
170 nitrogen through symbiotic associations with nitrogen-fixing bacteria (Brzostek
171 et al. 2014; Allen et al. 2020).

172 Carbon costs to acquire nitrogen likely vary in response to changes in soil
173 nitrogen availability. For example, if the primary mode of nitrogen acquisition
174 is through non-symbiotic active uptake, then nitrogen availability could decrease
175 carbon costs to acquire nitrogen as a result of increased per-root nitrogen up-
176 take (Franklin et al. 2009; Wang et al. 2018). However, if the primary mode of
177 nitrogen acquisition is through symbiotic active uptake, then nitrogen availabil-
178 ity may incur additional carbon costs to acquire nitrogen if it causes microbial
179 symbionts to shift toward parasitism along the parasitism–mutualism continuum
180 (Johnson et al. 1997; Hoek et al. 2016; Friel and Friesen 2019) or if it reduces

181 the nitrogen acquisition capacity of a microbial symbiont (van Diepen et al. 2007;
182 Soudzilovskaia et al. 2015; Muñoz et al. 2016). Species may respond to shifts in
183 soil nitrogen availability by switching their primary mode of nitrogen acquisition
184 to a strategy with lower carbon costs to acquire nitrogen in order to maximize
185 the magnitude of nitrogen acquired from a belowground carbon investment and
186 outcompete other individuals for soil resources (Rastetter et al. 2001; Menge et al.
187 2008).

188 Environmental conditions that affect demand to acquire nitrogen to sup-
189 port new and existing tissues could also be a source of variance in plant carbon
190 costs to acquire nitrogen. For example, an increase in plant nitrogen demand could
191 increase carbon costs to acquire nitrogen if this increases the carbon that must be
192 allocated belowground to acquire a proportional amount of nitrogen (Kulmatiski
193 et al. 2017; Noyce et al. 2019). This could be driven by a temporary state of
194 diminishing return associated with investing carbon toward building and main-
195 taining structures that are necessary to support enhanced nitrogen uptake, such
196 as fine roots (Matamala and Schlesinger 2000; Norby et al. 2004; Arndal et al.
197 2018), mycorrhizal hyphae (Saleh et al. 2020), or root nodules (Parvin et al.
198 2020). Alternatively, if the environmental factor that increases plant nitrogen de-
199 mand causes nitrogen to become more limiting in the system (e.g. atmospheric
200 CO₂) (Luo et al. 2004; LeBauer and Treseder 2008; Vitousek et al. 2010; Liang
201 et al. 2016), species might switch their primary mode of nitrogen acquisition to
202 a strategy with lower relative carbon costs to acquire nitrogen in order to gain a
203 competitive advantage over species with either different or more limited modes of
204 nitrogen acquisition (Ainsworth and Long 2005; Taylor and Menge 2018).

205 Using a plant economics approach, I examined the influence of plant ni-
206 trogen demand and soil nitrogen availability on plant carbon costs to acquire
207 nitrogen. This was done by growing a species capable of forming associations
208 with nitrogen-fixing bacteria (*Glycine max* L. (Merr)) and a species not capable
209 of forming these associations (*Gossypium hirsutum* L.) under four levels of light
210 availability (plant nitrogen demand proxy) and four levels of soil nitrogen fertil-
211 ization (soil nitrogen availability proxy) in a full-factorial, controlled greenhouse
212 experiment. I used this experimental set-up to test the following hypotheses:

- 213 1. An increase in plant nitrogen demand due to increasing light availability will
214 increase carbon costs to acquire nitrogen through a proportionally larger
215 increase in belowground carbon than whole-plant nitrogen acquisition. This
216 will be the result of an increased investment of carbon toward belowground
217 structures that support enhanced nitrogen uptake, but at a lower nitrogen
218 return.
- 219 2. An increase in soil nitrogen availability will decrease carbon costs to acquire
220 nitrogen as a result of increased per root nitrogen uptake in *G. hirsutum*.
221 However, soil nitrogen availability will not affect carbon costs to acquire
222 nitrogen in *G. max* because of the already high return of nitrogen supplied
223 through nitrogen fixation.

224 2.2 Methods

225 2.2.1 *Experiment setup*

226 *Gossypium hirsutum* and *G. max* were planted in individual 3 liter pots (NS-300; **227** Nursery Supplies, Orange, CA, USA) containing a 3:1 mix of unfertilized potting **228** mix (Sungro Sunshine Mix #2, Agawam, MA, USA) to native soil extracted from **229** an agricultural field most recently planted with *G. max* at the USDA-ARS Lab-**230** oratory in Lubbock, TX, USA (33.59°N, -101.90°W). The field soil was classified **231** as Amarillo fine sandy loam (75% sand, 10% silt, 15% clay). Upon planting, **232** all *G. max* pots were inoculated with *Bradyrhizobium japonicum* (Verdesian N-**233** Dure™ Soybean, Cary, NC, USA) to stimulate root nodulation. Individuals of **234** both species were grown under similar, unshaded, ambient greenhouse conditions **235** for 2 weeks to germinate and begin vegetative growth.

236 Three blocks were set up in the greenhouse, each containing four light **237** treatments created using shade cloth that reduced incoming radiation by either 0 **238** (full sun), 30, 50, or 80%. Two weeks post-germination, individuals were randomly **239** placed in the four light treatments in each block. Individuals received one of four **240** nitrogen fertilization doses as 100ml of a modified Hoagland solution (Hoagland **241** and Arnon 1950) equivalent to either 0, 70, 210, or 630 ppm N twice per week **242** within each light treatment. Nitrogen fertilization doses were received as topical **243** agents to the soil surface. Each Hoagland solution was modified to keep concen-**244** trations of other macro- and micronutrients equivalent (Table A1). Plants were **245** routinely well watered to eliminate water stress.

246 2.2.2 *Plant measurements and calculations*

247 Each individual was harvested after 5 weeks of treatment, and biomass was sepa-
248 rated by organ type (leaves, stems, and roots). Nodules on *G. max* roots were also
249 harvested. Except for the 0% shade cover and 630 ppm N treatment combination,
250 all treatment combinations in both species had lower average dry biomass:pot vol-
251 ume ratios than the 1:1 ratio recommended by Poorter et al. (2012) to minimize
252 the likelihood of pot volume-induced growth limitation (Table A2; Table A3; Fig.
253 A1).

254 All harvested material was dried, weighed, and ground by organ type.
255 Carbon and nitrogen content (g g^{-1}) was determined by subsampling from ground
256 and homogenized biomass of each organ type using an elemental analyzer (Costech
257 4010; Costech, Inc., Valencia, CA, USA). I scaled these values to total leaf, stem,
258 and root carbon and nitrogen biomass (g) by multiplying dry biomass of each
259 organ type by carbon or nitrogen content of each corresponding organ type. Whole
260 plant nitrogen biomass (g) was calculated as the sum of total leaf (g), stem (g),
261 and root (g) nitrogen biomass. Root nodule carbon biomass was not included in
262 the calculation of root carbon biomass; however, relative plant investment toward
263 root or root nodule standing stock was estimated as the ratio of root biomass to
264 root nodule biomass (g g^{-1}), following similar metrics to those adopted by Dovrat
265 et al. (2018) and Dovrat et al. (2020).

266 Carbon costs to acquire nitrogen (N_{cost} ; gC gN^{-1}) were estimated as the
267 ratio of total root carbon biomass (C_{bg} ; gC) to whole-plant nitrogen biomass
268 (N_{wp} ; gN). This calculation quantifies the relationship between carbon spent on
269 nitrogen acquisition and whole plant nitrogen acquisition by using root carbon

270 biomass as a proxy for estimating the magnitude of carbon allocated toward ni-
271 trogen acquisition. This calculation therefore assumes that the magnitude of root
272 carbon standing stock is proportional to carbon transferred to root nodules or my-
273 corrhizae, or lost through root exudation or turnover. The assumption has been
274 supported in species that associate with ectomycorrhizal fungi (Hobbie 2006; Hob-
275 bie and Hobbie 2008), but is less clear in species that acquire nitrogen through
276 non-symbiotic active uptake or symbiotic nitrogen fixation. It is also unclear
277 whether relationships between root carbon standing stock and carbon transfer to
278 root nodules are similar in magnitude to carbon lost through exudation or when
279 allocated toward other active uptake pathways. Thus, because of the way mea-
280 surements were calculated, proximal values of carbon costs to acquire nitrogen are
281 underestimates.

282 2.2.3 *Statistical analyses*

283 I explored the effects of light and nitrogen availability on carbon costs to acquire
284 nitrogen using separate linear mixed-effects models for each species. Models in-
285 cluded shade cover, nitrogen fertilization, and interactions between shade cover
286 and nitrogen fertilization as continuous fixed effects, and also included block as a
287 random intercept term. Three separate models for each species were built with
288 this independent variable structure for three different dependent variables: (i)
289 carbon costs to acquire nitrogen (gC gN^{-1}); (ii) whole plant nitrogen biomass
290 (denominator of carbon cost to acquire nitrogen; gN); and (iii) belowground car-
291 bon biomass (numerator of carbon cost to acquire nitrogen; gC). I constructed two
292 additional models for *G. max* with the same model structure described above to

293 investigate the effects of light availability and nitrogen fertilization on root nodule
294 biomass (g) and the ratio of root nodule biomass to root biomass (unitless).

295 I used Shapiro–Wilk tests of normality to determine whether species spe-
296 cific linear mixed-effects model residuals followed a normal distribution. Zero
297 models satisfied residual normality assumptions when models were fit using un-
298 transformed data (Shapiro–Wilk: $p < 0.05$ in all cases). I attempted to satisfy
299 residual normality assumptions by first fitting models using dependent variables
300 that were natural-log transformed. If residual normality assumptions were still
301 not met (Shapiro–Wilk: $p < 0.05$), then models were fit using dependent variables
302 that were square root transformed. All residual normality assumptions were satis-
303 fied when models were fit with either a natural-log or square root transformation
304 (Shapiro–Wilk: $p > 0.05$ in all cases). Specifically, I natural-log transformed *G.*
305 *hirsutum* carbon costs to acquire nitrogen and *G. hirsutum* whole-plant nitrogen
306 biomass. I also square root transformed *G. max* carbon costs to acquire nitrogen,
307 *G. max* whole-plant nitrogen biomass, root carbon biomass in both species, *G.*
308 *max* root nodule biomass, and the *G. max* ratio of root nodule biomass to root
309 biomass. I used the ‘lmer’ function in the ‘lme4’ R package (Bates et al. 2015) to
310 fit each model and the ‘Anova’ function in the ‘car’ R package (Fox and Weisberg
311 2019) to calculate Wald’s χ^2 to determine the significance ($\alpha = 0.05$) of each fixed
312 effect coefficient. Finally, I used the ‘emmeans’ R package (Lenth 2019) to conduct
313 post-hoc comparisons of our treatment combinations using Tukey’s tests. Degrees
314 of freedom for all Tukey’s tests were approximated using the Kenward–Roger ap-
315 proach (Kenward and Roger 1997). All analyses and plots were conducted in R
316 version 4.0.1 (R Core Team 2021).

317 2.3 Results

318 2.3.1 *Carbon costs to acquire nitrogen*

319 Carbon costs to acquire nitrogen in *G. hirsutum* increased with increasing light
320 availability ($p<0.001$; Table 2.1; Fig. 2.1) and decreased with increasing nitrogen
321 fertilization ($p<0.001$; Table 2.1; Fig. 2.1). There was no interaction between
322 light availability and nitrogen fertilization ($p=0.486$, Table 2.1; Fig. 2.1).

323 Carbon costs to acquire nitrogen in *G. max* also increased with increasing
324 light availability ($p<0.001$, Table 2.1; Fig. 2.1) and decreased with increasing
325 nitrogen fertilization ($p<0.001$; Table 2.1; Fig. 2.1). There was no interaction
326 between light availability and nitrogen fertilization ($p=0.261$, Table 2.1; Fig. 2.1).

Table 2.1. Analysis of variance results exploring species-specific effects of light availability, nitrogen fertilization, and their interactions on carbon costs to acquire nitrogen (N_{cost}), whole plant nitrogen biomass (N_{wp}), and root carbon biomass (C_{bg})

	N_{cost}			N_{wp}			C_{bg}			
	df	Coefficient	χ^2	p	Coefficient	χ^2	p	Coefficient	χ^2	p
<i>G. hirsutum</i>										
Intercept		1.594	-	-	-3.232	-	-	0.432	-	-
Light (L)	1	-1.09E-02	56.494	<0.001	-6.41E-03	91.275	<0.001	-2.62E-03	169.608	<0.001
Nitrogen (N)	1	-1.34E-03	54.925	<0.001	1.83E-03	118.784	<0.001	1.15E-04	2.901	0.089
L*N	1	3.88E-06	0.485	0.486	-1.34E-05	10.721	0.001	-1.67E-06	3.140	0.076
<i>G. max</i>										
Intercept		1.877	-	-	0.239	-	-	0.438	-	-
Light (L)	1	-7.67E-03	174.156	<0.001	-6.72E-04	39.799	<0.001	-2.55E-03	194.548	<0.001
Nitrogen (N)	1	-2.35E-04	21.948	<0.001	1.55E-04	70.771	<0.001	2.52E-04	19.458	<0.001
L*N	1	-2.89E-06	1.262	0.261	-6.32E-07	1.435	0.231	-3.16E-06	10.803	0.001

16

327 *Significance determined using Wald's χ^2 tests ($p=0.05$). P-values less than 0.05 are in bold and p-values between
 328 0.05 and 0.1 are italicized. Negative coefficients for light treatments indicate a positive effect of increasing light
 329 availability on all response variables, as light availability is treated as percent shade cover in all linear mixed-effects
 330 models.

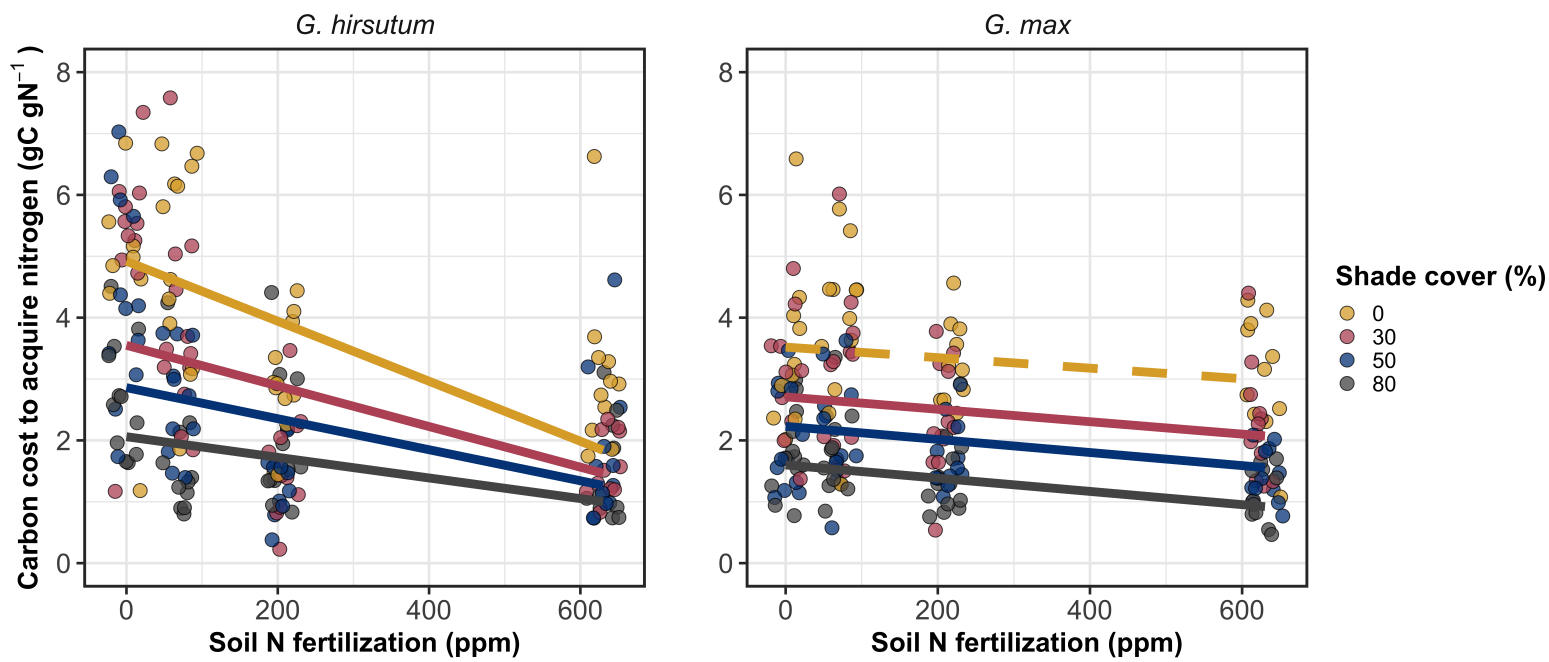


Figure 2.1. Relationships between soil nutrient fertilization and light availability on carbon costs to acquire nitrogen in *G. hirsutum* and *G. max*. Nitrogen fertilization treatments are represented on the x-axis. Shade cover treatments are represented through colored points and trendlines. Trendlines were created by back-transforming marginal mean slopes and intercepts from species-specific linear mixed-effects models. These values were calculated using the ‘emtrends’ and ‘emmeans’ functions in the ‘emmeans’ R package (Lenth, 2019). Yellow points and trendlines represent the 0% shade cover treatment, red points and trendlines represent the 30% shade cover treatment, blue points and trendlines represent the 50% shade cover treatment, and gray points and trendlines represent the 80% shade cover treatment. Solid trendlines indicate slopes that are significantly different from zero (Tukey: $p < 0.05$), while dashed trendlines indicate slopes that are not statistically different from zero.

331 2.3.2 *Whole plant nitrogen biomass*

332 Whole plant nitrogen biomass in *G. hirsutum* was driven by an interaction between
333 light availability and nitrogen fertilization ($p=0.001$; Table 2.1; Fig. 2.2). This
334 interaction indicated a greater stimulation of whole-plant nitrogen biomass by
335 nitrogen fertilization as light levels increased (Table 2.1; Fig. 2.2).

336 Whole plant nitrogen biomass in *G. max* increased with increasing light
337 availability ($p<0.001$) and nitrogen fertilization ($p<0.001$), with no interaction
338 between light availability and nitrogen fertilization ($p=0.231$; Table 2.1; Fig. 2.2).

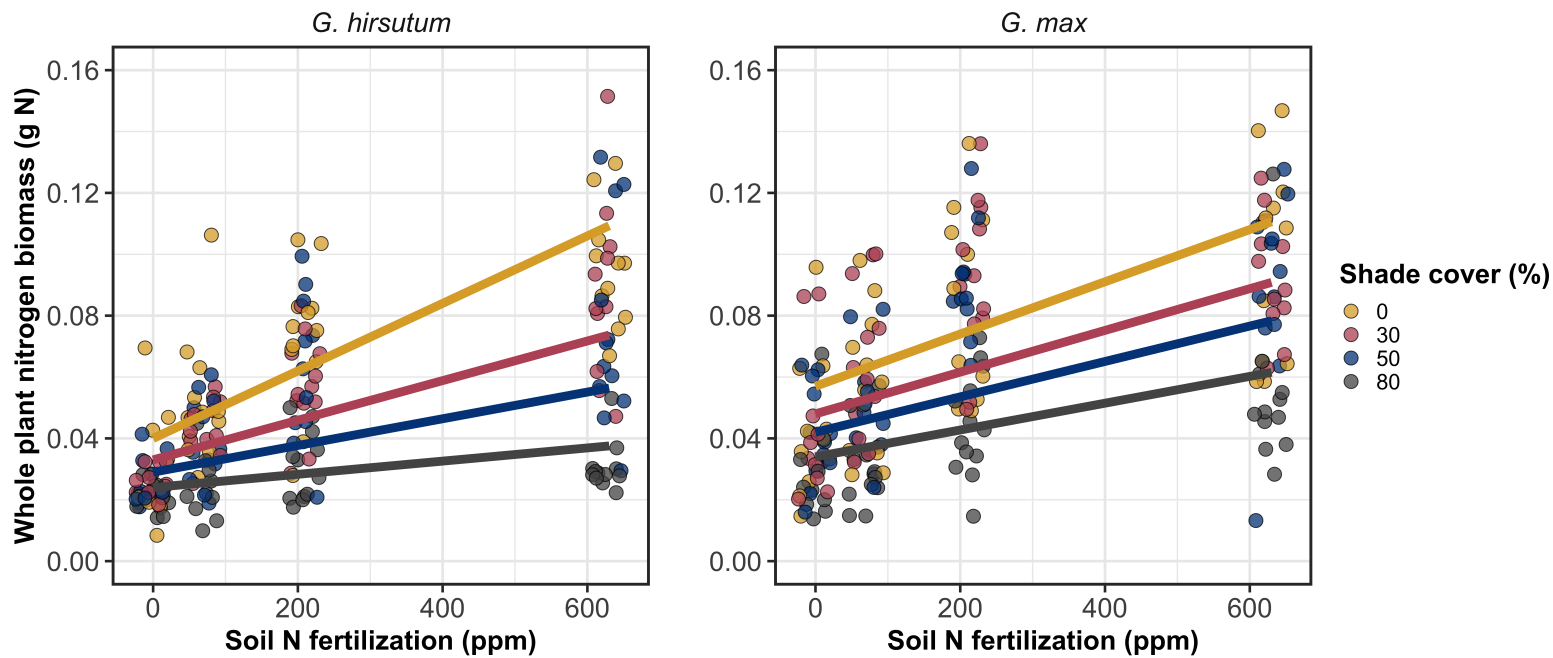


Figure 2.2. Relationships between soil nutrient fertilization and light availability on whole-plant nitrogen biomass in *G. hirsutum* and *G. max*. Whole-plant nitrogen biomass is the denominator of the carbon cost to acquire nitrogen calculation. Nitrogen fertilization treatments are represented on the x-axis. Shade cover treatments are represented through colored points and trendlines. Trendlines were created by back-transforming marginal mean slopes and intercepts from species-specific linear mixed-effects models. These values were calculated using the ‘emtrends’ and ‘emmeans’ functions in the ‘emmeans’ R package (Lenth 2019). Points are jittered for visibility. Colored points and trendlines are as explained in Fig. 2.1. Solid trendlines indicate slopes that are significantly different from zero (Tukey: $p < 0.05$), while dashed trendlines indicate slopes that are not statistically different from zero.

339 2.3.3 *Root carbon biomass*

340 Root carbon biomass in *G. hirsutum* significantly increased with increasing light
341 availability ($p<0.001$; Table 2.1; Fig. 2.3) and marginally increased with nitrogen
342 fertilization ($p=0.089$; Table 2.1; Fig. 2.3). There was also a marginal interaction
343 between light availability and nitrogen fertilization ($p=0.076$; Table 2.1), driven by
344 an increase in the positive response of root carbon biomass to increasing nitrogen
345 fertilization as light availability increased (Table 2.3). This resulted in significantly
346 positive trends between root carbon biomass and nitrogen fertilization in the two
347 highest light treatments (Tukey: $p<0.05$ in both cases; Table 2.3; Fig. 2.3) and no
348 effect of nitrogen fertilization in the two lowest light treatments (Tukey: $p>0.05$
349 in both cases; Table 2.3; Fig. 2.3).

350 There was an interaction between light availability and nitrogen fertiliza-
351 tion on root carbon biomass in *G. max* ($p=0.001$; Table 2.1; Fig. 2.3). Post-hoc
352 analyses indicated that the positive effects of nitrogen fertilization on *G. max*
353 root carbon biomass increased with increasing light availability (Table 2.3; Fig.
354 2.3). There were also positive individual effects of increasing nitrogen fertilization
355 ($p<0.001$) and light availability ($p<0.001$) on *G. max* root carbon biomass (Table
356 2.1; Fig. 2.3).

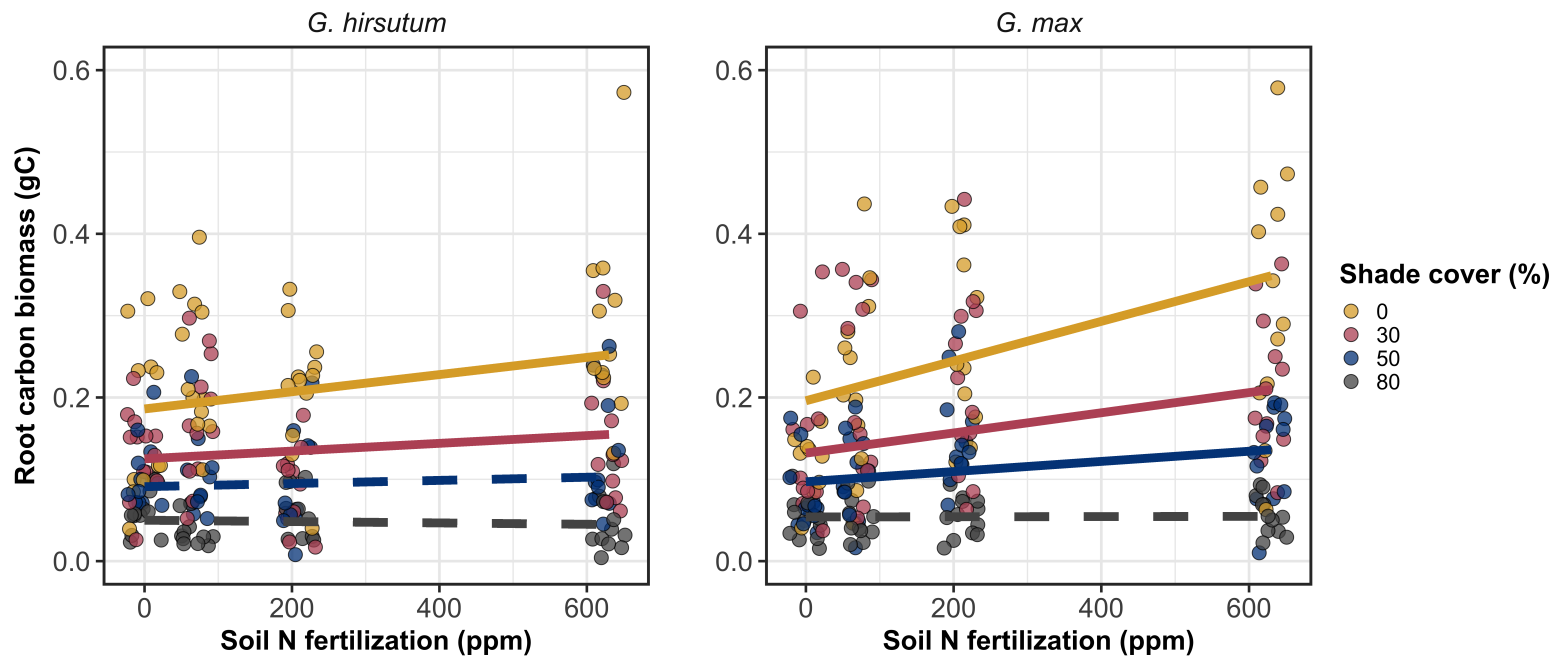


Figure 2.3. Relationships between soil nutrient fertilization and light availability on root carbon biomass in *G. hirsutum* and *G. max*. Root carbon biomass is the numerator of the carbon cost to acquire nitrogen calculation. Nitrogen fertilization treatments are represented on the x-axis. Colored points and trendlines are as explained in Fig. 2.1. Trendlines were created by back-transforming marginal mean slopes and intercepts from species-specific linear mixed-effects models. These values were calculated using the ‘emtrends’ and ‘emmeans’ functions in the ‘emmeans’ R package (Lenth 2019). Points are jittered for visibility. Colored points and trendlines are as explained in Fig. 2.1.

357 2.3.4 *Root nodule biomass*

358 Root nodule biomass in *G. max* increased with increasing light availability ($p<0.001$);
359 Table 2.2; Fig. 2.4a) and decreased with increasing nitrogen fertilization ($p<0.001$;
360 Table 2.2; Fig. 2.4a). There was no interaction between nitrogen fertilization and
361 light availability ($p=0.133$; Table 2.2; Fig. 2.4a). The ratio of root nodule biomass
362 to root biomass did not change in response to light availability ($p=0.481$; Table
363 2.2; Fig. 2.4b) but decreased with increasing nitrogen fertilization ($p<0.001$; Ta-
364 ble 2.2; Fig. 2.4b). There was no interaction between nitrogen fertilization and
365 light availability on the ratio of root nodule biomass to root biomass ($p=0.621$;
366 Table 2.2; Fig. 2.4b).

Table 2.2. Analysis of variance results exploring effects of light availability, nitrogen fertilization, and their interactions on *G. max* root nodule biomass and the ratio of root nodule biomass to root biomass*

	Nodule biomass			Nodule biomass: root biomass			<i>p</i>
	df	Coefficient	χ^2	<i>p</i>	Coefficient	χ^2	
(Intercept)		0.302	-	-	0.448	-	-
Light (L)	1	-1.81E-03	72.964	<0.001	-8.76E-05	0.496	0.481
Nitrogen (N)	1	-2.83E-04	115.377	<0.001	-5.09E-04	156.476	<0.001
L*N	1	1.14E-06	2.226	0.133	-7.30E-07	0.244	0.621

367 *Significance determined using Wald's χ^2 tests ($\alpha=0.05$). *P*-values less than 0.05 are in bold. Negative coefficients for
 368 light treatments indicate a positive effect of increasing light availability on all response variables, as light availability
 369 is treated as percent shade cover in all linear mixed-effects models. Root nodule biomass and nodule biomass: root
 370 biomass models were only constructed for *G. max* because *G. hirsutum* was not inoculated with *B. japonicum* and
 371 is not capable of forming root nodules.

Table 2.3. Slopes of the regression line describing the relationship between each dependent variable and nitrogen fertilization at each light level*

Shade cover	Carbon cost to acquire nitrogen	Whole plant nitrogen biomass	Belowground carbon biomass	Root nodule biomass	Nodule biomass: root biomass
<i>G. hirsutum</i>					
0%	-1.34E-03^a	1.83E-03^a	1.15E-04^b	-	-
30%	-1.22E-03^a	1.43E-03^a	1.17E-04^b	-	-
50%	-1.14E-03^a	1.17E-03^a	3.12E-05 ^b	-	-
80%	-1.02E-03^a	7.66E-04^a	-1.89E-06 ^b	-	-
<i>G. max</i>					
0%	-2.35E-04 ^b	1.55E-05^b	2.51E-04^b	-2.83E-04^b	-5.09E-04^b
30%	-3.22E-04^b	1.35E-05^b	1.57E-04^b	-2.49E-04^b	-5.31E-04^b
50%	-3.80E-04^b	1.23E-05^b	9.37E-05^b	-2.26E-04^b	-5.45E-04^b
80%	-4.66E-04^b	1.04E-05^b	-9.95E-07 ^b	-1.92E-04^b	-5.67E-04^b

24

372 * Slopes represent estimated marginal mean slopes from linear mixed-effects models described in the Methods. Slopes
373 were calculated using the ‘emmeans’ R package (Lenth 2019). Superscripts indicate slopes fit to natural-log (^a) or
374 square root (^b) transformed data. Slopes statistically different from zero (Tukey: $p<0.05$) are indicated in bold.
375 Marginally significant slopes (Tukey: $0.05< p<0.1$) are italicized.

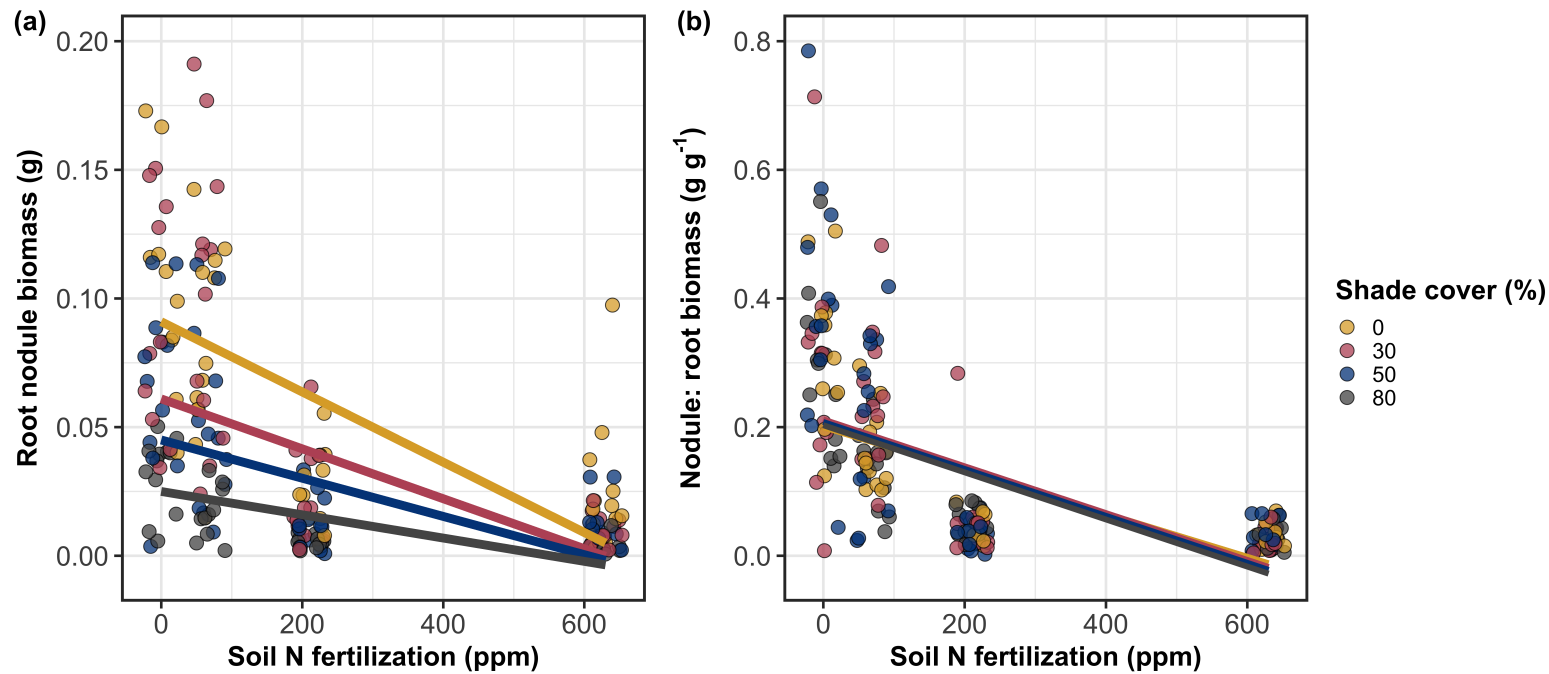


Figure 2.4. Effects of shade cover and nitrogen fertilization on root nodule biomass (a) and the ratio of root nodule biomass to root biomass (b) in *G. max*. Nitrogen fertilization treatments are represented on the x-axis. Shade cover treatments are represented through colored points and trendlines. Trendlines were created by back-transforming marginal mean slopes and intercepts from species-specific linear mixed-effects models. These values were calculated using the ‘emtrends’ and ‘emmmeans’ functions in the ‘emmeans’ R package (Lenth 2019). Points are jittered for visibility. Yellow points and trendlines represent the 0% shade cover treatment, blue points and trendlines represent the 30% shade cover treatment, green points and trendlines represent the 50% shade cover treatment, and purple points and trendlines represent the 80% shade cover treatment. Solid trendlines indicate slopes that are significantly different from zero (Tukey: $p < 0.05$), while dashed trendlines indicate slopes that are not statistically different from zero.

376 2.4 Discussion

377 In this chapter, I determined the effects of light availability and soil nitrogen
378 fertilization on root mass carbon costs to acquire nitrogen in *G. hirsutum* and *G.*
379 *max*. In support of my hypotheses, I found that carbon costs to acquire nitrogen
380 generally increased with increasing light availability and decreased with increasing
381 soil nitrogen fertilization in both species. These findings suggest that carbon costs
382 to acquire nitrogen are determined by factors that influence plant nitrogen demand
383 and soil nitrogen availability. In contrast to my second hypothesis, root nodulation
384 data suggested that *G. max* and *G. hirsutum* achieved similar directional carbon
385 cost responses to nitrogen fertilization despite a likely shift in *G. max* allocation
386 from nodulation to root biomass along the nitrogen fertilization gradient.

387 2.4.1 *Carbon costs to acquire nitrogen increase with light availability and*
388 *decrease with fertilization*

389 Both *G. max* and *G. hirsutum* experienced an increase in carbon costs to ac-
390 quire nitrogen due to increasing light availability. These patterns were driven by
391 a larger increase in root carbon biomass than whole-plant nitrogen biomass. In-
392 creases in root carbon biomass due to factors that increase plant nitrogen demand
393 are a commonly observed pattern, as carbon allocated belowground provides sub-
394 strate needed to produce and maintain structures that satisfy aboveground plant
395 nitrogen demand (Nadelhoffer and Raich 1992; Giardina et al. 2005; Raich et al.
396 2014). Findings suggest that plants allocate relatively more carbon for acquiring
397 nitrogen when demand increases over short temporal scales, which may cause a
398 temporary state of diminishing return due to asynchrony between belowground

399 carbon and whole-plant nitrogen responses to plant nitrogen demand (Kulmatiski
400 et al. 2017; Noyce et al. 2019). These responses might be attributed to a temporal
401 lag associated with producing structures that enhance nitrogen acquisition. For
402 example, fine roots (Matamala and Schlesinger 2000; Norby et al. 2004; Arndal
403 et al. 2018) and root nodules (Parvin et al. 2020) take time to build and first
404 require the construction of coarse roots. Thus, full nitrogen returns from these
405 investments may not occur immediately (Kayler et al. 2010; Kayler et al. 2017),
406 and may vary by species acquisition strategy. I speculate that increases in ni-
407 trogen acquisition from a given carbon investment may occur beyond the 5-week
408 scope of this experiment. A similar study conducted over a longer temporal scale
409 would address this.

410 Increasing soil nitrogen fertilization generally decreased carbon costs to
411 acquire nitrogen in both species. These patterns were driven by a larger increase
412 in whole-plant nitrogen biomass than root carbon biomass. In *G. hirsutum*, re-
413 ductions in carbon costs to acquire nitrogen may have been due to an increase in
414 per-root nitrogen uptake, allowing individuals to maximize the amount of nitro-
415 gen acquired from a belowground carbon investment. Interestingly, increased soil
416 nitrogen fertilization increased whole-plant nitrogen biomass in *G. max* despite
417 reductions in root nodule biomass that likely reduced the nitrogen-fixing capac-
418 ity of *G. max* (Andersen et al. 2005; Muñoz et al. 2016). While reductions in
419 root nodulation due to increased soil nitrogen availability are commonly observed
420 (Gibson and Harper 1985; Fujikake et al. 2003), root nodulation responses were
421 observed in tandem with increased root carbon biomass, implying that *G. max*
422 shifted relative carbon allocation from nitrogen fixation to soil nitrogen acquisition

423 (Markham and Zekveld 2007; Dovrat et al. 2020). This was likely because there
424 was a reduction in the carbon cost advantage of acquiring fixed nitrogen relative
425 to soil nitrogen, and suggests that species capable of associating with symbiotic
426 nitrogen-fixing bacteria shift their relative nitrogen acquisition pathway to opti-
427 mize nitrogen uptake (Rastetter et al. 2001). Future studies should investigate
428 these patterns with a larger quantity of phylogenetically related species, or differ-
429 ent varieties of a single species that differ in their ability to form associations with
430 symbiotic nitrogen-fixing bacteria to more directly test the impact of nitrogen
431 fixation on the patterns observed in this study.

432 2.4.2 *Modeling implications*

433 Carbon costs to acquire nitrogen are subsumed in the general discussion of eco-
434 nomic analogies to plant resource uptake (Bloom et al. 1985; Rastetter et al.
435 2001; Vitousek et al. 2002; Phillips et al. 2013; Terrer et al. 2018; Henneron
436 et al. 2020). Despite this, terrestrial biosphere models rarely include costs of
437 nitrogen acquisition within their framework for predicting plant nitrogen uptake.
438 There is currently one plant resource uptake model, FUN, that quantitatively
439 predicts carbon costs to acquire nitrogen within a framework for predicting plant
440 nitrogen uptake for different nitrogen acquisition strategies (Fisher et al. 2010;
441 Brzostek et al. 2014). Iterations of FUN are currently coupled to two terrestrial
442 biosphere models: the Community Land Model 5.0 and the Joint UK Land En-
443 vironment Simulator (Shi et al. 2016; Lawrence et al. 2019; Clark et al. 2011).
444 Recent work suggests that coupling FUN to CLM 5.0 caused a large overpredic-
445 tion of plant nitrogen uptake associated with nitrogen fixation (Davies-Barnard

446 et al. 2020) compared to other terrestrial biosphere model products. Thus, em-
447 pirical data from manipulative experiments that explicitly quantify carbon costs
448 to acquire nitrogen in species capable of associating with nitrogen-fixing bacteria
449 across different environmental contexts is an important step toward identifying
450 potential biases in models such as FUN.

451 These findings broadly support the FUN formulation of carbon costs to
452 acquire nitrogen in response to soil nitrogen availability. FUN calculates carbon
453 costs to acquire nitrogen based on the sum of carbon costs to acquire nitrogen
454 via nitrogen fixation, mycorrhizal active uptake, non-mycorrhizal active uptake,
455 and retranslocation (Fisher et al. 2010; Brzostek et al. 2014). Carbon costs to
456 acquire nitrogen via mycorrhizal or non-mycorrhizal active uptake pathways are
457 derived as a function of nitrogen availability, root biomass, and two parameterized
458 values based on nitrogen acquisition strategy (Brzostek et al. 2014). Due to this,
459 FUN simulates a net decrease in carbon costs to acquire nitrogen with increasing
460 nitrogen availability for mycorrhizal and non-mycorrhizal active uptake pathways,
461 assuming constant root biomass. This was a pattern I observed in *G. hirsutum* re-
462 gardless of light availability. In contrast, FUN would not simulate a net change in
463 carbon costs to acquire nitrogen via nitrogen fixation due to nitrogen availability.
464 This is because carbon costs to acquire nitrogen via nitrogen fixation are derived
465 from a well established function of soil temperature, which is independent of soil
466 nitrogen availability (Houlton et al. 2008; Fisher et al. 2010). I observed a net
467 reduction in carbon costs to acquire nitrogen in *G. max*, except when individu-
468 als were grown under 0% shade cover. While a net reduction of carbon costs in
469 response to nitrogen fertilization runs counter to nitrogen fixation carbon costs

470 simulated by FUN, these patterns were likely because *G. max* individuals switched
471 their primary mode of nitrogen acquisition from symbiotic nitrogen fixation to a
472 non-symbiotic active uptake pathway.

473 2.4.3 *Study limitations*

474 It should be noted that the metric used in this study to determine carbon costs
475 to acquire nitrogen has several limitations. Most notably, this metric uses root
476 carbon biomass as a proxy for estimating the amount of carbon spent on nitrogen
477 acquisition. While it is true that most carbon allocated belowground has at least
478 an indirect structural role in acquiring soil resources, it remains unclear whether
479 this assumption holds true for species that acquire nitrogen via symbiotic nitro-
480 gen fixation. I also cannot quantify carbon lost through root exudates or root
481 turnover, which may increase due to factors that increase plant nitrogen demand
482 (Tingey et al. 2000; Phillips et al. 2011), and can increase the magnitude of
483 available nitrogen from soil organic matter through priming effects on soil micro-
484 bial communities (Uselman et al. 2000; Bengtson et al. 2012). It is also not
485 clear whether these assumptions hold under all environmental conditions, such
486 as those that shift belowground carbon allocation toward a different mode of ni-
487 trogen acquisition (Taylor and Menge 2018; Friel and Friesen 2019) or between
488 species with different acquisition strategies. In this study, increasing soil nitrogen
489 fertilization increased carbon investment to roots relative to carbon transferred to
490 root nodules. By assuming that carbon allocated to root carbon was proportional
491 to carbon allocated to root nodules across all treatment combinations, these ob-
492 served responses to soil nitrogen fertilization were likely to be overestimated in *G.*

493 *max*. I encourage future research to quantify these carbon fates independently.

494 Researchers conducting pot experiments must carefully choose pot volume
495 to minimize the likelihood of growth limitations induced by pot volume (Poorter
496 et al. 2012). Poorter et al. (2012) indicate that researchers are likely to avoid
497 growth limitations associated with pot volume if measurements are collected when
498 the plant biomass:pot volume ratio is less than 1 g L^{-1} . In this experiment, all
499 treatment combinations in both species had biomass:pot volume ratios less than
500 1 g L^{-1} except for *G. max* and *G. hirsutum* that were grown under 0% shade
501 cover and had received 630 ppm N. Specifically, *G. max* and *G. hirsutum* had
502 average respective biomass:pot volume ratios of $1.24 \pm 0.07 \text{ g L}^{-1}$ and 1.34 ± 0.13
503 g L^{-1} , when grown under 0% shade cover and received 630 ppm N (Table A2;
504 Table A3; Fig. A1). If growth in this treatment combination was limited by pot
505 volume, then individuals may have had larger carbon costs to acquire nitrogen
506 than would be expected if they were grown in larger pots. This pot volume
507 induced growth limitation could cause a reduction in per-root nitrogen uptake
508 associated with more densely packed roots, which could reduce the positive effect
509 of nitrogen fertilization on whole-plant nitrogen biomass relative to root carbon
510 biomass (Poorter et al. 2012).

511 Growth limitation associated with pot volume provides a possible expla-
512 nation for the marginally insignificant effect of increasing nitrogen fertilization on
513 *G. max* carbon costs to acquire nitrogen when grown under 0% shade cover. This
514 is because the regression line describing the relationship between carbon costs to
515 acquire nitrogen and nitrogen fertilization in *G. max* grown under 0% shade cover
516 would have flattened if growth limitation had caused larger than expected carbon

517 costs to acquire nitrogen in the 0% shade cover, 630 ppm N treatment combi-
518 nation. This may have been exacerbated by the fact that *G. max* likely shifted
519 relative carbon allocation from nitrogen fixation to soil nitrogen acquisition, which
520 could have increased the negative effect of more densely packed roots on nitrogen
521 uptake. These patterns could have also occurred in *G. hirsutum* grown under 0%
522 shade cover; however, there was no change in the effect of nitrogen fertilization on
523 *G. hirsutum* carbon costs to acquire nitrogen grown under 0% shade cover relative
524 to other shade cover treatments. Regardless, the possibility of growth limitation
525 due to pot volume suggests that effects of increasing nitrogen fertilization on car-
526 bon costs to acquire nitrogen in both species grown under 0% shade cover could
527 have been underestimated. Follow-up studies using a similar experimental design
528 with a larger pot volume would be necessary in order to determine whether these
529 patterns were impacted by pot volume-induced growth limitation.

530 2.4.4 *Conclusions*

531 In conclusion, this chapter provides empirical evidence that carbon costs to ac-
532 quire nitrogen are influenced by light availability and soil nitrogen fertilization
533 in a species capable of acquiring nitrogen via symbiotic nitrogen fixation and a
534 species not capable of forming such associations. We show that carbon costs to
535 acquire nitrogen generally increase with increasing light availability and decrease
536 with increasing nitrogen fertilization. This chapter provides important empirical
537 data needed to evaluate the formulation of carbon costs to acquire nitrogen in
538 terrestrial biosphere models, particularly carbon costs to acquire nitrogen that
539 are associated with symbiotic nitrogen fixation. My findings broadly support the

540 general formulation of these carbon costs in the FUN biogeochemical model in
541 response to shifts in nitrogen availability. However, there is a need for future
542 studies to explicitly quantify carbon costs to acquire nitrogen under different en-
543 vironmental contexts, over longer temporal scales, and using larger selections of
544 phylogenetically related species. In addition, I suggest that future studies mini-
545 mize the limitations associated with the metric used here by explicitly measuring
546 belowground carbon fates independently.

547

Chapter 3

548 Soil nitrogen availability modifies leaf nitrogen economies in mature
549 temperate deciduous forests: a direct test of photosynthetic least-cost
550 theory

551 3.1 Introduction

552 Photosynthesis represents the largest carbon flux between the atmosphere and
553 land surface (IPCC 2021), and plays a central role in biogeochemical cycling at
554 multiple spatial and temporal scales (Vitousek and Howarth 1991; LeBauer and
555 Treseder 2008; Kaiser et al. 2015; Wieder et al. 2015). Therefore, carbon and
556 energy fluxes simulated by terrestrial biosphere models are sensitive to the formu-
557 lation of photosynthetic processes (Ziehn et al. 2011; Bonan et al. 2011; Booth
558 et al. 2012; Smith et al. 2016; Smith et al. 2017) and must be represented using
559 robust, empirically tested processes (Prentice et al. 2015; Wieder et al. 2019).
560 Current formulations of photosynthesis vary across terrestrial biosphere models
561 (Smith and Dukes 2013; Rogers et al. 2017), which causes variation in modeled
562 ecosystem processes (Knorr 2000; Knorr and Heimann 2001; Bonan et al. 2011;
563 Friedlingstein et al. 2014) and casts uncertainty on the ability of these models to
564 accurately predict terrestrial ecosystem responses and feedbacks to global change
565 (Zaehle et al. 2005; Schaefer et al. 2012; Davies-Barnard et al. 2020).

566 Terrestrial biosphere models commonly represent C₃ photosynthesis th-
567 rough variants of the Farquhar et al. (1980) biochemical model (Smith and Dukes
568 2013; Rogers 2014; Rogers et al. 2017). This well-tested photosynthesis model
569 estimates leaf-level carbon assimilation, or photosynthetic capacity, as a function
570 of the maximum rate of Ribulose-1,5-bisphosphate carboxylase-oxygenase (Ru-

571 bisco) carboxylation (V_{cmax}) and the maximum rate of Ribulose-1,5-bisphosphate
572 (RuBP) regeneration (J_{max}) (Farquhar et al. 1980). Many terrestrial biosphere
573 models predict these model inputs based on plant functional group specific lin-
574 ear relationships between leaf nutrient content and V_{cmax} (Smith and Dukes 2013;
575 Rogers 2014; Rogers et al. 2017) under the tenet that a large fraction of leaf nutri-
576 ents, and nitrogen in particular, are partitioned toward building and maintaining
577 enzymes that support photosynthetic capacity, such as Rubisco (Brix 1971; Gul-
578 mon and Chu 1981; Evans 1989; Kattge et al. 2009; Walker et al. 2014). Terres-
579 trial biosphere models predict leaf nutrient content from soil nutrient availability
580 based on the assumption that increasing soil nutrients generally increases leaf nu-
581 trients (Firn et al. 2019; Li et al. 2020; Liang et al. 2020) which, in the case of
582 nitrogen, generally corresponds with an increase in photosynthetic processes (Li
583 et al. 2020; Liang et al. 2020).

584 Recent work calls the generality of relationships between soil nutrient avail-
585 ability, leaf nutrient content, and photosynthetic capacity into question, suggest-
586 ing instead that leaf nutrients and photosynthetic capacity are better predicted as
587 an integrated product of aboveground climate, leaf traits, and soil nutrient avail-
588 ability, rather than soil nutrient availability alone (Dong et al. 2017; Dong et al.
589 2020; Dong et al. 2022; Firn et al. 2019; Smith et al. 2019; Peng et al. 2021).
590 It has been reasoned that this result is because plants allocate added nutrients to
591 growth and storage rather than alterations in leaf chemistry (Smith et al. 2019),
592 perhaps as a result of nutrient limitation of primary productivity (LeBauer and
593 Treseder 2008; Fay et al. 2015). Additionally, recent work suggests that relation-
594 ships between leaf nutrient content and photosynthesis vary across environments,

595 and that the proportion of leaf nutrient content allocated to photosynthetic tis-
596 sue varies over space and time with plant acclimation and adaptation responses
597 to light availability, vapor pressure deficit, soil pH, soil nutrient availability, and
598 environmental factors that influence leaf mass per area (Pons and Pearcy 1994;
599 Niinemets and Tenhunen 1997; Evans and Poorter 2001; Hikosaka and Shigeno
600 2009; Ghimire et al. 2017; Onoda et al. 2017; Luo et al. 2021). The use of linear
601 relationships between leaf nutrient content and V_{cmax} to predict photosynthetic
602 capacity, as commonly used in terrestrial biosphere models (Rogers 2014), is not
603 capable of detecting such responses.

604 Photosynthetic least-cost theory provides an alternative framework for un-
605 derstanding relationships between soil nutrient availability, leaf nutrient content,
606 and photosynthetic capacity (Harrison et al. 2021). Leveraging a two-input mi-
607 croeconomics approach (Wright et al. 2003), the theory posits that plants accli-
608 mate to a given environment by optimizing leaf photosynthesis rates at the lowest
609 summed cost of using nutrients and water (Prentice et al. 2014; Wang et al. 2017;
610 Smith et al. 2019; Paillassa et al. 2020). Across resource availability gradients,
611 the theory predicts that optimal photosynthetic rates can be achieved by trading
612 less efficient use of a resource that is less costly to acquire (or more abundant)
613 for more efficient use of a resource more costly to acquire (or less abundant). For
614 example, an increase in soil nutrient availability should reduce the cost of acquir-
615 ing and using nutrients (Bae et al. 2015; Eastman et al. 2021; Perkowski et al.
616 2021), which could increase leaf nutrient investments in photosynthetic proteins to
617 allow similar photosynthetic rates to be achieved with higher nutrient use (lower
618 nutrient use efficiency) but lower water use (greater water use efficiency). The

619 theory suggests similar tradeoffs in response to increasing soil pH (Paillassa et al.
620 2020), specifically, that increasing soil pH should reduce the cost of acquiring soil
621 nutrients due to an increase in plant-available nutrient concentration (Paillassa
622 et al. 2020; Dong et al. 2022). The theory is also capable of reconciling dynamic
623 leaf nutrient-photosynthesis relationships at global scales (Luo et al. 2021).

624 Patterns expected from photosynthetic least-cost theory have recently re-
625 ceived empirical support both in global environmental gradient (Smith et al.
626 2019; Paillassa et al. 2020; Luo et al. 2021; Querejeta et al. 2022; Wester-
627 band et al. 2023) and local manipulative invasion (Bialic-Murphy et al. 2021)
628 studies. However, nutrient addition experiments that directly examine nutrient-
629 water use tradeoffs expected from the theory are rare (but see Guerrieri et al.
630 2011), and only global gradient studies testing the theory have considered soil pH
631 in their analyses. As a result, there is a need to use nutrient addition and soil pH
632 manipulation experiments to test mechanisms driving responses predicted by the
633 theory.

634 In this study, I measured leaf responses to soil nitrogen availability in five
635 deciduous tree species growing in the upper canopy of mature closed canopy tem-
636 perate forests in the northeastern United States. Soil nitrogen availability and pH
637 were manipulated through a nitrogen-by-pH field manipulation experiment with
638 treatments applied since 2011, eight years prior to measurement. Two different
639 soil nitrogen treatments were applied to increase nitrogen availability with op-
640 posing effects on soil pH. An additional N-free acidifying treatment was expected
641 to decrease soil pH. I hypothesized that increased soil nitrogen availability would
642 enable plants to increase nutrient uptake and create more photosynthetic enzymes

643 per leaf, allowing similar photosynthetic rates achieved with lower leaf C_i:C_a and
644 increased leaf nitrogen content allocated to photosynthetic leaf tissue. I expected
645 that this response would be driven by a reduction in the cost of acquiring nitrogen,
646 which would cause trees to sacrifice efficient nitrogen use to enable more efficient
647 use of other limiting resources (i.e., water). Finally, I hypothesized similar leaf
648 responses to increasing soil pH.

649 3.2 Methods

650 3.2.1 *Study site description*

651 I conducted this study in summer 2019 at three stands located within a 20-km ra-
652 dius of Ithaca, NY, USA (42.444 °N, 76.502 °W). All stands contain mature,
653 closed-canopy forests dominated by deciduous tree species. Stands contained
654 abundant sugar maple (*Acer saccharum* Marshall), American beech (*Fagus gran-*
655 *difolia* Ehrh.), and white ash (*Fraxinus americana* L.), accounting for 43%, 15%,
656 and 17% of the total aboveground biomass across the three stands, respectively,
657 with less frequent red maple (*Acer rubrum* L.; 9% of total aboveground biomass)
658 and red oak occurrences (*Quercus rubra* L.; 10% of total aboveground biomass).
659 Soils at each site were broadly classified as a channery silt loam Inceptisols using
660 the USDA NRCS Web Soil Survey data product (Soil Survey Staff 2022). Between
661 2006 and 2020, study sites averaged 972 mm of precipitation per year and had an
662 average temperature of 7.9 °C per a weather station located near the Cornell Uni-
663 versity campus (42.449 °N, 76.449 °W) part of the NOAA NCEI Global Historical
664 Climatology Network (Menne et al. 2012).

665 3.2.2 *Experimental design*

666 Four 40 m x 40 m plots were set up at each site in 2009, each with an additional
667 10 m buffer along plot perimeters (60 m x 60 m total). The plots were set up as a
668 nitrogen-by-pH field manipulation experiment, with one each of four treatments
669 at each site. Two nitrogen treatments were applied, both at $50 \text{ kg N ha}^{-1} \text{ yr}^{-1}$, as
670 either sodium nitrate (NaNO_3) to raise soil pH, or ammonium sulfate ($(\text{NH}_4)_2\text{SO}_4$)
671 to acidify; an elemental sulfur treatment was selected to acidify without nitrogen,
672 applied at the same rate of S addition ($57 \text{ kg S ha}^{-1} \text{ yr}^{-1}$); and control plots
673 received no additions. All amendments were added in pelletized form using hand-
674 held fertilizer spreaders to both the main plots and buffers. Amendments were
675 divided into three equal doses distributed across the growing season from 2011-
676 2017 and added as a single dose from 2018 onward. During 2019, plots were
677 fertilized during the week of May 20.

678 3.2.3 *Leaf gas exchange and trait measurements*

679 I sampled one leaf each from 6 to 10 individuals per plot between June 25 and
680 July 12, 2019 for gas exchange measurements (Table B1). Leaves were collected
681 from deciduous broadleaf trees represented across all sites and plots and were
682 replicated in efforts to mimic the species abundance of each plot at each site.
683 We also attempted to collect leaves from the upper canopy to reduce differential
684 shading effects on leaf physiology. Leaves were accessed by pulling down small
685 branches using an arborist's slingshot and weighted beanbag attached to a throw
686 line. Branches were immediately recut under deionized water and remained sub-
687 merged to reduce stomatal closure and avoid xylem embolism, as done in Smith

688 and Dukes (2018), until gas exchange data were collected.

689 Randomly selected leaves with little to no visible external damage were
690 attached to a Li-COR LI-6800 (Li-COR Bioscience, Lincoln, Nebraska, USA)
691 portable photosynthesis machine to measure net photosynthesis (A_{net} ; $\mu\text{mol m}^{-2}$
692 s^{-1}), stomatal conductance (g_{sw} ; $\text{mol m}^{-2} \text{s}^{-1}$), and intercellular CO_2 concentra-
693 tion (C_i ; $\mu\text{mol mol}^{-1}$) at different reference CO_2 concentrations (C_a ; $\mu\text{mol mol}^{-1}$)
694 concentrations (i.e., an A_{net}/C_i curve) under saturating light conditions (2,000
695 $\mu\text{mol m}^{-2} \text{s}^{-1}$). Reference CO_2 concentrations followed the sequence: 400, 300,
696 200, 100, 50, 400, 400, 600, 800, 1000, 1200, 1500, and 2000 $\mu\text{mol mol}^{-1} \text{CO}_2$. Leaf
697 temperatures were not controlled in the cuvette and ranged from 21.8 °C to 31.7
698 °C (mean±SD: 27.2 ± 2.2 °C). A linear and second order log-polynomial nonlinear
699 regression suggested no effect of temperature on stomatal conductance measured
700 at 400 $\mu\text{mol mol}^{-1} \text{CO}_2$ or net photosynthesis measured at 400 $\mu\text{mol mol}^{-1} \text{CO}_2$
701 (Table B2-B3; Fig. B1). All A_{net}/C_i curves were generated within one hour of
702 branch severance.

703 Leaf morphological and chemical traits were collected on the same leaf used
704 to generate each A_{net}/C_i curve. Images of each leaf were taken using a flat-bed
705 scanner to determine fresh leaf area using the ‘LeafArea’ R package (Katabuchi
706 2015), which automates leaf area calculations using ImageJ software (Schneider
707 et al. 2012). Each leaf was dried at 65°C for at least 48 hours, weighed, and
708 ground using a Retsch MM200 ball mill grinder (Verder Scientific, Inc., Newtown,
709 PA, USA) until homogenized. Leaf mass per area (M_{area} , g m^{-2}) was calculated
710 as the ratio of dry leaf biomass to fresh leaf area. Using a subsample of ground
711 and homogenized leaf biomass, leaf nitrogen content (N_{mass} ; gN g^{-1}) and leaf

712 $\delta^{13}\text{C}$ (‰, relative to VPDB) were measured at the Cornell Stable Isotope Lab
713 with an elemental analyzer (NC 2500, CE Instruments, Wigan, UK) interfaced to
714 an isotope ratio mass spectrometer (Delta V Isotope Ratio Mass Spectrometer,
715 ThermoFisher Scientific, Waltham, MA, USA). Leaf nitrogen content per unit leaf
716 area (N_{area} ; gN m⁻²) was calculated by multiplying N_{mass} by M_{area} .

717 I used leaf $\delta^{13}\text{C}$ values to estimate χ (unitless), which is an isotope-derived
718 estimate of the leaf $C_i:C_a$ ratio. While intercellular and atmospheric CO₂ con-
719 centrations were directly measured during each A_{net}/C_i curve, deriving χ from
720 $\delta^{13}\text{C}$ provides a more integrative estimate of the $C_i:C_a$ over an individual leaf's
721 lifespan. We derived χ following the approach of Farquhar et al. (1989) described
722 in Cernusak et al. (2013):

$$\chi = \frac{\Delta^{13}C - a}{b - a} \quad (3.1)$$

723 where $\Delta^{13}\text{C}$ represents the relative difference between leaf $\delta^{13}\text{C}$ (‰) and air $\delta^{13}\text{C}$
724 (‰), and is calculated from the following equation:

$$\Delta^{13}C = \frac{\delta^{13}C_{\text{air}} - \delta^{13}C_{\text{leaf}}}{1 + \delta^{13}C_{\text{leaf}}} \quad (3.2)$$

725 where $\delta^{13}C_{\text{air}}$ is assumed to be -8‰ (Keeling et al. 1979; Farquhar et al. 1989), a
726 represents the fractionation between ¹²C and ¹³C due to diffusion in air, assumed
727 to be 4.4‰, and b represents the fractionation caused by Rubisco carboxylation,
728 assumed to be 27‰ (Farquhar et al. 1989).

729 3.2.4 A_{net}/C_i curve-fitting and parameter estimation

730 We fit A_{net}/C_i curves of each individual using the ‘fitaci’ function in the
731 ‘plantecophys’ R package (Duursma 2015). This function estimates the maxi-
732 mum rate of Rubisco carboxylation (V_{cmax} ; $\mu\text{mol m}^{-2} \text{s}^{-1}$) and maximum rate
733 of electron transport for RuBP regeneration (J_{max} ; $\mu\text{mol m}^{-2} \text{s}^{-1}$) based on the
734 Farquhar, von Caemmerer, and Berry biochemical model of C₃ photosynthesis
735 (Farquhar et al. 1980). For each curve fit, we included triose phosphate uti-
736 lization (TPU) limitation to avoid underestimating J_{max} (Gregory et al. 2021).
737 Curves were visually examined to confirm the likely presence of TPU limitation.

738 We determined Michaelis-Menten coefficients for Rubisco affinity to CO₂
739 (K_c ; $\mu\text{mol mol}^{-1}$) and O₂ (K_o ; $\mu\text{mol mol}^{-1}$), and the CO₂ compensation point
740 (Γ^* ; $\mu\text{mol mol}^{-1}$) using leaf temperature and equations described in Medlyn et al.
741 (2002) and derived in Bernacchi et al. (2001). Specifically, K_c and K_o were
742 calculated as:

$$K_c = 404.9 * \exp^{\frac{79430(T_k - 298)}{298RT_k}} \quad (3.3)$$

743 and

$$K_o = 278.4 * \exp^{\frac{36380(T_k - 298)}{298RT_k}} \quad (3.4)$$

744 while Γ^* was calculated as:

$$\Gamma^* = 42.75 * \exp^{\frac{37830(T_k - 298)}{298RT_k}} \quad (3.5)$$

745 In all three equations, T_k is the leaf temperature (in Kelvin) during each A_{net}/C_i

746 curve and R is the universal gas constant ($8.314 \text{ J mol}^{-1} \text{ K}^{-1}$).

747 We standardized V_{cmax} and J_{max} estimates to 25°C using a modified Ar-

748 rhenius equation (Kattge and Knorr 2007):

$$k_{25} = \frac{k_{\text{obs}}}{e^{\frac{H_a(T_{\text{obs}} - T_{\text{ref}})}{T_{\text{ref}}RT_{\text{obs}}}} * \frac{1+e^{\frac{T_{\text{ref}}\Delta S - H_d}{T_{\text{obs}}}}}{1+e^{\frac{T_{\text{obs}}\Delta S - H_d}{T_{\text{obs}}}}}} \quad (3.6)$$

749 k_{25} represents the standardized V_{cmax} or J_{max} rate at 25°C , k_{obs} represents

750 the V_{cmax} or J_{max} estimate at the average leaf temperature measured inside the

751 cuvette during the A_{net}/C_i curve. H_a is the activation energy of V_{cmax} ($71,513$

752 J mol^{-1}) Kattge and Knorr (2007) or J_{max} ($49,884 \text{ J mol}^{-1}$) (Kattge and Knorr

753 2007). H_d represents the deactivation energy of both V_{cmax} and J_{max} ($200,000 \text{ J}$

754 mol^{-1}) (Medlyn et al. 2002), and R represents the universal gas constant (8.314

755 $\text{J mol}^{-1} \text{ K}^{-1}$). T_{ref} represents the standardized temperature of 298.15 K (25°C)

756 and T_{obs} represents the mean leaf temperature (in K) during each A_{net}/C_i curve.

757 ΔS is an entropy term that (Kattge and Knorr 2007) derived as a linear relation-

758 ship with average growing season temperature (T_g ; $^\circ\text{C}$), where:

$$\Delta S_{vcmax} = -1.07 T_g + 668.39 \quad (3.7)$$

759 and

$$\Delta S_{jmax} = -0.75 T_g + 659.70 \quad (3.8)$$

760 We estimated T_g in Equations 3.7 and 3.8 based on mean daily (24-hour) air
761 temperature of the 30 days leading up to the day of each sample collection using
762 the same weather station reported in the site description. We then used V_{cmax25}
763 and J_{max25} estimates to calculate the ratio of J_{max25} to V_{cmax25} ($J_{max25}:V_{cmax25}$;
764 unitless).

765 3.2.5 *Proportion of leaf nitrogen allocated to photosynthesis and structure*

766 We used equations from Niinemets and Tenhunen (1997) to estimate the
767 proportion of leaf N content allocated to Rubisco and bioenergetics. The propor-
768 tion of leaf N allocated to Rubisco (ρ_{rub} ; gN gN $^{-1}$) was calculated as a function
769 of V_{cmax25} and N_{area} :

$$\rho_{rubisco} = \frac{V_{cmax25} N_r}{V_{cr} N_{area}} \quad (3.9)$$

770 where N_r is the amount of nitrogen in Rubisco, set to 0.16 gN (gN in Rubisco) $^{-1}$
771 and V_{cr} is the maximum rate of RuBP carboxylation per unit Rubisco protein,
772 set to 20.5 μ mol CO $_2$ (g Rubisco) $^{-1}$. The proportion of leaf nitrogen allocated to
773 bioenergetics (ρ_{bioe} ; gN gN $^{-1}$) was similarly calculated as a function of J_{max25} and
774 N_{area} :

$$\rho_{bioe} = \frac{J_{max25} N_b}{J_{mc} N_{area}} \quad (3.10)$$

775 where N_b is the amount of nitrogen in cytochrome f, set to 0.12407 gN (μ mol
776 cytochrome f) $^{-1}$ assuming a constant 1: 1: 1.2 cytochrome f: ferredoxin NADP
777 reductase: coupling factor molar ratio (Evans and Seemann 1989; Niinemets and

778 Tenhunen 1997), and J_{mc} is the capacity of electron transport per cytochrome f,
779 set to $156 \mu\text{mol electron} (\mu\text{mol cytochrome f})^{-1}\text{s}^{-1}$.

780 We estimated the proportion of leaf N content allocated to photosynthetic
781 tissue ($\rho_{photo}; \text{gN gN}^{-1}$) as the sum of ρ_{rub} and ρ_{bioe} . This calculation is an un-
782 derestimate of the proportion of leaf N allocated to photosynthetic tissue because
783 it does not include N allocated to light harvesting proteins. This leaf N pool was
784 not included because we did not perform chlorophyll extractions on focal leaves.
785 However, the proportion of leaf nitrogen content allocated to light harvesting pro-
786 teins tends to be small relative to ρ_{rub} and ρ_{bioe} , and may scale with changes in
787 ρ_{rub} and ρ_{bioe} (Niinemets and Tenhunen 1997).

788 Finally, we estimated the proportion of leaf N content allocated to struc-
789 tural tissue ($\rho_{str}; \text{gN gN}^{-1}$) using an empirical equation from Onoda et al. (2017):

$$N_{cw} = 0.000355 * M_{area}^{1.39} \quad (3.11)$$

790 where N_{cw} is the leaf N content allocated to cell walls (gN m^{-2}). ρ_{str} was estimated
791 by dividing N_{cw} by N_{area} .

792 3.2.6 *Tradeoffs between nitrogen and water use*

793 Photosynthetic nitrogen use efficiency (PNUE; $\mu\text{mol CO}_2 \text{ mol}^{-1} \text{ N s}^{-1}$)
794 was calculated by dividing A_{net} by N_{area} , first converting N_{area} to mol N m^{-2} using
795 the molar mass of N (14 g mol^{-1}). I used χ as an indicator of water use efficiency,
796 which exploratory analyses suggest had similar responses to soil nitrogen availabil-
797 ity and pH as intrinsic water use efficiency measured from gas exchange (A_{net}/g_s).

798 Tradeoffs between nitrogen and water use were determined by calculating the ratio
799 of N_{area} to χ ($N_{\text{area}}:\chi$; g N m⁻²) and V_{cmax25} to χ ($V_{\text{cmax25}}:\chi$; $\mu\text{mol m}^{-2} \text{s}^{-1}$). This
800 approach is similar to tradeoff calculations in which nitrogen-water use tradeoffs
801 are measured as the ratio of N_{area} or V_{cmax25} to g_{sw} (Paillassa et al. 2020; Bialic-
802 Murphy et al. 2021). In this chapter, I quantify these relationships using χ in lieu
803 of g_{sw} because g_{sw} rapidly changes with environmental conditions and therefore
804 may have been altered by recent tree branch severance and/or placement in the
805 cuvette.

806 3.2.7 *Soil nitrogen availability and pH*

807 To characterize soil nitrogen availability at the time of our leaf gas exchange
808 measurements, we used mixed bed resin bags to quantify mobile ammonium-N
809 and nitrate-N concentrations in each plot. Lycra mesh bags were filled with 5 g
810 of Dowex® Marathon MR-3 hydrogen and hydroxide form resin (MilliporeSigma,
811 Burlington, MA USA) and sealed with a zip tie. Each bag was activated by
812 soaking in 0.5 M HCl for 20 minutes, then in 2 M NaCl until pH of the saline
813 solution stabilized, as described in Allison et al. (2008). Five resin bags were
814 inserted about 10 cm below the soil surface at each plot on June 25, 2019: one
815 near each of the four plot corners and one near the plot center. All resin bags
816 were collected 24 days later on July 19, 2019 and were frozen until extracted.

817 Prior to anion and cation extraction, each resin bag was rinsed with ul-
818 trapure water (MilliQ IQ 7000; Millipore Sigma, Burlington, MA) to remove any
819 surface soil residues. Anions and cations were extracted from surface-cleaned resin
820 bags by individually soaking and shaking each bag in 100 mL of a 0.1 M HCl/2.0

821 M NaCl matrix for one hour. Using a microplate reader (Biotek Synergy H1;
822 Biotek Instruments, Winooski, VT USA), nitrate-N concentrations were quanti-
823 fied spectrophotometrically at 540 nm with the end product of a single reagent
824 vanadium (III) chloride reaction (Doane and Horwáth 2003), and ammonium-N
825 concentrations quantified at 650 nm with the end product of a modified phenol-
826 hypochlorite reaction (Weatherburn 1967; Rhine et al. 1998). Both the single
827 reagent vanadium (III) chloride and modified phenol-hypochlorite methodologies
828 have been well established for determining nitrate-N and ammonium-N concen-
829 trations in resin bag extracts (Arnone 1997; Allison et al. 2008). We used a
830 series of negative and positive controls throughout each well plate to verify the
831 accuracy and precision of our measurements, assaying each resin bag extract and
832 control in triplicate. Soil N availability was estimated as the sum of the nitrate-N
833 and ammonium-N concentration in each resin bag, normalized per g of resin and
834 duration in the field ($\mu\text{g N g}^{-1} \text{ resin d}^{-1}$), then subsequently averaged across all
835 resin bags in a plot for a plot-level mean.

836 Soil pH was measured on 0-10 cm mineral soil samples collected prior to
837 fertilization in 2019. Near each of the four plot corners, three 5.5 cm diameter soil
838 cores were collected after first removing the forest floor where present. Each set
839 of three cores was placed in a plastic bag, and later composited by hand mixing
840 and sieved to 4mm. Soil pH was determined for a 1:2 soil:water slurry (10 g field-
841 moist soil to 20 mL DI water) of each sample using an Accumet AB15 pH meter
842 with flushable junction probe (Fisher Scientific; Hampton, NH, USA), and was
843 estimated at the plot level as the mean soil pH within each plot.

844 3.2.8 *Statistical analyses*

845 We built two separate series of linear mixed-effects models to explore ef-
846 fects of soil nitrogen availability, soil pH, species, and leaf nitrogen content on leaf
847 physiological traits. In the first series of linear mixed-effects models, we explored
848 the effect of soil nitrogen availability, soil pH, and species on leaf nitrogen con-
849 tent, leaf photosynthesis, stomatal conductance, and nitrogen-water use tradeoffs.
850 Models included plot-level soil N availability and plot-level soil pH as continuous
851 fixed effects, species as a categorical fixed effect, and site as a categorical random
852 intercept term. Interaction terms between fixed effects were not included due
853 to the small number of experimental plots. We built a series of separate mod-
854 els with this independent variable structure to quantify individual effects of soil
855 nitrogen availability, soil pH, and species on N_{area} , M_{area} , N_{mass} , A_{net} , V_{cmax25} ,
856 J_{max25} , $J_{\text{max25}}:V_{\text{cmax25}}$, ρ_{rubisco} , $\rho_{\text{bioenergetics}}$, ρ_{photo} , $\rho_{\text{structure}}$, χ , PNUE, $N_{\text{area}}:\chi$, and
857 $V_{\text{cmax25}}:\chi$.

858 A second series of linear mixed-effects models were built to investigate
859 relationships between leaf N content and photosynthetic parameters. Statistical
860 models included N_{area} as a single continuous fixed effect with species and site des-
861 ignated as individual random intercept terms. We used this independent variable
862 structure to quantify individual effects of leaf nitrogen content on A_{net} , V_{cmax25} ,
863 J_{max25} , $J_{\text{max25}}:V_{\text{cmax25}}$, and χ .

864 For all linear mixed-effects models, we used Shapiro-Wilk tests of normal-
865 ity to determine whether linear mixed-effects models satisfied residual normality
866 assumptions. If residual normality assumptions were not met, then models were
867 fit using dependent variables that were natural log transformed. If residual nor-

868 mality assumptions were still not met (Shapiro-Wilk: $p < 0.05$), then models were
869 fit using dependent variables that were square root transformed. All residual nor-
870 mality assumptions for both sets of models that did not originally satisfy residual
871 normality assumptions were met with either a natural log or square root data
872 transformation (Shapiro-Wilk: $p > 0.05$ in all cases).

873 In the first series of models, models for N_{area} , M_{area} , N_{mass} , V_{cmax25} , J_{max25} ,
874 χ , $N_{\text{area}}:\chi$, and $V_{\text{cmax25}}:\chi$, ρ_{rubisco} , $\rho_{\text{bioenergetics}}$, ρ_{photo} , $\rho_{\text{structure}}$ satisfied residual
875 normality assumptions without data transformations (Shapiro-Wilk: $p > 0.05$ in
876 all cases). The model for $J_{\text{max25}}:V_{\text{cmax25}}$ satisfied residual normality assumptions
877 with a natural log data transformation, while models for A_{net} and PNUE each
878 satisfied residual normality assumptions with square root data transformations.
879 In the second series of models, models for V_{cmax25} , J_{max25} , χ , and $V_{\text{cmax25}}:\chi$ satisfied
880 residual normality assumptions without data transformations (Shapiro-Wilk: p
881 > 0.05 in all cases). The model for $J_{\text{max25}}:V_{\text{cmax25}}$ required a natural log data
882 transformation and the model for A_{net} required a square root data transformation
883 (Shapiro-Wilk: $p > 0.05$ in both cases).

884 In all models, we used the ‘lmer’ function in the ‘lme4’ R package (Bates
885 et al. 2015) to fit each model and the ‘Anova’ function in the ‘car’ R package (Fox
886 and Weisberg 2019) to calculate Type II Wald’s χ^2 and determine the significance
887 level ($\alpha=0.05$) of each fixed effect coefficient. Finally, we used the ‘emmeans’
888 R package (Lenth, 2019) to conduct post-hoc comparisons using Tukey’s tests,
889 where degrees of freedom were approximated using the Kenward-Roger approach
890 (Kenward and Roger 1997). All analyses and plots were conducted in R version
891 4.1.1 (R Core Team 2021). All figure regression lines and associated 95% confi-

892 dence interval error bars were plotted using predictions generated across the soil
893 nitrogen availability gradient using the ‘emmeans’ R package (Lenth 2019).

894 3.3 Results

895 3.3.1 *Leaf nitrogen content*

896 Increasing soil N availability generally increased N_{area} (Table 3.1; Fig.
897 3.1a). This pattern was driven by an increase in N_{mass} (Table 3.1; Fig. 3.1c)
898 and a marginal increase in M_{area} (Table 3.1; Fig. 3.1e) with increasing soil N
899 availability. There was no effect of soil pH on N_{area} , N_{mass} , or M_{area} (Table 3.1);
900 however, we did observe strong differences in N_{area} (Fig. 3.1b), N_{mass} (Fig. 3.1d),
901 and M_{area} (Fig. 3.1e) between species (Table 3.1).

Table 3.1. Effects of soil N availability, soil pH, and species on leaf N content per unit leaf area (N_{area}), leaf N content per unit leaf mass (N_{mass}), and leaf mass per unit leaf area (M_{area})

	N_{area}			N_{mass}			M_{area}			
	df	Coefficient	χ^2	p	Coefficient	χ^2	p	Coefficient	χ^2	p
Intercept	-	9.03E-01	-	-	1.68E+00	-	-	4.60E+01	-	-
Soil N	1	1.68E-02	11.990	0.001	1.25E-02	6.902	0.009	4.87E-01	4.143	0.042
Soil pH	1	9.28E-02	0.836	0.361	8.08E-02	0.663	0.415	4.05E+00	0.653	0.419
Species	4	-	72.128	<0.001	-	35.074	<0.001	-	29.869	<0.001

902 *Significance determined using Type II Wald χ^2 tests ($\alpha = 0.05$). P-values < 0.05 are in bold.

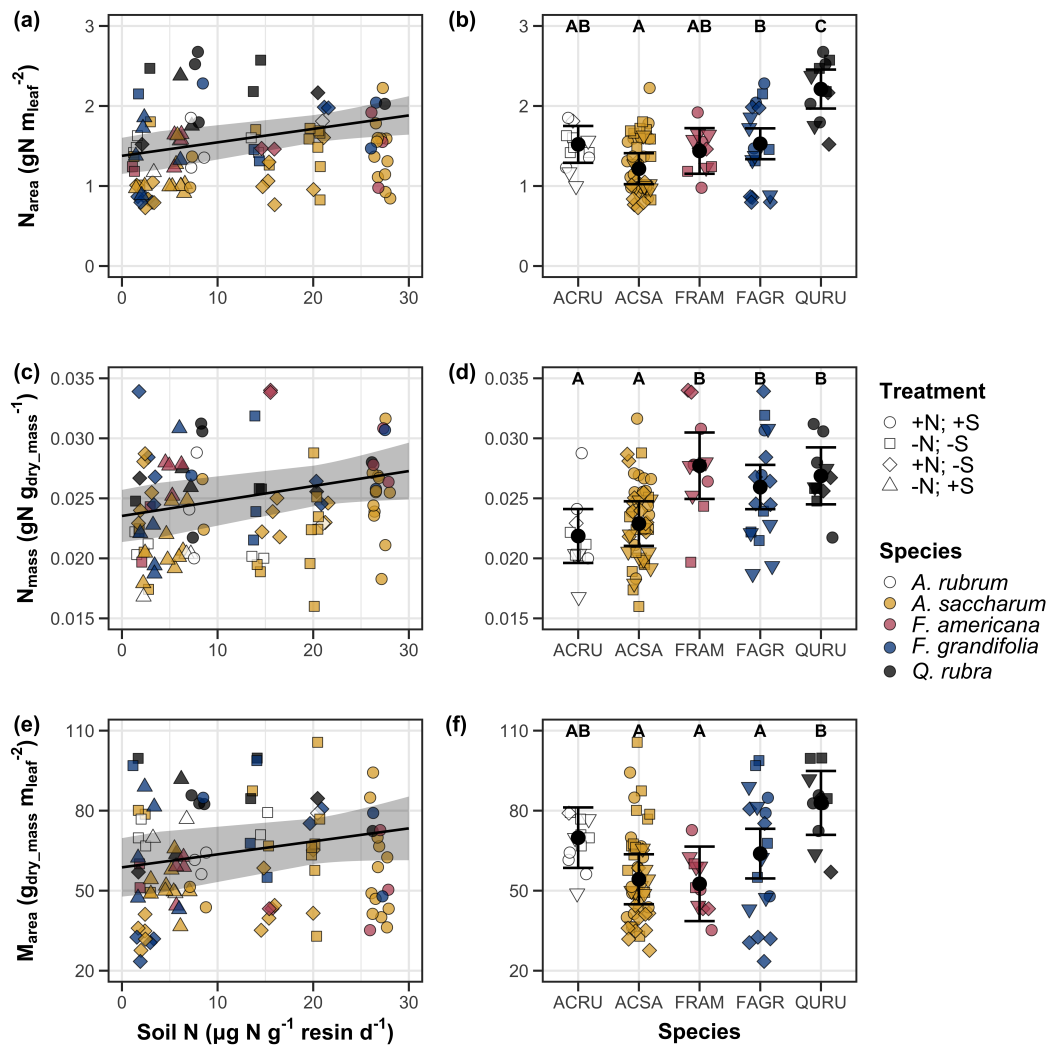


Figure 3.1. Effects of soil N availability and species on leaf N content per unit leaf area (a-b), leaf nitrogen content per unit leaf biomass (c-d), and leaf mass per leaf area (e-f). Soil N availability is represented on the x-axis in the left column of panels, while species is represented on the x-axis in the right column of panels. Tree species are represented as colored points and treatment plots are represented as shaped points, jittered for visibility. Species are abbreviated in the right column of panels through their assigned NRCS PLANTS Database symbol (USDA NRCS 2022), grouped along the x-axis per common mycorrhizal association, where the first three species commonly associate with arbuscular mycorrhizae (ACRU, ASCA, FAGR) and the second two species with ectomycorrhizae (FAGR, QURU). Trendlines are only included when the regression slope is statistically different from zero ($p < 0.05$).

903 3.3.2 *Net photosynthesis and leaf biochemistry*

904 Increasing soil N availability generally had no effect on A_{net} , V_{cmax25} , J_{max25} ,
905 or $J_{\text{max25}}:V_{\text{cmax25}}$ (Table 3.2, Figs. 3.2a, 3.2d, 3.2g). We also observed strong
906 species effects on all measured leaf photosynthetic traits (Table 3.2; Figs. 3.2b,
907 3.2e, 3.2h). Increasing soil pH had a marginal negative effect on A_{net} , but had no
908 effect on V_{cmax25} , J_{max25} , or $J_{\text{max25}}:V_{\text{cmax25}}$ (Table 3.2). There was a weak positive
909 effect of increasing N_{area} on A_{net} (Fig. 3.2c), but quite strong positive effects of
910 increasing N_{area} on V_{cmax25} and J_{max25} (Table 3.2; Fig. 3.2f and 3.2i).

Table 3.2. Effects of soil N availability, soil pH, species, and N_{area} on leaf biochemistry

	A_{net}			V_{cmax25}			J_{max25}			
	df	Coefficient	χ^2	p	Coefficient	χ^2	p	Coefficient	χ^2	p
(Intercept)	-	3.29E+00 ^b	-	-	6.38E+01	-	-	1.12E+02	-	-
Soil N	1	-1.23E-03 ^b	1.798	0.180	-3.84E-01	1.745	0.187	-6.70E-01	2.172	0.141
Soil pH	1	-3.09E-01 ^b	3.312	0.069	-4.91E+00	0.655	0.418	-8.18E+00	0.742	0.389
Species	4	-	11.838	0.019	-	31.748	<0.001	-	27.291	<0.001
(N_{area} int.)	-	6.59E-01 ^b	-	-	1.45E-01	-	-	2.86E+01	-	-
N_{area}	4	3.13E-01 ^b	4.790	0.029	2.43E+01	22.616	<0.001	4.04E+01	28.259	<0.001

	$J_{\text{max25}}:V_{\text{cmax25}}$			
	df	Coefficient	χ^2	p
(Intercept)	-	6.59E-01 ^a	-	-
Soil N	1	7.04E-04 ^a	0.088	0.767
Soil pH	1	-7.84E-03 ^a	0.025	0.874
Species	4	-	12.745	0.013
(N_{area} int.)	-	6.69E-01 ^a	-	-
N_{area}	4	-4.69E-02 ^a	1.142	0.285

911 *Significance determined using Type II Wald χ^2 tests ($\alpha = 0.05$). P-values < 0.05 are in bold, while p-values between
 912 0.05 and 0.1 are italicized. Superscript letters indicate model coefficients fit to natural-log (^a) or square-root (^b)
 913 transformed data. Relationships between N_{area} and each response variable were fit using the second series of bivariate
 914 mixed-effects models, so model coefficients and results are independent of model coefficients and results reported
 915 for relationships between soil N, soil pH, and species for each response variable. Key: A_{net} – light saturated net
 916 photosynthesis rate; V_{cmax25} – maximum rate of Rubisco carboxylation at 25°C; J_{max25} – maximum rate of electron
 917 transport for RuBP regeneration at 25°C, $J_{\text{max25}}:V_{\text{cmax25}}$ – the ratio of J_{max25} to V_{cmax25} .

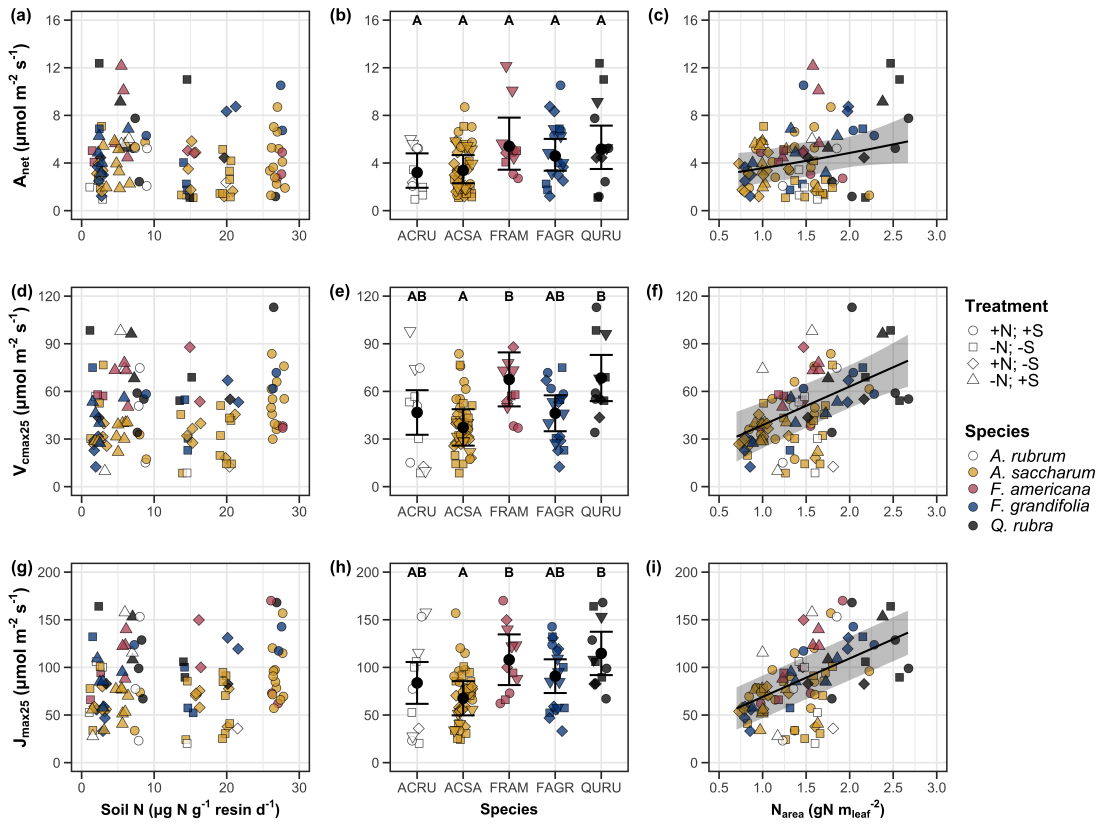


Figure 3.2. Effects of soil N availability (left column of panels), species (middle column of panels), and leaf N content per unit leaf area (right column of panels) on net photosynthesis (a-c), maximum Rubisco carboxylation rate (d-f), and maximum RuBP regeneration rate (g-i). Soil N availability is represented on the x-axis in the left column of panels, species is represented on the x-axis in the middle column of panels, and leaf N content per unit leaf area is represented continuously on the x-axis in the right column of panels. Species abbreviations and position along the x-axis in the middle column of panels, colored points, shapes, and trendlines are as explained in Figure 3.1.

918 3.3.3 *Leaf N allocation*

919 Neither soil N availability nor soil pH affected the proportion of leaf N
920 allocated to Rubisco or bioenergetics (Table 3.3; Fig. 3.3a, Fig. 3.3c), nor was
921 there any subsequent effect on the proportion of leaf N allocated to photosynthesis
922 (Table 3.3; Fig. 3.3f). We also found no effect of soil N availability or soil pH on
923 the proportion of leaf N allocated to structure (Table 3.3; Fig 3.3g). Species varied
924 in the proportion of leaf N allocated to Rubisco, photosynthesis, and structure (Fig
925 3.3b, Fig. 3.3d, Fig 3.3h), with no detectable species effect on the proportion of
926 leaf N allocated to bioenergetics (Table 3.3).

Table 3.3. Effects of soil N availability, soil pH, and species on the proportion of leaf nitrogen content allocated to photosynthesis, Rubisco, bioenergetics, and structure

	ρ_{photo}			ρ_{rub}			ρ_{bioe}			
	df	Coefficient	χ^2	p	Coefficient	χ^2	p	Coefficient	χ^2	p
Intercept	-	4.93E-01	-	-	4.17E-01	-	-	7.64E-02	-	-
Soil N	1	-1.23E-03	0.521	0.470	-1.04E-03	0.501	0.479	-1.77E-04	0.557	0.455
Soil pH	1	-4.37E-02	1.581	0.209	-3.70E-02	1.511	0.219	-6.84E-03	1.941	0.164
Species	4	-	13.106	0.011	-	14.152	0.007	-	7.300	0.121

	ρ_{str}			
	df	Coefficient	χ^2	p
Intercept	-	9.77E-02	-	-
Soil N	1	-2.29E-04	1.165	0.280
Soil pH	1	-1.87E-03	0.179	0.672
Species	4	-	16.428	0.002

57

927 *Significance determined using Type II Wald χ^2 tests ($\alpha = 0.05$). P-values < 0.05 are in bold. Key: ρ_{photo} -
 928 proportion of leaf nitrogen content allocated to photosynthesis; ρ_{rub} - proportion of leaf nitrogen content allocated
 929 to Rubisco; ρ_{bioe} - proportion of leaf nitrogen content allocated to bioenergetics; ρ_{str} - proportion of leaf nitrogen
 930 content allocated to structure.

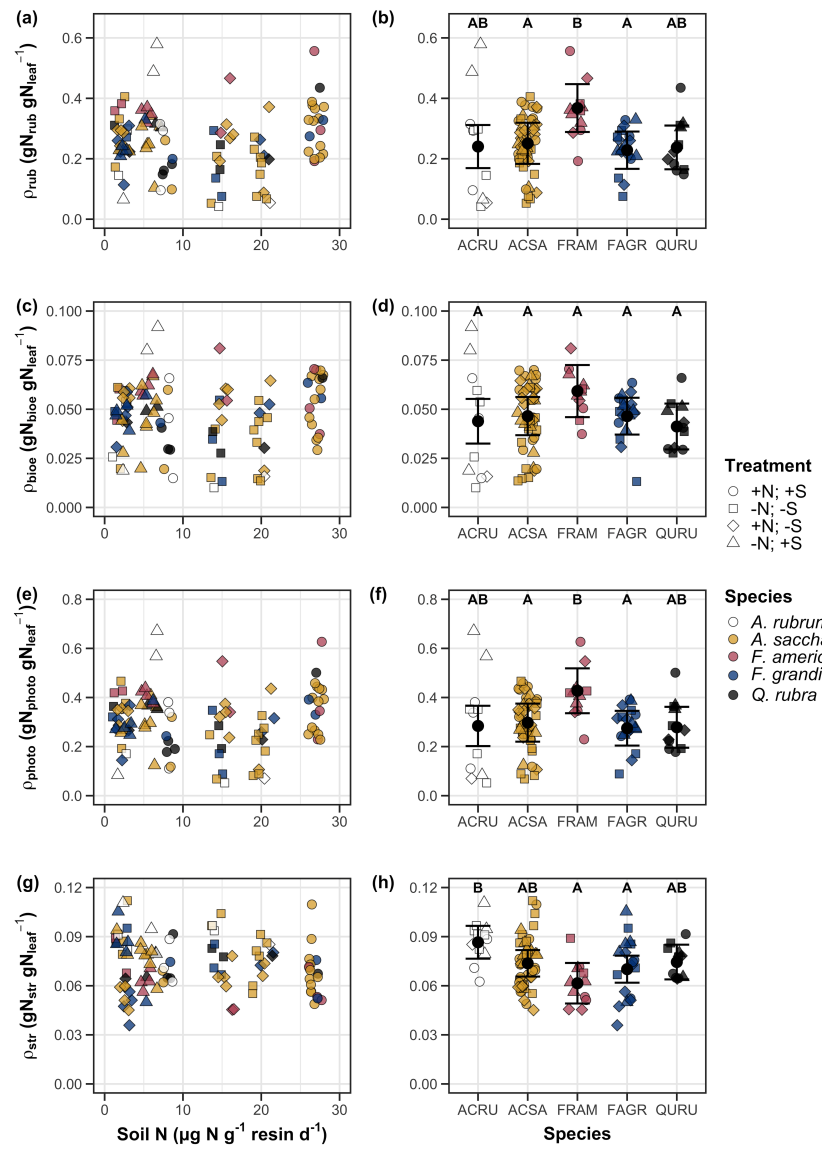


Figure 3.3. Effects of soil nitrogen availability and species on the proportion of leaf nitrogen content allocated to Rubisco (a-b), bioenergetics (c-d), photosynthesis (e-f), and structure (g-h). Soil nitrogen availability is represented on the x-axis in the left column of panels and species are represented on the x-axis in the right column of panels. Species abbreviations and position along the x-axis in the middle column of panels, colored points, shapes, trendlines, error bars, and compact lettering are as explained in Figure 3.1.

931 3.3.4 *Tradeoffs between nitrogen and water use*

932 Although soil N availability did not affect χ (Table 3.4; Fig. 3.4a), increasing
933 soil N availability decreased PNUE (Table 3.4; Fig. 3.4d) and increased the
934 ratio of $N_{\text{area}}:\chi$ (Table 3.4; Fig. 3.4f). Specifically, this response yielded a 26%
935 reduction in PNUE and 37% stimulation in $N_{\text{area}}:\chi$ across the soil nitrogen avail-
936 ability gradient. There was no apparent effect of soil N availability on $V_{\text{cmax25}}:\chi$
937 (Table 3.4; Fig. 3.4h). Increasing soil pH had a weak marginal negative effect
938 on PNUE, but did not influence χ , $N_{\text{area}}:\chi$, or $V_{\text{cmax25}}:\chi$ (Table 3.4). We also
939 observed differences in χ (Fig. 3.4b), PNUE (Fig. 3.4e), $N_{\text{area}}:\chi$ (Fig. 3.4g), and
940 $V_{\text{cmax25}}:\chi$ (Fig. 3.4i) between species (Table 3.4). Finally, increasing N_{area} had a
941 strong negative effect on χ (Table 3.4; Fig. 3.4c) and a strong positive effect on
942 $V_{\text{cmax25}}:\chi$ (Table 3.4; Fig. 3.4j).

Table 3.4. Effects of soil N availability, soil pH, species, and N_{area} on tradeoffs between nitrogen and water use

	χ	PNUE				$N_{\text{area}}:\chi$				
	df	Coefficient	χ^2	p	Coefficient	χ^2	p	Coefficient	χ^2	p
(Intercept)	-	8.12E-01	-	-	9.57E+00	-	-	9.19E-01	-	-
Soil N	1	-1.14E-03	1.698	0.193	-6.63E-02	6.396	0.011	2.60E-02	9.533	0.002
Soil pH	1	-1.91E-02	1.087	0.297	-9.25E-01	2.843	<i>0.092</i>	2.03E-01	1.321	0.250
Species	4	-	18.843	0.001	-	13.454	0.009	-	52.983	<0.001
$(N_{\text{area}} \text{ int.})$	-	8.93E-01	-	-	-	-	-	-	-	-
N_{area}	1	-1.11E-01	80.606	<0.001	-	-	-	-	-	-

	$V_{\text{cmax25}}:\chi$			
	df	Coefficient	χ^2	p
(Intercept)	-	7.20E+01	-	-
Soil N	1	3.99E-01	0.963	0.326
Soil pH	1	-3.12E+00	0.138	0.711
Species	4	-	31.450	<0.001
$(N_{\text{area}} \text{ int.})$	-	1.18E+01	-	-
N_{area}	4	3.87E+01	32.797	<0.001

*Significance determined using Type II Wald χ^2 tests ($\alpha = 0.05$). P-values < 0.05 are in bold, while p-values between 0.05 and 0.1 are italicized. Superscript letters indicate model coefficients fit to natural-log ^(a) or square-root ^(b) transformed data. Relationships between N_{area} and each response variable were fit using the second series of bivariate mixed-effects models, so model coefficients and results are independent of model coefficients and results reported for relationships between soil N, soil pH, and species for each response variable. Key: χ - isotope-derived estimate of the $C_i:C_a$; PNUE - photosynthetic N use efficiency, ratio of net photosynthesis to leaf N content per unit leaf area; $N_{\text{area}}:\chi$ - ratio of N_{area} to χ ; $V_{\text{cmax25}}:\chi$ - ratio of V_{cmax25} to χ .

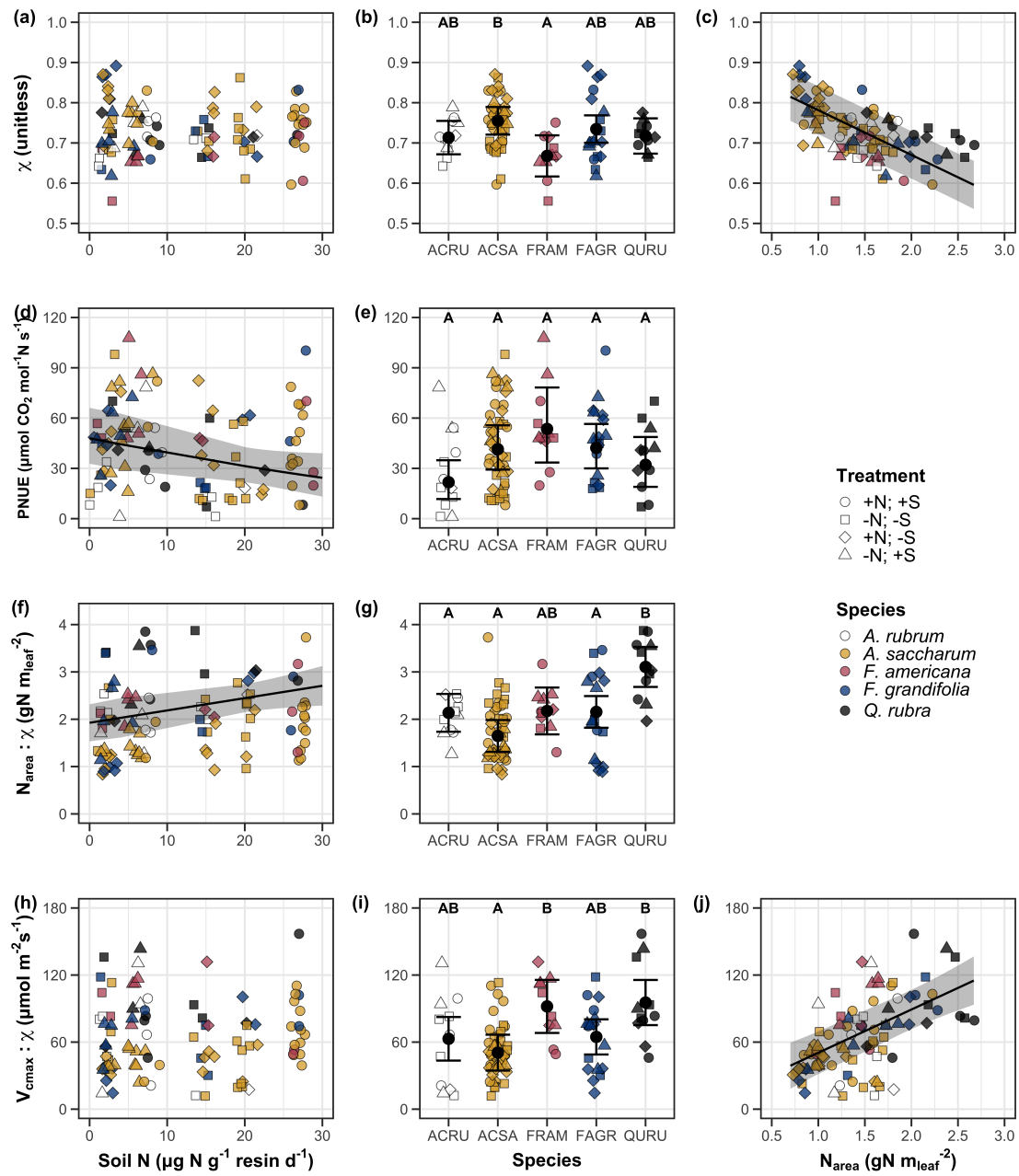


Figure 3.4. Effects of soil nitrogen availability and species on the proportion of leaf nitrogen content allocated to Rubisco (a-b), bioenergetics (c-d), photosynthesis (Rubisco + bioenergetics; e-f), and structure (g-h). Soil nitrogen availability is represented on the x-axis in the left column of panels and species are represented on the x-axis in the right column of panels. Species abbreviations and position along the x-axis in the middle column of panels, colored points, shapes, trendlines, error bars, and compact lettering are as explained in Figure 3.1.

950 3.4 Discussion

951 Photosynthetic least-cost theory provides an explanation for understand-
952 ing relationships between soil nutrient availability, leaf nutrient allocation, and
953 photosynthetic capacity. The theory suggests that plants acclimate to a given
954 environment by optimizing leaf photosynthesis rates at the lowest summed cost
955 of using nutrients and water Prentice et al. (2014), Wang et al. (2017), Smith
956 et al. (2019), Paillassa et al. (2020). The theory predicts that an increase in
957 soil nutrient availability should allow similar photosynthesis rates to be achieved
958 with increased leaf nutrient content and photosynthetic capacity (i.e., V_{cmax25} and
959 J_{max25}) at lower leaf $C_i:C_a$ (χ), resulting in an increase in water use efficiency,
960 decrease in nutrient use efficiency, and increase in both leaf nutrient content and
961 photosynthetic capacity per unit χ . The theory predicts similar leaf responses to
962 increasing soil pH under acidic conditions, presumably due to generally faster nu-
963 trient cycle dynamics and consequent reductions in the cost of acquiring nutrients
964 relative to water with increasing soil pH (Wang et al. 2017; Paillassa et al. 2020;
965 Dong et al. 2020).

966 Supporting the theory, we showed that increasing soil N availability was
967 associated with increased leaf N content (Fig 3.1a, 3.1c), a pattern that reduced
968 photosynthetic N use efficiency (Fig 3.4d) and increased leaf N content per unit
969 χ (Fig 3.4f). Increasing soil N coincided with slight, but non-significant decreases
970 in χ and increases in V_{cmax25} and J_{max25} ($p < 0.2$, Table 3.2). The positive trend
971 between soil N availability and photosynthetic capacity was supported by the con-
972 current strong increase in leaf N content with increasing soil N availability, which
973 resulted in no change in the proportion of leaf N content allocated to photosynthe-

974 sis across the soil N availability gradient. Additionally, leaf N content exhibited a
975 strong negative correlation with χ , indicative of strong nitrogen-water use trade-
976 offs at the leaf level. Responses tended to vary more due to soil N availability
977 than soil pH. Overall, these findings are consistent with the nutrient-water use
978 tradeoffs predicted from theory.

979 3.4.1 *Soil nitrogen availability modifies tradeoffs between nitrogen and water use*

980 In support of expected least-cost outcomes and past environmental gradient
981 studies (Dong et al. 2017; Paillassa et al. 2020), we found that increasing soil N
982 availability was associated with increased leaf N content. Soil N availability had
983 smaller impacts on measures of net photosynthesis and χ , which led to reductions
984 in PNUE and increases in leaf N content per unit χ , as expected from theory.
985 Photosynthetic least-cost theory suggests that reductions in PNUE should be
986 driven by an increase in the proportion of leaf N allocated to photosynthetic tissue,
987 a pattern that should allow plants to achieve optimal photosynthetic rates with
988 greater photosynthetic capacity to make better use of available light. Contrasting
989 theory predictions, we found no effect of soil N availability on photosynthetic
990 capacity. However, photosynthetic capacity did tend to increase with increasing
991 soil N availability ($p < 0.20$; Table 3.2) resulting in no effect of soil N availability on
992 the relative fraction of leaf N allocated to photosynthesis, Rubisco, or bioenergetics
993 (Fig. 3.3). These lines of evidence support the idea that trees use additional N
994 to support increased leaf N allocation toward photosynthetic tissue and enhance
995 photosynthetic capacity (Wright et al. 2003).

996 Soil N availability had a stronger effect on leaf N than photosynthetic ca-

997 pacity. This pattern suggests that additional plant N uptake due to increased
998 soil N availability was also being used to support non-photosynthetic N pools,
999 possibly to structural tissue or stress-induced amino acid and polyamine synthe-
1000 sis (Minocha et al. 2000; Onoda et al. 2004; Bubier et al. 2011). While we
1001 found no change in the proportion of leaf N allocated to leaf structural tissue, the
1002 overall stimulation in leaf N content with increasing soil N availability suggests an
1003 increase in the net amount of N invested in leaf structural tissue along the N avail-
1004 ability gradient. Importantly, leaf N allocated to structure was calculated using
1005 an empirical relationship between M_{area} and the amount of leaf N allocated to cell
1006 walls (Onoda et al. 2017). As the generality of relationships between M_{area} and
1007 the amount of leaf N allocated to cell walls has been called into question (Harrison
1008 et al. 2009), future work should consider explicitly measuring N allocation to cell
1009 wall tissue and stress-induced amino acid synthesis to confirm these patterns.

1010 In opposition to patterns expected from least-cost theory, increasing soil
1011 N availability had no apparent effect on χ (Fig. 3.4a). Interestingly, despite
1012 the null effect of soil N availability on χ , we observed a strong negative effect of
1013 increasing N_{area} on χ (Fig. 3.4c), consistent with the nitrogen-water use tradeoffs
1014 expected from theory. The null response of χ to increasing soil N availability may
1015 have been due to a lack of water limitation in the system, given that the area
1016 received approximately 20% more precipitation (1167 mm) during the 12-month
1017 period leading up to our measurement period than normally expected (972 mm).
1018 However, droughts can and do occur in temperate forests of the northeastern
1019 United States (Sweet et al. 2017), so the observed increase in leaf N content
1020 with increasing soil N availability could be a strategy that allows trees to hedge

1021 bets against drier than normal growing seasons (Onoda et al. 2004; Onoda et al.
1022 2017; Hallik et al. 2009). As was suggested in Paillassa et al. (2020), and more
1023 recently by Querejeta et al. (2022), negative effects of soil N availability on χ may
1024 increase with increasing aridity. This strategy would be especially advantageous if
1025 it allows individuals growing in arid regions to maintain carbon assimilation rates
1026 with reduced water loss. Future work should attempt to quantify interactive roles
1027 of climate and soil nitrogen availability on nitrogen-water use tradeoffs, which
1028 could be done by leveraging coordinated and multifactor nutrient (Borer et al.
1029 2014) and water (Knapp et al. 2017) manipulation experiments across broad
1030 climatic gradients.

1031 3.4.2 *Soil pH did not modify tradeoffs between nitrogen and water usage*

1032 While the primary purpose of this study was to examine the role of soil N
1033 availability on nitrogen-water use tradeoffs, our experimental design manipulated
1034 both soil N and pH, providing an opportunity to isolate the roles of these variables.
1035 Previous correlational studies along environmental gradients identified soil pH as
1036 a particularly important factor that can modify tradeoffs between nutrient and
1037 water use (Smith et al. 2019; Paillassa et al. 2020; Westerband et al. 2023)
1038 and the proportion of leaf nitrogen allocated to photosynthesis (Luo et al. 2021).
1039 Such studies implied that these patterns may be driven by reductions in the cost of
1040 acquiring nutrients relative to water with increasing pH, which may be exacerbated
1041 in acidic soils.

1042 Consistent with theory (Wright et al. 2003; Prentice et al. 2014), our
1043 results indicate that increasing soil pH was negatively associated with PNUE.

1044 However, there was no effect of soil pH on leaf N content, χ , or leaf N content per
1045 unit χ , most likely because the experimental N additions increased soil N sup-
1046 ply while both increasing (sodium nitrate) and decreasing (ammonium sulfate)
1047 soil pH. These results suggest that soil pH did not play a major role in modify-
1048 ing expected photosynthetic least-cost theory patterns, contrasting findings from
1049 Paillassa et al. (2020) and other gradient studies that note positive effects of in-
1050 creasing soil pH on leaf N content, Rubisco carboxylation, and χ (Viet et al. 2013;
1051 Cornwell et al. 2018; Luo et al. 2021). Instead, null responses to soil pH show
1052 that leaf photosynthetic parameters depend more on soil N availability than pH
1053 per se, and that inferences from gradient studies might be confounding covariation
1054 between N availability and soil acidity.

1055 3.4.3 *Species identity explains a large amount of variation in leaf and whole*
1056 *plant traits*

1057 Species generally explained a larger amount of variation in measured leaf
1058 traits than soil N availability or soil pH. Interspecies variation is an important
1059 factor to consider when deducing mechanisms that drive photosynthetic least-
1060 cost theory, particularly for species that form distinct mycorrhizal associations or
1061 have different photosynthetic pathways, growth forms, or leaf habit (Espelta et al.
1062 2005; Adams et al. 2016; Bialic-Murphy et al. 2021; Scott and Smith 2022). The
1063 need to consider species may also be important when comparing nutrient-water
1064 use tradeoffs in early and late successional species, or in species with different
1065 resource economic strategies (Abrams and Mostoller 1995; Ellsworth and Reich
1066 1996; Wright et al. 2004; Reich 2014; Onoda et al. 2017; Ziegler et al. 2020).

1067 A strength of the study design and sampling effort is that it controls for
1068 many species differences that should modify nitrogen-water use tradeoffs expected
1069 from theory. All tree species measured in this study shared the leaf habit of decid-
1070 uous broadleaves, were growing in forests of similar successional stage, but differed
1071 in mycorrhizal association and consequent resource economic strategies. As stands
1072 tended to be dominated by trees that associate with arbuscular mycorrhizae (*Frax-*
1073 *inus* and both *Acer* species made up 70% of total aboveground biomass across
1074 stands), ecosystem biogeochemical cycle dynamics may be more closely aligned
1075 to the inorganic nutrient economy proposed in Phillips et al. (2013), which may
1076 promote stronger nitrogen-water use tradeoffs in tree species that associate with
1077 arbuscular mycorrhizae. This result was not observed here, as photosynthetic
1078 properties varied as much within as across the two mycorrhizal associations rep-
1079 resented. Given the high variability in measured photosynthetic traits within
1080 and across species, effects of mycorrhizal association likely require more intensive
1081 sampling efforts to detect than were possible here.

1082 3.4.4 *Implications for photosynthetic least-cost theory model development*

1083 In the field, soil nutrient availability is heterogeneous across time and space
1084 (Table S4). Unaccounted within-plot heterogeneity may have contributed to the
1085 low amount of variation explained by soil N availability in our statistical mod-
1086 els, as resin bags are a coarse surrogate for soil N availability. Despite this, we
1087 still observed evidence for nutrient-water use tradeoffs, suggesting that observed
1088 responses reported here may be an underestimate toward the net effect of soil
1089 N availability on these tradeoffs. While we urge caution in the interpretation of

1090 these results, they do provide a promising baseline for future studies investigating
1091 patterns expected from photosynthetic least-cost theory at finer spatiotemporal
1092 resolutions.

1093 The general stronger relationship between leaf N content and photosynthetic parameters versus between leaf N content and soil N availability suggests
1094 that leaf N content is more directly tied to photosynthesis than soil N availability.
1095 While this could be due to the high spatiotemporal heterogeneity of soil N availability,
1096 principles from photosynthetic least-cost theory suggest that leaf N content is the downstream product of leaf nutrient demand to build and maintain
1097 photosynthetic machinery, which is set by aboveground environmental conditions
1098 such as light availability, CO₂, temperature, or vapor pressure deficit (Smith
1099 et al. 2019; Paillassa et al. 2020; Peng et al. 2021; Westerband et al. 2023). The
1100 stronger relationship between leaf N and photosynthetic parameters paired with
1101 the strong negative relationship between leaf N and χ could indicate a relatively
1102 stronger effect of climate on leaf N-photosynthesis relationships than soil resource
1103 availability. However, the short distance between plots and across sites limited
1104 our ability to test this mechanism.

1107 Variation in soil pH affected least cost responses less than variations in
1108 soil N availability, in part because experimental treatments directly increased soil
1109 N and affected soil pH in opposite directions. While soil pH has been shown
1110 to drive nitrogen-water tradeoffs in global gradient analyses (Viet et al. 2013;
1111 Paillassa et al. 2020), these responses may be due to covariations between soil pH
1112 and nutrient cycling rather than a role of pH per se. The direct manipulations
1113 of soil pH and soil N availability in this study allowed us to partly disentangle

1114 these factors and show that variation in N availability matters more for least-cost
1115 tradeoffs than pH alone.

1116 3.4.5 *Conclusions*

1117 Increasing soil N availability generally increased leaf N content (both area-
1118 and mass-based), but did not significantly influence χ . This shift in leaf N led
1119 to a reduction in PNUE, and an increase in leaf N per unit χ with increasing
1120 soil N availability. Despite null effects of soil N availability on χ , we observed a
1121 strong negative relationship between leaf N content and χ . These results provide
1122 empirical support for the nutrient-water use tradeoffs expected from photosyn-
1123 thetic least-cost theory in response to soil nutrient availability, but suggest that
1124 all tenets of the theory may not hold in every environment. These results exper-
1125 imentially test previous work suggesting that leaf water-nitrogen economies vary
1126 across gradients of soil nutrient availability and pH, and show that variations in
1127 nutrient availability matter more for determining variation in leaf photosynthetic
1128 traits than soil pH.

1129

Chapter 4

1130 The relative cost of resource use for photosynthesis drives variance in
1131 leaf nitrogen content across a climate and soil resource availability
1132 gradient

1133 4.1 Introduction

1134 Terrestrial biosphere models, which comprise the land surface component
1135 of Earth system models, are sensitive to the formulation of photosynthetic pro-
1136 cesses (Knorr and Heimann 2001; Ziehn et al. 2011; Booth et al. 2012; Walker
1137 et al. 2021). This is because photosynthesis is the largest carbon flux between the
1138 atmosphere and terrestrial biosphere (IPCC 2021), and is constrained by ecosys-
1139 tem carbon and nutrient cycles (Hungate et al. 2003; LeBauer and Treseder
1140 2008; Fay et al. 2015). Many terrestrial biosphere models formulate photosyn-
1141 thesis by parameterizing photosynthetic capacity within plant functional groups
1142 through empirical linear relationships between area-based leaf nitrogen content
1143 (N_{area}) and the maximum carboxylation rate of Ribulose-1,5-bisphosphate car-
1144 boxylase/oxygenase (Kattge et al. 2009; Rogers 2014; Rogers et al. 2017). Models
1145 are also beginning to include connected carbon-nitrogen cycles (Wieder et al. 2015;
1146 Shi et al. 2016; Davies-Barnard et al. 2020; Braghieri et al. 2022), which allows
1147 leaf photosynthesis to be predicted directly through changes in N_{area} and indirectly
1148 through changes in soil nitrogen availability (e.g., LPJ-GUESS, CLM5.0) (Smith
1149 et al. 2014; Lawrence et al. 2019). Despite recent model developments, open
1150 questions remain regarding the generality of ecological relationships between soil
1151 nitrogen availability, leaf nitrogen content, and leaf photosynthesis across edaphic
1152 and climatic gradients.

1153 Empirical support for positive relationships between soil nitrogen availabil-
1154 ity and N_{area} is abundant (Firn et al. 2019; Liang et al. 2020), and is a result
1155 often attributed to the high nitrogen cost of building and maintaining Rubisco
1156 (Evans 1989; Evans and Seemann 1989; Onoda et al. 2004; Onoda et al. 2017;
1157 Walker et al. 2014; Dong et al. 2020). Such patterns imply that positive rela-
1158 tionships between soil nitrogen availability and N_{area} should cause an increase in
1159 leaf photosynthesis and photosynthetic capacity by increasing the maximum rate
1160 of Rubisco carboxylation through increased investments to Rubisco construction
1161 and maintenance. This integrated N_{area} -photosynthesis response to soil nitrogen
1162 availability has been observed both in manipulative experiments and across envi-
1163 ronmental gradients (Field and Mooney 1986; Evans 1989; Walker et al. 2014; Li
1164 et al. 2020), and is thought to be driven by ecosystem nitrogen limitation, which
1165 limits primary productivity globally (LeBauer and Treseder 2008; Fay et al. 2015).
1166 However, this response is not consistently observed, as recent studies note variable
1167 N_{area} -photosynthesis relationships across soil nitrogen availability gradients (Liang
1168 et al. 2020; Luo et al. 2021) and that aboveground growing conditions (e.g., light
1169 availability, temperature, vapor pressure deficit) or species identity traits (e.g.,
1170 photosynthetic pathway, nitrogen acquisition strategy) may be more important
1171 for explaining variance in N_{area} and photosynthetic capacity across environmental
1172 gradients (Adams et al. 2016; Dong et al. 2017; Dong et al. 2020; Dong et al.
1173 2022; Smith et al. 2019; Peng et al. 2021; Westerband et al. 2023).

1174 One hypothesized mechanism to explain variance in N_{area} across environ-
1175 mental gradients has been proposed via photosynthetic least-cost theory (Wright
1176 et al. 2003; Prentice et al. 2014; Paillassa et al. 2020; Harrison et al. 2021).

1177 The theory predicts that plants acclimate to environments by optimizing photo-
1178 synthetic assimilation rates at the lowest summed cost of nitrogen and water use
1179 (Wright et al. 2003; Prentice et al. 2014). In a given environment, the theory pro-
1180 poses that nitrogen and water use can be substituted for each other to maintain
1181 the lowest summed cost to satisfy leaf resource demand, such that optimal photo-
1182 synthetic rates are achieved with less efficient use of the more abundant and less
1183 costly resource to acquire in exchange for more efficient use of the less abundant
1184 and more costly resource to acquire. The theory predicts that, all else equal, an
1185 increase in soil nitrogen availability should decrease the cost of acquiring and us-
1186 ing nitrogen relative to water (a ratio referred to herein as β), resulting in optimal
1187 photosynthetic rates achieved with greater N_{area} at lower stomatal conductance
1188 and lower leaf $C_i:C_a$ (Wright et al. 2003; Prentice et al. 2014). Alternatively, an
1189 increase in soil moisture should reduce costs of water acquisition and use, increas-
1190 ing β , stomatal conductance, and leaf $C_i:C_a$, resulting in optimal photosynthetic
1191 rates achieved with decreased N_{area} . The theory also predicts variability in stom-
1192 atal conductance and N_{area} in response to climatic factors, suggesting that the
1193 optimal response to increased vapor pressure deficit (VPD) should be a reduction
1194 in stomatal conductance and leaf $C_i:C_a$ that is counterbalanced by an increase
1195 in N_{area} to support the higher photosynthetic capacity needed to maintain high
1196 assimilation at lower conductance (Grossiord et al. 2020; Dong et al. 2020; López
1197 et al. 2021; Westerband et al. 2023).

1198 Leaf nitrogen allocation responses to changing climates or soil resource
1199 availability may also depend on their mode of nutrient acquisition or photo-
1200 synthetic pathway. For example, species that form associations with symbiotic

1201 nitrogen-fixing bacteria (referred as “N-fixing species” from this point forward)
1202 should, in theory, have access to a less finite nitrogen supply, which may result in
1203 lower β values than species not capable of forming such associations (referred as
1204 “non-fixing species” from this point forward). This result was previously shown in
1205 a greenhouse experiment, where a leguminous species generally had lower costs of
1206 nitrogen acquisition compared to a non-leguminous species, although these differ-
1207 ences were generally stronger under increased nitrogen limitation (Perkowski et al.
1208 2021). Lower β values could be a possible explanation for why N-fixing species
1209 commonly have higher leaf nitrogen content than non-fixing species (Adams et al.
1210 2016; Dong et al. 2017). Similarly, leaf nitrogen allocation patterns across en-
1211 vironmental gradients may be dependent on photosynthetic pathway. Lower leaf
1212 $C_i:C_a$ values in C₄ species suggests that C₄ species should have lower β values
1213 than C₃ species (Scott and Smith 2022), a pattern that could be the result of
1214 increased costs associated with water acquisition and use or reduced costs of ni-
1215 trogen acquisition and use relative to C₃ species. No study to date has directly
1216 quantified β in C₄ species aside from the dataset used to initially parameterize
1217 an optimality model for C₄ species (Scott and Smith 2022).

1218 While photosynthetic least-cost theory provides a unified hypothesis for un-
1219 derstanding effects of climate and soil resource availability on N_{area} , empirical tests
1220 of the theory are sparse. Increasing soil nitrogen availability has been previously
1221 shown to decrease the cost of acquiring nutrients (Bae et al. 2015; Perkowski et al.
1222 2021; Lu et al. 2022), which can induce predictable nutrient-water use tradeoffs
1223 expected from the theory across broad environmental gradients (Paillassa et al.
1224 2020; Querejeta et al. 2022; Westerband et al. 2023) and in manipulation experi-

ments (Bialic-Murphy et al. 2021). Additionally, increasing VPD has been shown to have a positive effect on N_{area} (Dong et al. 2017; Dong et al. 2020; Firn et al. 2019; López et al. 2021). However, studies have been restricted to exploring these patterns with C3 species and, while previous studies have shown that variance in N_{area} across environmental gradients is driven by strong negative relationships with leaf $C_i:C_a$ (3.4, (Dong et al. 2017; Paillassa et al. 2020; Westerband et al. 2023)), no study to date has explicitly investigated effects of soil resource availability or plant functional group on N_{area} using β as a direct predictor of leaf $C_i:C_a$. Additionally, as N_{area} can be broken down into structural (leaf mass per area; M_{area} ; g m⁻²) and metabolic (mass-based leaf nitrogen content; N_{mass} ; gN g⁻¹) components (Dong et al. 2017), no study has investigated which component of N_{area} drives the hypothesized response of N_{area} to leaf $C_i:C_a$. Understanding whether changes in N_{area} due to leaf $C_i:C_a$ are driven by changes in leaf morphology or stoichiometry is important, especially because N_{mass} tends to covary with M_{area} due to tradeoffs between leaf longevity and leaf productivity (Wright et al. 2004; Reich 2014; Onoda et al. 2017; Wang et al. 2023).

In this chapter, I measured N_{area} , N_{mass} , M_{area} , leaf $\delta^{13}\text{C}$ -derived estimates of leaf $C_i:C_a$, and leaf $\delta^{13}\text{C}$ -derived estimates of β in 520 individuals spanning 57 species scattered across 24 grassland sites in Texas, USA (Table S1). Texas contains a diverse climatic gradient, indicated by 2006-2020 mean annual precipitation totals ranging from 204 to 1803 mm and 2006-2020 mean annual temperature ranging from 11.8° to 24.6°C. Variability in soil nitrogen availability and soil moisture was expected across sites, owing to differences in soil texture and aboveground climate that would drive differential rates of water retention and

1249 nitrogen transformations to plant-available substrate. I leveraged the expected
1250 climatic and soil resource variability across sites to test the following hypotheses:

- 1251 1. Soil nitrogen availability will decrease β through a reduction in costs of
1252 nitrogen acquisition and use, while soil moisture will increase β through a
1253 reduction in costs of water acquisition and use. Following previous results,
1254 we expected that N-fixing species would have lower β values and that C₄
1255 species would have lower β values.
- 1256 2. Leaf $C_i:C_a$ will be positively related to β , a pattern that will result in a
1257 negative indirect effect of increasing soil nitrogen availability on leaf $C_i:C_a$,
1258 a positive indirect effect of increasing soil moisture on leaf $C_i:C_a$, and lower
1259 leaf $C_i:C_a$ in both N-fixing species and C₄ species. We also expected that
1260 leaf $C_i:C_a$ would be negatively related to VPD, as increasing atmospheric
1261 dryness should cause plants to close stomata to minimize water loss.
- 1262 3. N_{area} will be negatively related to leaf $C_i:C_a$ and β . This response will result
1263 in an indirect positive effect of increasing soil nitrogen availability, a negative
1264 effect of increasing soil moisture on N_{area} , and generally larger N_{area} values
1265 in both N-fixing species. While theory predicts that negative relationships
1266 between N_{area} and leaf $C_i:C_a$ should yield generally larger N_{area} in C₄ species,
1267 we expected that C₄ species would have lower N_{area} due to generally greater
1268 nitrogen use efficiency in C₄ species than C₃ species. Additionally, VPD
1269 was expected to increase N_{area} , a pattern that would be directly mediated
1270 through the reduction in leaf $C_i:C_a$ with increasing VPD.

1271 4.2 Methods

1272 4.2.1 *Site descriptions and sampling methodology*

1273 I collected leaf and soil samples from 24 open grassland sites across central and
1274 eastern Texas in summer 2020 and summer 2021 (Fig. 4.1). Twelve sites were vis-
1275 ited between June and July 2020 and 14 sites (11 unique from 2020) were visited
1276 between May and June 2021 (Table 4.1). I explicitly chose sites that maximized
1277 variability in precipitation and edaphic variability between sites while minimiz-
1278 ing temperature variability across the environmental gradient (Table 4.1). No
1279 site with personally communicated or anecdotal evidence of grazing or distur-
1280 bance (e.g., mowing, feral hog activity, etc.) were used. I collected leaf material
1281 from three individuals each of the five most abundant species at random locations
1282 at each site, only selecting species that were broadly classified as graminoid or
1283 forb/herb growth habits per the USDA PLANTS database (USDA NRCS 2022).
1284 All collected leaves were fully expanded with no visible herbivory or other external
1285 damage and also free from shading by nearby shrubs or trees. Five soil samples
1286 were collected from 0-15cm below the soil surface at each site near the leaf collec-
1287 tion sample locations. Soil samples were later mixed together by hand to create
1288 one composite soil sample per site.

1289 4.2.2 *Leaf trait measurements*

1290 Images of each leaf were taken immediately following each site visit using a flat-
1291 bed scanner. Fresh leaf area was determined from each image using the 'LeafArea'
1292 R package (Katabuchi 2015), which automates leaf area calculations using ImageJ
1293 software (Schneider et al. 2012). Each leaf was dried at 65°C for at least 48 hours

1294 to a constant mass, weighed, and manually ground in a mortar and pestle until
1295 homogenized. Leaf mass per area (M_{area} ; g m⁻²) was calculated as the ratio of
1296 dry leaf biomass to fresh leaf area. Subsamples of dried and homogenized leaf
1297 tissue were used to measure leaf nitrogen content (N_{mass} ; gN g⁻¹) through ele-
1298 mental combustion analysis (Costech-4010, Costech Instruments, Valencia, CA).
1299 Leaf nitrogen content per unit leaf area (N_{area} ; gN m⁻²) was then calculated as
1300 the product of N_{mass} and M_{area} .

1301 Subsamples of dried and homogenized leaf tissue were sent to the University
1302 of California-Davis Stable Isotope Facility to determine leaf $\delta^{13}\text{C}$. Leaf $\delta^{13}\text{C}$ values
1303 were determined using an elemental analyzer (PDZ Europa ANCA-GSL; Sercon
1304 Ltd., Chestshire, UK) interfaced to an isotope ratio mass spectrometer (PDZ
1305 Europa 20-20 Isotope Ratio Mass Spectrometer, Sercon Ltd., Chestshire, UK).
1306 I used leaf $\delta^{13}\text{C}$ values (‰; relative to Vienna Pee Dee Belemnite international
1307 reference standard) to estimate the ratio of intercellular (C_i) to extracellular (C_a)
1308 CO₂ ratio (leaf $C_i:C_a$; unitless) following the approach of Farquhar et al. (1989)
1309 described in Cernusak et al. (2013). Specifically, I derived leaf C_i:C_a as:

$$\text{Leaf } \frac{C_i}{C_a} = \frac{\Delta^{13}\text{C} - a}{b - a} \quad (4.1)$$

1310 where $\Delta^{13}\text{C}$ represents the relative difference between leaf $\delta^{13}\text{C}$ (‰) and air $\delta^{13}\text{C}$
1311 (‰), and is calculated as:

$$\Delta^{13}\text{C} = \frac{\delta^{13}\text{C}_{\text{air}} - \delta^{13}\text{C}_{\text{leaf}}}{1 + \delta^{13}\text{C}_{\text{leaf}}} \quad (4.2)$$

1312 $\delta^{13}\text{C}_{\text{air}}$, traditionally assumed to be -8‰ (Keeling et al. 1979; Farquhar et al.

1313 1989), was calculated as a function of calendar year t using an empirical equation
1314 derived in Feng (1999):

$$\delta^{13}C_{air} = -6.429 - 0.006e^{0.0217(t-1740)} \quad (4.3)$$

1315 This calculation resulted in $\delta^{13}C_{air}$ values for 2020 and 2021 as -9.04‰ and -
1316 9.09‰, respectively. a represents the fractionation between ^{12}C and ^{13}C due to
1317 diffusion in air, assumed to be 4.4‰, and b represents the fractionation caused
1318 by Rubisco carboxylation, assumed to be 27‰ (Farquhar et al. 1989). For C_4
1319 species, b in Eqn. 4.1 was set to 6.3‰, and was derived from:

$$b = c + (d \cdot \phi) \quad (4.4)$$

1320 Where c was set to -5.7‰ and d was set to 30‰ (Farquhar et al. 1989). ϕ , which
1321 is the bundle sheath leakiness term, was set to 0.4. All leaf $C_i:C_a$ values less than
1322 0.1 and greater than 0.95 were assumed to be incorrect and removed.

1323 I derived the unit cost of resource use (β) using leaf $C_i:C_a$ and site climate
1324 data with equations first described in Prentice et al. (2014) and simplified in
1325 Lavergne et al. (2020):

$$\beta = 1.6\eta^*D \frac{\chi - (\frac{\Gamma^*}{C_a})^2}{(1 - \chi)^2(K_m + \Gamma^*)} \quad (4.5)$$

1326 where η^* is the viscosity of water relative to 25°C, calculated using elevation and
1327 mean air temperature of the seven days leading up to each site visit following
1328 equations in Huber et al. (2009). D represents vapor pressure deficit (Pa), set

1329 to the mean vapor pressure deficit of the seven days leading up to each site visit,
1330 C_a represents atmospheric CO₂ concentration, arbitrarily set to 420 $\mu\text{mol mol}^{-1}$
1331 CO₂. K_m (Pa) is the Michaelis-Menten coefficient for Rubisco affinity to CO₂ and
1332 O₂, calculated as:

$$K_m = K_c \cdot \left(1 + \frac{O_i}{K_o}\right) \quad (4.6)$$

1333 where K_c (Pa) and K_o (Pa) are the Michaelis-Menten coefficients for Rubisco
1334 affinity to CO₂ and O₂, respectively, and O_i is the intercellular O₂ concentration.
1335 Γ^* (Pa) is the CO₂ compensation point in the absence of dark respiration. K_c , K_o ,
1336 and Γ^* were determined using equations described in Medlyn et al. (2002) and
1337 derived in Bernacchi et al. (2001), invoking an elevation correction for atmospheric
1338 pressure as explained in Stocker et al. (2020).

Table 4.1. Site locality information, sampling year(s), 2006-2020 mean annual precipitation (MAP; mm), mean annual temperature (MAT; °C), and water holding capacity (WHC; mm)*

Site	Latitude	Longitude	Sampling year	MAP	MAT	WHC
Edwards_2019_17	29.95	-100.36	2020	563.5	19.0	224.7
Uvalde_2020_02	29.59	-100.09	2020, 2021	648.5	19.5	224.7
Menard_2020_01	30.91	-99.59	2020	641.9	18.3	220.2
Kerr_2020_03	30.06	-99.34	2021	672.4	18.3	237.5
Bandera_2020_03	29.85	-99.30	2021	789.4	18.8	235.1
Sansaba_2020_01	31.29	-98.62	2020	733.0	18.8	234.3
Comal_2020_21	29.79	-98.43	2020	878.5	19.9	220.7
Blanco_2019_16	29.99	-98.43	2020	833.0	19.2	222.2
Bexar_2019_13	29.24	-98.43	2020	759.3	21.5	206.0
Burnet_2020_14	30.84	-98.34	2021	763.3	19.5	217.8
Comal_2020_19	30.01	-98.32	2021	845.0	19.3	220.4
Hays_2020_54	29.96	-98.17	2021	861.3	20.0	225.6
Burnet_2020_12	30.82	-98.06	2021	815.1	19.4	245.3
Williamson_2019_09	30.71	-97.86	2020	867.7	19.7	270.2
Williamson_2019_10	30.54	-97.77	2020	819.5	19.9	239.8
Bell_2021_08	31.06	-97.55	2021	937.3	19.6	232.3
Fayette_2021_12	29.86	-97.21	2021	985.7	20.4	165.6
Fayette_2019_04	30.09	-96.78	2020	1017.4	20.6	226.9
Fayette_2020_09	29.86	-96.71	2021	1002.7	20.8	187.6
Washington_2020_08	30.28	-96.41	2021	1077.4	20.4	203.9
Austin_2020_03	29.78	-96.24	2021	1108.7	20.6	253.0
Brazos_2020_16	30.93	-96.23	2021	1078.0	20.1	202.2
Brazos_2020_18	30.52	-96.21	2020, 2021	1099.4	20.4	233.5
Harris_2020_03	29.88	-95.31	2020, 2021	1492.0	21.6	265.6

1339 * Rows are arranged by longitude to visualize precipitation variability across sites

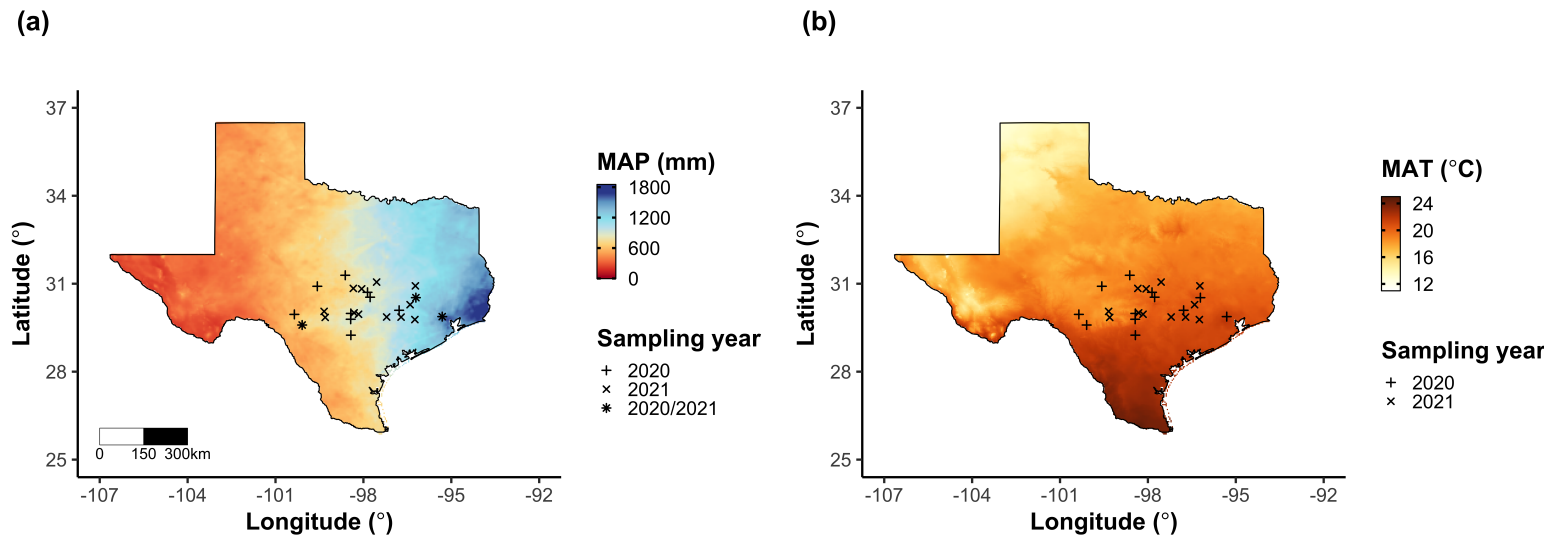


Figure 4.1. Maps that detail site locations along 2006-2020 mean annual precipitation (a) and mean annual temperature (b) gradients in Texas, USA. Precipitation and temperature data were plotted at a 4-km grid resolution and are masked to include only grid cells that occur in the Texas state boundary in the United States. In both panels, open circles refer to sites visited in 2020, open triangles to sites visited in 2021, and closed circles to sites visited in 2020 and 2021. The scale bar in (a) also applies to (b).

1340 4.2.3 *Site climate data*

1341 I used the Parameter-elevation Regressions on Independent Slopes Model (PRISM)
1342 (Daly et al. 2008) climate product to access gridded daily temperature and precip-
1343 itation data for the coterminous United States at a 4-km grid resolution between
1344 January 1, 2006 and July 31, 2021 (PRISM Climate Group, Oregon State Uni-
1345 versity, <https://prism.oregonstate.edu>, data created 4 Feb 2014, accessed 24 Mar
1346 2022). Daily mean air temperature, mean VPD, and total precipitation data were
1347 extracted from the grid cell that contained the latitude and longitude of each
1348 property using the ‘extract’ function in the ‘terra’ R package (Hijmans 2022).
1349 PRISM data were used in lieu of local weather station data because several rural
1350 sites did not have a local weather station present within a 20-km radius of the site.
1351 Daily site climate data were used to estimate mean annual precipitation and mean
1352 annual temperature for each site between 2006 and 2020 (Table 1). I calculated
1353 total precipitation and mean daily VPD for the prior 1, 2, 3, 4, 5, 6, 7, 8, 9, 10,
1354 15, 20, 25, 30, 60, and 90 days leading up to each site visit.

1355 4.2.4 *Site edaphic characteristics*

1356 Subsamples of composited soil samples were sent to the Texas A & M Soil, Water
1357 and Forage Laboratory to quantify soil nitrate concentration (NO₃-N; ppm). Soil
1358 NO₃-N was determined by extracting composite soil samples in 1 M KCl, measur-
1359 ing absorbance values of extracts at 520 nm using the end product of a NO₃-N to
1360 NO₂-N cadmium reduction reaction (Kachurina et al. 2000; Keeney and Nelson
1361 1983). Soil texture data from 0-15cm below the soil surface were accessed using
1362 the SoilGrids2.0 data product (Poggio et al. 2021) through the ‘fetchSoilGrids’

1363 function in the ‘soilDB’ R package (Beaudette et al. 2022). I used SoilGrids2.0
1364 to access soil texture data in lieu of analyses using the collected composite soil
1365 sample due to a lack of soil material from some sites after sending samples for soil
1366 NO₃-N.

1367 Soil moisture was not measured in the field, but was estimated using the
1368 ‘Simple Process-Led Algorithms for Simulating Habitats’ model (SPLASH) (Davis
1369 et al. 2017). This model, derived from the STASH model (Cramer and Prentice
1370 1988), spins up a bucket model using Priestley-Taylor equations (Priestley and
1371 Taylor 1972) to calculate daily soil moisture (W_n ; mm) as a function of the previous
1372 day’s soil moisture (W_{n-1} ; mm), daily precipitation (P_n ; mm), condensation (C_n ;
1373 mm), actual evapotranspiration (E_n^a ; mm), and runoff (RO; mm):

$$W_n = W_{n-1} + P_n + C_n - E_n^a - RO \quad (4.7)$$

1374 Models were spun up by equilibrating the previous day’s soil moisture using succes-
1375 sive model iterations with daily mean air temperature, daily precipitation total,
1376 the number of daily sunlight hours, and latitude as model inputs (Davis et al.
1377 2017). Daily sunlight hours were estimated for each day at each site using the
1378 ‘getSunlightTimes’ function in the ‘suncalc’ R package, which estimated sunrise
1379 and sunset times of each property using date and site coordinates (Thieurmel and
1380 Elmarhraoui 2019). Water holding capacity (mm), or bucket size, was estimated
1381 as a function of soil texture using pedotransfer equations explained in Saxton and
1382 Rawls (2006), as done in Stocker et al. (2020) and Bloomfield et al. (2023). A
1383 summary of these equations is included in the Supplemental Information.

1384 Daily soil moisture outputs from the SPLASH model for each site were
1385 used to calculate mean daily soil moisture for the prior 1, 2, 3, 4, 5, 6, 7, 8, 9,
1386 10, 15, 20, 25, 30, 60, and 90 days leading up to each site visit. Mean daily
1387 soil moisture values were then expressed as a fraction of water holding capacity
1388 to normalize across sites with different bucket depths, as done in Stocker et al.
1389 (2018).

1390 4.2.5 *Plant functional group assignments*

1391 Plant functional group was assigned to each species and used as the primary
1392 descriptor of species identity. Specifically, I assigned plant functional groups
1393 based on photosynthetic pathway (C_3 , C_4) and ability to form associations with
1394 symbiotic nitrogen-fixing bacteria. The ability to form associations with symbi-
1395 otic nitrogen-fixing bacteria was assigned based on whether species were in the
1396 *Fabaceae* family, and photosynthetic pathway of each species was determined from
1397 past literature and confirmed through leaf $\delta^{13}C$ values. We chose these plant func-
1398 tional groups based on *a priori* hypotheses regarding the functional role of nitrogen
1399 fixation and photosynthetic pathway on the sensitivity of plant nitrogen uptake
1400 and leaf nitrogen allocation to soil nutrient availability and aboveground growing
1401 conditions. These plant functional group classifications resulted in three distinct
1402 plant functional groups within our dataset: C_3 legumes ($n = 53$), C_3 non-legumes
1403 ($n = 350$), and C_4 non-legumes ($n = 117$).

1404 4.2.6 *Data analysis*

1405 All analyses and plotting were conducted in R version 4.1.1 (R Core Team 2021).

1406 I constructed a series of separate linear mixed-effects models to investigate en-

1407 vironmental drivers of β , leaf $C_i:C_a$, N_{area} , N_{mass} , and M_{area} , followed by a path

1408 analysis using a piecewise structural equation model to investigate direct and

1409 indirect effects of climate and soil resource availability on N_{area} .

1410 To explore environmental drivers of β , I built a linear mixed-effects model

1411 that included soil moisture, soil nitrogen availability, and plant functional group

1412 as fixed effect coefficients. Species were designated as a random intercept term.

1413 Interaction coefficients between all possible combinations of the three fixed effect

1414 coefficients were also included. β was natural log transformed to linearize data.

1415 I used an information-theoretic model selection approach to determine whether

1416 90-, 60-, 30-, 20-, 15-, 10-, 9-, 8-, 7-, 6-, 5-, 4-, 3-, 2-, or 1-day mean daily soil

1417 moisture conferred the best model fit for β . To do this, I constructed 16 separate

1418 linear mixed-effects models where log-transformed β was included as the response

1419 variable and each soil moisture time step was separately included as a single

1420 continuous fixed effect. Species were included as a random intercept term for all

1421 models. I used corrected Akaike Information Criterion (AICc) to select the soil

1422 moisture timescale that conferred the best model fit, indicated by the model with

1423 the lowest AICc score (Table S2; Fig. S2).

1424 To explore environmental drivers of leaf $C_i:C_a$, I constructed a second linear

1425 mixed effects model that included VPD, soil moisture, soil nitrogen availability,

1426 and plant functional group as fixed effect coefficients. Two-way interactions be-

1427 tween plant functional group and VPD, soil nitrogen availability, or soil moisture

1428 were also included as fixed effect coefficients, in addition to a three-way interaction
1429 between soil moisture, soil nitrogen availability, and plant functional group.
1430 Species were included as a random intercept term. I used an information-theoretic
1431 model selection approach to determine whether 90-, 60-, 30-, 20-, 15-, 10-, 9-, 8-,
1432 7-, 6-, 5-, 4-, 3-, 2-, or 1-day mean daily VPD conferred the best model fit for leaf
1433 $C_i:C_a$ using the same approach explained above for the soil moisture effect on β .
1434 The soil moisture timescale was set to the same timescale that conferred the best
1435 fit for β .

1436 To explore environmental drivers of N_{area} , N_{mass} , and M_{area} , I constructed
1437 three separate linear mixed effects model that each included leaf $C_i:C_a$, soil ni-
1438 trogen availability, soil moisture, and plant functional group as fixed effect coef-
1439 ficients. Two-way interactions between plant functional group and β , leaf $C_i:C_a$,
1440 soil nitrogen availability, or soil moisture were included as additional fixed effect
1441 coefficients, in addition to a three-way interaction between soil nitrogen availabil-
1442 ity, soil moisture, and plant functional group. Species were included as a random
1443 intercept term, with the soil moisture timescale set to the same timescale that
1444 conferred the best fit for β .

1445 In all linear mixed-effects models explained above, including those to select
1446 relevant timescales, I used the 'lmer' function in the 'lme4' R package (Bates et al.
1447 2015) to fit each model and the 'Anova' function in the 'car' R package (Fox and
1448 Weisberg 2019) to calculate Type II Wald's χ^2 and determine the significance
1449 level ($\alpha = 0.05$) of each fixed effect coefficient. I used the 'emmeans' R package
1450 (Lenth 2019) to conduct post-hoc comparisons using Tukey's tests, where degrees
1451 of freedom were approximated using the Kenward-Roger approach (Kenward and

1452 Roger 1997). Trendlines and error ribbons for all plots were drawn using a series
1453 of ‘emmeans’ outputs across the range in plotted x-axis values.

1454 Finally, I conducted a path analysis using a piecewise structural equation
1455 model to examine direct and indirect pathways that determined variance in N_{area} .
1456 Six separate linear mixed effects models were loaded into the piecewise structural
1457 equation model. Models were constructed per *a priori* hypotheses following pat-
1458 terns expected from photosynthetic least-cost theory. The first model regressed
1459 N_{area} against N_{mass} and M_{area} . The second model regressed M_{area} against leaf
1460 $C_i:C_a$. The third model regressed N_{mass} against leaf $C_i:C_a$ and M_{area} (Dong et al.
1461 2017; Dong et al. 2020). The fourth model regressed leaf $C_i:C_a$ against β and
1462 VPD. The fifth model regressed β against soil nitrogen availability, soil moisture,
1463 ability to associate with symbiotic nitrogen-fixing bacteria, and photosynthetic
1464 pathway. The sixth model regressed soil nitrogen availability against soil mois-
1465 ture. All models included the relevant timescale selected in the individual linear
1466 mixed effect models explained above. Models included species as a random inter-
1467 cept term, were built using the ‘lme’ function in the ‘nlme’ R package (Pinheiro
1468 and Bates 2022), and subsequently loaded into the piecewise structural equation
1469 model using the ‘psem’ function in the ‘piecewiseSEM’ R package (Lefcheck 2016).

1470 4.3 Results

1471 4.3.1 *Cost to acquire nitrogen relative to water*

1472 Model selection indicated that 90-day soil moisture conferred the best model fit
1473 for β ($AICc=1429.14$; Table S2; Fig. S1).

1474 Increasing soil nitrogen availability generally decreased β ($p < 0.001$; Table

1475 4.2; Fig. 4.2a), a pattern driven by a negative effect of increasing soil nitrogen on β
1476 in C₃ nonlegumes (Tukey: $p = 0.002$) and C₃ legumes (Tukey: $p = 0.031$) despite
1477 a null effect of soil nitrogen on β in C₄ nonlegumes (Tukey: $p = 0.905$). There
1478 was no effect of soil moisture on β ($p = 0.902$; Table 4.2; Fig. 4.2b). A functional
1479 group effect ($p < 0.001$; Table 4.2) indicated that C₄ nonlegumes generally had
1480 lower β values than both C₃ legumes and C₃ non-legumes (Tukey: $p < 0.001$
1481 in both cases), while β values in C₃ legumes did not differ from C₃ nonlegumes
1482 (Tukey: $p = 0.804$).

Table 4.2. Effects of soil moisture, soil nitrogen availability, and plant functional group on β

	df	Coefficient	χ^2	p
Intercept	-	3.39E+00	-	-
Soil moisture (SM ₉₀)	1	-2.03E-01	0.015	0.902
Soil N (N)	1	-1.49E-02	13.832	<0.001
PFT	2	-	225.049	<0.001
SM ₉₀ *N	1	-8.86E-04	1.016	0.313
SM ₉₀ *PFT	2	-	0.754	0.686
N*PFT	2	-	5.236	0.073
SM ₉₀ *N*PFT	2	-	3.633	0.163

1483 *Significance determined using Type II Wald χ^2 tests ($\alpha = 0.05$). P-values < 0.05

1484 are in bold. Model coefficients are expressed on the natural-log scale and are only

1485 included for continuous fixed effects. Key: df = degrees of freedom, χ^2 = Wald

1486 Type II chi-square test statistic

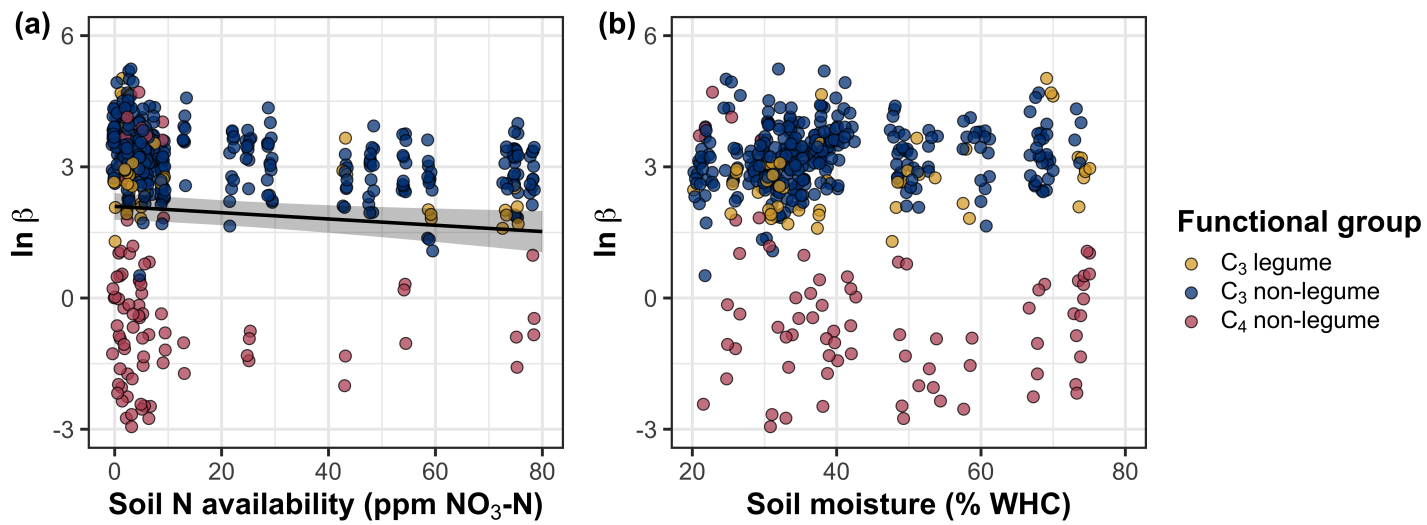


Figure 4.2. Effects of soil nitrogen availability (a) and 90-day soil moisture (b) on the unit cost ratio β . In (b), soil moisture is represented as a percent of site water holding capacity. Yellow shading and trendlines indicate C₃ legumes, blue shading and trendlines indicate C₃ non-legumes, and red shading and trendlines indicate C₄ non-legumes. Points are jittered for visibility. Variably colored trendlines are only included if there is an interaction between the x-axis and plant functional group, where solid trendlines indicate slopes that are different from zero ($p < 0.05$) and dashed trendlines indicate slopes that are not different from zero ($p > 0.05$). Error ribbons represent the upper and lower 95% confidence intervals of each fitted trendline.

1487 4.3.2 $C_i:C_a$

1488 Model selection indicated that 4-day daily VPD was the timescale that conferred

1489 the best model fit for leaf $C_i:C_a$ (AICc = -793.49; Table S1; Fig. S2).

1490 Model results revealed that increasing VPD generally decreased leaf $C_i:C_a$

1491 ($p < 0.001$; Table 4.3; Fig. 4.3a). There was no effect of soil moisture ($p =$

1492 0.843; Table 4.3; Fig. 4.3b) or soil nitrogen availability ($p = 0.544$; Table 4.3;

1493 Fig. 4.3c) on leaf $C_i:C_a$. A strong plant functional group effect ($p < 0.001$; Table

1494 4.3) indicated that C₄ nonlegumes had lower leaf $C_i:C_a$ than C₃ legumes and C₃

1495 nonlegumes (Tukey: $p < 0.001$ in both cases), with no difference between C₃

1496 legumes and C₃ nonlegumes (Tukey: $p = 0.865$).

Table 4.3. Effects of soil moisture, soil nitrogen availability, and plant functional group on leaf $C_i:C_a$ ^{*}

	df	Coefficient	χ^2	p
Intercept	-	1.32E+00	-	-
Vapor pressure deficit (VPD_4)	1	-4.53E-01	11.211	<0.001
Soil moisture (SM_{90})	1	-1.71E-01	0.039	0.843
Soil N (N)	1	-3.33E-03	0.369	0.544
PFT	2	-	227.005	<0.001
SM_{90}^*N	1	need this	2.361	0.124
VPD_4^*PFT	2	-	0.927	0.629
SM_{90}^*PFT	2	-	0.817	0.664
N^*PFT	2	-	4.085	0.130
$SM_{90}^*N^*PFT$	2	-	3.677	0.159

1497 *Significance determined using Type II Wald χ^2 tests ($\alpha = 0.05$). *P*-values less
1498 than 0.05 are in bold and *p*-values where $0.05 < p < 0.1$ are italicized. Leaf $C_i:C_a$
1499 was not transformed prior to model fitting, so model coefficients are reported
1500 on the response scale. Model coefficients are only included for continuous fixed
1501 effects.

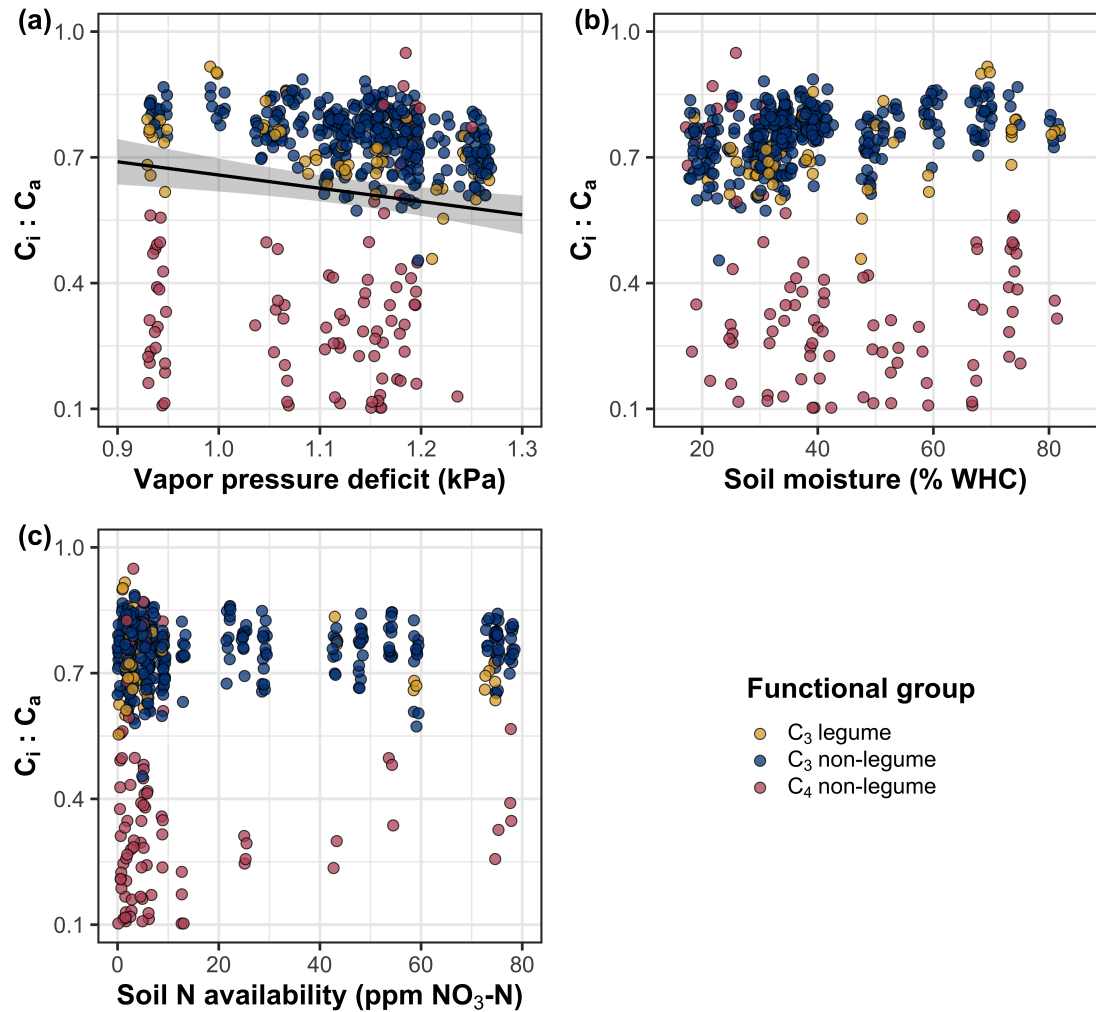


Figure 4.3. Effects of 4-day mean vapor pressure deficit (a), 90-day soil moisture (per water holding capacity; b), and soil nitrogen availability (c) on leaf $C_i:C_a$. Shading and trendlines are as explained in Figure 4.3. Points are jittered for visibility. Variably colored trendlines are only included if there is an interaction between the x-axis and plant functional group, where solid trendlines indicate slopes that are different from zero ($p < 0.05$) and dashed trendlines indicate slopes that are not different from zero ($p < 0.05$). Error ribbons represent the upper and lower 95% confidence intervals of each fitted trendline.

1502 4.3.3 *Leaf nitrogen content*

1503 An interaction between leaf $C_i:C_a$ and plant functional group ($p < 0.001$;
1504 Table 4.4) revealed that the negative effect of increasing leaf $C_i:C_a$ on N_{area} ($p <$
1505 0.001; Table 4.4) was driven by a negative effect of increasing leaf $C_i:C_a$ on N_{area}
1506 in C₃ nonlegumes (Tukey: $p < 0.001$) and C₃ legumes (Tukey: $p = 0.002$), with no
1507 observable effect in C₄ nonlegumes (Tukey: $p = 0.795$; Fig. 4.4a). An interaction
1508 between soil nitrogen availability and plant functional group ($p = 0.041$; Table
1509 4.4) indicated that the positive effect of increasing soil nitrogen ($p = 0.007$; Table
1510 4.4) was only apparent in C₃ legumes (Tukey: $p < 0.001$; Table 4.4; Fig. 4.4d),
1511 with no observable effect in C₃ nonlegumes (Tukey: $p = 0.449$) or C₄ nonlegumes
1512 (Tukey: $p = 0.680$). Increasing soil moisture increased N_{area} ($p=0.010$, Table
1513 4.4). A plant functional group effect ($p < 0.001$; Table 4.4) indicated that C₄
1514 nonlegumes had lower N_{area} compared to C₃ legumes (Tukey: $p < 0.001$) and C₃
1515 nonlegumes (Tukey: $p < 0.001$), while C₃ legumes had lower N_{area} compared to
1516 C₃ nonlegumes (Tukey: $p = 0.030$).

1517 A marginal interaction between soil nitrogen availability and soil moisture
1518 ($p = 0.097$; Table 4.4) indicated that the positive effect of increasing soil nitrogen
1519 on N_{mass} ($p < 0.001$; Table 4.4; Fig. 4.4e) was only apparent when soil moisture
1520 was less than 50% of the maximum water holding capacity (Tukey: $p < 0.05$ in
1521 all cases). There was no effect of leaf $C_i:C_a$ on N_{mass} ($p = 0.447$; Table 4.4; Fig.
1522 4.4b), but a positive effect of increasing soil moisture on N_{mass} . A plant functional
1523 group effect ($p < 0.001$; Table 4.4) indicated that C₄ nonlegumes had lower N_{mass}
1524 compared to C₃ legumes (Tukey: $p=0.003$) and C₃ nonlegumes (Tukey: $p =$
1525 0.011), while N_{mass} did not differ between C₃ legumes and C₃ nonlegumes (Tukey:

1526 $p = 0.231$).

1527 Variance in M_{area} was driven by a three-way interaction between soil ni-
1528 trogen availability, soil moisture, and plant functional group ($p = 0.018$; Table
1529 4.4). This interaction indicated that increasing soil moisture increased the posi-
1530 tive effect of increasing soil nitrogen availability on M_{area} in C₃ legumes (Tukey:
1531 $p = 0.030$) but did not modify the negative effect of increasing soil nitrogen on
1532 M_{area} in C₄ nonlegumes (Tukey: $p = 0.511$) or C₃ nonlegumes (Tukey: $p > 0.999$).
1533 There was otherwise no effect of soil moisture on M_{area} ($p = 0.696$; Table 4.4).
1534 An interaction between leaf $C_i:C_a$ and plant functional group ($p < 0.001$; Table
1535 4.4; Fig. 4.4c) indicated that negative effect of increasing leaf $C_i:C_a$ on M_{area} (p
1536 < 0.001 ; Table 4.4) was driven by a negative effect of increasing leaf $C_i:C_a$ on
1537 M_{area} in C₃ legumes and C₃ nonlegumes (Tukey: $p < 0.001$ in both cases), with
1538 no effect in C₄ nonlegumes (Tukey: $p = 0.343$; Fig. 4.4c).

Table 4.4. Effects of soil nitrogen fertilization, inoculation, and CO₂ treatments on N_{area} , N_{mass} , and M_{area}

	df	N_{area}			N_{mass}			M_{area}		
		Coefficient	χ^2	p	Coefficient	χ^2	p	Coefficient	χ^2	p
(Intercept)	-	2.41E+00	-	-	6.28E-02	-	-	6.90E+00	-	-
$C_i:C_a$	1	-2.32E+00	7.386	0.007	8.04E-01	0.578	0.447	-3.13E+00	15.913	<0.001
Soil N (N)	1	1.26E-02	6.070	0.014	1.12E-02	90.940	<0.001	-2.66E-02	43.529	<0.001
Soil moisture (SM ₉₀)	1	5.60E-01	6.717	0.010	7.81E-01	11.205	<0.001	-2.53E-01	0.153	0.696
PFT	1	-	52.277	<0.001	-	17.184	<0.001	-	7.289	0.026
SM ₉₀ *N	1	5.44E-02	0.444	0.505	-1.91E-02	2.749	0.097	8.16E-02	1.690	0.194
$C_i:C_a$ *PFT	1	-	25.631	<0.001	-	4.864	0.078	-	34.683	<0.001
N*PFT	1	-	6.389	0.041	-	1.219	0.544	-	19.949	<0.001
SM ₉₀ *PFT	1	-	3.548	0.170	-	0.911	0.634	-	3.293	0.193
SM ₉₀ *N*PFT	1	-	3.520	0.172	-	0.092	0.955	-	7.987	0.018

939 *Significance determined using Type II Wald χ^2 tests ($\alpha = 0.05$). P-values less than 0.05 are in bold and p-values
 1540 where $0.05 < p < 0.1$ are italicized. Coefficients are reported on the natural-log scale and are only included for
 1541 continuous fixed effects.

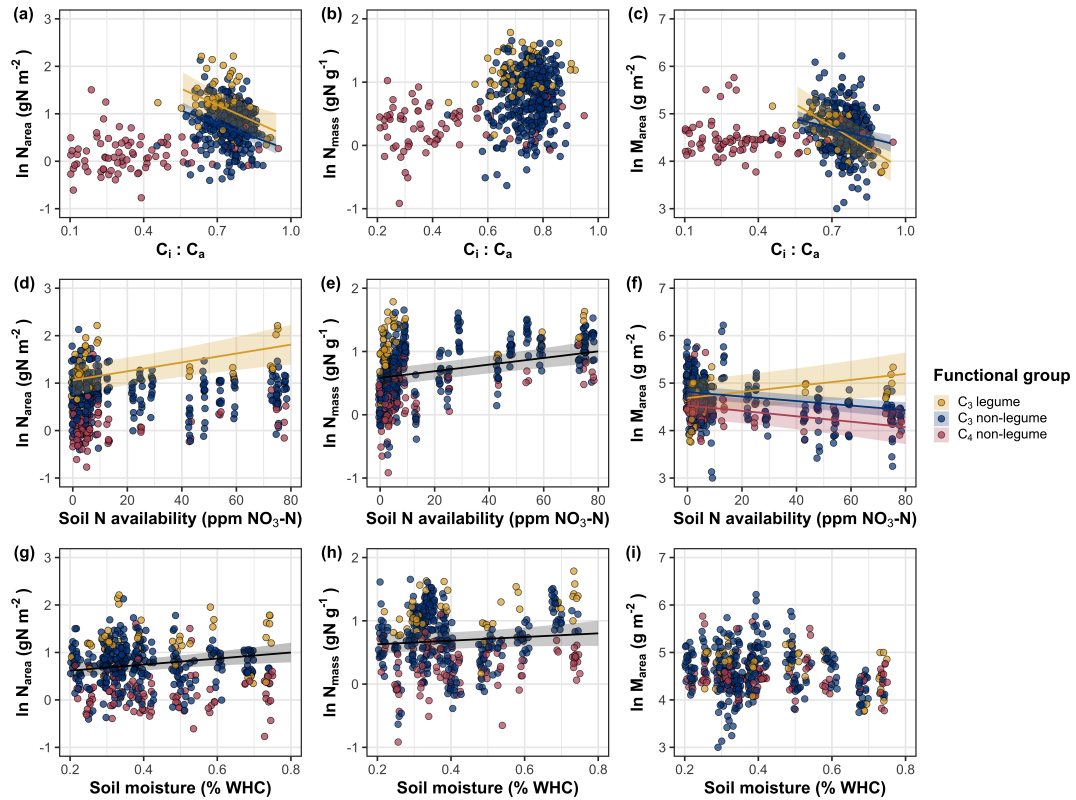


Figure 4.4. Effects of leaf $C_i:C_a$ (a-c), soil nitrogen availability (d-f), and soil moisture (g-i) on leaf nitrogen content per unit leaf area (a, d, g), leaf nitrogen content per unit leaf biomass (b, e, h), and leaf mass per area (c, f, i). Yellow points and trendlines indicate C₃ legumes, blue points and trendlines indicate C₃ nonlegumes, and red points and trendlines indicate C₄ nonlegumes. Points are jittered for visibility. Variably colored trendlines are only included if there is an interaction between plant functional group and the x-axis. Black solid trendlines denote bivariate slopes that are different from zero ($p < 0.05$) where there is no apparent interaction between plant functional group and the x-axis.

1542 4.3.4 *Structural equation model*

1543 The piecewise structural equation model explained 89%, 56%, 77%, 82%, and 37%
1544 of variance in N_{area} , N_{mass} , M_{area} , leaf $C_i:C_a$, and β , respectively (Table 4.5; Fig.
1545 4.5). Variance in N_{area} was driven by a positive effect of increasing N_{mass} and
1546 M_{area} ($p < 0.001$ in both cases; Table 4.5; Fig. 4.5). Model results indicated that
1547 an indirect negative effect of $C_i:C_a$ on N_{area} was driven by a strong reduction in
1548 M_{area} with increasing leaf $C_i:C_a$ ($p < 0.001$; Table 4.5) paired with no effect of
1549 increasing $C_i:C_a$ on N_{mass} ($p = 0.111$; Table 4.5). However, there was a strong
1550 negative effect of increasing M_{area} on N_{mass} ($p < 0.001$; Table 4.5; Fig. 4.5).
1551 Leaf $C_i:C_a$ increased with increasing β ($p < 0.001$; Table 4.5) and decreased with
1552 increasing VPD ($p < 0.001$; Table 4.5; Fig. 4.5). Variance in β was driven by a
1553 negative effect of increasing soil nitrogen availability ($p < 0.001$; Table 4.5) and
1554 was generally higher in C3 species ($p < 0.001$; Table 4.5; Fig. 4.5). However,
1555 β did not change with soil moisture ($p = 0.904$; Table 4.5) or with ability to
1556 acquire nitrogen via symbiotic nitrogen fixation ($p = 0.495$; Table 4.5). Finally,
1557 soil nitrogen availability was positively associated with increasing soil moisture (p
1558 = 0.002; Table 4.5; Fig. 4.5).

Table 4.5. Structural equation model results investigating direct effects of climatic and soil resource availability on N_{area} , N_{mass} , M_{area} , leaf $C_i:C_a$, and β

Predictor	Coefficient	<i>p</i>
N_{area} ($R^2_c = 0.89$)		
M_{area}	0.758	<0.001
N_{mass}	0.781	<0.001
N_{mass} ($R^2_c = 0.56$)		
Leaf $C_i:C_a$	0.092	0.111
M_{area}	-0.311	<0.001
M_{area} ($R^2_c = 0.77$)		
Leaf $C_i:C_a$	-0.237	<0.001
Leaf $C_i:C_a$ ($R^2_c = 0.82$)		
β	0.309	<0.001
VPD_4	-0.110	<0.001
β ($R^2_c = 0.37$)		
Soil N	-0.213	<0.001
SM_{90}	-0.006	0.904
Photo. pathway	0.446	<0.001
N-fixing ability	-0.056	0.495
Soil N ($R^2_c = 0.35$)		
SM_{90}	-0.154	0.002

1559 *Reported coefficients are standardized across the structural equation model. *P*-
1560 values less than 0.05 are noted in bold. Positive coefficients for photosynthetic
1561 pathway indicate generally larger values in C₃ species, while positive coefficients
1562 for N-fixing ability indicate generally larger values in N-fixing species. Key: N_{area}
1563 = leaf nitrogen content per unit leaf area, M_{area} = leaf mass per unit leaf dry
1564 biomass, N_{mass} = leaf nitrogen content per unit leaf dry biomass, β = cost of
1565 acquiring nitrogen relative to water, VPD_4 = 4-day mean vapor pressure deficit,
1566 SM_{90} = 90-day mean soil moisture, R^2_c = conditional R² value

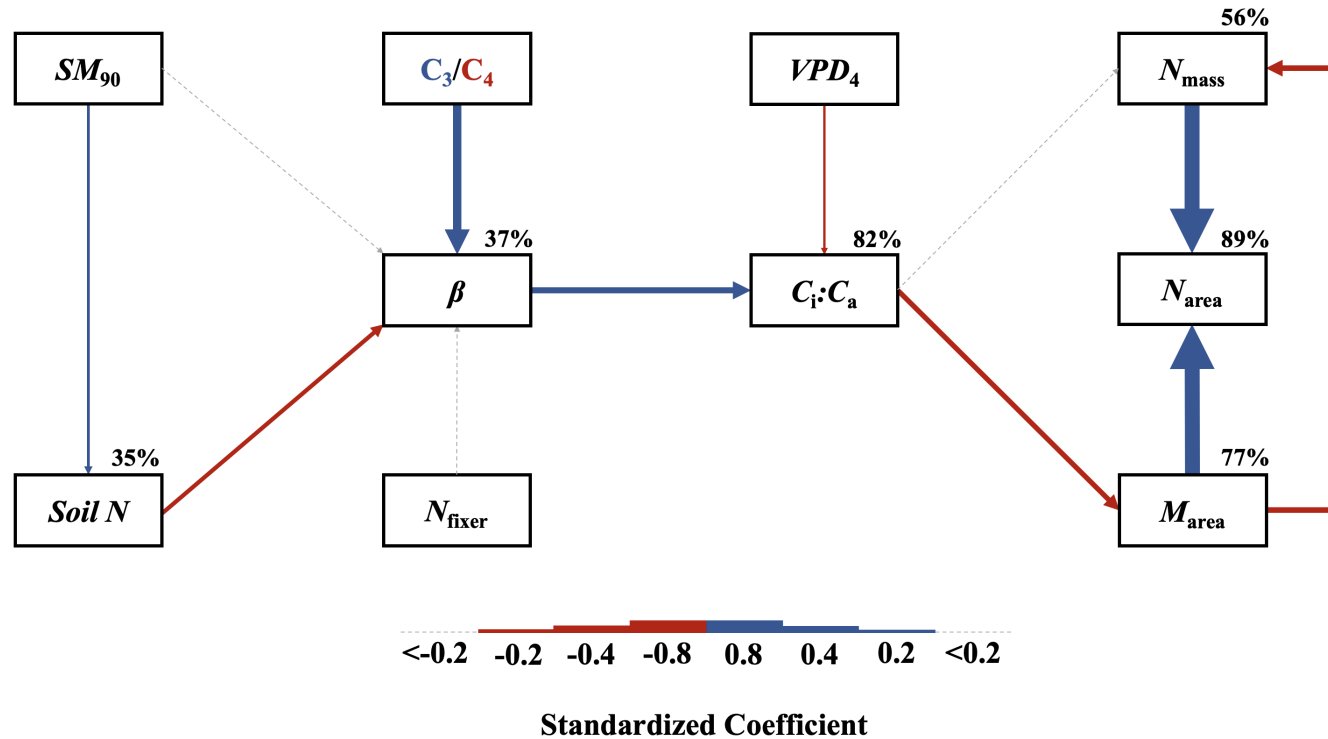


Figure 4.5. Structural equation model results exploring drivers of N_{area} . Boxes indicate measured edaphic factors, climatic factors, and leaf traits. Solid arrows indicate bivariate relationships where $p < 0.05$, while dashed arrows indicate relationships where $p > 0.05$. Positive model coefficients are indicated through blue arrows, negative model coefficients are indicated through red arrows, and insignificant coefficients ($p > 0.05$) are indicated through gray dashed arrows. Arrow thickness scales with the standardized model coefficient of each bivariate relationship. A positive coefficient for photosynthetic pathway indicates larger values in C_3 species, while a positive coefficient for N_{fixer} indicates larger values in N-fixing species. Standardized model coefficients and associated p -values are reported in Table 4.5, with conditional R^2 values for each response variable reported on the top right of each box.

1567 4.4 Discussion

1568 In this study, we quantified direct and indirect effects of soil resource availability,
1569 climate, leaf $C_i:C_a$, and β on N_{area} and components of N_{area} (N_{mass} and M_{area}) in
1570 520 individuals spanning across a soil resource availability and climate gradient
1571 in Texas, USA. We found consistent support for patterns expected from photo-
1572 synthetic least-cost theory, a result driven by a strong direct negative relationship
1573 between the relative costs to acquire nitrogen versus water (β) on N_{area} as me-
1574 diated through changes in the leaf $C_i:C_a$ ratio. In further support of patterns
1575 expected from theory, increasing soil nitrogen availability had a strong negative
1576 effect on β , resulting in an indirect stimulation in N_{area} . Increasing VPD also
1577 indirectly increased N_{area} through a direct negative effect of increasing VPD on
1578 leaf $C_i:C_a$. Interestingly, a strong positive association between soil moisture and
1579 N_{area} was driven by positive covariance between soil moisture and soil nitrogen
1580 availability and was not associated with a direct effect of soil moisture on β .
1581 Overall, results provide strong and consistent support for patterns expected from
1582 photosynthetic least-cost theory, showing that both soil resource availability and
1583 climate drive variance in N_{area} through changes in leaf $C_i:C_a$.

1584 4.4.1 *Negative effects of leaf $C_i:C_a$ on N_{area} are driven by reductions in M_{area} ,*
1585 *not N_{mass}*

1586 A strong negative effect of increasing leaf $C_i:C_a$ on N_{area} was detected in both
1587 the linear mixed effect and piecewise structural equation models. The negative
1588 response of N_{area} to increasing leaf $C_i:C_a$ is consistent with previous environmental
1589 gradient (Dong et al. 2017; Querejeta et al. 2022) and manipulation experiments

1590 (Perkowski et al. n.d.), showing strong support for the nitrogen-water use tradeoffs
1591 expected from photosynthetic least cost theory (Wright et al. 2003; Prentice et al.
1592 2014). Negative effects of increasing leaf $C_i:C_a$ on N_{area} were driven by a strong
1593 negative effect of increasing $C_i:C_a$ on M_{area} , with no apparent effect of leaf $C_i:C_a$
1594 on N_{mass} , suggesting that changes in N_{area} were driven by changes in leaf structure
1595 and not leaf chemistry. Interestingly, increasing M_{area} was negatively associated
1596 with N_{mass} , indicating that an increase in N_{mass} was associated with larger, thinner
1597 leaves (i.e. lower M_{area}). These results are consistent with patterns reported
1598 from previous studies indicating that variance in N_{area} is driven by changes in
1599 M_{area} across environmental gradients, and that part of this response is due to
1600 negative covariance between M_{area} and N_{mass} associated with tradeoffs between
1601 leaf longevity and leaf productivity (Wright et al. 2004; Dong et al. 2017; Dong
1602 et al. 2022; Querejeta et al. 2022; Wang et al. 2023).

1603 The negative relationship between leaf $C_i:C_a$ and M_{area} could be also re-
1604 sponse that allows leaves to maximize productivity in shorter-lived leaves. Trade-
1605 offs between leaf longevity and leaf productivity are commonly observed and are
1606 included in a continuum of coordinated leaf traits that position individuals along
1607 a fast- or slow-growing leaf economics spectrum (Wright et al. 2003; Onoda et al.
1608 2004; Onoda et al. 2017; Reich 2014; Wang et al. 2023). Negative relationships
1609 between $C_i:C_a$ and M_{area} indicate that increased stomatal conductance and re-
1610 duced water use efficiency were associated with thinner, larger leaves (i.e., lower
1611 M_{area}). These patterns, combined with the negative relationship between M_{area}
1612 and N_{mass} mentioned above, likely allowed individuals to maximize light intercep-
1613 tion and productivity by exploiting high light environments, though this may come

1614 at the expense of increased water loss and decreased water-use efficiency. This
1615 strategy may be especially advantageous for fast-growing species in open canopy
1616 systems. In this study, C₃ legumes and C₃ nonlegumes dominated the dataset
1617 (78% of total sampling effort), of which 22% (17% of total sampling effort) were
1618 classified as annual species with short growing seasons. We observed no effect of
1619 leaf C_i:C_a on N_{area} or M_{area} in C₄ nonlegumes, which made up 22% of the sampling
1620 effort and were generally classified as warm season graminoid species with slower
1621 growth rates and longer growing seasons. These patterns indicate that stronger
1622 tradeoffs between nitrogen and water use may be more apparent in fast-growing
1623 species with high demand for building and maintaining productive leaf tissues.

1624 4.4.2 *Soil nitrogen availability increases N_{area} through changes in the cost to*
1625 *acquire nitrogen*

1626 The null effect of soil nitrogen availability on N_{area} was driven by positive
1627 and negative respective effects of increasing soil nitrogen availability on N_{mass} and
1628 M_{area} that were equal in magnitude. The null response of N_{area} to soil nitrogen
1629 availability occurred alongside a negative effect of increasing soil nitrogen availabil-
1630 ity on β , which, paired with the negative relationship between leaf C_i:C_a and N_{area},
1631 suggests a general positive effect of increasing soil nitrogen availability on N_{area},
1632 but only when mediated through changes in β . This result is consistent with our
1633 hypotheses and patterns expected from photosynthetic least-cost theory. These
1634 results suggest that positive direct effects of increasing soil nitrogen availability
1635 on N_{area} are not ubiquitous across environmental gradients. Instead, as predicted
1636 by our hypotheses and patterns expected from theory, positive responses of N_{area}

1637 to increasing soil nitrogen availability are a deterministic acclimation response to
1638 shifts in climate-related demand to build and maintain photosynthetic enzymes,
1639 which allows plants to optimize photosynthetic processes and resource use to a
1640 given environment (Paillassa et al. 2020; Peng et al. 2021; Dong et al. 2022;
1641 Westerband et al. 2023).

1642 4.4.3 *Soil moisture increases N_{area} by facilitating increases in soil nitrogen
1643 availability*

1644 Increasing soil moisture generally had no effect on N_{area} , a response that was as-
1645 sociated with a null effect of soil moisture on β . These results contrast patterns
1646 expected from theory, where increasing soil moisture is expected to indirectly de-
1647 crease N_{area} through an increase in β due to a reduction in costs associated with
1648 water acquisition and use (Wright et al. 2003; Prentice et al. 2014; Lavergne
1649 et al. 2020). Interestingly, structural equation model results revealed a strong
1650 positive association between soil moisture and soil nitrogen availability, indicat-
1651 ing an indirect positive effect of increasing soil moisture on N_{area} mediated by the
1652 negative effect of increasing soil nitrogen availability on β . In Texan grasslands,
1653 productivity and nutrient uptake are often co-limited by precipitation and nutrient
1654 availability (Yahdjian et al. 2011; Wang et al. 2017). Thus, increases in soil mois-
1655 ture may have facilitated more favorable and productive environments for soil
1656 microbial communities, thereby stimulating the accumulation of plant-available
1657 nitrogen substrate through increased ammonification or nitrification rates (Reich-
1658 man et al. 1966; Stark and Firestone 1995; Paul et al. 2003). Alternatively, soil
1659 moisture may have facilitated greater nitrogen mobility through soil solution. As
1660 discussed above, the positive indirect response of N_{area} to increasing soil nitrogen
1661 availability as mediated through reductions in β follow patterns expected from

1662 theory.

1663 4.4.4 *Indirect effects of climate on N_{area} are mediated through changes in leaf*
1664 $C_i:C_a$ *and β*

1665 In support of our hypothesis and patterns expected from theory, increasing VPD
1666 indirectly increased N_{area} , mediated through the negative effect of increasing VPD
1667 on leaf $C_i:C_a$. These responses are consistent with previous work noting strong
1668 reductions in stomatal conductance with increasing VPD (Oren et al. 1999; Novick
1669 et al. 2016; Sulman et al. 2016; Grossiord et al. 2020; López et al. 2021), a
1670 response that allows plants to minimize water loss as a result of high atmospheric
1671 water demand. Results also support findings from previous experiments across
1672 environmental gradients, where increasing VPD generally increases N_{area} at lower
1673 stomatal conductance across environmental gradients (Dong et al. 2017; Dong
1674 et al. 2022; Paillassa et al. 2020; Westerband et al. 2023).

1675 4.4.5 *Species identity traits modify effects of the environment on β , leaf $C_i:C_a$,*
1676 *and N_{area}*

1677 N-fixing species generally had higher N_{area} values on average compared to non-
1678 fixing species, a pattern driven by a stronger stimulation in N_{mass} in N-fixing
1679 species coupled with no change in M_{area} between species with different N-fixation
1680 ability. We found no evidence to suggest that N-fixing species had different β or
1681 leaf $C_i:C_a$ values compared to non-fixing species across the environmental gradient.
1682 These results follow patterns from previous environmental gradient experiments
1683 that investigate variance in leaf nitrogen allocation in N-fixing species (Adams
1684 et al. 2016; Dong et al. 2017; Dong et al. 2020), and that increases in N_{mass}
1685 and N_{area} in N-fixing species are not necessarily correlated to increases in water

1686 use efficiency or reductions in leaf $C_i:C_a$ (Adams et al. 2016). While our results
1687 are consistent with results from previous environmental gradient experiments,
1688 they do not necessarily support our hypothesis or patterns expected from theory,
1689 which predicts that stimulations in N_{area} by N-fixing species should be driven
1690 by a reduction in β relative to non-fixing species, and that this response should
1691 decrease stomatal conductance and leaf $C_i:C_a$.

1692 C_4 species generally had lower β , leaf $C_i:C_a$, and N_{area} than C_3 species.
1693 Reduced β and leaf $C_i:C_a$ values in C_4 species follow our hypothesis, a pattern
1694 that could be the result of either reduced costs of nitrogen acquisition and use or
1695 increased costs of water acquisition and use or both (Wright et al. 2003, Prentice
1696 et al. 2014). Results also indicate that β in C_4 nonlegumes was unresponsive to
1697 changes in soil nitrogen availability despite an apparent negative effect of increas-
1698 ing soil nitrogen availability on β in C_3 legumes and C_3 nonlegumes. Combined
1699 with a general null response of β to soil moisture regardless of plant functional
1700 group, these patterns imply that reduced β values in C_4 species may be the re-
1701 sult of lower costs of nitrogen acquisition and use relative to C_3 species. While
1702 lower β values in C_4 species provides a possible explanation for why C_4 species
1703 often have lower leaf $C_i:C_a$ and greater water use efficiency, theory predicts that
1704 this response should cause C_4 species to have greater N_{area} values compared to
1705 C_3 species, though C_4 species commonly exhibit lower N_{area} and higher nitrogen
1706 use efficiency than C_3 species (Schmitt and Edwards 1981; Sage and Pearcy 1987;
1707 Ghannoum et al. 2011). We speculate that lowered costs of nitrogen acquisition
1708 and use in C_4 species could be driven by more efficient Rubisco carboxylation effi-
1709 ciency in C_4 species associated with CO_2 concentrating mechanisms that eliminate

1710 photorespiration (Ghannoum et al. 2011), which could reduce or eliminate the
1711 need to sacrifice inefficient nitrogen use for efficient water use to achieve optimal
1712 photosynthesis rates.

1713 4.4.6 *Next steps for optimality model development*

1714 Optimality models for both C₃ and C₄ species have been developed using principles
1715 from photosynthetic least-cost theory (Prentice et al. 2014; Wang et al. 2017;
1716 Smith et al. 2019; Stocker et al. 2020; Scott and Smith 2022). In both C₃ and
1717 C₄ model variants, β values are held constant using global datasets of leaf $\delta^{13}\text{C}$
1718 (Wang et al. 2017; Cornwell et al. 2018). Specifically, the C₃ optimality model
1719 initially assumed a constant β value of 240 (Wang et al. 2017), later corrected to
1720 146 (Stocker et al. 2020), while the C₄ optimality model assumes a constant β
1721 value of 166 (Scott and Smith 2022). Our results, which build on findings from
1722 Paillassa et al. (2020), demonstrate high variability in calculated β values across
1723 environmental gradients. Specifically, β values in C₃ species ranged from 1.7 to
1724 188.0 (mean: 30.2; median: 23.1; standard deviation: 25.4), while ranged from 0.1
1725 to 110.6 in C₄ species (mean: 7.2; median: 0.7; standard deviation: 18.6). Mean
1726 β values in both C₃ and C₄ species were consistently lower than values currently
1727 implemented in optimality models, though this was likely the result of increased
1728 water limitation across our sites relative to global averages. Regardless, the high
1729 degree of β variability across this environmental gradient, together with findings
1730 from Lavergne et al. (2020) and Paillassa et al. (2020), suggests that the use of
1731 constant β values may contribute to erroneous errors when conducting optimality
1732 model simulations. We therefore build on suggestions from Wang et al. (2017),
1733 recommending future photosynthetic least-cost model developments to consider

1734 the use of dynamic β values.

1735 4.4.7 *Conclusions*

1736 To summarize, variability in N_{area} across an environmental gradient in Texan
1737 grasslands was driven by indirect effects of climate and soil resource availability
1738 mediated. Results from this experiment provide strong and consistent support
1739 for patterns expected from photosynthetic least-cost theory, demonstrating that
1740 negative relationships between $C_i:C_a$ and N_{area} unify expected effects of climatic
1741 and edaphic characteristics on N_{area} across environmental gradients. Our results
1742 also demonstrate a need to consider the dynamic nature of the relative cost of
1743 nitrogen versus water uptake (β) across environmental gradients in optimality
1744 models that leverage principles of photosynthetic least-cost theory.

1745

Chapter 5

1746 Optimal resource investment to photosynthetic capacity maximizes
1747 nutrient allocation to whole plant growth under elevated CO₂

1748 5.1 Introduction

1749 Terrestrial ecosystems are regulated by complex carbon and nitrogen cy-
1750 cles. As a result, terrestrial biosphere models, which are beginning to include
1751 coupled carbon and nitrogen cycles (Shi et al. 2016; Davies-Barnard et al. 2020;
1752 Braghieri et al. 2022), must accurately represent these cycles under different
1753 environmental scenarios to reliably simulate carbon and nitrogen atmosphere-
1754 biosphere fluxes (Hungate et al. 2003; Prentice et al. 2015). While the inclusion
1755 of coupled carbon and nitrogen cycles tends to reduce model uncertainty (Arora
1756 et al. 2020), large uncertainty in role of soil nitrogen availability and nitrogen ac-
1757 quisition strategy on leaf and whole plant acclimation responses to CO₂ remains
1758 (Smith and Dukes 2013; Terrer et al. 2018; Smith and Keenan 2020). This source
1759 of uncertainty likely contributes to the widespread divergence in future carbon
1760 and nitrogen flux simulations across terrestrial biosphere models (Friedlingstein
1761 et al. 2014; Zaehle et al. 2014; Meyerholt et al. 2020).

1762 Plants grown under elevated CO₂ generally have less leaf nitrogen content
1763 than those grown under ambient CO₂, a response that often corresponds with
1764 reductions in photosynthetic capacity and stomatal conductance at the leaf-level
1765 and biomass stimulation over time at the whole plant level (Curtis 1996; Drake
1766 et al. 1997; Ainsworth et al. 2002; Makino 2003; Morgan et al. 2004; Ainsworth
1767 and Long 2005; Ainsworth and Rogers 2007; Smith and Dukes 2013; Poorter et al.
1768 2022). As net primary productivity is generally limited by nitrogen availability

1769 (Vitousek and Howarth 1991; LeBauer and Treseder 2008; Fay et al. 2015), and
1770 soil nitrogen availability is often positively correlated with leaf nitrogen content
1771 and photosynthetic capacity (Field and Mooney 1986; Evans and Seemann 1989;
1772 Evans 1989; Walker et al. 2014; Firn et al. 2019; Liang et al. 2020), some
1773 have hypothesized that leaf and whole plant acclimation responses to CO₂ are
1774 constrained by soil nitrogen availability. The progressive nitrogen limitation hy-
1775 pothesis predicts that elevated CO₂ will increase plant nitrogen demand, which
1776 will increase plant nitrogen uptake and progressively deplete soil nitrogen if soil
1777 nitrogen supply does not exceed plant nitrogen demand (Luo et al. 2004). The
1778 hypothesis predicts that this response should result in strong acute stimulations in
1779 whole plant growth and primary productivity that diminish over time as nitrogen
1780 becomes more limiting. Assuming a positive relationship between soil nitrogen
1781 availability, leaf nitrogen content, and photosynthetic capacity, this hypothesis
1782 also implies that progressive reductions in soil nitrogen availability should be the
1783 mechanism that drives the downregulation in leaf nitrogen content and photosyn-
1784 thetic capacity under elevated CO₂. This hypothesis has received some support
1785 from free air CO₂ enrichment experiments (Reich et al. 2006; Norby et al. 2010),
1786 although is not consistently observed across experiments (Finzi et al. 2006; Moore
1787 et al. 2006; Liang et al. 2016).

1788 While possible that progressive nitrogen limitation may determine leaf and
1789 whole plant acclimation responses to CO₂, growing evidence indicates that leaf ni-
1790 trogen and photosynthetic capacity are more strongly determined through above-
1791 ground growing conditions than by soil resource availability (Dong et al. 2017;
1792 Dong et al. 2020; Dong et al. 2022; Smith et al. 2019; Smith and Keenan 2020;

1793 Paillassa et al. 2020; Peng et al. 2021; Querejeta et al. 2022; Westerband et al.
1794 2023), and satellite-derived chlorophyll fluorescence data indicate that increasing
1795 atmospheric CO₂ may decrease leaf and canopy demand for nitrogen (Dong et al.
1796 2022). Together, results from these studies suggest that the downregulation in
1797 leaf nitrogen content and photosynthetic capacity due to increasing CO₂ may not
1798 be as tightly linked to progressive nitrogen limitation as previously hypothesized.

1799 A unification of optimal coordination and photosynthetic least-cost the-
1800 ories predicts that leaves acclimate to elevated CO₂ by downregulating nitrogen
1801 allocation to Ribulose-1,5-bisphosphate (RuBP) carboxylase/oxygenase (Rubisco)
1802 to optimize resource use efficiencies at the leaf level, which allows for greater re-
1803 source allocation to whole plant growth (Drake et al. 1997; Wright et al. 2003;
1804 Prentice et al. 2014; Smith et al. 2019). The theory predicts that the downregu-
1805 lation in nitrogen allocation to Rubisco results in a stronger downregulation in the
1806 maximum rate of Rubisco carboxylation (V_{cmax}) than the maximum rate of RuBP
1807 regeneration (J_{max}), which maximizes photosynthetic efficiency by allowing net
1808 photosynthesis rates to be equally co-limited by Rubisco carboxylation and RuBP
1809 regeneration (Chen et al. 1993; Maire et al. 2012). This acclimation response
1810 allows plants to make more efficient use of available light while avoiding overin-
1811 vestment in Rubisco, which has high nitrogen and energetic costs of building and
1812 maintaining (Evans 1989; Evans and Clarke 2019). Instead, additional acquired
1813 resources not needed to optimize leaf photosynthesis are allocated to the mainte-
1814 nance of structures that support whole plant growth (e.g., total leaf area, whole
1815 plant biomass, etc.) or to allocation processes not related to leaf photosynthesis
1816 or growth, such as plant defense mechanisms or leaf structural tissue. Regardless,

1817 optimized resource allocation at the leaf level should allow for greater resource
1818 allocation to whole plant growth. The theory indicates that leaf acclimation re-
1819 sponses to CO₂ should be independent of changes in soil nitrogen availability.
1820 While this leaf acclimation response maximizes nitrogen allocation to structures
1821 that support whole plant growth, the theory suggests that the positive effect of
1822 elevated CO₂ on whole plant growth may be further stimulated by soil nitrogen
1823 availability through a reduction in the cost of acquiring nitrogen (Bae et al. 2015;
1824 Perkowski et al. 2021; Lu et al. 2022).

1825 Plants acquire nitrogen by allocating photosynthetically derived carbon be-
1826 lowground in exchange for nitrogen through different nitrogen acquisition strate-
1827 gies. These nitrogen acquisition strategies can include direct uptake pathways
1828 such as mass flow or diffusion (Barber 1962), symbioses with mycorrhizal fungi or
1829 symbiotic nitrogen-fixing bacteria (Vance and Heichel 1991; Marschner and Dell
1830 1994; Smith and Read 2008; Udvardi and Poole 2013), or through the release
1831 of root exudates that prime free-living soil microbial communities (Phillips et al.
1832 2011; Wen et al. 2022). Plants cannot acquire nitrogen without first allocating
1833 carbon belowground, which implies an inherent carbon cost to the plant for acquir-
1834 ing nitrogen regardless of nitrogen acquisition strategy. Carbon costs to acquire
1835 nitrogen often vary in species with different nitrogen acquisition strategies and
1836 are dependent on external environmental factors such as atmospheric CO₂, light
1837 availability, and soil nitrogen availability (Brzostek et al. 2014; Terrer et al. 2016;
1838 Terrer et al. 2018; Allen et al. 2020; Perkowski et al. 2021; Lu et al. 2022), which
1839 suggests that acquisition strategy may be an important factor in determining ef-
1840 fects of soil nitrogen availability on leaf and whole plant acclimation responses to

1841 elevated CO₂.

1842 A recent meta-analysis using data across 20 grassland and forest CO₂ en-
1843 richment experiments suggested that species which acquire nitrogen from sym-
1844 biotic nitrogen-fixing bacteria had reduced costs of nitrogen acquisition under
1845 elevated CO₂ (Terrer et al. 2018). Findings from this meta-analysis indicated
1846 that reductions in costs of nitrogen acquisition in species that form associations
1847 with symbiotic nitrogen-fixing bacteria under elevated CO₂ may drive stronger
1848 stimulations in whole plant growth and downregulations in V_{cmax} than species that
1849 associate with arbuscular mycorrhizal fungi (Smith and Keenan 2020), which gen-
1850 erally have higher costs of nitrogen acquisition under elevated CO₂ (Terrer et al.
1851 2018). However, plant investments in symbiotic nitrogen fixation generally de-
1852 cline with increasing nitrogen availability (Dovrat et al. 2018; Perkowski et al.
1853 2021), a response that has been previously inferred to be the result of a shift in
1854 the dominant mode of nitrogen acquisition to direct uptake pathways as costs of
1855 direct uptake decrease with increasing soil nitrogen availability (Rastetter et al.
1856 2001; Perkowski et al. 2021). Thus, effects of symbiotic nitrogen fixation on plant
1857 acclimation responses to CO₂ should decline with increasing soil nitrogen avail-
1858 ability, although manipulative experiments that directly test these patterns are
1859 rare.

1860 Here, I conducted a 7-week growth chamber experiment using *Glycine max*
1861 L. (Merr.) to examine the effects of soil nitrogen fertilization and inoculation with
1862 symbiotic nitrogen-fixing bacteria on leaf and whole plant acclimation responses
1863 to elevated CO₂. Following patterns expected from theory, I hypothesized that in-
1864 dividual leaves should acclimate to elevated CO₂ by more strongly downregulating

1865 V_{cmax} relative to J_{max} , allowing leaf photosynthesis to approach optimal coordi-
1866 nation. I expected this response to correspond with a stronger downregulation in
1867 leaf nitrogen content than V_{cmax} and J_{max} , which would increase the fraction of
1868 leaf nitrogen content allocated to photosynthesis and photosynthetic nitrogen use
1869 efficiency. At the whole-plant level, I hypothesized that plants would acclimate
1870 to elevated CO₂ by stimulating whole plant growth and productivity, a response
1871 that would be driven by a strong positive response of total leaf area and above-
1872 ground biomass to elevated CO₂. I predicted that leaf acclimation responses to
1873 elevated CO₂ would be independent of soil nitrogen fertilization and inoculation
1874 with symbiotic nitrogen-fixing bacteria; however, I expected that increasing soil
1875 nitrogen fertilization would increase the positive effect of elevated CO₂ on mea-
1876 sures of whole plant growth due to a stronger reduction in the cost of acquiring
1877 nitrogen under elevated CO₂ with increasing fertilization. I also expected stronger
1878 stimulations in whole plant growth due to inoculation, but that this effect would
1879 only be apparent under low fertilization due to a reduction in root nodulation
1880 with increasing fertilization.

1881 5.2 Methods

1882 5.2.1 *Seed treatments and experimental design*

1883 *Glycine max* L. (Merr) seeds were planted in 144 6-liter surface sterilized
1884 pots (NS-600, Nursery Supplies, Orange, CA, USA) containing a steam-sterilized
1885 70:30 v:v mix of Sphagnum peat moss (Premier Horticulture, Quakertown, PA,
1886 USA) to sand (Pavestone, subsidiary of Quikrete Companies, Atlanta, GA, USA).
1887 Before planting, all *G. max* seeds were surface sterilized in 2% sodium hypochlorite

1888 for 3 minutes, followed by three separate 3-minute washes with ultrapure water
1889 (MilliQ 7000; MilliporeSigma, Burlington, MA USA). A subset of surface steril-
1890 ized seeds were inoculated with *Bradyrhizobium japonicum* (Verdesian N-Dure™
1891 Soybean, Cary, NC, USA) in a slurry following manufacturer recommendations
1892 (3.12 g inoculant and 241 g deionized water per 1 kg seed).

1893 Seventy-two pots were randomly planted with surface-sterilized seeds inoc-
1894 ulated with *B. japonicum*, while the remaining 72 pots were planted with surface-
1895 sterilized uninoculated seeds. Thirty-six pots within each inoculation treatment
1896 were randomly placed in one of two atmospheric CO₂ treatments (ambient and
1897 1000 μmol mol⁻¹ CO₂). Pots within each unique inoculation-by-CO₂ treatment
1898 combination randomly received one of nine soil nitrogen fertilization treatments
1899 equivalent to 0, 35, 70, 105, 140, 210, 280, 350, or 630 ppm N. Nitrogen fertil-
1900 ization treatments were created using a modified Hoagland solution (Hoagland
1901 and Arnon 1950) designed to keep concentrations of other macronutrients and
1902 micronutrients equivalent across treatments (Table S1). Pots received the same
1903 fertilization treatment throughout the entire duration experiment, which were ap-
1904 plied twice per week in 150 mL doses as topical agents to the soil surface through-
1905 out the duration of the experiment. This experimental design yielded a fully
1906 factorial experiment with four replicates per unique fertilization-by-inoculation-
1907 by-CO₂ combination.

1908 5.2.2 *Growth chamber conditions*

1909 Upon experiment initiation, pots were randomly placed in one of six Per-
1910 cival LED-41L2 growth chambers (Percival Scientific Inc., Perry, IA, USA) over

1911 two experimental iterations due to chamber space limitation. Two iterations were
1912 conducted such that one iteration included all elevated CO₂ pots and the second
1913 iteration included all ambient CO₂ pots. Average (\pm SD) CO₂ concentrations
1914 across chambers throughout the experiment were $439 \pm 5 \mu\text{mol mol}^{-1}$ for the
1915 ambient CO₂ treatment and $989 \pm 4 \mu\text{mol mol}^{-1}$ for the elevated CO₂ treatment.

1916 Daytime growing conditions were simulated using a 16-hour photoperiod,
1917 with incoming light radiation set to chamber maximum (mean \pm SD: 1240 ± 32
1918 $\mu\text{mol m}^{-2} \text{s}^{-1}$ across chambers), air temperature set to 25°C, and relative humid-
1919 ity set to 50%. The remaining 8 hours simulated nighttime growing conditions,
1920 with incoming light radiation set to 0 $\mu\text{mol m}^{-2} \text{s}^{-1}$, chamber temperature set
1921 to 17°C, and relative humidity set to 50%. Transitions between daytime and
1922 nighttime growing conditions were simulated by ramping incoming light radiation
1923 in 45-minute increments and temperature in 90-minute increments over a 3-hour
1924 period (Table S2).

1925 Including the two, 3-hour ramping periods, pots grew under average (\pm
1926 SD) daytime light intensity of $1049 \pm 27 \mu\text{mol m}^{-2} \text{s}^{-1}$. In the elevated CO₂
1927 iteration, pots grew under $24.0 \pm 0.2^\circ\text{C}$ during the day, $16.4 \pm 0.8^\circ\text{C}$ during the
1928 night, and $51.6 \pm 0.4\%$ relative humidity. In the ambient CO₂ iteration, pots grew
1929 under $23.9 \pm 0.2^\circ\text{C}$ during the day, $16.0 \pm 1.4^\circ\text{C}$ during the night, and $50.3 \pm 0.2\%$
1930 relative humidity. We accounted for climatic differences across the six chambers
1931 by shuffling the same group of pots daily throughout the growth chambers. This
1932 process was done by iteratively moving the group of pots on the top rack of a
1933 chamber to the bottom rack of the same chamber, while simultaneously moving
1934 the group of pots on the bottom rack of a chamber to the top rack of the adjacent

1935 chamber. I moved pots within and across chambers every day throughout the
1936 course of each experiment iteration.

1937 5.2.3 *Leaf gas exchange measurements*

1938 Gas exchange measurements were collected for all individuals on the sev-
1939 enth week of development. All gas exchange measurements were collected on
1940 the center leaf of the most recent fully expanded trifoliate leaf set. Specifi-
1941 cally, I measured net photosynthesis (A_{net} ; $\mu\text{mol m}^{-2} \text{s}^{-1}$), stomatal conductance
1942 (g_{sw} ; $\text{mol m}^{-2} \text{s}^{-1}$), and intercellular CO₂ (C_i ; $\mu\text{mol mol}^{-1}$) concentrations across
1943 a range of atmospheric CO₂ concentrations (i.e., an A_{net}/C_i curve) using the
1944 Dynamic Assimilation Technique™. The Dynamic Assimilation Technique™ has
1945 been shown to correspond well with traditional steady-state CO₂ response curves
1946 in *G. max* (Saathoff and Welles 2021). A_{net}/C_i curves were generated along a
1947 reference CO₂ ramp down from 420 $\mu\text{mol mol}^{-1}$ CO₂ to 20 $\mu\text{mol mol}^{-1}$ CO₂, fol-
1948 lowed by a ramp up from 420 $\mu\text{mol mol}^{-1}$ CO₂ to 1620 $\mu\text{mol mol}^{-1}$ CO₂ after
1949 a 90-second wait period at 420 $\mu\text{mol mol}^{-1}$ CO₂. The ramp rate for each curve
1950 was set to 200 $\mu\text{mol mol}^{-1} \text{min}^{-1}$, logging every five seconds, which generated 96
1951 data points per response curve. All A_{net}/C_i curves were generated after A_{net} and
1952 g_{sw} stabilized in a LI-6800 cuvette set to a 500 mol s^{-1} , 10,000 rpm mixing fan
1953 speed, 1.5 kPa vapor pressure deficit, 25°C leaf temperature, 2000 $\mu\text{mol m}^{-2} \text{s}^{-1}$
1954 incoming light radiation, and initial reference CO₂ set to 420 $\mu\text{mol mol}^{-1}$.

1955 With the same focal leaf used to generate A_{net}/C_i curves, I measured dark
1956 respiration (R_{d25} ; $\mu\text{mol m}^{-2} \text{s}^{-1}$) following at least a 30-minute period of darkness.
1957 Measurements were collected on a 5-second log interval for 60 seconds after stabi-

1958 lizing in a LI-6800 cuvette set to a 500 mol s^{-1} , 10,000 rpm mixing fan speed, 1.5
1959 kPa vapor pressure deficit, 25°C leaf temperature, and $420 \mu\text{mol mol}^{-1}$ reference
1960 CO₂ concentration (for both CO² concentrations), with incoming light radiation
1961 set to $0 \mu\text{mol m}^{-2} \text{ s}^{-1}$. A single dark respiration value was determined for each
1962 focal leaf by calculating the mean dark respiration value (i.e. the absolute value
1963 of A_{net} during the logging period) across the logging interval.

1964 5.2.4 *Leaf trait measurements*

1965 The focal leaf used to generate A_{net}/C_i curves and dark respiration was
1966 harvested immediately following gas exchange measurements. Images of each focal
1967 leaf were curated using a flat-bed scanner to determine wet leaf area using the
1968 'LeafArea' R package (Katabuchi 2015), which automates leaf area calculations
1969 using ImageJ software (Schneider et al. 2012). Each leaf was dried at 65°C for
1970 at least 48 hours, and subsequently weighed and ground until homogenized. Leaf
1971 mass per area (M_{area} ; g m⁻²) was calculated as the ratio of dry leaf biomass
1972 to fresh leaf area. Using subsamples of ground and homogenized leaf tissue, I
1973 measured leaf nitrogen content (N_{mass} ; gN g⁻¹) through elemental combustion
1974 analysis (Costech-4010, Costech, Inc., Valencia, CA, USA). Leaf nitrogen content
1975 per unit leaf area (N_{area} ; gN m⁻²) was calculated by multiplying N_{mass} and M_{area} .

1976 I extracted chlorophyll content from a second leaf in the same trifoliolate
1977 leaf set as the focal leaf used to generate A_{net}/C_i curves. Prior to chlorophyll
1978 extraction, I used a cork borer to punch between 3 and 5 0.6 cm² disks from the
1979 leaf. Separate images of each punched leaf and set of leaf disks were curated using
1980 a flat-bed scanner to determine wet leaf area, again quantified using the 'LeafArea'

1981 R package (Katabuchi 2015). The punched leaf was dried and weighed after at
1982 least 65°C in the drying oven to determine M_{area} of the chlorophyll leaf.

1983 Leaf disks were shuttled into a test tube containing 10mL dimethyl sul-
1984 foxide, vortexed, and incubated at 65degreeC for 120 minutes (Barnes et al.
1985 1992). Incubated test tubes were vortexed again before loaded in 150 μL trip-
1986 licate aliquots to a 96-well plate. Dimethyl sulfoxide was also loaded in a 150
1987 μL triplicate aliquot as a blank. Absorbance measurements at 649.1 nm ($A_{649.1}$)
1988 and 665.1 nm ($A_{665.1}$) were read in each well using a plate reader (Biotek Synergy
1989 H1; Biotek Instruments, Winooski, VT USA) (Wellburn 1994), with triplicates
1990 subsequently averaged and corrected by the mean of the blank absorbance value.
1991 Blank-corrected absorbance values were used to estimate Chl_a ($\mu\text{g mL}^{-1}$) and
1992 Chl_b ($\mu\text{g mL}^{-1}$) following equations from Wellburn (1994):

$$Chl_a = 12.47A_{665.1} - 3.62A_{649.1} \quad (5.1)$$

1993 and

$$Chl_b = 25.06A_{665.1} - 6.50A_{649.1} \quad (5.2)$$

1994 Chl_a and Chl_b were converted to mmol mL^{-1} using the molar mass of chlorophyll a
1995 (893.51 g mol^{-1}) and the molar mass of chlorophyll b (907.47 g mol^{-1}), then added
1996 together to calculate total chlorophyll content in the dimethyl sulfoxide extractant
1997 (mmol mL^{-1}). Total chlorophyll content was multiplied by the volume of the
1998 dimethyl sulfoxide extractant (10 mL) and converted to area-based chlorophyll
1999 content by dividing by the total area of the leaf disks (Chl_{area} ; mmol m^{-2}). Mass-
2000 based chlorophyll content (Chl_{mass} ; mmol g^{-1}) was calculated by dividing Chl_{area}

2001 by the leaf mass per area of the punched leaf.

2002 5.2.5 *A/C_i curve fitting and parameter estimation*

2003 I fit A_{net}/C_i curves of each individual using the ‘fitaci’ function in the
2004 ‘plantecophys’ R package (Duursma 2015). This function estimates the maxi-
2005 mum rate of Rubisco carboxylation (V_{cmax} ; $\mu\text{mol m}^{-2} \text{s}^{-1}$) and maximum rate
2006 of electron transport for RuBP regeneration (J_{max} ; $\mu\text{mol m}^{-2} \text{s}^{-1}$) based on the
2007 Farquhar biochemical model of C₃ photosynthesis (Farquhar et al. 1980). Triose
2008 phosphate utilization (TPU) limitation was included in all curve fits, and all curve
2009 fits included measured dark respiration values. As A_{net}/C_i curves were generated
2010 using a common leaf temperature, curves were fit using Michaelis-Menten coeffi-
2011 cients for Rubisco affinity to CO₂ (K_c ; $\mu\text{mol mol}^{-1}$) and O₂ (K_o ; $\mu\text{mol mol}^{-1}$), and
2012 the CO₂ compensation point (Γ^* ; $\mu\text{mol mol}^{-1}$) reported in Bernacchi et al. (2001).
2013 Specifically, K_c was set to 404.9 $\mu\text{mol mol}^{-1}$, K_o was set to 278.4 $\mu\text{mol mol}^{-1}$, and
2014 Γ^* was set to 42.75 $\mu\text{mol mol}^{-1}$. The use of a common leaf temperature across
2015 curves and dark respiration measurements also eliminated the need to manually
2016 temperature standardize rate estimates. For clarity, I reference V_{cmax} , J_{max} , and
2017 R_d estimates throughout the rest of the paper as $V_{\text{cmax}25}$, $J_{\text{max}25}$, and R_{d25} .

2018 5.2.6 Stomatal limitation

2019 I quantified the extent by which stomatal conductance limited photosynthe-
2020 sis (l; unitless) following equations originally described in Farquhar and Sharkey
2021 (1982). Stomatal limitation was calculated as:

$$l = 1 - \frac{A_{net}}{A_{mod}} \quad (5.3)$$

2022 where A_{mod} represents the photosynthetic rate where $C_i = C_a$. A_{mod} was calcu-

2023 lated as:

$$A_{mod} = V_{cmax25} - \frac{420 - \Gamma^*}{420 + K_m} - R_{d25} \quad (5.4)$$

2024 K_m is the Michaelis-Menten coefficient for Rubisco-limited photosynthesis, calcu-

2025 lated as:

$$K_m = K_c \cdot \left(1 + \frac{O_i}{K_o}\right) \quad (5.5)$$

2026 where O_i refers to leaf intercellular O₂ concentrations, set to 210 μmol mol⁻¹.

2027 5.2.7 *Proportion of leaf nitrogen allocated to photosynthesis and structure*

2028 I used equations from Niinemets and Tenhunen (1997) to estimate the

2029 proportion of leaf N content allocated to Rubisco bioenergetics, and light harvest-

2030 ing proteins. The proportion of leaf N allocated to Rubisco (ρ_{rub} ; gN gN⁻¹) was

2031 calculated as a function of V_{cmax25} and N_{area} :

$$\rho_{rubisco} = \frac{V_{cmax25} N_r}{V_{cr} N_{area}} \quad (5.6)$$

2032 where N_r is the amount of nitrogen in Rubisco, set to 0.16 gN (gN in Rubisco)⁻¹

2033 and V_{cr} is the maximum rate of RuBP carboxylation per unit Rubisco protein,

2034 set to 20.5 μmol CO₂ (g Rubisco)⁻¹. The proportion of leaf nitrogen allocated to

2035 bioenergetics (ρ_{bioe} ; gN gN⁻¹) was similarly calculated as a function of J_{max25} and

2036 N_{area} :

$$\rho_{\text{bioe}} = \frac{J_{\text{max}25} N_b}{J_{\text{mc}} N_{\text{area}}} \quad (5.7)$$

2037 where N_b is the amount of nitrogen in cytochrome f, set to 0.12407 gN (μmol cytochrome f) $^{-1}$ assuming a constant 1: 1: 1.2 cytochrome f: ferredoxin NADP reductase: coupling factor molar ratio (Evans and Seemann 1989; Niinemets and Tenhunen 1997), and J_{mc} is the capacity of electron transport per cytochrome f, set to 156 μmol electron (μmol cytochrome f) $^{-1}\text{s}^{-1}$.

2042 The proportion of leaf nitrogen allocated to light harvesting proteins was calculated as a function of Chl_{mass} and N_{mass} :

$$\rho_{\text{light}} = \frac{Chl_{\text{mass}}}{N_{\text{mass}} c_b} \quad (5.8)$$

2044 where c_b is the stoichiometry of the light-harvesting chlorophyll complexes of photosystem II, set to 2.75 mmol chlorophyll (gN in chlorophyll) $^{-1}$. We used the N_{mass} value of the focal leaf used to generate A_{net}/C_i curves instead of the leaf used to extract chlorophyll content, as the two leaves are from the same trifoliolate leaf set and are highly correlated with each other (Figure SX).

2049 The proportion of leaf nitrogen content allocated to photosynthetic tissue (ρ_{photo} ; gN gN $^{-1}$) was estimated as the sum of ρ_{rubisco} , ρ_{bioe} , and ρ_{light} .

2051 Finally, the proportion of leaf N content allocated to structural tissue (ρ_{str} ; gN gN $^{-1}$) was estimated as:

$$\rho_{\text{structure}} = \frac{N_{\text{cw}}}{N_{\text{area}}} \quad (5.9)$$

2053 where N_{cw} is the leaf N content allocated to cell walls (gN m^{-2}), calculated as a
2054 function of M_{area} using an empirical equation from Onoda et al. (2017):

$$N_{cw} = 0.000355 * M_{area}^{1.39} \quad (5.10)$$

2055 5.2.8 *Whole plant traits*

2056 Seven weeks after experiment initiation and immediately following gas ex-
2057 change measurements, I harvested all experimental individuals and separated
2058 biomass of each experimental individual into major organ types (leaves, stems,
2059 roots, and nodules when present). Fresh leaf area of all harvested leaves was mea-
2060 sured using an LI-3100C (Li-COR Biosciences, Lincoln, Nebraska, USA). Total
2061 fresh leaf area (cm^2) was calculated as the sum of all leaf areas, including the focal
2062 leaf used to collect gas exchange data and the focal leaf used to extract chlorophyll
2063 content. All harvested material was dried in an oven set to 65°C for at least 48
2064 hours, weighed, and ground to homogeneity. Leaves and nodules were manually
2065 ground either with a mortar and pestle, while stems and roots were ground using
2066 a Wiley mill (E3300 Mini Mill; Eberbach Corp., MI, USA). Total dry biomass (g)
2067 was calculated as the sum of dry leaf (including focal leaf for both the A_{net}/C_i
2068 curve and leaf used to extract chlorophyll content), stem, root, and root nodule
2069 biomass. I quantified carbon and nitrogen content of each respective organ type
2070 through elemental combustion (Costech-4010, Costech, Inc., Valencia, CA, USA)
2071 using subsamples of ground and homogenized organ tissue.

2072 Following the approach explained in the first experimental chapter, I calcu-
2073 lated structural carbon costs to acquire nitrogen as the ratio of total belowground

2074 carbon biomass to whole plant nitrogen biomass (N_{cost} ; gC gN⁻¹). Belowground
2075 carbon biomass (C_{bg} ; gC) was calculated as the sum of root carbon biomass
2076 and root nodule carbon biomass. Root carbon biomass and root nodule carbon
2077 biomass was calculated as the product of the organ biomass and the respective
2078 organ carbon content. Whole plant nitrogen biomass (N_{wp} ; gN) was similarly
2079 calculated as the sum of total leaf, stem, root, and root nodule nitrogen biomass,
2080 including the focal leaf used for A_{net}/C_i curve and chlorophyll extractions. Leaf,
2081 stem, root, and root nodule nitrogen biomass was calculated as the product of
2082 the organ biomass and the respective organ nitrogen content. This calculation
2083 only quantifies plant structural carbon costs to acquire nitrogen and does not
2084 include any additional costs of nitrogen acquisition associated with respiration,
2085 root exudation, or root turnover. An explicit explanation of the limitations for
2086 interpreting this calculation can be found in Perkowski et al. (2021) and Terrer
2087 et al. (2018).

2088 Finally, plant investments in nitrogen fixation were calculated as the ra-
2089 tio of root nodule biomass to root biomass, where increasing values indicate an
2090 increase in plant investments to nitrogen fixation (Dovrat et al. 2018; Dovrat
2091 et al. 2020; Perkowski et al. 2021). I also calculated the percent of leaf nitrogen
2092 acquired from the atmosphere (% N_{dfa}) using leaf $\delta^{15}\text{N}$ and the following equation
2093 from Andrews et al. (2011):

$$\%N_{\text{dfa}} = \frac{\delta^{15}N_{\text{reference}} - \delta^{15}N_{\text{sample}}}{\delta^{15}N_{\text{reference}} - B} \quad (5.11)$$

2094 where $\delta^{15}\text{N}_{\text{reference}}$ refers to a reference plant that exclusively acquires nitrogen via

2095 direct uptake, $\delta^{15}\text{N}_{\text{sample}}$ refers to an individual's leaf $\delta^{15}\text{N}$, and B refers to individuals that are entirely reliant on nitrogen fixation. Within each unique nitrogen
2096 fertilization treatment-by-CO₂ treatment combination, I calculated the mean leaf
2097 $\delta^{15}\text{N}$ for individuals growing in the non-inoculated treatment for $\delta^{15}\text{N}_{\text{reference}}$. Any
2098 individuals with visual confirmation of root nodule formation or nodule initiation
2099 were omitted from the calculation of $\delta^{15}\text{N}_{\text{reference}}$. Following recommendations
2100 from Andrews et al. (2011) I calculated B within each CO₂ treatment using
2101 the mean leaf $\delta^{15}\text{N}$ of inoculated individuals that received 0 ppm N. I did not
2102 calculate B within each unique soil nitrogen-by-CO₂ treatment combination, as
2103 previous studies suggest decreased reliance on nitrogen fixation with increasing
2104 soil nitrogen availability (Perkowski et al. 2021). This approach for estimating
2105 nitrogen fixation standardizes values such that approaching 1 indicates increasing
2106 reliance on nitrogen fixation.

2108 5.2.9 *Statistical analyses*

2109 Any uninoculated pots that had substantial root nodule formation (nodule
2110 biomass: root biomass values greater than 0.05 g g⁻¹) were removed from analyses.
2111 This was because they were assumed to have been colonized by symbiotic nitrogen-
2112 fixing bacteria from outside sources. This decision resulted in the removal of
2113 sixteen pots from our analysis: two pots in the elevated CO₂ treatment that
2114 received 35 ppm N, three pots in the elevated CO₂ treatment that received 70
2115 ppm N, one pot in the elevated CO₂ treatment that received 210 ppm N, two pots
2116 in the elevated CO₂ treatment that received 280 ppm N, two pots in the ambient
2117 CO₂ treatment that received 0 ppm N, three pots in the ambient CO₂ treatment

2118 that received 70 ppm N, two pots in the ambient CO₂ treatment that received
2119 105 ppm N, and one pot in the ambient CO₂ treatment that received 280 ppm N.

2120 I built a series of linear mixed effects models to investigate the impacts of
2121 CO₂ concentration, soil nitrogen fertilization, and inoculation with *B. japonicum*
2122 on *G. max* gas exchange, tradeoffs between nitrogen and water use, whole plant
2123 growth, and investment in nitrogen fixation. All models included CO₂ treatment
2124 as a categorical fixed effect, inoculation treatment as a categorical fixed effect,
2125 soil nitrogen fertilization as a continuous fixed effect, with interaction terms be-
2126 tween all three fixed effects. All models also accounted for climatic difference
2127 between chambers across experiment iterations by including a random intercept
2128 term that nested starting chamber rack by CO₂ treatment. Models with this
2129 independent variable structure were created for each of the following dependent
2130 variables: N_{area} , M_{area} , N_{mass} , Chl_{area} , V_{cmax25} , J_{max25} , $J_{\text{max25}}:V_{\text{cmax25}}$, R_{d25} , g_{sw} ,
2131 stomatal limitation, ρ_{rubisco} , ρ_{bioe} , ρ_{light} , ρ_{photo} , $\rho_{\text{structure}}$, N_{cost} , C_{bg} , N_{wp} , total
2132 biomass, total leaf area, nodule biomass, and the ratio of nodule biomass to root
2133 biomass.

2134 I used Shapiro-Wilk tests of normality to determine whether linear mixed
2135 effects models satisfied residual normality assumptions. If residual normality as-
2136 sumptions were not met (Shapiro-Wilk: $p < 0.05$), then models were fit using
2137 dependent variables that were natural log transformed. All residual normality
2138 assumptions that did not originally satisfy residual normality assumptions were
2139 met with either a natural log or square root data transformation (Shapiro-Wilk:
2140 $p > 0.05$ in all cases). Specifically, models for N_{area} , N_{mass} , Chl_{area} , V_{cmax25} ,
2141 J_{max25} , $J_{\text{max25}}:V_{\text{cmax25}}$, g_{sw} , stomatal limitation, ρ_{rubisco} , ρ_{bioe} , ρ_{light} , ρ_{photo} , and to-

2142 tal leaf area satisfied residual normality assumptions without data transformation.

2143 Models for M_{area} , $\rho_{\text{structure}}$, N_{cost} , C_{bg} , N_{wp} , and total biomass satisfied residual

2144 normality assumptions with a natural log data transformation, while models for

2145 nodule biomass and nodule biomass: root biomass satisfied residual normality

2146 assumptions with a square root data transformation.

2147 In all statistical models, I used the 'lmer' function in the 'lme4' R package

2148 (Bates et al. 2015) to fit each model and the 'Anova' function in the 'car' R

2149 package (Fox and Weisberg 2019) to calculate Type II Wald's χ^2 and determine

2150 the significance ($\alpha = 0.05$) of each fixed effect coefficient. I used the 'emmeans'

2151 R package (Lenth 2019) to conduct post-hoc comparisons using Tukey's tests,

2152 where degrees of freedom were approximated using the Kenward-Roger approach

2153 (Kenward and Roger 1997). All analyses and plots were conducted in R version

2154 4.2.0 (R Core Team 2021).

2155 5.3 Results

2156 5.3.1 Leaf nitrogen and chlorophyll content

2157 Elevated CO₂ reduced N_{area} , N_{mass} , and Chl_{area} by 29%, 50%, and 31%,

2158 respectively, and stimulated M_{area} by 44% ($p < 0.001$ in all cases; Table 5.1). An

2159 interaction between fertilization and CO₂ (CO₂-by-fertilization interaction: $p_{N_{\text{area}}}$

2160 = 0.017, $p_{N_{\text{mass}}} < 0.001$, $p_{M_{\text{area}}} = 0.006$, $p_{Chl_{\text{area}}} = 0.083$; Table 5.1) indicated

2161 that the general positive effect of increasing fertilization on N_{area} , N_{mass} , and

2162 Chl_{area} ($p < 0.001$ in all cases; Table 5.1) was generally stronger under ambient

2163 CO₂ (Tukey _{N_{area}} : $p = 0.026$; Tukey _{N_{mass}} : $p < 0.001$; Tukey _{M_{area}} : $p = 0.009$;

2164 Tukey _{Chl_{area}} : $p = 0.065$; Table 5.1; Figs. 5.1a-d). This pattern resulted in a

2165 stronger reduction in N_{area} , N_{mass} , and Chl_{area} as well as a stronger stimulation
2166 in M_{area} under elevated CO₂ with increasing fertilization. An additional interac-
2167 tion between inoculation and CO₂ on N_{area} (CO₂-by-inoculation interaction: $p =$
2168 0.030; Table 5.1) indicated that the general positive effect of inoculation on N_{area}
2169 ($p < 0.001$; Table 5.1) was stronger under elevated CO₂ (45% increase; Tukey: p
2170 < 0.001) than under ambient CO₂ (18% increase; Tukey: $p < 0.001$), a result that
2171 increased the reduction in N_{area} in inoculated pots under elevated CO₂. Inocula-
2172 tion treatment did not modify the downregulation in N_{mass} (CO₂-by-inoculation
2173 interaction: $p = 0.148$; Table 5.1) and Chl_{area} ($p = 0.147$; Table 5.1) or the stimu-
2174 lation in M_{area} ($p = 0.866$; Table 5.1) under elevated CO₂. However, interactions
2175 between fertilization and inoculation on N_{area} (fertilization-by-inoculation inter-
2176 action: $p < 0.001$; Table 5.1; Fig. 5.1a), N_{mass} ($p = 0.001$; Table 5.1; Fig. 5.1b),
2177 M_{area} ($p = 0.025$; Table 5.1; Fig. 5.1c), and Chl_{area} ($p < 0.001$; Table 5.1; Fig.
2178 5.1d) indicated that the general positive effect of increasing fertilization on each
2179 trait was stronger in uninoculated pots (Tukey _{N_{area}} : $p < 0.001$; Tukey _{N_{mass}} : $p =$
2180 0.001; Tukey _{M_{area}} : $p = 0.031$; Tukey _{Chl_{area}} : $p < 0.001$).

Table 5.1. Effects of soil nitrogen fertilization, inoculation, and CO₂ treatments on N_{area} , N_{mass} , M_{area} , and Chl_{area}

	N_{area}			N_{mass}			M_{area}^a			
	df	Coefficient	χ^2	p	Coefficient	χ^2	p	Coefficient	χ^2	p
(Intercept)	-	1.10E+00	-	-	3.05E-02	-	-	3.64E+00	-	-
CO ₂	1	-5.67E-01	155.908	<0.001	-1.80E-02	272.362	<0.001	3.04E-01	151.319	<0.001
Inoculation (I)	1	6.21E-01	86.029	<0.001	7.54E-03	15.576	<0.001	1.81E-01	19.158	<0.001
Fertilization (N)	1	3.06E-03	316.408	<0.001	5.78E-05	106.659	<0.001	3.10E-04	21.440	<0.001
CO ₂ *I	1	2.63E-01	4.729	0.030	3.96E-03	2.025	0.155	-3.37E-02	0.029	0.866
CO ₂ *N	1	-3.68E-04	5.723	0.017	-2.85E-05	22.542	<0.001	2.80E-04	7.619	0.006
I*N	1	-1.36E-03	43.381	<0.001	-2.00E-05	11.137	0.001	-3.36E-04	5.022	0.025
CO ₂ *I*N	1	-3.23E-04	0.489	0.484	-2.59E-06	0.041	0.839	1.15E-04	0.208	0.649
<hr/>										
Chl_{area}										
	df	Coefficient	χ^2	p						
(Intercept)	-	2.13E-02	-	-						
CO ₂	1	-1.33E-02	69.233	<0.001						
Inoculation (I)	1	1.24E-01	136.341	<0.001						
Fertilization (N)	1	3.35E-04	163.111	<0.001						
CO ₂ *I	1	-3.18E-02	2.102	0.147						
CO ₂ *N	1	-8.79E-05	2.999	<i>0.083</i>						
I*N	1	-2.65E-04	75.769	<0.001						
CO ₂ *I*N	1	7.68E-05	2.144	0.147						

129

2181 *Significance determined using Type II Wald χ^2 tests ($\alpha = 0.05$). P -values < 0.05 are in bold, while p -values between
 2182 0.05 and 0.1 are italicized. A superscript “a” is included after trait labels to indicate if models were fit with natural
 2183 log transformed response variables. Key: df = degrees of freedom, N_{area} = leaf nitrogen content per unit leaf area,
 2184 N_{mass} = leaf nitrogen content, M_{area} = leaf mass per unit leaf area.

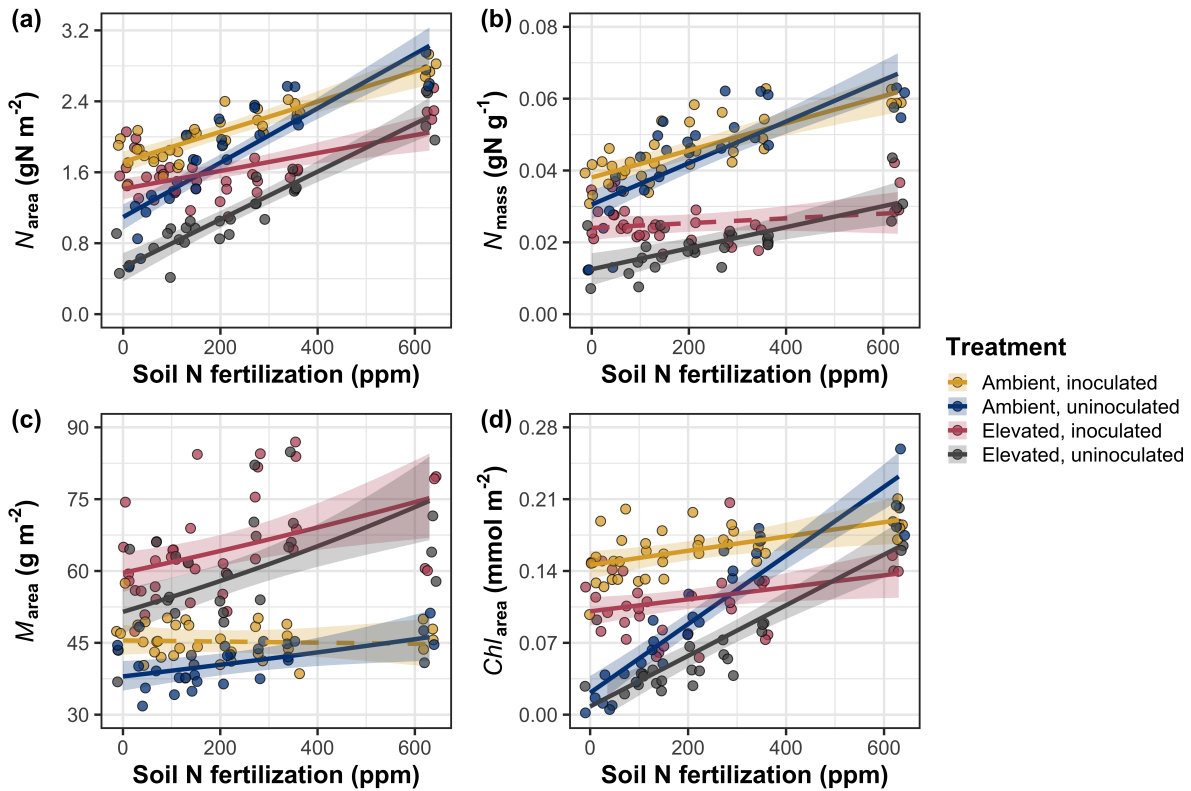


Figure 5.1. Effects of CO₂, fertilization, and inoculation on leaf nitrogen per unit leaf area (a), leaf nitrogen content (b), leaf mass per unit leaf area (c), and chlorophyll content per unit leaf area (d). Soil nitrogen fertilization is represented on the x-axis in all panels. Yellow points and trendlines indicate inoculated individuals grown under ambient CO₂, blue points and trendlines indicate uninoculated individuals grown under ambient CO₂, red points and trendlines indicate inoculated individuals grown under elevated CO₂, and grey points indicate uninoculated individuals grown under elevated CO₂. Solid trendlines indicate regression slopes that are different from zero ($p < 0.05$), while dashed trendlines indicate slopes that are not distinguishable from zero ($p > 0.05$).

2185 5.3.2 Leaf biochemistry and stomatal conductance

2186 Elevated CO₂ resulted in plants with 16% lower V_{cmax25} ($p < 0.001$; Table
2187 5.2) and 10% lower J_{max25} ($p = 0.014$; Table 5.2) as compared to those grown under
2188 ambient CO₂. However, CO₂ concentration did not influence R_{d25} ($p = 0.613$;
2189 Table 5.2). A relatively stronger downregulation in V_{cmax25} than J_{max25} resulted
2190 in an 8% stimulation in $J_{max25}:V_{cmax25}$ under elevated CO₂ ($p < 0.001$; Table 5.2;
2191 Fig. 2E). The downregulatory effect of CO₂ on V_{cmax25} and J_{max25} was not modified
2192 across the fertilization gradient (CO₂-by-fertilization interaction: $p = 0.185$, $p =$
2193 0.389 for V_{cmax25} and J_{max25} , respectively; Table 5.2; Fig. 5.2a-b) or between
2194 inoculation treatments (CO₂-by-inoculation interaction: $p = 0.799$ and $p = 0.714$
2195 for V_{cmax25} and J_{max25} , respectively; Table 5.2). However, a strong interaction
2196 between fertilization and inoculation (fertilization-by-inoculation interaction: $p \leq$
2197 0.001 in all cases; Table 5.2) indicated that the general positive effect of increasing
2198 fertilization on V_{cmax25} ($p < 0.001$; Table 5.2), J_{max25} ($p < 0.001$; Table 5.2), and
2199 R_{d25} ($p = 0.015$; Table 2) was only observed in uninoculated pots (Tukey: p
2200 ≤ 0.001 in all cases), as there was no apparent effect of fertilization on V_{cmax25}
2201 (Tukey: $p = 0.456$), J_{max25} (Tukey: $p = 0.180$), or R_{d25} (Tukey: $p = 0.443$) in
2202 inoculated pots (Figs. 5.2a-d). A relatively stronger positive effect of increasing
2203 fertilization on V_{cmax25} than J_{max25} resulted in a general reduction in $J_{max25}:V_{cmax25}$
2204 with increasing fertilization ($p < 0.001$), though this pattern was only seen in
2205 uninoculated pots (Tukey: $p = 0.003$) and not inoculated plants (Tukey: $p >$
2206 0.05).

2207 Elevated CO₂ reduced stomatal conductance by 20% ($p < 0.001$; Table
2208 5.2; Fig. 5.2e) compared to ambient CO₂, but this downregulation did not influ-

2209 ence stomatal limitation of photosynthesis ($p = 0.355$; Table 5.2; Fig. 5.2f). As
2210 with V_{cmax25} and J_{max25} , the downregulation of stomatal conductance due to ele-
2211 vated CO₂ was not modified across the fertilization gradient (CO₂-by-fertilization
2212 interaction: $p = 0.141$; Table 5.2) or between inoculation treatments (CO₂-by-
2213 inoculation interaction: $p = 0.179$; Table 5.2). Fertilization also did not modify
2214 the general null effect of CO₂ on stomatal limitation (CO₂-by-fertilization interac-
2215 tion: $p = 0.554$; Table 5.2), although an interaction between CO₂ and inoculation
2216 (CO₂-by-inoculation interaction: $p = 0.043$; Table 5.2) indicated that inoculation
2217 increased stomatal limitation under ambient CO₂ (Tukey: $p = 0.021$), but not
2218 under elevated CO₂ (Tukey: $p > 0.999$). An interaction between inoculation and
2219 fertilization on stomatal conductance (fertilization-by-inoculation interaction: p
2220 < 0.001 ; Table 5.2) indicated that increasing fertilization increased stomatal con-
2221 ductance in uninoculated pots (Tukey: $p = 0.003$) but decreased stomatal con-
2222 ductance in inoculated pots (Tukey: $p = 0.021$). The similar in magnitude, but
2223 opposite direction, trend in the effect of increasing fertilization on stomatal con-
2224 ductance between inoculation treatments likely drove a null general response of
2225 stomatal conductance to increasing fertilization ($p = 0.642$; Table 5.2).

Table 5.2. Effects of soil nitrogen fertilization, inoculation, and CO₂ on leaf biochemistry

	<i>V_{cmax25}</i>			<i>J_{max25}</i>			<i>R_{d25}</i>			
	df	Coefficient	χ^2	p	Coefficient	χ^2	p	Coefficient	χ^2	p
(Intercept)	-	4.36E+01	-	-	8.30E+01	-	-	1.69E+00	-	-
CO ₂	1	-7.05E+00	18.039	<0.001	-9.11E+00	6.042	0.014	4.53E-01	0.256	0.613
Inoculation (I)	1	5.87E+01	98.579	<0.001	9.62E+01	85.064	<0.001	1.04E+00	3.094	0.079
Fertilization (N)	1	1.32E-01	37.053	<0.001	2.09E-01	25.356	<0.001	2.86E-03	5.965	0.015
CO ₂ *I	1	-4.65E+00	0.065	0.799	7.84E-01	0.667	0.414	-5.71E-01	2.563	0.109
CO ₂ *N	1	-3.58E-02	1.758	0.185	-4.33E-02	0.742	0.389	-1.55E-03	2.675	0.102
I*N	1	-1.35E-01	60.394	<0.001	-2.30E-01	57.410	<0.001	-2.84E-03	12.083	0.001
CO ₂ *I*N	1	2.73E-02	0.748	0.387	3.46E-02	0.377	0.539	7.21E-04	0.244	0.622

	<i>J_{max25}:V_{cmax25}</i>			<i>g_{sw}</i>			Stomatal limitation			
	df	Coefficient	χ^2	p	Coefficient	χ^2	p	Coefficient	χ^2	p
(Intercept)	-	1.92E+00	-	-	1.95E-01	-	-	2.12E-01	-	-
CO ₂	1	5.71E-02	92.010	<0.001	-6.23E-02	9.718	0.002	3.91E-02	0.856	0.355
Inoculation (I)	1	-1.79E-01	27.768	<0.001	1.30E-01	22.351	<0.001	7.87E-02	4.582	0.032
Fertilization (N)	1	-4.61E-04	28.147	<0.001	2.50E-04	0.066	0.797	2.60E-04	32.218	<0.001
CO ₂ *I	1	8.94E-02	2.916	0.088	6.69E-02	1.810	0.179	-7.84E-02	4.093	0.043
CO ₂ *N	1	2.35E-04	3.210	0.073	-8.50E-05	2.165	0.141	-1.24E-04	0.350	0.554
I*N	1	3.27E-04	9.607	0.002	-3.09E-04	14.696	<0.001	-1.67E-04	2.547	0.110
CO ₂ *I*N	1	-1.66E-04	1.102	0.294	-8.89E-05	0.234	0.629	1.67E-04	2.231	0.135

133

2226 *Significance determined using Type II Wald χ^2 tests ($\alpha = 0.05$). *P*-values < 0.05 are in bold, while *p*-values between
 2227 0.05 and 0.1 are italicized. Key: *V_{cmax25}* = maximum rate of Rubisco carboxylation at 25°C; *J_{max25}* = maximum rate
 2228 of electron transport for RuBP regeneration at 25°C, *R_{d25}* = dark respiration at 25°C; *J_{max25}:V_{cmax25}* = the ratio of
 2229 *J_{max25}* to *V_{cmax25}*; *g_{sw}* = stomatal conductance.

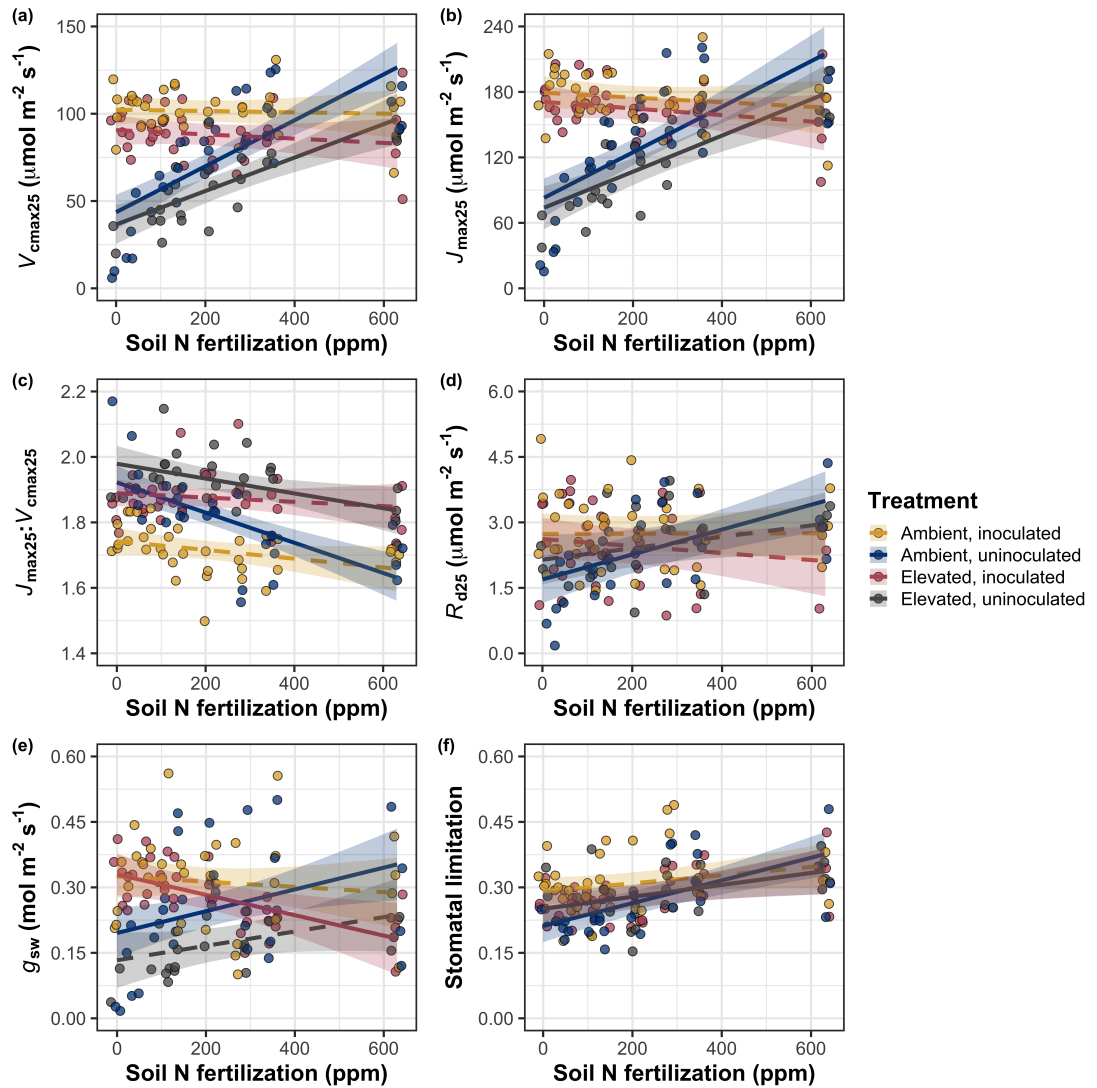


Figure 5.2. Effects of CO₂, fertilization, and inoculation on maximum rate of Rubisco carboxylation (a), the maximum rate of RuBP regeneration (b), and the ratio of the maximum rate of RuBP regeneration to the maximum rate of Rubisco carboxylation leaf mass per unit leaf area (c), dark respiration (d), stomatal conductance (e), and stomatal limitation (f). Soil nitrogen fertilization is represented on the x-axis in all panels. Colored points and trendlines are as explained in Figure 1.

2230 5.3.3 *Leaf nitrogen allocation*

2231 A relatively stronger downregulation in N_{area} than $V_{\text{cmax}25}$ or $J_{\text{max}25}$ resulted
2232 in an 20% and 29% respective stimulation in ρ_{rubisco} and ρ_{bioe} under elevated CO₂
2233 ($p < 0.001$ in both cases; Table 5.3). There was no apparent CO₂ effect on ρ_{light}
2234 ($p = 0.700$; Table 5.3), but the strong stimulation in ρ_{rubisco} and ρ_{bioe} resulted
2235 in a 21% stimulation of ρ_{photo} under elevated CO₂ ($p < 0.001$; Table 5.3; Fig.
2236 5.3a). The stimulation of ρ_{rubisco} , ρ_{bioe} , and ρ_{photo} due to elevated CO₂ was not
2237 modified across the fertilization gradient (CO₂-by-fertilization interaction: p_{rubisco}
2238 = 0.269, $p_{\text{bioe}} = 0.298$, $p_{\text{photo}} = 0.281$; Table 5.3). A marginal interaction between
2239 inoculation and CO₂ on ρ_{rubisco} and ρ_{photo} (CO₂-by-inoculation interaction: p_{rubisco}
2240 = 0.057, $p_{\text{photo}} = 0.057$; Table 5.3) indicated that the general positive effect of
2241 inoculation on ρ_{rubisco} and ρ_{photo} ($p < 0.001$ in both cases; Table 5.3) was only
2242 apparent under ambient CO₂ (Tukey: $p < 0.001$ in both cases), with no apparent
2243 effect of inoculation under elevated CO₂ (Tukey_{rubisco}: $p = 0.200$; Tukey_{photo}: p
2244 = 0.147). Inoculation did not modify the stimulation of ρ_{bioe} under elevated CO₂
2245 (CO₂-by-inoculation interaction: $p = 0.122$; Table 5.3) or the null effect of CO₂ on
2246 ρ_{bioe} (CO₂-by-inoculation interaction: $p = 0.298$; Table 5.3). Strong interactions
2247 between fertilization and inoculation on ρ_{rubisco} , ρ_{bioe} , and ρ_{photo} (fertilization-
2248 by-inoculation interaction: $p < 0.001$ in all cases; Table 5.3) indicated that the
2249 general negative effect of increasing fertilization ($p < 0.001$ in all cases; Table
2250 5.3) was only observed in inoculated pots (Tukey: $p < 0.001$ in all cases), with
2251 no apparent effect of fertilization on ρ_{rubisco} (Tukey: $p = 0.612$), ρ_{bioe} (Tukey:
2252 $p = 0.544$), or ρ_{photo} (Tukey: $p = 0.521$; Fig 5.3a) in uninoculated pots. An
2253 additional interaction between fertilization and inoculation on ρ_{light} (fertilization-

2254 by-inoculation interaction: $p < 0.001$; Table 5.3) indicated a negative effect of
2255 increasing fertilization on ρ_{light} in inoculated pots (Tukey: $p = 0.041$), but a
2256 positive effect of increasing fertilization in uninoculated pots (Tukey: $p < 0.001$).

2257 The stimulation in M_{area} resulted in an 133% stimulation of $\rho_{\text{structure}}$ under
2258 elevated CO₂ ($p < 0.001$; Table 5.3; Fig 5.3b). An interaction between fertiliza-
2259 tion and CO₂ (CO₂-by-fertilization interaction: $p = 0.039$; Table 5.3) indicated
2260 that the general negative effect of increasing fertilization ($p < 0.001$; Table 5.3) on
2261 $\rho_{\text{structure}}$ was marginally stronger under ambient CO₂ (Tukey: $p = 0.055$), resulting
2262 in a stronger stimulation in $\rho_{\text{structure}}$ under elevated CO₂ with increasing fertiliza-
2263 tion. A marginal interaction between inoculation and CO₂ (CO₂-by-inoculation
2264 interaction: $p = 0.057$; Table 5.3) indicated that the general positive effect of
2265 inoculation on $\rho_{\text{structure}}$ ($p < 0.001$; Table 5.3) was only observed under elevated
2266 CO₂ (Tukey: $p < 0.001$), with no apparent inoculation effect observed under am-
2267 bient CO₂ (Tukey: $p = 0.513$). Finally, an interaction between fertilization and
2268 inoculation (fertilization-by-inoculation interaction: $p < 0.001$; Table 5.3) indi-
2269 cated that, while increasing fertilization generally increased $\rho_{\text{structure}}$ ($p < 0.001$;
2270 Table 5.3), this response was generally stronger in uninoculated pots (Tukey: p
2271 = 0.001; Fig. 5.3b).

Table 5.3. Effects of soil N availability, soil pH, species, and N_{area} on leaf nitrogen allocation

		ρ_{rubisco}			ρ_{bioe}			ρ_{light}		
	df	Coefficient	χ^2	p	Coefficient	χ^2	p	Coefficient	χ^2	p
(Intercept)	-	2.70E-01	-	-	5.26E-02	-	-	8.48E-03	-	-
CO_2	1	1.42E-01	23.510	<0.001	3.00E-02	53.899	<0.001	2.03E-03	0.149	0.700
Inoculation (I)	1	1.83E-01	23.475	<0.001	2.80E-02	13.860	<0.001	2.04E-02	147.234	<0.001
Fertilization (N)	1	1.35E-04	16.609	<0.001	1.22E-05	26.827	<0.001	3.22E-05	19.378	<0.001
CO_2*I	1	-1.07E-01	3.629	<i>0.057</i>	-1.67E-02	2.390	0.122	-5.33E-03	0.684	0.408
CO_2*N	1	-2.16E-04	1.223	0.269	-3.59E-05	1.085	0.298	-7.01E-06	0.351	0.553
$I*N$	1	-4.26E-04	20.045	<0.001	-6.87E-05	15.458	<0.001	-4.37E-05	64.042	<0.001
CO_2*I*N	1	2.50E-04	3.327	<i>0.068</i>	4.08E-05	2.651	0.103	1.74E-05	3.735	<i>0.053</i>

		ρ_{photo}			$\rho_{\text{structure}}^a$					
	df	Coefficient	χ^2	p	Coefficient	χ^2	p			
(Intercept)	-	3.32E-01	-	-	-2.93E+00	-	-			
CO_2	1	1.81E-01	27.651	<0.001	8.77E-01	229.571	<0.001			
Inoculation (I)	1	2.31E-01	26.238	<0.001	-2.55E-01	13.872	<0.001			
Fertilization (N)	1	1.76E-04	15.899	<0.001	-1.51E-03	38.128	<0.001			
CO_2*I	1	-1.36E-01	3.671	<i>0.055</i>	-2.99E-01	3.622	<i>0.057</i>			
CO_2*N	1	-2.72E-04	1.163	0.281	3.14E-04	4.266	0.039			
$I*N$	1	-5.37E-04	21.355	<0.001	7.00E-04	11.025	0.001			
CO_2*I*N	1	3.29E-04	4.009	0.045	4.52E-04	0.669	0.413			

137

2272 *Significance determined using Type II Wald χ^2 tests ($\alpha = 0.05$). P -values < 0.05 are in bold, while p -values
 2273 between 0.05 and 0.1 are italicized. A superscript “a” is included after trait labels to indicate if models were fit with
 2274 natural log transformed response variables. Key: df=degrees of freedom, ρ_{rubisco} = proportion of leaf N allocated
 2275 to photosynthesis, ρ_{bioe} = proportion of leaf N allocated to bioenergetics, ρ_{light} = proportion of leaf N allocated to
 2276 light harvesting proteins, ρ_{photo} = proportion of leaf N allocated to photosynthesis, $\rho_{\text{structure}}$ = proportion of leaf N
 2277 allocated to cell wall structural tissue

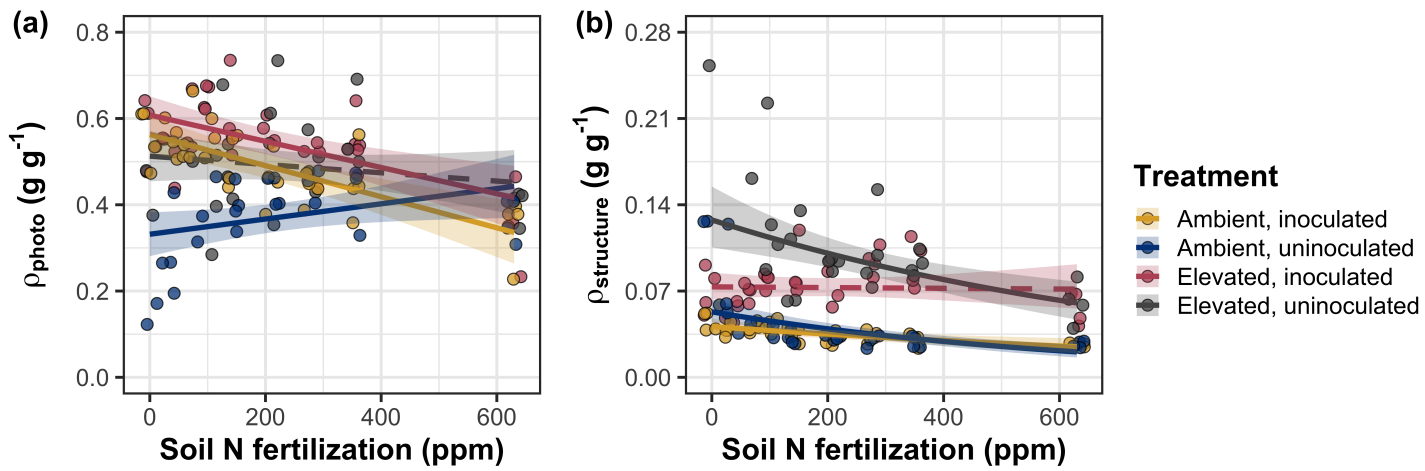


Figure 5.3. Effects of CO_2 , fertilization, and inoculation on the relative fraction of leaf nitrogen allocated to photosynthesis (a) and the fraction of leaf nitrogen allocated to structure (b). Soil nitrogen fertilization is represented on the x-axis in both panels. Colored points and trendlines are as explained in Figure 1.

2278 5.3.4 *Whole plant traits*

2279 Total leaf area was 51% greater and total biomass was 102% greater under
2280 elevated CO₂ ($p < 0.001$ in both cases; Table 5.4), a pattern that was enhanced
2281 by fertilization (CO₂-by-fertilization interaction: $p < 0.001$ in both cases; Table
2282 5.4; Figs. 5.4a-b) but was not modified across inoculation treatments (CO₂-by-
2283 inoculation interaction: $p_{total_leaf_area} = 0.151$, $p_{total_biomass} = 0.472$; Table 5.4).
2284 Specifically, the general positive effect of increasing fertilization on total leaf area
2285 and whole plant biomass ($p < 0.001$ in both cases; Table 5.4) was stronger under
2286 elevated CO₂ (Tukey: $p < 0.001$ in both cases). The general positive effect of
2287 increasing fertilization on total leaf area was modified by inoculation treatment
2288 (fertilization-by-inoculation interaction: $p < 0.001$ in both cases; Table 5.4), in-
2289 dicating a stronger positive effect of increasing fertilization in uninoculated pots
2290 (Tukey: $p_{total_leaf_area} = 0.002$, $p_{total_biomass} = 0.001$, Fig. 5.4a).

2291 A 62% stimulation in N_{cost} under elevated CO₂ was modified through a
2292 strong three-way interaction between CO₂, fertilization, and inoculation (CO₂-
2293 by-inoculation-by-fertilization interaction: $p < 0.001$; Table 5.4; Fig. 5.4). This
2294 interaction revealed a general negative effect of increasing fertilization on N_{cost}
2295 ($p < 0.001$; Table 5.4) that was observed in all treatment combinations (Tukey:
2296 $p < 0.001$ in all cases) except for inoculated pots grown under elevated CO₂
2297 (Tukey: $p = 0.779$; Fig. 5.4c). This response also resulted in generally stronger
2298 negative effects of increasing fertilization on N_{cost} in uninoculated pots grown
2299 under elevated CO₂ than uninoculated pots grown under ambient CO₂ (Tukey:
2300 $p = 0.001$) and inoculated pots grown under either ambient CO₂ (Tukey: $p <$
2301 0.001) or elevated CO₂ (Tukey: $p < 0.001$), while uninoculated pots grown under

2302 ambient CO₂ had generally stronger negative effects of increasing fertilization on
2303 N_{cost} than inoculated pots grown under elevated CO₂ (Tukey: $p = 0.002$), but
2304 not inoculated pots grown under ambient CO₂ (Tukey: $p = 0.216$; Fig. 5.4).
2305 The general reduction in N_{cost} with increasing fertilization and in uninoculated
2306 pots were driven by a stronger positive effect of increasing fertilization on N_{wp}
2307 (denominator of N_{cost}) than C_{bg} (numerator of N_{cost}), while the general stimulation
2308 in N_{cost} under elevated CO₂ was driven by a stronger positive effect of elevated
2309 CO₂ on C_{bg} than N_{wp} (Table 5.4).

Table 5.4. Effects of soil N availability, soil pH, species, and N_{area} on total leaf area, whole plant biomass, and carbon costs to acquire nitrogen

	Total leaf area			Total biomass			N_{cost}			
	df	Coefficient	χ^2	p	Coefficient	χ^2	p	Coefficient	χ^2	p
(Intercept)	-	8.78E+01	-	-	9.96E-01	-	-	8.67E+00	-	-
CO_2	1	3.36E+01	69.291	<0.001	5.07E-01	131.477	<0.001	8.75E+00	88.189	<0.001
Inoculation (I)	1	1.88E+02	35.715	<0.001	7.96E-01	34.264	<0.001	-1.68E+00	136.343	<0.001
Fertilization (N)	1	9.35E-01	274.199	<0.001	3.14E-03	269.046	<0.001	-8.50E-03	80.501	<0.001
$\text{CO}_2 * \text{I}$	1	6.44E+01	2.064	0.151	-7.69E-02	0.518	0.472	-8.38E+00	85.237	<0.001
$\text{CO}_2 * \text{N}$	1	5.05E-01	18.655	<0.001	1.61E-03	16.877	<0.001	-9.17E-03	1.050	0.306
$\text{I} * \text{N}$	1	-3.84E-01	10.804	0.001	-1.45E-03	15.779	<0.001	4.20E-03	46.489	<0.001
$\text{CO}_2 * \text{I} * \text{N}$	1	-2.97E-03	<0.001	0.990	-1.14E-04	0.023	0.880	1.32E-02	18.125	<0.001

	C_{bg}			N_{wp}			
	df	Coefficient	χ^2	p	Coefficient	χ^2	p
(Intercept)	-	-1.70E+00	-	-	1.24E-01	-	-
CO_2	1	9.21E-01	84.134	<0.001	-3.41E-03	23.890	<0.001
Inoculation (I)	1	1.18E+00	41.030	<0.001	1.68E-01	134.460	<0.001
N fertilization (N)	1	3.38E-03	152.248	<0.001	6.69E-04	529.021	<0.001
$\text{CO}_2 * \text{I}$	1	-6.18E-01	8.965	0.003	3.68E-02	1.190	0.275
$\text{CO}_2 * \text{N}$	1	-3.66E-05	1.188	0.276	1.58E-04	5.915	0.015
$\text{I} * \text{N}$	1	-2.22E-03	22.648	<0.001	-3.20E-04	55.562	<0.001
$\text{CO}_2 * \text{I} * \text{N}$	1	8.09E-04	1.109	0.292	-7.54E-05	0.620	0.431

141

2310 *Significance determined using Type II Wald χ^2 tests ($\alpha = 0.05$). P-values < 0.05 are in bold, while p-values between
 2311 0.05 and 0.1 are italicized. Key: df = degrees of freedom; N_{cost} = structural carbon cost to acquire nitrogen; C_{bg} =
 2312 belowground carbon biomass; N_{wp} = whole plant nitrogen biomass

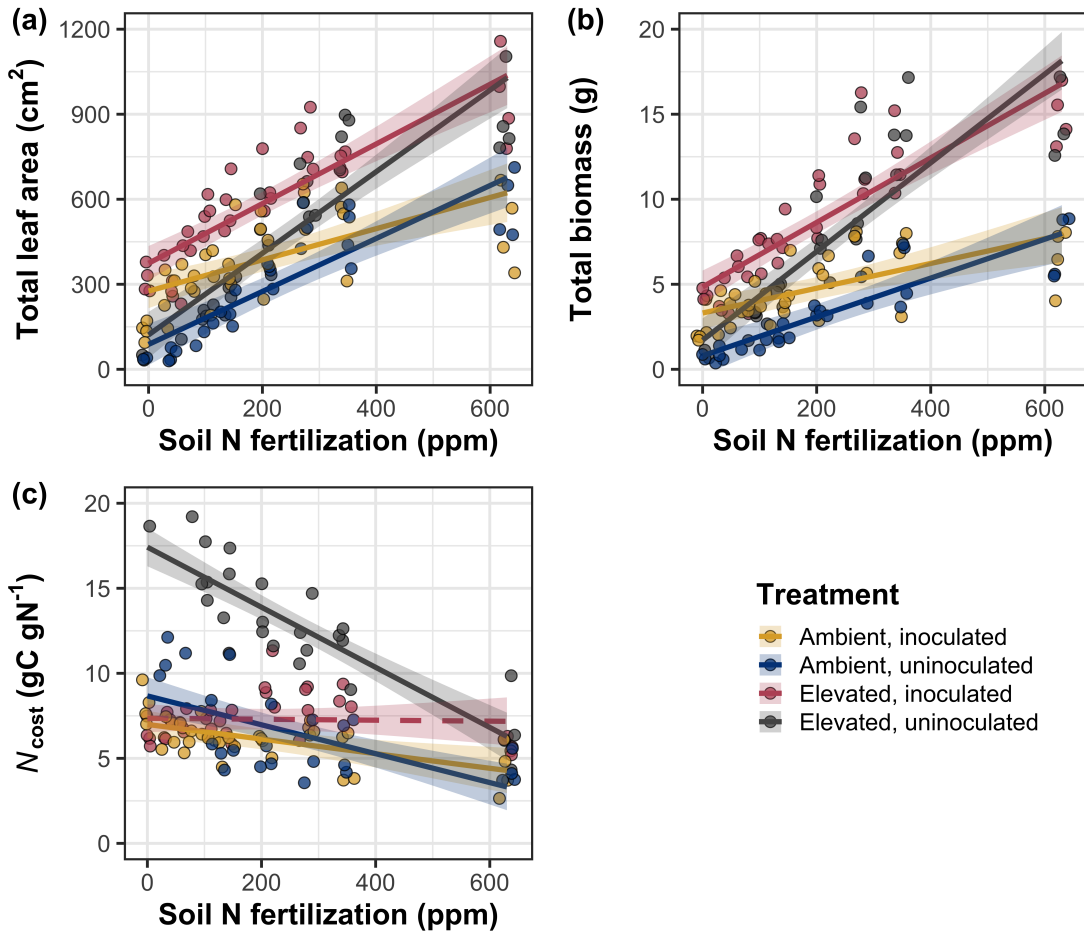


Figure 5.4. Effects of CO_2 , fertilization, and inoculation on total leaf area (a), total biomass (b), and structural carbon costs to acquire nitrogen (c). Soil nitrogen fertilization is represented continuously on the x-axis in all panels. Colored points and trendlines are as explained in Figure 1.

2313 5.3.5 *Nitrogen fixation*

2314 Nodule biomass was stimulated by 30% under elevated CO₂ ($p < 0.001$;
2315 Table 5.5), a pattern that was modified across the fertilization gradient (CO₂-
2316 by-fertilization interaction: $p = 0.479$; Table 5.5), but not between inoculation
2317 treatments (CO₂-by-inoculation interaction: $p = 0.404$; Table 5.5). Specifically,
2318 the general negative effect of increasing fertilization on nodule biomass ($p < 0.001$;
2319 Table 5.5) was stronger under elevated CO₂ than ambient CO₂ (Tukey: $p <$
2320 0.001; Fig. 5.5a), which reduced the stimulation in nodule biomass under elevated
2321 CO₂ with increasing fertilization. A strong interaction between fertilization and
2322 inoculation (fertilization-by-inoculation interaction: $p < 0.001$; Table 5.5) was
2323 driven by a stronger negative effect of increasing fertilization in inoculated pots
2324 (Tukey: $p < 0.001$; Fig. 5.5a).

2325 There was no effect of CO₂ on nodule: root biomass ($p = 0.767$; Table
2326 5.5), although an interaction between CO₂ and inoculation (CO₂-by-inoculation
2327 interaction: $p < 0.001$; Table 5.5) indicated that the general positive effect of in-
2328 oculation on nodule: root biomass ($p < 0.001$; Table 5.5) was stronger under am-
2329 bient CO₂ (3129% increase; Tukey: $p < 0.001$) than elevated CO₂ (379% increase;
2330 Tukey: $p < 0.001$; Fig. 5.5b). The null effect of CO₂ on nodule: root biomass
2331 was consistently observed across the fertilization gradient ($p = 0.183$; Table 5.5;
2332 Fig. 5.5b). An interaction between fertilization and inoculation (fertilization-by-
2333 inoculation interaction: $p < 0.001$; Table 5.5) indicated that the general negative
2334 effect of increasing fertilization on nodule: root biomass ($p < 0.001$; Table 5.5)
2335 was stronger in inoculated pots (Tukey: $p < 0.001$; Fig. 5.5b).

2336 There was no effect of CO₂ on %N_{dfa} ($p = 0.472$; Table 5.5), a pattern

2337 that was not modified by inoculation (CO_2 -by-inoculation interaction: $p = 0.156$;
2338 Table 5.5) or fertilization (CO_2 -by-fertilization interaction: $p = 0.099$; Table 5.5).
2339 An interaction between fertilization and inoculation (fertilization-by-inoculation
2340 interaction: $p < 0.001$; Table 5.5) indicated that the general negative effect of
2341 increasing fertilization on $\%N_{dfa}$ ($p < 0.001$; Table 5.5) was only observed in
2342 inoculated pots (Tukey: $p < 0.001$), with no apparent effect of fertilization on
2343 $\%N_{dfa}$ in uninoculated pots (Tukey: $p = 0.651$; Table 5.5; Fig. 5.5c).

Table 5.5. Effects of soil N availability, soil pH, species, and N_{area} on root nodule biomass and plant investments in symbiotic nitrogen fixation

	Root nodule biomass ^b			Root nodule: root biomass ^b			% N_{dfa}^b			
	df	Coefficient	χ^2	p	Coefficient	χ^2	p	Coefficient	χ^2	p
(Intercept)	-	9.41E-03	-	-	1.33E-02	-	-	7.48E-01	-	-
CO ₂	1	1.20E-01	19.258	<0.001	9.94E-02	0.087	0.768	-1.00E-01	0.518	0.472
Inoculation (I)	1	5.74E-01	755.020	<0.001	5.40E-01	903.691	<0.001	9.01E+00	955.570	<0.001
Fertilization (N)	1	7.71E-06	84.376	<0.001	-5.99E-06	258.099	<0.001	3.64E-04	292.938	<0.001
CO ₂ *I	1	-4.68E-02	0.950	0.330	-1.38E-01	20.614	<0.001	-1.44E-01	2.010	0.156
CO ₂ *N	1	-1.59E-04	2.106	0.147	-1.73E-04	1.773	0.183	-6.21E-05	2.716	0.099
I*N	1	-5.82E-04	44.622	<0.001	-7.45E-04	133.918	<0.001	-1.58E-02	231.290	<0.001
CO ₂ *I*N	1	7.26E-05	0.196	0.658	1.76E-04	2.359	0.125	2.77E-03	2.119	0.145

2344 *Significance determined using Type II Wald χ^2 tests ($\alpha = 0.05$). P-values < 0.05 are in bold, while p-values between 0.05 and 0.1 are italicized. Superscript letters indicate model coefficients fit to square-root (^b) transformed data.
2345 Key: df = degrees of freedom % N_{dfa} = percent nitrogen fixed from the atmosphere.

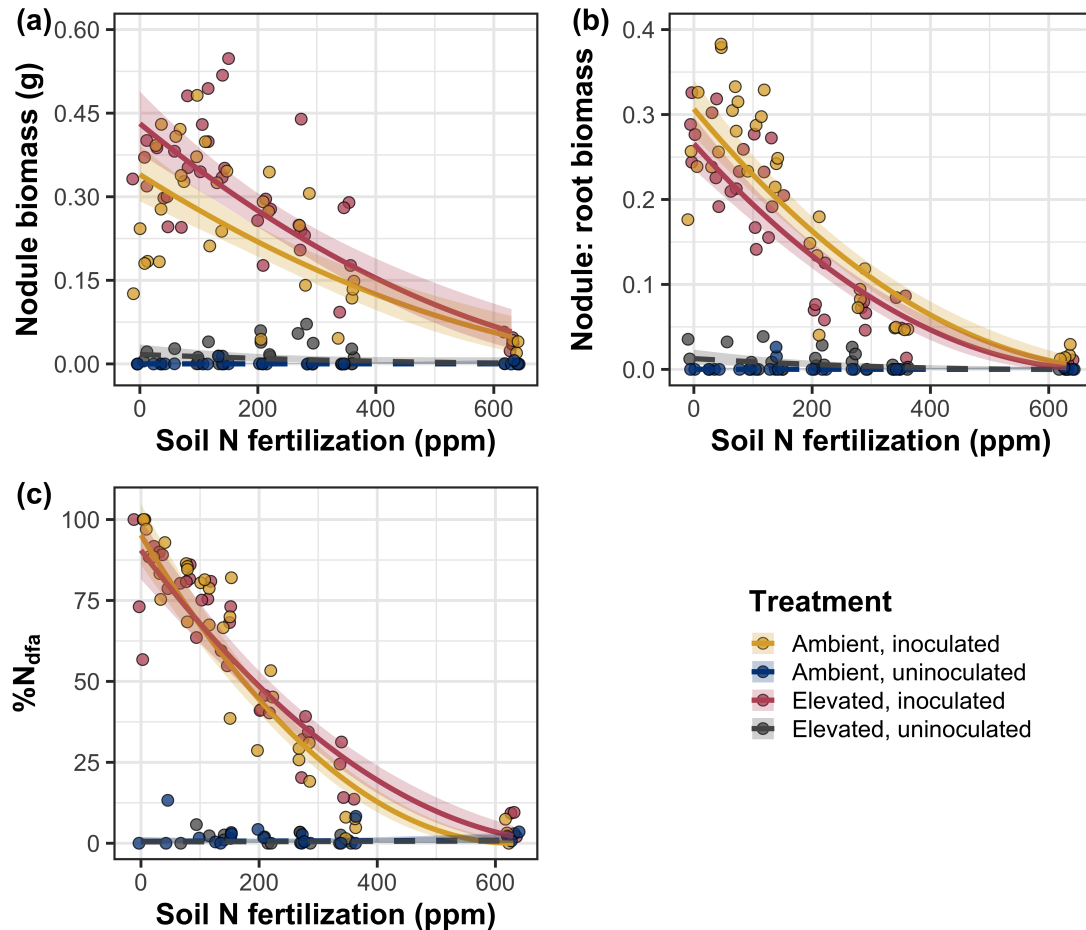


Figure 5.5. Effects of CO_2 , fertilization, and inoculation on nodule biomass (a), nodule: root biomass (b), and percent nitrogen fixed from the atmosphere (c). Soil nitrogen fertilization is represented on the x-axis. Yellow points and trendlines indicate inoculated individuals grown under ambient CO_2 , blue points and trendlines indicate uninoculated individuals grown under ambient CO_2 , red points and trendlines indicate inoculated individuals grown under elevated CO_2 , and grey points indicate uninoculated individuals grown under elevated CO_2 . Solid trendlines indicate slopes that are different from zero ($p < 0.05$), while dashed trendlines indicate slopes that are not different from zero ($p > 0.05$). Curvilinear trendlines occur as a result of back-transforming models where response variables received either a natural log or square root transformation prior to fitting.

2347 5.4 Discussion

2348 In this study, I determined leaf and whole plant acclimation responses of
2349 7-week *G. max* seedlings grown under two CO₂ concentrations, two inoculation
2350 treatments, and nine soil nitrogen fertilization treatments in a full-factorial growth
2351 chamber experiment. In support of my hypotheses and patterns expected from
2352 theory, elevated CO₂ reduced N_{area} , V_{cmax25} , and J_{max25} . The relatively stronger
2353 downregulation in V_{cmax25} than J_{max25} under elevated CO₂ resulted in a stimulation
2354 in $J_{\text{max25}}:V_{\text{cmax25}}$ under elevated CO₂. The downregulation of V_{cmax25} and J_{max25}
2355 under elevated CO₂ was similar across fertilization and inoculation treatments,
2356 indicating that the CO₂ responses were not due to nitrogen limitation. Interest-
2357 ingly, results indicate that elevated CO₂ increased the fraction of leaf nitrogen
2358 allocated to photosynthesis and structure, leading to a stimulation in nitrogen
2359 use efficiency under elevated CO₂ despite the apparent downregulation in N_{area} ,
2360 V_{cmax25} , and J_{max25} . The downregulation in leaf photosynthetic processes under
2361 elevated CO₂ also corresponded with a strong stimulation in total leaf area and to-
2362 tal biomass. Strong stimulations in whole plant growth due to elevated CO₂ were
2363 generally enhanced with increasing fertilization and were negatively related to
2364 structural carbon costs to acquire nitrogen. Inoculation generally did not modify
2365 whole plant responses to elevated CO₂ across the fertilization gradient, likely due
2366 to a strong reduction in root nodulation with increasing fertilization. However,
2367 strong positive effects of inoculation on whole plant growth were observed under
2368 low fertilization, consistent with our hypothesis. Overall, observed leaf and whole
2369 plant acclimation responses to CO₂ support hypotheses and patterns expected
2370 from photosynthetic least-cost theory, showing that leaf acclimation responses to

2371 CO₂ were decoupled from soil nitrogen availability and ability to acquire nitro-
2372 gen via symbiotic nitrogen fixation. Instead, leaf and whole plant acclimation
2373 responses to CO₂ were driven by optimal resource investment to photosynthetic
2374 capacity, where optimal resource investment at the leaf level maximized nitrogen
2375 allocation to structures that support whole plant growth.

2376 5.4.1 *Soil nitrogen fertilization has divergent effects on leaf and whole plant*
2377 *acclimation responses to CO₂*

2378 Elevated CO₂ reduced N_{area} , V_{cmax25} , J_{max25} , and stomatal conductance by
2379 29%, 16%, 10%, and 20%, respectively (Table 5.2). The larger downregulation in
2380 V_{cmax25} than J_{max25} led to an 8% stimulation in $J_{\text{max25}}:V_{\text{cmax25}}$ (Table 5.2), while
2381 the larger downregulation in N_{area} than V_{cmax25} resulted in a 21% stimulation
2382 in the fraction of leaf nitrogen allocated to photosynthesis under elevated CO₂.
2383 These acclimation responses are directionally consistent with previous studies that
2384 have investigated or reviewed leaf acclimation responses to CO₂ (Drake et al.
2385 1997; Makino et al. 1997; Ainsworth et al. 2002; Ainsworth and Long 2005;
2386 Ainsworth and Rogers 2007; Smith and Dukes 2013; Smith and Keenan 2020;
2387 Poorter et al. 2022), and follow patterns expected from photosynthetic least-cost
2388 theory (Wright et al. 2003; Prentice et al. 2014; Smith et al. 2019; Smith and
2389 Keenan 2020). Together, the stimulation in $J_{\text{max25}}:V_{\text{cmax25}}$ and the fraction of leaf
2390 nitrogen allocated to photosynthesis, and nitrogen use efficiency under elevated
2391 CO₂ provide strong support for the idea that leaves were downregulating V_{cmax25}
2392 in response to elevated CO₂ in order to optimally coordinate photosynthesis such
2393 that net photosynthesis rates approached becoming equally co-limited by Rubisco

2394 carboxylation and RuBP regeneration (Chen et al. 1993; Maire et al. 2012).

2395 Increasing fertilization and inoculation induced strong positive effects on
2396 N_{area} (Fig. 1a), $V_{\text{cmax}25}$ (Fig. 5.2a), $J_{\text{max}25}$ (Fig. 5.2b). The general positive
2397 response of N_{area} to increasing fertilization and in inoculated pots was enhanced
2398 under ambient CO_2 , which, paired with the general downregulation in N_{area} un-
2399 der elevated CO_2 , resulted in a stronger downregulation of N_{area} under elevated
2400 CO_2 with increasing fertilization and in inoculated pots (Fig. 5.1a). These pat-
2401 terns suggest that N_{area} responses to CO_2 were at least partially dependent on
2402 soil nitrogen fertilization and nitrogen acquisition strategy. However, the general
2403 stimulation in the fraction of leaf nitrogen allocated to Rubisco, bioenergetics,
2404 or photosynthesis under elevated CO_2 was not modified across the fertilization
2405 gradient and was only marginally enhanced in inoculated pots. These patterns
2406 suggest that the increased downregulation of N_{area} under elevated CO_2 with in-
2407 creasing fertilization was not associated with a change in relative investment to
2408 photosynthetic tissue. Instead, a stronger downregulation in the fraction of leaf
2409 nitrogen allocated to structure under ambient CO_2 resulted in a stronger stim-
2410 ulation in $\rho_{\text{structure}}$ under elevated CO_2 with increasing fertilization (Fig. 5.3b),
2411 indicating that fertilization shifted relative investment in leaf structural tissue un-
2412 der elevated CO_2 . These results, combined with a stimulation in PNUE (Fig. SX)
2413 and iWUE (Fig. SX) under elevated CO_2 that was independent of fertilization
2414 or inoculation treatment, provide additional support for the hypothesis that leaf
2415 acclimation photosynthetic responses to CO_2 were independent of fertilization;
2416 though fertilization may contribute to changes in leaf morphology under elevated
2417 CO_2 through shifts in M_{area} (Onoda et al. 2017; Wang et al. 2017; Dong et al.

2418 2022).

2419 The downregulation in N_{area} , $V_{\text{cmax}25}$, and $J_{\text{max}25}$ under elevated CO₂ cor-
2420 responded with a respective 62% and 100% stimulation in total leaf area (Fig.
2421 5.4a) and total biomass (Fig. 5.4b). The stimulation in total leaf area and total
2422 biomass under elevated CO₂ also corresponded with generally higher structural
2423 carbon costs to acquire nitrogen (Fig. 5.4c), a pattern driven by a stimulation
2424 in belowground carbon biomass and reduction in whole plant nitrogen biomass.
2425 Alone, this result suggests that elevated CO₂ reduces plant nitrogen uptake effi-
2426 ciency, which does not explain why plants grown under elevated CO₂ generally had
2427 higher biomass and total leaf area. However, a strong negative effect of increasing
2428 fertilization on structural carbon costs to acquire nitrogen, which were generally
2429 similar between CO₂ concentrations, was driven by a stronger increase in whole
2430 plant nitrogen biomass than belowground carbon biomass. Thus, increases in the
2431 positive response of whole plant growth and total leaf area under elevated CO₂
2432 with increasing fertilization were likely driven by an increase in nitrogen uptake
2433 efficiency, allowing plants to satisfy any increase in whole plant nitrogen demand
2434 associated with increased CO₂.

2435 Interestingly, these results indicate that the general stimulation in total
2436 leaf area and whole plant growth under elevated CO₂ was not modified by inoc-
2437 ulation despite an apparent general negative effect of inoculation on N_{cost} . This
2438 response could have been due to strong negative effect of increasing fertilization on
2439 nodulation (Fig. 5.5), which may have caused the strong increase in the positive
2440 effect of elevated CO₂ on whole plant growth with increasing fertilization to mask
2441 any increase in the positive effect of elevated CO₂ on whole plant growth due to

2442 inoculation. Reductions in nodulation with increasing fertilization are commonly
2443 observed patterns that have been inferred to be a response that allows species
2444 optimize nitrogen uptake efficiency as costs to acquire nitrogen via direct uptake
2445 become more similar (Fig. 5.4c) (Gibson and Harper 1985; Rastetter et al. 2001).
2446 In this study, pairwise comparisons indicated strong positive effects of inocula-
2447 tion on total leaf area and total biomass (158% increase in total leaf area, 119%
2448 increase in total biomass) under elevated CO₂ at 0 ppm N, but no observable
2449 inoculation effect on total leaf area or total biomass under elevated CO₂ at 350
2450 ppm N or 630 ppm N. While these responses did not generally differ from those
2451 observed under ambient CO₂, they do confirm the hypothesis that positive effects
2452 of inoculation on whole plant growth responses to elevated CO₂ would decrease
2453 with increasing fertilization.

2454 Combined, results reported here suggest that soil nitrogen availability has
2455 a divergent role in modifying leaf and whole plant acclimation responses to CO₂.
2456 Leaf acclimation responses were generally decoupled from fertilization, while whole
2457 plant acclimation responses relied heavily on an increase in nitrogen uptake ef-
2458 ficiency and consequent reduction in costs of acquiring nitrogen associated with
2459 increasing fertilization. However, whole plant responses to CO₂ indicated that
2460 fertilization may play a more important role in determining whole plant acclima-
2461 tion responses to CO₂ than nitrogen acquisition strategy, although these patterns
2462 were likely driven by reductions in nodulation with increasing fertilization. These
2463 results suggest that plants acclimate to CO₂ in nitrogen-limited systems by mini-
2464 mizing the number of optimally coordinated leaves, and that the downregulation
2465 in leaf nitrogen content under elevated CO₂ is not a direct response to changes in

2466 soil nitrogen availability as previously implied.

2467 5.4.2 *Implications for future model development*

2468 Many terrestrial biosphere models predict photosynthetic capacity through
2469 plant functional group-specific linear regressions between N_{area} and V_{cmax} (Rogers
2470 2014; Rogers et al. 2017), which assumes that leaf nitrogen-photosynthesis rela-
2471 tionships are constant across growing environments. Our results build on previ-
2472 ous work suggesting that leaf nitrogen-photosynthesis relationships dynamically
2473 change across growing environments (Luo et al. 2021; Dong et al. 2022). Specif-
2474 ically, results from this experiment indicate that CO_2 concentration increased
2475 the fraction of leaf nitrogen content allocated to photosynthesis, while a general
2476 negative effect of increasing fertilization on the fraction of leaf nitrogen content
2477 allocated to photosynthesis was dependent on inoculation treatment. Similar in-
2478 creases in N_{area} , $V_{\text{cmax}25}$, and $J_{\text{max}25}$ with increasing fertilization resulted in no
2479 change in the fraction of leaf nitrogen allocated to photosynthesis in uninoculated
2480 pots, while larger increases in N_{area} than $V_{\text{cmax}25}$ and $J_{\text{max}25}$ with increasing fertil-
2481 ization decreased the fraction of leaf nitrogen allocated to photosynthesis in inoc-
2482 ulated pots (Fig. 5.3a). As inoculated pots were able to access less finite supply of
2483 nitrogen across the fertilization gradient, these patterns suggest that constant leaf
2484 nitrogen-photosynthesis relationships may only apply in environments where ni-
2485 trogen is limiting and will likely change with increasing CO_2 concentrations. Thus,
2486 terrestrial biosphere models that parameterize photosynthetic capacity through
2487 linear relationships between N_{area} and V_{cmax} (Rogers 2014; Rogers et al. 2017)
2488 may be overestimating photosynthetic capacity in systems where nitrogen is not

2489 as limiting and may contribute to erroneous model simulations under future CO₂
2490 concentrations.

2491 These results also demonstrate that optimal resource investment to photo-
2492 synthetic capacity defines leaf acclimation responses to elevated CO₂, and that
2493 these responses were independent of fertilization or inoculation treatment. Cur-
2494 rent approaches for simulating photosynthetic responses to CO₂ generally invoke
2495 patterns expected from progressive nitrogen limitation, where the downregulation
2496 in N_{area} , and therefore photosynthetic capacity, due to elevated CO₂ are com-
2497 monly a function of progressive reductions in soil nitrogen availability. Results
2498 reported here contradict this formulation, suggesting that the leaf acclimation re-
2499 sponse is driven by optimal resource investment to photosynthetic capacity and
2500 is independent of soil resource supply. Optimality models that leverage prin-
2501 ciples from optimal coordination and photosynthetic least-cost theories (Wang
2502 et al. 2017; Stocker et al. 2020; Scott and Smith 2022) are capable of capturing
2503 such acclimation responses to CO₂ (Smith and Keenan 2020), suggesting that the
2504 implementation of these models may improve the simulation of photosynthetic
2505 processes in terrestrial biosphere models under increasing CO₂ concentrations.

2506 5.4.3 *Study limitations and future directions*

2507 There are two study limitations that must be addressed to contextualize
2508 patterns observed in this study. First, restricting the volume of belowground
2509 substrate via a potted experiment does not adequately replicate belowground en-
2510 vironments of natural systems, and therefore may modify effects of soil resource
2511 availability and inoculation on plant nitrogen uptake, particularly if pot size limits

2512 whole plant growth (Poorter et al. 2012). I attempted to minimize the extent of
2513 pot size limitation experienced in the first experimental chapters while account-
2514 ing for the expected stimulation in whole plant growth under elevated CO₂ by
2515 using 6-liter pots. Despite attempts to minimize growth limitation imposed by
2516 pot volume, fertilization and CO₂ treatments increased the biomass: pot volume
2517 ratio such that all treatment combinations to exceed 1 g L⁻¹ biomass: pot volume
2518 under high fertilization. The 1 g L⁻¹ biomass: pot volume recommendation from
2519 Poorter et al. (2012) was designated to avoid growth limitation imposed by pot
2520 volume. However, if pot size limitation indeed limited whole plant growth, then
2521 structural carbon costs to acquire nitrogen, belowground carbon biomass, whole
2522 plant nitrogen biomass, and whole plant biomass should each exhibit strong sat-
2523 uration points with increasing fertilization, which was not observed here. Addi-
2524 tionally, a second set of photosynthetic measurements from one week prior to the
2525 harvest (6 weeks post-germination) revealed ... As pot limitation is expected
2526 to decrease net photosynthesis, and focal leaves were of similar ages between the
2527 sixth and seventh week, one might expect growth limitation induced by constricted
2528 pot volume to result in a dampened effect of inoculation and fertilization on net
2529 photosynthesis, V_{cmax} , and J_{max25} . Analyses from the sixth week of development
2530 revealed ... Additionally, analyses revealed a stronger/weaker downregulation in
2531 V_{cmax25} and J_{max25} on week 7, though disentangling the causality of this response
2532 (i.e. whether due to pot size limitation or simply a stronger acclimation response)
2533 would be difficult.

2534 Second, this study evaluated leaf and whole plant responses to CO₂ in 7-
2535 week seedlings. Given the long-term scale of the progressive nitrogen limitation

2536 hypothesis, patterns observed here should be validated in longer-term nitrogen
2537 manipulation experiments. Previous work in free air CO₂ enrichment experiments
2538 show some support for patterns expected from the progressive nitrogen limitation
2539 hypothesis (Reich et al. 2006; Norby et al. 2010), although results are not consis-
2540 tent across experimental sites (Finzi et al. 2006; Moore et al. 2006; Liang et al.
2541 2016). We found some support for patterns expected by the progressive nitrogen
2542 limitation hypothesis, namely an increase in plant nitrogen uptake under elevated
2543 CO₂ (Luo et al. 2004), though leaf acclimation responses to CO₂ were strongly
2544 indicative of optimal resource investment to photosynthetic capacity as expected
2545 from photosynthetic least-cost theory (Prentice et al. 2014; Smith et al. 2019;
2546 Smith and Keenan 2020).

2547 5.4.4 *Conclusions*

2548 This study provides strong evidence suggesting that leaf acclimation re-
2549 sponds to elevated CO₂ did not vary with soil nitrogen fertilization or ability
2550 to acquire nitrogen through symbiotic nitrogen fixation. However, whole plant
2551 acclimation responses to CO₂ were dependent on fertilization, where increasing
2552 fertilization increased the positive effect of whole plant growth under elevated
2553 CO₂. Results also indicate that fertilization played a relatively more important
2554 role in modifying whole plant responses to CO₂, perhaps due to a reduction in
2555 nodulation across the fertilization gradient. These patterns strongly support the
2556 hypothesis that leaf and whole plant acclimation responses are driven by opti-
2557 mal resource investment to photosynthetic capacity, and that leaf acclimation
2558 responses to CO₂ were not modified by changes in soil nitrogen availability. Ad-

2559 ditionally, strong interactions between fertilization and inoculation on leaf and
2560 whole plant traits indicated positive effects of fertilization on leaf and whole plant
2561 traits in uninoculated pots, but null effects of fertilization on leaf and whole plant
2562 traits in inoculated pots. These results build on previous work suggesting that
2563 constant leaf nitrogen-photosynthesis relationships are dynamic and change across
2564 growing environments, calling the use of constant relationships by terrestrial bio-
2565 sphere models into question.

2566

Chapter 6

2567

Conclusions

2568 The experiments included in this dissertation were designed to test mechanisms
2569 that drive patterns expected from photosynthetic least-cost theory across various
2570 edaphic and climatic gradients. Specifically, I evaluate the context dependency
2571 of carbon costs to acquire nitrogen across soil nitrogen availability and how vari-
2572 ance in carbon costs to acquire nitrogen scales to influence leaf and whole plant
2573 acclimation responses to changing environments.

2574 In the first experimental chapter, I quantified carbon costs to acquire ni-
2575 trogen in a species capable of forming associations with symbiotic nitrogen-fixing
2576 bacteria (*Glycine max*) and a species not capable of forming such associations
2577 (*Gossypium hirsutum*) grown under four soil nitrogen fertilization treatments and
2578 four light availability treatments in a full factorial greenhouse experiment. I found
2579 that increasing light availability increased carbon costs to acquire nitrogen in both
2580 species due to a larger increase in belowground carbon biomass than whole plant
2581 nitrogen biomass. These patterns were observed in both species. I also found
2582 that increasing fertilization decreased carbon costs to acquire nitrogen due to a
2583 larger increase in whole plant nitrogen biomass than belowground carbon biomass.
2584 While these patterns were observed in both species, carbon costs to acquire nitro-
2585 gen in *G. max* were less responsive to increasing fertilization than *G. hirsutum*,
2586 providing some support for my second hypothesis. Root nodulation data indicated
2587 that *G. max* shifted relative carbon allocation from nitrogen fixation to direct up-
2588 take with increasing fertilization, which may explain the reduced responsiveness

2589 of *G. max* carbon costs to acquire nitrogen across the fertilization gradient.

2590 Despite evidence that reductions in the response of *G. max* carbon costs
2591 to acquire nitrogen to increasing fertilization may have been driven by shifts away
2592 from nitrogen fixation with increasing fertilization, I urge caution in assigning
2593 causality to the differential response of carbon costs to acquire nitrogen between
2594 species. This is because *G. max* and *G. hirsutum* are not phylogenetically related
2595 and have different life histories. Specifically, *G. max* is a herbaceous annual species,
2596 while *G. hirsutum* is a woody perennial species. Differences in life history between
2597 the two species limit my ability to assess whether reductions in the negative effect
2598 of increasing fertilization on carbon costs to acquire nitrogen in *G. max* were
2599 driven by shifts to direct uptake with increasing fertilization. However, these
2600 patterns were later confirmed in the fourth experimental chapter, where I quantify
2601 similar weaker negative effects of increasing fertilization on carbon costs to acquire
2602 nitrogen in *G. max* that were inoculated with symbiotic nitrogen-fixing bacteria
2603 compared to *G. max* that were left uninoculated across a similar soil nitrogen
2604 fertilization gradient.

2605 In the second experimental chapter, I assessed whether changes in soil
2606 nitrogen availability or soil pH drove changes in nitrogen-water use tradeoffs pre-
2607 dicted by photosynthetic least-cost theory. I measured leaf traits of mature upper
2608 canopy deciduous trees growing in a nine-year nitrogen-by-sulfur field manipula-
2609 tion experiment, where experimental sulfur additions were added with intent to
2610 acidify plots. Following patterns expected from the theory, increasing soil nitrogen
2611 availability was associated with increased leaf nitrogen content, but not net pho-
2612 tosynthesis, resulting in an increase in photosynthetic nitrogen use efficiency. In

2613 further support of theory, increasing soil nitrogen availability exhibited slight, but
2614 nonsignificant, decreases in leaf $C_i:C_a$ and increases in measures of photosynthetic
2615 capacity. Perhaps the strongest evidence for the theory was a strong negative
2616 relationship between leaf nitrogen content and leaf $C_i:C_a$, of which increased with
2617 increasing soil nitrogen availability through a stronger increase in leaf nitrogen
2618 content than leaf $C_i:C_a$.

2619 I found no effect of soil pH on nitrogen-water use tradeoffs aside from a
2620 marginal reduction in net photosynthesis rates that marginally reduced photosyn-
2621 thetic nitrogen use efficiency with increasing soil pH. Directionally, reductions in
2622 photosynthetic nitrogen use efficiency with increasing soil pH were as expected per
2623 theory; however, this response was driven by no change in leaf nitrogen content
2624 and a reduction in net photosynthesis. Theory predicts that these tradeoffs should
2625 be driven by no change in net photosynthesis and an increase in leaf nitrogen con-
2626 tent. Regardless, the general null leaf response to changing soil pH may have
2627 been due to experimental treatments directly increased soil nitrogen availability
2628 and affected soil pH in opposite patterns, suggesting that soil nitrogen availability
2629 may be more important in dictating nitrogen-water use tradeoffs than soil pH per
2630 se.

2631 In the third experimental chapter, I quantified variance in leaf nitrogen
2632 content across a precipitation and soil resource availability gradient in Texan
2633 grasslands. Specifically, I measured area-based leaf nitrogen content, components
2634 of area-based leaf nitrogen content (leaf mass per unit leaf area, leaf nitrogen per
2635 unit dry biomass), leaf $C_i:C_a$, and the unit cost of acquiring nitrogen relative to
2636 water in 520 individuals comprising 57 species. I found that variance in area-

2637 based leaf nitrogen content was positively associated with increasing soil nitrogen
2638 availability, soil moisture, vapor pressure deficit, and was negatively related to
2639 increasing leaf $C_i:C_a$. Following patterns expected from theory, a path analysis
2640 revealed that the positive soil nitrogen-leaf nitrogen relationship was driven by a
2641 positive relationship between soil nitrogen availability and the unit cost of acquir-
2642 ing and using nitrogen relative to water, a positive relationship between the unit
2643 cost of acquiring and using nitrogen relative to water, and negative relationship
2644 between leaf $C_i:C_a$ and leaf mass per unit leaf area. Interestingly, there was no
2645 effect of $C_i:C_a$ on leaf nitrogen content per unit dry biomass, indicating that vari-
2646 ance in area-based leaf nitrogen content across the environmental gradient was
2647 driven by a change in leaf morphology and not leaf chemistry.

2648 In the fourth experimental chapter, I quantified leaf and whole plant accli-
2649 mation responses in *G. max* grown under two atmospheric CO₂ levels, with and
2650 without inoculation with *Bradyrhizobium japonicum*, and across nine nitrogen fer-
2651 tilization treatments in a full factorial growth chamber experiment. I found strong
2652 evidence that leaf nitrogen content, V_{cmax} , and J_{max} were each downregulated un-
2653 der elevated CO₂. A stronger downregulation in V_{cmax} than J_{max} and stronger
2654 downregulation in leaf nitrogen content than V_{cmax} or J_{max} provided strong sup-
2655 port suggesting that leaves were acclimating to elevated CO₂ by optimizing leaf
2656 photosynthetic resource use efficiency to achieve optimal coordination. In striking
2657 support of my hypotheses, I find strong evidence suggesting that leaf acclimation
2658 responses to elevated CO₂ were decoupled from soil nitrogen fertilization and in-
2659 oculation treatment, despite apparent strong increases in leaf nitrogen content,
2660 V_{cmax} , and J_{max} with increasing fertilization and in inoculated pots. These find-

2661 ings contrast the current formulation of photosynthetic processes in terrestrial
2662 biosphere models, where many models simulate downregulations in leaf nitrogen
2663 content under elevated CO₂ schemes as a function of progressive nitrogen limita-
2664 tion.

2665 There are currently two iterations of optimality models that employ the
2666 use of patterns expected from photosynthetic least-cost theory, one for C₃ species
2667 (Wang et al. 2017; Smith et al. 2019; Stocker et al. 2020) and one more recently
2668 developed for C₄ species (Scott and Smith 2022). In both model variants, costs to
2669 acquire and use nitrogen relative to water are held constant using a global dataset
2670 of δ¹³C (Cornwell et al. 2018). The C₃ optimality model initially assumed a
2671 constant cost to acquire and use nitrogen relative to water value of 240 (Wang et al.
2672 2017), later corrected to 146 (Stocker et al. 2020), while the C₄ optimality model
2673 assumes a constant value of 166 (Scott and Smith 2022). Throughout experiments,
2674 I show strong evidence suggesting that costs to acquire and use nitrogen are
2675 dynamic and vary predictably across environmental gradients, and that changes
2676 in these costs yield predictable changes in leaf nitrogen-water use tradeoffs and
2677 acclimation responses to changing environments. Thus, optimality models that
2678 hold unit costs of resource use constant may contribute to erroneous errors in
2679 model simulations. Future iterations of optimality models that leverage patterns
2680 expected from photosynthetic least-cost theory should consider development of
2681 explicit schemes for dynamically calculating costs to acquire and use nitrogen
2682 relative to water, or be coupled with previously established plant nitrogen uptake
2683 models (e.g., FUN) (Fisher et al. 2010; Brzostek et al. 2014; Allen et al. 2020).

2684 First principles of photosynthetic least-cost theory suggest that plants can

2685 optimize photosynthesis rates by sacrificing inefficient use of a relatively more
2686 abundant (and less costly to acquire) resource for more efficient use of a relatively
2687 less abundant (and more costly to acquire) resource. I show strong support for
2688 these patterns across experiments, where increasing soil nitrogen fertilization gen-
2689 erally decreased the cost of acquiring nitrogen relative to water, a pattern that
2690 scaled to influence leaf nitrogen-water use tradeoffs. These findings provide im-
2691 portant empirical validation of photosynthetic least-cost theory needed to further
2692 develop optimality models and eventually implement in terrestrial biosphere model
2693 products. Many current terrestrial biosphere model products do not include ro-
2694 bust frameworks for simulating acclimation responses to changing environmental
2695 conditions, and empirical findings shown here provide some support that optimal-
2696 ity models that leverage photosynthetic least-cost theory predictions may improve
2697 the ability of terrestrial biosphere models to accurately simulate photosynthetic
2698 processes. Future work should leverage data collected from these experiments,
2699 particularly the environmental gradient experiment across Texan grasslands, to
2700 conduct model-data comparisons to evaluate optimality model performance.

2701 Many terrestrial biosphere models predict photosynthetic capacity through
2702 plant functional group-specific linear regressions between area-based leaf nitrogen
2703 content and V_{cmax} (Rogers 2014; Rogers et al. 2017), which assumes that leaf
2704 nitrogen-photosynthesis relationships are constant across growing environments.
2705 I found constant leaf nitrogen-photosynthesis relationships with increasing soil ni-
2706 trogen availability in the nitrogen-by-sulfur field manipulation experiment. How-
2707 ever, results from the CO₂-by-nitrogen-by-inoculation manipulation experiment
2708 indicated that leaf nitrogen-photosynthesis responses to soil nitrogen availability

2709 were dependent on whether nitrogen was limiting. Specifically, similar increases in
2710 area-based leaf nitrogen content, $V_{\text{cmax}25}$, and $J_{\text{max}25}$ with increasing fertilization
2711 resulted in no change in the fraction of leaf nitrogen allocated to photosynthesis in
2712 uninoculated pots, while larger increases in area-based leaf nitrogen content than
2713 $V_{\text{cmax}25}$ and $J_{\text{max}25}$ with increasing fertilization decreased the fraction of leaf nitro-
2714 gen allocated to photosynthesis in inoculated pots. As inoculated pots were able
2715 to access less finite supply of nitrogen across the fertilization gradient, these pat-
2716 terns suggest that constant leaf nitrogen-photosynthesis relationships may only
2717 apply in environments where nitrogen is limiting. Further investigation is cer-
2718 tainly warranted regarding the effect of soil nitrogen availability in modifying leaf
2719 nitrogen-photosynthesis relationships, but findings from these experiments suggest
2720 that representing photosynthetic processes through positive relationships between
2721 soil nitrogen availability, leaf nitrogen, and photosynthetic capacity are likely con-
2722 tributing to erroneous errors in model simulations and may be an explanation for
2723 the high degree of divergence between carbon and nutrient flux simulations across
2724 terrestrial biosphere model products (Friedlingstein et al. 2014; Davies-Barnard
2725 et al. 2020).

2726 The experiments included in this dissertation have provided a strong foun-
2727 dation for me to continue growing as a plant physiological ecologist. I envision
2728 five primary avenues for future research that build on the work presented here,
2729 which are briefly summarized below:

2730 1. Manipulative and environmental gradient experiments included in this dis-
2731 sertation were designed to provide empirical data needed to test photosyn-
2732 thetic least-cost theory assumptions. While these results show promising

- 2733 patterns for patterns expected from photosynthetic least-cost theory, they
2734 do not necessarily address whether these patterns follow those simulated by
2735 optimality models that leverage photosynthetic least-cost principles. Thus,
2736 a clear future direction of this research could be to conduct model-data
2737 comparisons using data collected here (or similar experiments) to compare
2738 against optimality model simulations.
- 2739 2. Experiments included in this dissertation explicitly quantify effects of sym-
2740 biotic nitrogen fixation on carbon costs to acquire nitrogen, nitrogen-water
2741 use tradeoffs, and leaf nitrogen-photosynthesis relationships. However, car-
2742 bon costs to acquire nitrogen also vary in species that associate with dif-
2743 ferent mycorrhizal types (Brzostek et al. 2014; Terrer et al. 2018), and
2744 dominant mycorrhizal type in an ecosystem may dictate net biogeochemical
2745 cycle dynamics (Phillips et al. 2013). Thus, future work should consider
2746 conducting similar experiments while manipulating mycorrhizal association
2747 to comprehensively understand how microbial symbioses modify leaf and
2748 whole plant acclimation responses to changing environments. This avenue
2749 of research would be particularly useful in forested ecosystems, as previous
2750 work suggests that dominant mycorrhizal type in hardwood forests dictate
2751 net biogeochemical cycle dynamics
- 2752 3. Recent work indicates a high degree of variance in symbiotic nitrogen fixa-
2753 tion rates across terrestrial biosphere models (Davies-Barnard et al. 2020;
2754 Meyerholt et al. 2016), perhaps due to nitrogen fixation rates that are im-
2755 plemented across terrestrial biosphere models as a function of temperature
2756 (Houlton et al. 2008). While energetic costs of nitrogen fixation are cer-

2757 tainly temperature dependent, I show that structural costs of nitrogen fix-
2758 ation are driven by shifts in soil resource availability. The light-by-nitrogen
2759 greenhouse experiment was recently published in *Journal of Experimental*
2760 *Botany*, and a reviewer encouraged future work to include a model-data
2761 comparison comparing carbon costs to acquire nitrogen measured in the
2762 experiment to carbon costs to acquire nitrogen simulated by the FUN bio-
2763 geochemical model (Fisher et al. 2010; Brzostek et al. 2014; Allen et al.
2764 2020). Conveniently, FUN calculates carbon costs to acquire nitrogen follow-
2765 ing the same calculation used in the first and fourth experimental chapter,
2766 and doing this would be a useful next step toward understanding why ni-
2767 trogen fixation simulations in terrestrial biosphere models might deviate to
2768 such a large degree between products.

2769 4. Carbon costs to acquire nitrogen relative to water were quantified at the
2770 leaf level as a function of $\delta^{13}\text{C}$ and vapor pressure deficit, while structural
2771 carbon costs to acquire nitrogen were quantified at the whole plant level
2772 as the ratio of belowground carbon allocation per unit whole plant nitro-
2773 gen biomass. As increasing soil nitrogen availability decreases both leaf and
2774 whole plant estimates of costs to acquire and use nitrogen, one might expect
2775 leaf and whole plant carbon cost to acquire nitrogen estimates to covary. Fu-
2776 ture work should consider investigating if leaf and whole plant estimates of
2777 carbon costs to acquire nitrogen covary and evaluate whether environmental
2778 conditions (or species acquisition strategy) modifies any of this possible co-
2779 variance. Strong covariance between leaf and whole plant costs of nitrogen
2780 acquisition could be a possible avenue to implement frameworks for allowing

2781 costs of nitrogen acquisition to vary in optimality models, as the FUN model
2782 calculates carbon costs of nitrogen acquisition at the whole plant level.

2783 5. While experiments included in this dissertation target effects of soil nitrogen
2784 availability on carbon costs to acquire nitrogen and associated leaf nitrogen-
2785 water use tradeoffs, photosynthetic least-cost theory predicts that costs of
2786 nutrient use, not just nitrogen, relative to water are substitutable. Recent
2787 iterations of the FUN biogeochemical cycle includes the carbon and nitro-
2788 gen cost of acquiring and using phosphorus, which similarly varies in species
2789 with different nutrient acquisition strategies (Allen et al. 2020). The im-
2790 plementation of this model in a terrestrial biosphere model (E3SM) was
2791 recently shown to improve model performance of ecosystem nutrient lim-
2792 itation (Braghiere et al. 2022). As phosphorus commonly co-limits leaf
2793 photosynthesis and primary productivity, extending experiments reported
2794 here to investigate carbon and nitrogen costs of phosphorus use may be a
2795 useful next step in understanding extensions and limitations of photosyn-
2796 thetic least-cost theory.

2797 I conclude this dissertation with a brief word of thanks to all who have
2798 shaped me into the plant physiological ecologist that I am today. Specifically,
2799 I am thankful for the incredible mentorship of my advisor and committee chair,
2800 Dr. Nick Smith, who provided invaluable insight for each of these experimental
2801 chapters, and for my committee members for their helpful advise and support
2802 throughout these experiments. I am excited to continue growing as a plant phys-
2803 iological ecologist, look forward to continuing to understand nutrient acquisition
2804 and allocation responses to global change, and am excited to help mentor future

2805 generations of young researchers.

2806

References

- 2807** Abrams, M. D. and S. A. Mostoller (1995). Gas exchange, leaf structure and
2808 nitrogen in contrasting successional tree species growing in open and under-
2809 story sites during a drought. *Tree Physiology* 15(6), 361–370.
- 2810** Adams, M. A., T. L. Turnbull, J. I. Sprent, and N. Buchmann (2016). Legumes
2811 are different: Leaf nitrogen, photosynthesis, and water use efficiency. *Pro-
2812 ceedings of the National Academy of Sciences of the United States of Amer-
2813 ica* 113(15), 4098–4103.
- 2814** Ainsworth, E. A., P. A. Davey, C. J. Bernacchi, O. C. Dermody, E. A. Heaton,
2815 D. J. Moore, P. B. Morgan, S. L. Naidu, H. S. Y. Ra, X. G. Zhu, P. S. Curtis,
2816 and S. P. Long (2002). A meta-analysis of elevated [CO₂] effects on soybean
2817 (*Glycine max*) physiology, growth and yield. *Global Change Biology* 8(8),
2818 695–709.
- 2819** Ainsworth, E. A. and S. P. Long (2005). What have we learned from 15 years of
2820 free-air CO₂ enrichment (FACE)? A meta-analytic review of the responses
2821 of photosynthesis, canopy properties and plant production to rising CO₂.
2822 *New Phytologist* 165(2), 351–372.
- 2823** Ainsworth, E. A. and A. Rogers (2007). The response of photosynthesis and
2824 stomatal conductance to rising [CO₂]: mechanisms and environmental in-
2825 teractions. *Plant, Cell and Environment* 30(3), 258–270.
- 2826** Allen, K., J. B. Fisher, R. P. Phillips, J. S. Powers, and E. R. Brzostek (2020).
2827 Modeling the carbon cost of plant nitrogen and phosphorus uptake across
2828 temperate and tropical forests. *Frontiers in Forests and Global Change* 3,

- 2829 1–12.
- 2830 Allison, S. D., C. I. Czimczik, and K. K. Treseder (2008). Microbial activity
2831 and soil respiration under nitrogen addition in Alaskan boreal forest. *Global
2832 Change Biology* 14(5), 1156–1168.
- 2833 Andersen, M. K., H. Hauggaard-Nielsen, P. Ambus, and E. S. Jensen (2005).
2834 Biomass production, symbiotic nitrogen fixation and inorganic N use in dual
2835 and tri-component annual intercrops. *Plant and Soil* 266(1-2), 273–287.
- 2836 Andrews, M., E. K. James, J. I. Sprent, R. M. Boddey, E. Gross, and F. B. dos
2837 Reis (2011). Nitrogen fixation in legumes and actinorhizal plants in natural
2838 ecosystems: Values obtained using ^{15}N natural abundance. *Plant Ecology
2839 and Diversity* 4(2-3), 117–130.
- 2840 Arndal, M. F., A. Tolver, K. S. Larsen, C. Beier, and I. K. Schmidt (2018). Fine
2841 root growth and vertical distribution in response to elevated CO₂, warming
2842 and drought in a mixed heathland–grassland. *Ecosystems* 21(1), 15–30.
- 2843 Arnone, J. A. (1997). Indices of plant N availability in an alpine grassland under
2844 elevated atmospheric CO₂. *Plant and Soil* 190(1), 61–66.
- 2845 Arora, V. K., A. Katavouta, R. G. Williams, C. D. Jones, V. Brovkin,
2846 P. Friedlingstein, J. Schwinger, L. Bopp, O. Boucher, P. Cadule, M. A.
2847 Chamberlain, J. R. Christian, C. Delire, R. A. Fisher, T. Hajima, T. Ilyina,
2848 E. Joetzjer, M. Kawamiya, C. D. Koven, J. P. Krasting, R. M. Law, D. M.
2849 Lawrence, A. Lenton, K. Lindsay, J. Pongratz, T. Raddatz, R. Séférian,
2850 K. Tachiiri, J. F. Tjiputra, A. Wiltshire, T. Wu, and T. Ziehn (2020).
2851 Carbon-concentration and carbon-climate feedbacks in CMIP6 models and
2852 their comparison to CMIP5 models. *Biogeosciences* 17(16), 4173–4222.

- 2853 Bae, K., T. J. Fahey, R. D. Yanai, and M. Fisk (2015). Soil nitrogen availability affects belowground carbon allocation and soil respiration in northern
2854 hardwood forests of New Hampshire. *Ecosystems* 18(7), 1179–1191.
- 2855
- 2856 Barber, S. A. (1962). A diffusion and mass-flow concept of soil nutrient availability. *Soil Science* 93(1), 39–49.
- 2857
- 2858 Barnes, J. D., L. Balaguer, E. Manrique, S. Elvira, and A. W. Davison (1992).
2859 A reappraisal of the use of DMSO for the extraction and determination
2860 of chlorophylls a and b in lichens and higher plants. *Environmental and
2861 Experimental Botany* 32(2), 85–100.
- 2862 Bates, D., M. Mächler, B. Bolker, and S. Walker (2015). Fitting linear mixed-
2863 effects models using lme4. *Journal of Statistical Software* 67(1), 1–48.
- 2864 Beaudette, D., J. Skovlin, S. Roeker, and A. Brown (2022). soilDB: Soil
2865 Database Interface.
- 2866 Bengtson, P., J. Barker, and S. J. Grayston (2012). Evidence of a strong cou-
2867 pling between root exudation, C and N availability, and stimulated SOM
2868 decomposition caused by rhizosphere priming effects. *Ecology and Evolu-
2869 tion* 2(8), 1843–1852.
- 2870 Bernacchi, C. J., E. L. Singsaas, C. Pimentel, A. R. Portis, and S. P. Long
2871 (2001). Improved temperature response functions for models of Rubisco-
2872 limited photosynthesis. *Plant, Cell and Environment* 24(2), 253–259.
- 2873 Bialic-Murphy, L., N. G. Smith, P. Voothuluru, R. M. McElderry, M. D.
2874 Roche, S. T. Cassidy, S. N. Kivlin, and S. Kalisz (2021). Invasion-induced
2875 root–fungal disruptions alter plant water and nitrogen economies. *Ecology*

- 2876** *Letters* 24(6), 1145–1156.
- 2877** Bloom, A. J., F. S. Chapin, and H. A. Mooney (1985). Resource limitation
2878 in plants - an economic analogy. *Annual Review of Ecology and Systemat-*
2879 *ics* 16(1), 363–392.
- 2880** Bloomfield, K. J., B. D. Stocker, T. F. Keenan, and I. C. Prentice (2023).
2881 Environmental controls on the light use efficiency of terrestrial gross primary
2882 production. *Global Change Biology* 29(4), 0–2.
- 2883** Bonan, G. B., M. D. Hartman, W. J. Parton, and W. R. Wieder (2013). Eval-
2884 uating litter decomposition in earth system models with long-term litter
2885 bag experiments: an example using the Community Land Model version 4
2886 (CLM4). *Global Change Biology* 19(3), 957–974.
- 2887** Bonan, G. B., P. J. Lawrence, K. W. Oleson, S. Levis, M. Jung, M. Reich-
2888 stein, D. M. Lawrence, and S. C. Swenson (2011). Improving canopy pro-
2889 cesses in the Community Land Model version 4 (CLM4) using global flux
2890 fields empirically inferred from FLUXNET data. *Journal of Geophysical Re-*
2891 *search* 116(G2), G02014.
- 2892** Booth, B. B. B., C. D. Jones, M. Collins, I. J. Totterdell, P. M. Cox, S. Sitch,
2893 C. Huntingford, R. A. Betts, G. R. Harris, and J. Lloyd (2012). High sen-
2894 sitivity of future global warming to land carbon cycle processes. *Environ-*
2895 *mental Research Letters* 7(2), 024002.
- 2896** Borer, E. T., W. S. Harpole, P. B. Adler, E. M. Lind, J. L. Orrock, E. W.
2897 Seabloom, and M. D. Smith (2014). Finding generality in ecology: A model
2898 for globally distributed experiments. *Methods in Ecology and Evolution* 5(1),
2899 65–73.

- 2900 Braghieri, R. K., J. B. Fisher, K. Allen, E. Brzostek, M. Shi, X. Yang, D. M.
2901 Ricciuto, R. A. Fisher, Q. Zhu, and R. P. Phillips (2022). Modeling global
2902 carbon costs of plant nitrogen and phosphorus acquisition. *Journal of Ad-*
2903 *vances in Modeling Earth Systems* 14(8), 1–23.
- 2904 Brix, H. (1971). Effects of nitrogen fertilization on photosynthesis and respi-
2905 ration in Douglas-fir. *Forest Science* 17(4), 407–414.
- 2906 Brzostek, E. R., J. B. Fisher, and R. P. Phillips (2014). Modeling the carbon
2907 cost of plant nitrogen acquisition: Mycorrhizal trade-offs and multipath
2908 resistance uptake improve predictions of retranslocation. *Journal of Geo-*
2909 *physical Research: Biogeosciences* 119, 1684–1697.
- 2910 Bubier, J. L., R. Smith, S. Juutinen, T. R. Moore, R. Minocha, S. Long, and
2911 S. Minocha (2011). Effects of nutrient addition on leaf chemistry, morphol-
2912 ogy, and photosynthetic capacity of three bog shrubs. *Oecologia* 167(2),
2913 355–368.
- 2914 Cernusak, L. A., N. Ubierna, K. Winter, J. A. M. Holtum, J. D. Marshall, and
2915 G. D. Farquhar (2013). Environmental and physiological determinants of
2916 carbon isotope discrimination in terrestrial plants. *New Phytologist* 200(4),
2917 950–965.
- 2918 Chen, J.-L., J. F. Reynolds, P. C. Harley, and J. D. Tenhunen (1993). Coor-
2919 dination theory of leaf nitrogen distribution in a canopy. *Oecologia* 93(1),
2920 63–69.
- 2921 Clark, D. B., L. M. Mercado, S. Sitch, C. D. Jones, N. Gedney, M. J. Best,
2922 M. Pryor, G. G. Rooney, R. L. H. Essery, E. Blyth, O. Boucher, R. J.
2923 Harding, C. Huntingford, and P. M. Cox (2011). The Joint UK Land Envi-

- 2924 ronment Simulator (JULES), model description. Part 2: Carbon fluxes and
2925 vegetation dynamics. *Geoscientific Model Development* 4(3), 701–722.
- 2926 Cornwell, W. K., J. H. C. Cornelissen, K. Amatangelo, E. Dorrepaal, V. T.
2927 Eviner, O. Godoy, S. E. Hobbie, B. Hoorens, H. Kurokawa, N. Pérez-
2928 Harguindeguy, H. M. Quested, L. S. Santiago, D. A. Wardle, I. J. Wright,
2929 R. Aerts, S. D. Allison, P. van Bodegom, V. Brovkin, A. Chatain, T. V.
2930 Callaghan, S. Díaz, E. Garnier, D. E. Gurvich, E. Kazakou, J. A. Klein,
2931 J. Read, P. B. Reich, N. A. Soudzilovskaia, M. V. Vaieretti, and M. Westoby
2932 (2008). Plant species traits are the predominant control on litter decompo-
2933 sition rates within biomes worldwide. *Ecology Letters* 11(10), 1065–1071.
- 2934 Cornwell, W. K., I. J. Wright, J. Turner, V. Maire, M. M. Barbour, L. A.
2935 Cernusak, T. E. Dawson, D. S. Ellsworth, G. D. Farquhar, H. Griffiths,
2936 C. Keitel, A. Knohl, P. B. Reich, D. G. Williams, R. Bhaskar, J. H. C. Cor-
2937 nelissen, A. Richards, S. Schmidt, F. Valladares, C. Körner, E.-D. Schulze,
2938 N. Buchmann, and L. S. Santiago (2018). Climate and soils together regulate
2939 photosynthetic carbon isotope discrimination within C₃ plants worldwide.
2940 *Global Ecology and Biogeography* 27(9), 1056–1067.
- 2941 Cramer, W. and I. C. Prentice (1988). Simulation of regional soil moisture
2942 deficits on a European scale. *Norsk Geografisk Tidsskrift - Norwegian Jour-*
2943 *nal of Geography* 42(2-3), 149–151.
- 2944 Curtis, P. S. (1996). A meta-analysis of leaf gas exchange and nitrogen in trees
2945 grown under elevated carbon dioxide. *Plant, Cell and Environment* 19(2),
2946 127–137.
- 2947 Daly, C., M. Halbleib, J. I. Smith, W. P. Gibson, M. K. Doggett, G. H. Taylor,

- 2948** J. Curtis, and P. P. Pasteris (2008). Physiographically sensitive mapping
2949 of climatological temperature and precipitation across the conterminous
2950 United States. *International Journal of Climatology* 28(15), 2031–2064.
- 2951** Davies-Barnard, T., J. Meyerholt, S. Zaehle, P. Friedlingstein, V. Brovkin,
2952 Y. Fan, R. A. Fisher, C. D. Jones, H. Lee, D. Peano, B. Smith, D. Wårlind,
2953 and A. J. Wiltshire (2020). Nitrogen cycling in CMIP6 land surface models:
2954 progress and limitations. *Biogeosciences* 17(20), 5129–5148.
- 2955** Davis, T. W., I. C. Prentice, B. D. Stocker, R. T. Thomas, R. J. Whitley,
2956 H. Wang, B. J. Evans, A. V. Gallego-Sala, M. T. Sykes, and W. Cramer
2957 (2017). Simple process-led algorithms for simulating habitats (SPLASH
2958 v.1.0): robust indices of radiation, evapotranspiration and plant-available
2959 moisture. *Geoscientific Model Development* 10, 689–708.
- 2960** Delaire, M., E. Frak, M. Sigogne, B. Adam, F. Beaujard, and X. Le Roux
2961 (2005). Sudden increase in atmospheric CO₂ concentration reveals strong
2962 coupling between shoot carbon uptake and root nutrient uptake in young
2963 walnut trees. *Tree Physiology* 25(2), 229–235.
- 2964** Doane, T. A. and W. R. Horwáth (2003). Spectrophotometric determination of
2965 nitrate with a single reagent. *Analytical Letters* 36(12), 2713–2722.
- 2966** Dong, N., I. C. Prentice, B. J. Evans, S. Caddy-Retalic, A. J. Lowe, and I. J.
2967 Wright (2017). Leaf nitrogen from first principles: field evidence for adaptive
2968 variation with climate. *Biogeosciences* 14(2), 481–495.
- 2969** Dong, N., I. C. Prentice, I. J. Wright, B. J. Evans, H. F. Togashi, S. Caddy-
2970 Retalic, F. A. McInerney, B. Sparrow, E. Leitch, and A. J. Lowe (2020).
2971 Components of leaf-trait variation along environmental gradients. *New Phy-*

- 2972** *tologist* 228(1), 82–94.
- 2973** Dong, N., I. C. Prentice, I. J. Wright, H. Wang, O. K. Atkin, K. J. Bloomfield,
- 2974** T. F. Domingues, S. M. Gleason, V. Maire, Y. Onoda, H. Poorter, and N. G.
- 2975** Smith (2022). Leaf nitrogen from the perspective of optimal plant function.
- 2976** *Journal of Ecology* 110(11), 2585–2602.
- 2977** Dong, N., I. J. Wright, J. M. Chen, X. Luo, H. Wang, T. F. Keenan, N. G.
- 2978** Smith, and I. C. Prentice (2022). Rising CO₂ and warming reduce global
- 2979** canopy demand for nitrogen. *New Phytologist* 235(5), 1692–1700.
- 2980** Dovrat, G., H. Bakhshian, T. Masci, and E. Sheffer (2020). The nitrogen eco-
- 2981** nomic spectrum of legume stoichiometry and fixation strategy. *New Phytol-*
- 2982** *ogist* 227(2), 365–375.
- 2983** Dovrat, G., T. Masci, H. Bakhshian, E. Mayzlish Gati, S. Golan, and E. Shef-
- 2984** fer (2018). Drought-adapted plants dramatically downregulate dinitrogen
- 2985** fixation: Evidences from Mediterranean legume shrubs. *Journal of Ecol-*
- 2986** *ogy* 106(4), 1534–1544.
- 2987** Drake, B. G., M. A. Gonzàlez-Meler, and S. P. Long (1997). More efficient
- 2988** plants: a consequence of rising atmospheric CO₂? *Annual Review of Plant*
- 2989** *Biology* 48, 609–639.
- 2990** Duursma, R. A. (2015). Plantecophys - An R package for analyzing and mod-
- 2991** elling leaf gas exchange data. *PLOS ONE* 10(11), e0143346.
- 2992** Eastman, B. A., M. B. Adams, E. R. Brzostek, M. B. Burnham, J. E. Carrara,
- 2993** C. Kelly, B. E. McNeil, C. A. Walter, and W. T. Peterjohn (2021). Altered
- 2994** plant carbon partitioning enhanced forest ecosystem carbon storage after 25

- 2995** years of nitrogen additions. *New Phytologist* 230(4), 1435–1448.
- 2996** Ellsworth, D. S. and P. B. Reich (1996). Photosynthesis and leaf nitrogen in five
- 2997** Amazonian tree species during early secondary succession. *Ecology* 77(2),
- 2998** 581–594.
- 2999** Espelta, J. M., P. Cortés, M. Mangirón, and J. Retana (2005). Differences
- 3000** in biomass partitioning, leaf nitrogen content, and water use efficiency δ^{13}
- 3001** result in similar performance of seedlings of two Mediterranean oaks with
- 3002** contrasting leaf habit. *Ecoscience* 12(4), 447–454.
- 3003** Evans, J. R. (1989). Photosynthesis and nitrogen relationships in leaves of C₃
- 3004** plants. *Oecologia* 78(1), 9–19.
- 3005** Evans, J. R. and V. C. Clarke (2019). The nitrogen cost of photosynthesis.
- 3006** *Journal of Experimental Botany* 70(1), 7–15.
- 3007** Evans, J. R. and H. Poorter (2001). Photosynthetic acclimation of plants to
- 3008** growth irradiance: the relative importance of specific leaf area and nitrogen
- 3009** partitioning in maximizing carbon gain. *Plant, Cell and Environment* 24(8),
- 3010** 755–767.
- 3011** Evans, J. R. and J. R. Seemann (1989). The allocation of protein nitrogen in
- 3012** the photosynthetic apparatus: costs, consequences, and control. *Photosyn-*
- 3013** *thesis* 8, 183–205.
- 3014** Exbrayat, J.-F., A. A. Bloom, P. Falloon, A. Ito, T. L. Smallman, and
- 3015** M. Williams (2018). Reliability ensemble averaging of 21st century projec-
- 3016** tions of terrestrial net primary productivity reduces global and regional
- 3017** uncertainties. *Earth System Dynamics* 9(1), 153–165.

- 3018** Farquhar, G. D., J. R. Ehleringer, and K. T. Hubick (1989). Carbon isotope
3019 discrimination and photosynthesis. *Annual Review of Plant Physiology and*
3020 *Plant Molecular Biology* 40(1), 503–537.
- 3021** Farquhar, G. D. and T. D. Sharkey (1982). Stomatal conductance and photo-
3022 synthesis. *Annual Review of Plant Physiology* 33(1), 317–345.
- 3023** Farquhar, G. D., S. von Caemmerer, and J. A. Berry (1980). A biochemical
3024 model of photosynthetic CO₂ assimilation in leaves of C₃ species.
3025 *Planta* 149(1), 78–90.
- 3026** Fay, P. A., S. M. Prober, W. S. Harpole, J. M. H. Knops, J. D. Bakker, E. T.
3027 Borer, E. M. Lind, A. S. MacDougall, E. W. Seabloom, P. D. Wragg, P. B.
3028 Adler, D. M. Blumenthal, Y. M. Buckley, C. Chu, E. E. Cleland, S. L.
3029 Collins, K. F. Davies, G. Du, X. Feng, J. Firn, D. S. Gruner, N. Hagenah,
3030 Y. Hautier, R. W. Heckman, V. L. Jin, K. P. Kirkman, J. A. Klein, L. M.
3031 Ladwig, Q. Li, R. L. McCulley, B. A. Melbourne, C. E. Mitchell, J. L. Moore,
3032 J. W. Morgan, A. C. Risch, M. Schütz, C. J. Stevens, D. A. Wedin, and
3033 L. H. Yang (2015). Grassland productivity limited by multiple nutrients.
3034 *Nature Plants* 1(7), 15080.
- 3035** Feng, X. (1999). Trends in intrinsic water-use efficiency of natural trees for the
3036 past 100-200 years: A response to atmospheric CO₂ concentration. *Geochim-
3037* *ica et Cosmochimica Acta* 63(13-14), 1891–1903.
- 3038** Field, C. B. and H. A. Mooney (1986). The photosynthesis-nitrogen relationship
3039 in wild plants. In T. J. Givnish (Ed.), *On the Economy of Plant Form and*
3040 *Function*, pp. 25–55. Cambridge: Cambridge University Press.
- 3041** Finzi, A. C., D. J. P. Moore, E. H. DeLucia, J. Lichter, K. S. Hofmockel, R. B.

- 3042 Jackson, H. S. Kim, R. Matamala, H. R. McCarthy, R. Oren, J. S. Pippen,
3043 and W. H. Schlesinger (2006). Progressive nitrogen limitation of ecosystem
3044 processes under elevated CO₂ in a warm-temperate forest. *Ecology* 87(1),
3045 15–25.
- 3046 Firn, J., J. M. McGree, E. Harvey, H. Flores Moreno, M. Schutz, Y. M. Buckley,
3047 E. T. Borer, E. W. Seabloom, K. J. La Pierre, A. M. MacDougall, S. M.
3048 Prober, C. J. Stevens, L. L. Sullivan, E. Porter, E. Ladouceur, C. Allen,
3049 K. H. Moromizato, J. W. Morgan, W. S. Harpole, Y. Hautier, N. Eisen-
3050 hauer, J. P. Wright, P. B. Adler, C. A. Arnillas, J. D. Bakker, L. Biederman,
3051 A. A. D. Broadbent, C. S. Brown, M. N. Bugalho, M. C. Caldeira, E. E. Cle-
3052 land, A. Ebeling, P. A. Fay, N. Hagenah, A. R. Kleinhesselink, R. Mitchell,
3053 J. L. Moore, C. Nogueira, P. L. Peri, C. Roscher, M. D. Smith, P. D. Wragg,
3054 and A. C. Risch (2019). Leaf nutrients, not specific leaf area, are consistent
3055 indicators of elevated nutrient inputs. *Nature Ecology and Evolution* 3(3),
3056 400–406.
- 3057 Fisher, J. B., S. Sitch, Y. Malhi, R. A. Fisher, C. Huntingford, and S.-Y. Tan
3058 (2010). Carbon cost of plant nitrogen acquisition: A mechanistic, globally
3059 applicable model of plant nitrogen uptake, retranslocation, and fixation.
3060 *Global Biogeochemical Cycles* 24(1), 1–17.
- 3061 Fox, J. and S. Weisberg (2019). *An R companion to applied regression* (Third
3062 edit ed.). Thousand Oaks, California: Sage.
- 3063 Franklin, O., R. E. McMurtrie, C. M. Iversen, K. Y. Crous, A. C. Finzi, D. Tis-
3064 sue, D. S. Ellsworth, R. Oren, and R. J. Norby (2009). Forest fine-root
3065 production and nitrogen use under elevated CO₂: contrasting responses

- 3066** in evergreen and deciduous trees explained by a common principle. *Global
3067 Change Biology* 15(1), 132–144.
- 3068** Friedlingstein, P., M. Meinshausen, V. K. Arora, C. D. Jones, A. Anav, S. K.
3069 Liddicoat, and R. Knutti (2014). Uncertainties in CMIP5 climate projections
3070 due to carbon cycle feedbacks. *Journal of Climate* 27(2), 511–526.
- 3071** Friel, C. A. and M. L. Friesen (2019). Legumes modulate allocation to rhizobial
3072 nitrogen fixation in response to factorial light and nitrogen manipulation.
3073 *Frontiers in Plant Science* 10, 1316.
- 3074** Fujikake, H., A. Yamazaki, N. Ohtake, K. Sueoshi, S. Matsuhashi, T. Ito,
3075 C. Mizuniwa, T. Kume, S. Hoshimoto, N.-S. Ishioka, S. Watanabe, A. Osa,
3076 T. Sekine, H. Uchida, A. Tsuji, and T. Ohyama (2003). Quick and reversible
3077 inhibition of soybean root nodule growth by nitrate involves a decrease in
3078 sucrose supply to nodules. *Journal of Experimental Botany* 54(386), 1379–
3079 1388.
- 3080** Ghannoum, O., J. R. Evans, and S. von Caemmerer (2011). Nitrogen and water
3081 use efficiency of C₄ plants. In A. S. Raghavendra and R. F. Sage (Eds.), *C₄
3082 Photosynthesis and Related CO₂ Concentrating Mechanisms*, Chapter 8, pp.
3083 129–146. Springer.
- 3084** Ghimire, B., W. J. Riley, C. D. Koven, J. Kattge, A. Rogers, P. B. Reich, and
3085 I. J. Wright (2017). A global trait-based approach to estimate leaf nitrogen
3086 functional allocation from observations:. *Ecological Applications* 27(5),
3087 1421–1434.
- 3088** Giardina, C. P., M. D. Coleman, J. E. Hancock, J. S. King, E. A. Lilleskov,
3089 W. M. Loya, K. S. Pregitzer, M. G. Ryan, and C. C. Trettin (2005). The

- 3090 response of belowground carbon allocation in forests to global change. In
3091 D. Binkley and O. Manyailo (Eds.), *Tree Species Effects on Soils: Implications for Global Change* (Volume 55 ed.), Chapter Chapter 7, pp. 119–154.
3092 Berlin/Heidelberg: Springer-Verlag.
- 3093
- 3094 Gibson, A. H. and J. E. Harper (1985). Nitrate effect on nodulation of soybean
3095 by *Bradyrhizobium japonicum*. *Crop Science* 25(3), 497–501.
- 3096 Gill, A. L. and A. C. Finzi (2016). Belowground carbon flux links biogeochemical
3097 cycles and resource-use efficiency at the global scale. *Ecology Letters* 19(12),
3098 1419–1428.
- 3099 Goll, D. S., V. Brovkin, B. R. Parida, C. H. Reick, J. Kattge, P. B. Reich, P. M.
3100 van Bodegom, and Ü. Niinemets (2012). Nutrient limitation reduces land
3101 carbon uptake in simulations with a model of combined carbon, nitrogen
3102 and phosphorus cycling. *Biogeosciences Discussions* 9(3), 3173–3232.
- 3103 Gregory, L. M., A. M. McClain, D. M. Kramer, J. D. Pardo, K. E. Smith, O. L.
3104 Tessmer, B. J. Walker, L. G. Ziccardi, and T. D. Sharkey (2021, oct). The
3105 triose phosphate utilization limitation of photosynthetic rate: Out of global
3106 models but important for leaf models. *Plant, Cell and Environment* 44(10),
3107 3223–3226.
- 3108 Grossiord, C., T. N. Buckley, L. A. Cernusak, K. A. Novick, B. Poulter, R. T. W.
3109 Siegwolf, J. S. Sperry, and N. G. McDowell (2020). Plant responses to rising
3110 vapor pressure deficit. *New Phytologist* 226(6), 1550–1566.
- 3111 Gulmon, S. L. and C. C. Chu (1981). The effects of light and nitrogen on pho-
3112 tosynthesis, leaf characteristics, and dry matter allocation in the chaparral
3113 shrub, *Diplacus aurantiacus*. *Oecologia* 49(2), 207–212.

- 3114** Gutschick, V. P. (1981). Evolved strategies in nitrogen acquisition by plants.
- 3115** *The American Naturalist* 118(5), 607–637.
- 3116** Hallik, L., Ü. Niinemets, and I. J. Wright (2009). Are species shade and drought
- 3117** tolerance reflected in leaf-level structural and functional differentiation in
- 3118** Northern Hemisphere temperate woody flora? *New Phytologist* 184(1), 257–
- 3119** 274.
- 3120** Harrison, M. T., E. J. Edwards, G. D. Farquhar, A. B. Nicotra, and J. R.
- 3121** Evans (2009). Nitrogen in cell walls of sclerophyllous leaves accounts for
- 3122** little of the variation in photosynthetic nitrogen-use efficiency. *Plant, Cell*
- 3123** and *Environment* 32(3), 259–270.
- 3124** Harrison, S. P., W. Cramer, O. Franklin, I. C. Prentice, H. Wang,
- 3125** Å. Bränström, H. de Boer, U. Dieckmann, J. Joshi, T. F. Keenan,
- 3126** A. Lavergne, S. Manzoni, G. Mengoli, C. Morfopoulos, J. Peñuelas,
- 3127** S. Pietsch, K. T. Rebel, Y. Ryu, N. G. Smith, B. D. Stocker, and I. J.
- 3128** Wright (2021). Eco-evolutionary optimality as a means to improve vegeta-
- 3129** tion and land-surface models. *New Phytologist* 231(6), 2125–2141.
- 3130** Henneron, L., P. Kardol, D. A. Wardle, C. Cros, and S. Fontaine (2020). Rhizo-
- 3131** sphere control of soil nitrogen cycling: a key component of plant economic
- 3132** strategies. *New Phytologist* 228(4), 1269–1282.
- 3133** Hijmans, R. J. (2022). terra: Spatial Data Analysis.
- 3134** Hikosaka, K. and A. Shigeno (2009). The role of Rubisco and cell walls in the
- 3135** interspecific variation in photosynthetic capacity. *Oecologia* 160(3), 443–
- 3136** 451.

- 3137** Hoagland, D. R. and D. I. Arnon (1950). The water culture method for growing
3138 plants without soil. *California Agricultural Experiment Station: 347* 347(2),
3139 1–32.
- 3140** Hobbie, E. A. (2006). Carbon allocation to ectomycorrhizal fungi correlates
3141 with belowground allocation in culture studies. *Ecology* 87(3), 563–569.
- 3142** Hobbie, E. A. and J. E. Hobbie (2008). Natural abundance of ^{15}N in nitrogen-
3143 limited forests and tundra can estimate nitrogen cycling through mycorrhizal
3144 fungi: a review. *Ecosystems* 11(5), 815–830.
- 3145** Hoek, T. A., K. Axelrod, T. Biancalani, E. A. Yurtsev, J. Liu, and J. Gore
3146 (2016). Resource availability modulates the cooperative and competitive na-
3147 ture of a microbial cross-feeding mutualism. *PLOS Biology* 14(8), e1002540.
- 3148** Höglberg, M. N., M. J. I. Briones, S. G. Keel, D. B. Metcalfe, C. Campbell, A. J.
3149 Midwood, B. Thornton, V. Hurry, S. Linder, T. Näsholm, and P. Höglberg
3150 (2010). Quantification of effects of season and nitrogen supply on tree below-
3151 ground carbon transfer to ectomycorrhizal fungi and other soil organisms in
3152 a boreal pine forest. *New Phytologist* 187(2), 485–493.
- 3153** Höglberg, P., M. N. Höglberg, S. G. Göttlicher, N. R. Betson, S. G. Keel, D. B.
3154 Metcalfe, C. Campbell, A. Schindlbacher, V. Hurry, T. Lundmark, S. Linder,
3155 and T. Näsholm (2008). High temporal resolution tracing of photosynthate
3156 carbon from the tree canopy to forest soil microorganisms. *New Phytolo-*
3157 *gist* 177(1), 220–228.
- 3158** Houlton, B. Z., Y.-P. Wang, P. M. Vitousek, and C. B. Field (2008). A uni-
3159 fying framework for dinitrogen fixation in the terrestrial biosphere. *Na-*
3160 *ture* 454(7202), 327–330.

- 3161** Huber, M. L., R. A. Perkins, A. Laesecke, D. G. Friend, J. V. Sengers, M. J.
3162 Assael, I. N. Metaxa, E. Vogel, R. Mareš, and K. Miyagawa (2009). New
3163 international formulation for the viscosity of H₂O. *Journal of Physical and*
3164 *Chemical Reference Data* 38(2), 101–125.
- 3165** Hungate, B. A., J. S. Dukes, M. R. Shaw, Y. Luo, and C. B. Field (2003).
3166 Nitrogen and climate change. *Science* 302(5650), 1512–1513.
- 3167** IPCC (2021). *Climate Change 2021: The Physical Science Basis. Contribution*
3168 *of Working Group I to the Sixth Assessment Report of the Intergovernmental*
3169 *Panel on Climate Change*, Volume In Press. Cambridge, United Kingdom
3170 and New York, NY, USA: Cambridge University Press.
- 3171** Johnson, N. C., J. H. Graham, and F. A. Smith (1997). Functioning of mycor-
3172 rhizal associations along the mutualism-parasitism continuum. *New Phytol-*
3173 *ogist* 135(4), 575–585.
- 3174** Kachurina, O. M., H. Zhang, W. R. Raun, and E. G. Krenzer (2000). Simul-
3175 taneous determination of soil aluminum, ammonium- and nitrate- nitrogen
3176 using 1 M potassium chloride. *Communications in Soil Science and Plant*
3177 *Analysis* 31(7-8), 893–903.
- 3178** Kaiser, C., M. R. Kilburn, P. L. Clode, L. Fuchslueger, M. Koranda, J. B. Cliff,
3179 Z. M. Solaiman, and D. V. Murphy (2015). Exploring the transfer of recent
3180 plant photosynthates to soil microbes: mycorrhizal pathway vs direct root
3181 exudation. *New Phytologist* 205(4), 1537–1551.
- 3182** Katabuchi, M. (2015). LeafArea: An R package for rapid digital analysis of leaf
3183 area. *Ecological Research* 30(6), 1073–1077.

- 3184** Kattge, J. and W. Knorr (2007). Temperature acclimation in a biochemical
3185 model of photosynthesis: a reanalysis of data from 36 species. *Plant, Cell*
3186 and *Environment* 30(9), 1176–1190.
- 3187** Kattge, J., W. Knorr, T. Raddatz, and C. Wirth (2009). Quantifying photosyn-
3188 thetic capacity and its relationship to leaf nitrogen content for global-scale
3189 terrestrial biosphere models. *Global Change Biology* 15(4), 976–991.
- 3190** Kayler, Z., A. Gessler, and N. Buchmann (2010). What is the speed of link
3191 between aboveground and belowground processes? *New Phytologist* 187(4),
3192 885–888.
- 3193** Kayler, Z., C. Keitel, K. Jansen, and A. Gessler (2017). Experimental evidence
3194 of two mechanisms coupling leaf-level C assimilation to rhizosphere CO₂
3195 release. *Environmental and Experimental Botany* 135, 21–26.
- 3196** Keeling, C. D., W. G. Mook, and P. P. Tans (1979, jan). Recent trends in the
3197 ¹³C:¹²C ratio of atmospheric carbon dioxide. *Nature* 277(5692), 121–123.
- 3198** Keeney, D. R. and D. W. Nelson (1983). Nitrogen—Inorganic Forms. In A. L.
3199 Page (Ed.), *Methods of Soil Analysis* (2nd ed.), Chapter 33, pp. 643–698.
3200 Madison, WI, USA: ASA and SSSA.
- 3201** Kenward, M. G. and J. H. Roger (1997). Small sample inference for fixed effects
3202 from restricted maximum likelihood. *Biometrics* 53(3), 983.
- 3203** Knapp, A. K., M. L. Avolio, C. Beier, C. J. W. Carroll, S. L. Collins, J. S.
3204 Dukes, L. H. Fraser, R. J. Griffin-Nolan, D. L. Hoover, A. Jentsch, M. E.
3205 Loik, R. P. Phillips, A. K. Post, O. E. Sala, I. J. Slette, L. Yahdjian, and
3206 M. D. Smith (2017). Pushing precipitation to the extremes in distributed

- 3207 experiments: recommendations for simulating wet and dry years. *Global*
3208 *Change Biology* 23(5), 1774–1782.
- 3209 Knorr, W. (2000). Annual and interannual CO₂ exchanges of the
3210 terrestrial biosphere: process-based simulations and uncertainties. *Global*
3211 *Ecology and Biogeography* 9(3), 225–252.
- 3212 Knorr, W. and M. Heimann (2001). Uncertainties in global terrestrial biosphere
3213 modeling: 1. A comprehensive sensitivity analysis with a new photosynthesis
3214 and energy balance scheme. *Global Biogeochemical Cycles* 15(1), 207–225.
- 3215 Kulmatiski, A., P. B. Adler, J. M. Stark, and A. T. Tredennick (2017). Water
3216 and nitrogen uptake are better associated with resource availability than
3217 root biomass. *Ecosphere* 8(3), e01738.
- 3218 Lavergne, A., D. Sandoval, V. J. Hare, H. Graven, and I. C. Prentice (2020).
3219 Impacts of soil water stress on the acclimated stomatal limitation of pho-
3220 tosynthesis: Insights from stable carbon isotope data. *Global Change Biol-*
3221 *ogy* 26(12), 7158–7172.
- 3222 Lawrence, D. M., R. A. Fisher, C. D. Koven, K. W. Oleson, S. C. Swen-
3223 son, G. B. Bonan, N. Collier, B. Ghimire, L. Kampenhout, D. Kennedy,
3224 E. Kluzek, P. J. Lawrence, F. Li, H. Li, D. L. Lombardozzi, W. J. Riley,
3225 W. J. Sacks, M. Shi, M. Vertenstein, W. R. Wieder, C. Xu, A. A. Ali,
3226 A. M. Badger, G. Bisht, M. Broeke, M. A. Brunke, S. P. Burns, J. Buzan,
3227 M. Clark, A. Craig, K. M. Dahlin, B. Drewniak, J. B. Fisher, M. Flanner,
3228 A. M. Fox, P. Gentine, F. M. Hoffman, G. Keppel-Aleks, R. Knox, S. Ku-
3229 mar, J. Lenaerts, L. R. Leung, W. H. Lipscomb, Y. Lu, A. Pandey, J. D.
3230 Pelletier, J. Perket, J. T. Randerson, D. M. Ricciuto, B. M. Sanderson,

- 3231** A. Slater, Z. M. Subin, J. Tang, R. Q. Thomas, M. Val Martin, and X. Zeng
3232 (2019). The Community Land Model Version 5: description of new features,
3233 benchmarking, and impact of forcing uncertainty. *Journal of Advances in*
3234 *Modeling Earth Systems* 11(12), 4245–4287.
- 3235** LeBauer, D. S. and K. K. Treseder (2008). Nitrogen limitation of net primary
3236 productivity. *Ecology* 89(2), 371–379.
- 3237** Lefcheck, J. S. (2016). piecewiseSEM: Piecewise structural equation modelling
3238 in r for ecology, evolution, and systematics. *Methods in Ecology and Evolu-*
3239 *tion* 7(5), 573–579.
- 3240** Lenth, R. (2019). emmeans: estimated marginal means, aka least-squares
3241 means.
- 3242** Li, W., H. Zhang, G. Huang, R. Liu, H. Wu, C. Zhao, and N. G. McDowell
3243 (2020). Effects of nitrogen enrichment on tree carbon allocation: A global
3244 synthesis. *Global Ecology and Biogeography* 29(3), 573–589.
- 3245** Liang, J., X. Qi, L. Souza, and Y. Luo (2016). Processes regulating progressive
3246 nitrogen limitation under elevated carbon dioxide: a meta-analysis. *Biogeosciences*
3247 13(9), 2689–2699.
- 3248** Liang, X., T. Zhang, X. Lu, D. S. Ellsworth, H. BassiriRad, C. You, D. Wang,
3249 P. He, Q. Deng, H. Liu, J. Mo, and Q. Ye (2020). Global response patterns of
3250 plant photosynthesis to nitrogen addition: A meta-analysis. *Global Change*
3251 *Biology* 26(6), 3585–3600.
- 3252** López, J., D. A. Way, and W. Sadok (2021). Systemic effects of rising atmo-
3253 spheric vapor pressure deficit on plant physiology and productivity. *Global*

- 3254** *Change Biology* 27(9), 1704–1720.
- 3255** Lu, J., J. Yang, C. Keitel, L. Yin, P. Wang, W. Cheng, and F. A. Dijkstra
- 3256** (2022). Belowground carbon efficiency for nitrogen and phosphorus acqui-
- 3257** sition varies between *Lolium perenne* and *Trifolium repens* and depends on
- 3258** phosphorus fertilization. *Frontiers in Plant Science* 13, 1–9.
- 3259** Luo, X., T. F. Keenan, J. M. Chen, H. Croft, I. C. Prentice, N. G. Smith,
- 3260** A. P. Walker, H. Wang, R. Wang, C. Xu, and Y. Zhang (2021). Global
- 3261** variation in the fraction of leaf nitrogen allocated to photosynthesis. *Nature*
- 3262** *Communications* 12(1), 4866.
- 3263** Luo, Y., W. S. Currie, J. S. Dukes, A. C. Finzi, U. A. Hartwig, B. A. Hungate,
- 3264** R. E. McMurtrie, R. Oren, W. J. Parton, D. E. Pataki, R. M. Shaw, D. R.
- 3265** Zak, and C. B. Field (2004). Progressive nitrogen limitation of ecosystem
- 3266** responses to rising atmospheric carbon dioxide. *BioScience* 54(8), 731–739.
- 3267** Maire, V., P. Martre, J. Kattge, F. Gastal, G. Esser, S. Fontaine, and J.-F.
- 3268** Soussana (2012). The coordination of leaf photosynthesis links C and N
- 3269** fluxes in C₃ plant species. *PLoS ONE* 7(6), e38345.
- 3270** Makino, A. (2003). Rubisco and nitrogen relationships in rice: leaf photosyn-
- 3271** thesis and plant growth. *Soil Science and Plant Nutrition* 49(3), 319–327.
- 3272** Makino, A., M. Harada, T. Sato, H. Nakano, and T. Mae (1997). Growth and N
- 3273** Allocation in Rice Plants under CO₂ Enrichment. *Plant Physiology* 115(1),
- 3274** 199–203.
- 3275** Markham, J. H. and C. Zekveld (2007). Nitrogen fixation makes biomass al-
- 3276** location to roots independent of soil nitrogen supply. *Canadian Journal of*

- 3277** *Botany* (9), 787–793.
- 3278** Marschner, H. and B. Dell (1994). Nutrient uptake in mycorrhizal symbiosis.
- 3279** *Plant and Soil* 159(1), 89–102.
- 3280** Matamala, R. and W. H. Schlesinger (2000). Effects of elevated atmospheric
- 3281** CO₂ on fine root production and activity in an intact temperate forest
- 3282** ecosystem. *Global Change Biology* 6(8), 967–979.
- 3283** Medlyn, B. E., E. Dreyer, D. S. Ellsworth, M. Forstreuter, P. C. Harley,
- 3284** M. U. F. Kirschbaum, X. Le Roux, P. Montpied, J. Strassmeyer, A. Wal-
- 3285** croft, K. Wang, and D. Loustau (2002). Temperature response of parameters
- 3286** of a biochemically based model of photosynthesis. II. A review of experimen-
- 3287** tal data. *Plant, Cell and Environment* 25(9), 1167–1179.
- 3288** Menge, D. N. L., S. A. Levin, and L. O. Hedin (2008). Evolutionary tradeoffs can
- 3289** select against nitrogen fixation and thereby maintain nitrogen limitation.
- 3290** *Proceedings of the National Academy of Sciences* 105(5), 1573–1578.
- 3291** Menne, M. J., I. Durre, R. S. Vose, B. E. Gleason, and T. G. Houston (2012).
- 3292** An overview of the global historical climatology network-daily database.
- 3293** *Journal of Atmospheric and Oceanic Technology* 29(7), 897–910.
- 3294** Meyerholt, J., K. Sickel, and S. Zaehle (2020). Ensemble projections elucidate
- 3295** effects of uncertainty in terrestrial nitrogen limitation on future carbon up-
- 3296** take. *Global Change Biology* 26(7), 3978–3996.
- 3297** Meyerholt, J., S. Zaehle, and M. J. Smith (2016). Variability of projected ter-
- 3298** restrial biosphere responses to elevated levels of atmospheric CO₂ due to
- 3299** uncertainty in biological nitrogen fixation. *Biogeosciences* 13(5), 1491–1518.

- 3300** Minocha, R., S. Long, A. H. Magill, J. D. Aber, and W. H. McDowell (2000).
- 3301** Foliar free polyamine and inorganic ion content in relation to soil and soil
- 3302** solution chemistry in two fertilized forest stands at the Harvard Forest,
- 3303** Massachusetts. *Plant and Soil* 222(1-2), 119–137.
- 3304** Moore, D. J., S. Aref, R. M. Ho, J. S. Pippen, J. G. Hamilton, and E. H. De
- 3305** Lucia (2006). Annual basal area increment and growth duration of *Pinus*
- 3306** *taeda* in response to eight years of free-air carbon dioxide enrichment. *Global*
- 3307** *Change Biology* 12(8), 1367–1377.
- 3308** Morgan, J. A., D. E. Pataki, C. Körner, H. Clark, S. J. Del Grosso, J. M.
- 3309** Grünzweig, A. K. Knapp, A. R. Mosier, P. C. D. Newton, P. A. Niklaus,
- 3310** J. B. Nippert, R. S. Nowak, W. J. Parton, H. W. Polley, and M. R. Shaw
- 3311** (2004). Water relations in grassland and desert ecosystems exposed to ele-
- 3312** vated atmospheric CO₂. *Oecologia* 140(1), 11–25.
- 3313** Muñoz, N., X. Qi, M. W. Li, M. Xie, Y. Gao, M. Y. Cheung, F. L. Wong, and
- 3314** H.-M. Lam (2016). Improvement in nitrogen fixation capacity could be part
- 3315** of the domestication process in soybean. *Heredity* 117(2), 84–93.
- 3316** Nadelhoffer, K. J. and J. W. Raich (1992). Fine root production estimates and
- 3317** belowground carbon allocation in forest ecosystems. *Ecology* 73(4), 1139–
- 3318** 1147.
- 3319** Niinemets, Ü. and J. D. Tenhunen (1997). A model separating leaf structural
- 3320** and physiological effects on carbon gain along light gradients for the shade-
- 3321** tolerant species *Acer saccharum*. *Plant, Cell and Environment* 20(7), 845–
- 3322** 866.
- 3323** Norby, R. J., J. Ledford, C. D. Reilly, N. E. Miller, and E. G. O'Neill

- 3324** (2004). Fine-root production dominates response of a deciduous forest to
3325 atmospheric CO₂ enrichment. *Proceedings of the National Academy of Sci-
ences* 101(26), 9689–9693.
- 3327** Norby, R. J., J. M. Warren, C. M. Iversen, B. E. Medlyn, and R. E. Mc-
3328 Murtrie (2010). CO₂ enhancement of forest productivity constrained by
3329 limited nitrogen availability. *Proceedings of the National Academy of Sci-
ences* 107(45), 19368–19373.
- 3331** Novick, K. A., D. L. Ficklin, P. C. Stoy, C. A. Williams, G. Bohrer, A. C.
3332 Oishi, S. A. Papuga, P. D. Blanken, A. Noormets, B. N. Sulman, R. L.
3333 Scott, L. Wang, and R. P. Phillips (2016). The increasing importance of
3334 atmospheric demand for ecosystem water and carbon fluxes. *Nature Climate
Change* 6(11), 1023–1027.
- 3336** Noyce, G. L., M. L. Kirwan, R. L. Rich, and J. P. Megonigal (2019). Asyn-
3337 chronous nitrogen supply and demand produce nonlinear plant allocation re-
3338 sponds to warming and elevated CO₂. *Proceedings of the National Academy
of Sciences* 116(43), 21623–21628.
- 3340** Onoda, Y., K. Hikosaka, and T. Hirose (2004). Allocation of nitrogen to
3341 cell walls decreases photosynthetic nitrogen-use efficiency. *Functional Ecol-
ogy* 18(3), 419–425.
- 3343** Onoda, Y., I. J. Wright, J. R. Evans, K. Hikosaka, K. Kitajima, Ü. Niinemets,
3344 H. Poorter, T. Tosens, and M. Westoby (2017). Physiological and structural
3345 trade-offs underlying the leaf economics spectrum. *New Phytologist* 214(4),
3346 1447–1463.
- 3347** Oren, R., J. S. Sperry, G. G. Katul, D. E. Pataki, B. E. Ewers, N. Phillips,

- 3348** and K. V. R. Schäfer (1999). Survey and synthesis of intra- and interspecific
3349 variation in stomatal sensitivity to vapor pressure deficit. *Plant, Cell and*
3350 *Environment* 22(12), 1515–1526.
- 3351** Oreskes, N., K. Shrader-Frechette, and K. Belitz (1994). Verification, vali-
3352 dation, and confirmation of numerical models in the Earth sciences. *Sci-
ence* 263(5147), 641–646.
- 3353** Paillassa, J., I. J. Wright, I. C. Prentice, S. Pepin, N. G. Smith, G. Ethier,
3354 A. C. Westerband, L. J. Lamarque, H. Wang, W. K. Cornwell, and V. Maire
3355 (2020). When and where soil is important to modify the carbon and water
3356 economy of leaves. *New Phytologist* 228(1), 121–135.
- 3357** Parvin, S., S. Uddin, S. Tausz Posch, R. Armstrong, and M. Tausz (2020). Car-
3358 bon sink strength of nodules but not other organs modulates photosynthesis
3359 of faba bean (*Vicia faba*) grown under elevated [CO₂] and different water
3360 supply. *New Phytologist* 227(1), 132–145.
- 3361** Paul, K. I., P. J. Polglase, A. M. O'Connell, J. C. Carlyle, P. J. Smethurst, and
3362 P. K. Khanna (2003). Defining the relation between soil water content and
3363 net nitrogen mineralization. *European Journal of Soil Science* 54(1), 39–48.
- 3364** Peng, Y., K. J. Bloomfield, L. A. Cernusak, T. F. Domingues, and I. C. Pren-
3365 tice (2021). Global climate and nutrient controls of photosynthetic capacity.
3366 *Communications Biology* 4(1), 462.
- 3367** Perkowski, E. A., E. F. Waring, and N. G. Smith (2021). Root mass carbon
3368 costs to acquire nitrogen are determined by nitrogen and light availabil-
3369 ity in two species with different nitrogen acquisition strategies. *Journal of*
3370 *Experimental Botany* 72(15), 5766–5776.
- 3371**

- 3372** Phillips, R. P., E. R. Brzostek, and M. G. Midgley (2013). The mycorrhizal-
3373 associated nutrient economy: a new framework for predicting carbon-
3374 nutrient couplings in temperate forests. *New Phytologist* 199(1), 41–51.
- 3375** Phillips, R. P., A. C. Finzi, and E. S. Bernhardt (2011). Enhanced root ex-
3376 udation induces microbial feedbacks to N cycling in a pine forest under
3377 long-term CO₂ fumigation. *Ecology Letters* 14(2), 187–194.
- 3378** Pinheiro, J. and D. Bates (2022). nlme: linear and nonlinear mixed effects
3379 models.
- 3380** Poggio, L., L. M. De Sousa, N. H. Batjes, G. B. M. Heuvelink, B. Kempen,
3381 E. Ribeiro, and D. Rossiter (2021). SoilGrids 2.0: Producing soil information
3382 for the globe with quantified spatial uncertainty. *Soil* 7(1), 217–240.
- 3383** Pons, T. L. and R. W. Pearcy (1994). Nitrogen reallocation and photosynthetic
3384 acclimation in response to partial shading in soybean plants. *Physiologia*
3385 *Plantarum* 92(4), 636–644.
- 3386** Poorter, H., J. Bühler, D. Van Dusschoten, J. Climent, and J. A. Postma (2012).
3387 Pot size matters: A meta-analysis of the effects of rooting volume on plant
3388 growth. *Functional Plant Biology* 39(11), 839–850.
- 3389** Poorter, H., O. Knopf, I. J. Wright, A. A. Temme, S. W. Hogewoning, A. Graf,
3390 L. A. Cernusak, and T. L. Pons (2022). A meta-analysis of responses of C₃
3391 plants to atmospheric CO₂: dose-response curves for 85 traits ranging from
3392 the molecular to the whole-plant level. *New Phytologist* 233(4), 1560–1596.
- 3393** Prentice, I. C., N. Dong, S. M. Gleason, V. Maire, and I. J. Wright (2014).
3394 Balancing the costs of carbon gain and water transport: testing a new theo-

- 3395 retical framework for plant functional ecology. *Ecology Letters* 17(1), 82–91.
- 3396 Prentice, I. C., X. Liang, B. E. Medlyn, and Y.-P. Wang (2015). Reliable, ro-
- 3397 bust and realistic: The three R’s of next-generation land-surface modelling.
- 3398 *Atmospheric Chemistry and Physics* 15, 5987–6005.
- 3399 Priestley, C. H. B. and R. J. Taylor (1972). On the Assessment of Surface
- 3400 Heat Flux and Evaporation Using Large-Scale Parameters. *Monthly Weather*
- 3401 *Review* 100(2), 81–92.
- 3402 Querejeta, J. I., I. Prieto, C. Armas, F. Casanoves, J. S. Diémé, M. Diouf,
- 3403 H. Yossi, B. Kaya, F. I. Pugnaire, and G. M. Rusch (2022). Higher leaf
- 3404 nitrogen content is linked to tighter stomatal regulation of transpiration
- 3405 and more efficient water use across dryland trees. *New Phytologist* 235(4),
- 3406 1351–1364.
- 3407 R Core Team (2021). R: A language and environment for statistical computing.
- 3408 Raich, J. W., D. A. Clark, L. Schwendenmann, and T. E. Wood (2014). Above-
- 3409 ground tree growth varies with belowground carbon allocation in a tropical
- 3410 rainforest environment. *PLoS ONE* 9(6), e100275.
- 3411 Rastetter, E. B., P. M. Vitousek, C. B. Field, G. R. Shaver, D. Herbert, and
- 3412 G. I. Ågren (2001). Resource optimization and symbiotic nitrogen fixation.
- 3413 *Ecosystems* 4(4), 369–388.
- 3414 Reich, P. B. (2014). The world-wide ‘fast-slow’ plant economics spectrum: a
- 3415 traits manifesto. *Journal of Ecology* 102(2), 275–301.
- 3416 Reich, P. B., S. E. Hobbie, T. Lee, D. S. Ellsworth, J. B. West, D. Tilman,
- 3417 J. M. H. Knops, S. Naeem, and J. Trost (2006). Nitrogen limitation con-

- 3418 strains sustainability of ecosystem response to CO₂. *Nature* 440(7086), 922–
3419 925.
- 3420 Reichman, G. A., D. L. Grunes, and F. G. Viets (1966). Effect of soil moisture
3421 on ammonification and nitrification in two Northern Plains soils. *Soil Science
3422 Society of America Journal* 30(3), 363–366.
- 3423 Rhine, E. D., R. L. Mulvaney, E. J. Pratt, and G. K. Sims (1998). Improving
3424 the Berthelot reaction for determining ammonium in soil extracts and water.
3425 *Soil Science Society of America Journal* 62(2), 473.
- 3426 Rogers, A. (2014). The use and misuse of V_{cmax} in Earth System Models. *Photo-
3427 synthesis Research* 119(1-2), 15–29.
- 3428 Rogers, A., B. E. Medlyn, J. S. Dukes, G. B. Bonan, S. Caemmerer, M. C.
3429 Dietze, J. Kattge, A. D. B. Leakey, L. M. Mercado, Ü. Niinemets, I. C.
3430 Prentice, S. P. Serbin, S. Sitch, D. A. Way, and S. Zaehle (2017). A roadmap
3431 for improving the representation of photosynthesis in Earth system models.
3432 *New Phytologist* 213(1), 22–42.
- 3433 Saathoff, A. J. and J. Welles (2021). Gas exchange measurements in the un-
3434 steady state. *Plant Cell and Environment* 44(11), 3509–3523.
- 3435 Sage, R. F. and R. W. Pearcy (1987). The nitrogen use efficiency of C₃ and C₄
3436 plants: I. Leaf nitrogen, growth, and biomass partitioning in *Chenopodium
3437 album* (L.) and *Amaranthus retroflexus* (L.). *Plant Physiology* 84(3), 954–
3438 958.
- 3439 Saleh, A. M., M. Abdel-Mawgoud, A. R. Hassan, T. H. Habeeb, R. S. Yehia,
3440 and H. AbdElgawad (2020). Global metabolic changes induced by arbuscular

- 3441** mycorrhizal fungi in oregano plants grown under ambient and elevated levels
3442 of atmospheric CO₂. *Plant Physiology and Biochemistry* 151, 255–263.
- 3443** Saxton, K. E. and W. J. Rawls (2006). Soil water characteristic estimates by
3444 texture and organic matter for hydrologic solutions. *Soil Science Society of*
3445 *America Journal* 70(5), 1569–1578.
- 3446** Schaefer, K., C. R. Schwalm, C. Williams, M. A. Arain, A. Barr, J. M. Chen,
3447 K. J. Davis, D. Dimitrov, T. W. Hilton, D. Y. Hollinger, E. Humphreys,
3448 B. Poulter, B. M. Racza, A. D. Richardson, A. Sahoo, P. Thornton, R. Var-
3449 gas, H. Verbeeck, R. Anderson, I. Baker, T. A. Black, P. Bolstad, J. Chen,
3450 P. S. Curtis, A. R. Desai, M. C. Dietze, D. Dragoni, C. M. Gough, R. F.
3451 Grant, L. Gu, A. K. Jain, C. Kucharik, B. E. Law, S. Liu, E. Lokipitiya,
3452 H. A. Margolis, R. Matamala, J. H. McCaughey, R. Monson, J. W. Munger,
3453 W. Oechel, C. Peng, D. T. Price, D. Ricciuto, W. J. Riley, N. Roulet,
3454 H. Tian, C. Tonitto, M. Torn, E. Weng, and X. Zhou (2012). A model-
3455 data comparison of gross primary productivity: Results from the North
3456 American Carbon Program site synthesis. *Journal of Geophysical Research:*
3457 *Biogeosciences* 117(G3), G03010.
- 3458** Schmitt, M. R. and G. E. Edwards (1981). Photosynthetic capacity and nitrogen
3459 use efficiency of maize, wheat, and rice: A comparison between C₃ and C₄
3460 photosynthesis. *Journal of Experimental Botany* 32(3), 459–466.
- 3461** Schneider, C. A., W. S. Rasband, and K. W. Eliceiri (2012). NIH Image to
3462 ImageJ: 25 years of image analysis. *Nature Methods* 9(7), 671–675.
- 3463** Scott, H. G. and N. G. Smith (2022). A Model of C₄ photosynthetic acclima-
3464 tion based on least-cost optimality theory suitable for Earth system model

- 3465** incorporation. *Journal of Advances in Modeling Earth Systems* 14(3), 1–16.
- 3466** Shi, M., J. B. Fisher, E. R. Brzostek, and R. P. Phillips (2016). Carbon cost
3467 of plant nitrogen acquisition: Global carbon cycle impact from an improved
3468 plant nitrogen cycle in the Community Land Model. *Global Change Biology*
3469 22(3), 1299–1314.
- 3470** Shi, M., J. B. Fisher, R. P. Phillips, and E. R. Brzostek (2019). Neglecting
3471 plant–microbe symbioses leads to underestimation of modeled climate im-
3472 pacts. *Biogeosciences* 16(2), 457–465.
- 3473** Smith, B., D. Wärllind, A. Arneth, T. Hickler, P. Leadley, J. Siltberg, and
3474 S. Zaehle (2014). Implications of incorporating N cycling and N limitations
3475 on primary production in an individual-based dynamic vegetation model.
3476 *Biogeosciences* 11(7), 2027–2054.
- 3477** Smith, N. G. and J. S. Dukes (2013). Plant respiration and photosynthesis in
3478 global-scale models: incorporating acclimation to temperature and CO₂.
3479 *Global Change Biology* 19(1), 45–63.
- 3480** Smith, N. G. and J. S. Dukes (2018). Drivers of leaf carbon exchange capacity
3481 across biomes at the continental scale. *Ecology* 99(7), 1610–1620.
- 3482** Smith, N. G. and T. F. Keenan (2020). Mechanisms underlying leaf photosyn-
3483 thetic acclimation to warming and elevated CO₂ as inferred from least-cost
3484 optimality theory. *Global Change Biology* 26(9), 5202–5216.
- 3485** Smith, N. G., T. F. Keenan, I. C. Prentice, H. Wang, I. J. Wright, Ü. Niinemets,
3486 K. Y. Crous, T. F. Domingues, R. Guerrieri, F. oko Ishida, J. Kattge, E. L.
3487 Kruger, V. Maire, A. Rogers, S. P. Serbin, L. Tarvainen, H. F. Togashi,

- 3488 P. A. Townsend, M. Wang, L. K. Weerasinghe, and S.-X. Zhou (2019).
3489 Global photosynthetic capacity is optimized to the environment. *Ecology*
3490 *Letters* 22(3), 506–517.
- 3491 Smith, N. G., D. L. Lombardozzi, A. Tawfik, G. B. Bonan, and J. S. Dukes
3492 (2017). Biophysical consequences of photosynthetic temperature acclimation
3493 for climate. *Journal of Advances in Modeling Earth Systems* 9(1), 536–547.
- 3494 Smith, N. G., S. L. Malyshev, E. Shevliakova, J. Kattge, and J. S. Dukes
3495 (2016). Foliar temperature acclimation reduces simulated carbon sensitivity
3496 to climate. *Nature Climate Change* 6(4), 407–411.
- 3497 Smith, S. E. and D. J. Read (2008). *Mycorrhizal Symbiosis*. Academic Press.
- 3498 Soil Survey Staff (2022). Web Soil Survey.
- 3499 Soudzilovskaia, N. A., J. C. Douma, A. A. Akhmetzhanova, P. M. van Bode-
3500 gom, W. K. Cornwell, E. J. Moens, K. K. Treseder, and J. H. C. Cornelissen
3501 (2015). Global patterns of plant root colonization intensity by mycorrhizal
3502 fungi explained by climate and soil chemistry. *Global Ecology and Biogeog-
3503 raphy* 24(3), 371–382.
- 3504 Stark, J. M. and M. K. Firestone (1995). Mechanisms for soil moisture ef-
3505 fects on activity of nitrifying bacteria. *Applied and Environmental Microbi-
3506 ology* 61(1), 218–221.
- 3507 Stocker, B. D., H. Wang, N. G. Smith, S. P. Harrison, T. F. Keenan, D. San-
3508 doval, T. Davis, and I. C. Prentice (2020). P-model v1.0: An optimality-
3509 based light use efficiency model for simulating ecosystem gross primary pro-
3510 duction. *Geoscientific Model Development* 13(3), 1545–1581.

- 3511 Stocker, B. D., J. Zscheischler, T. F. Keenan, I. C. Prentice, J. Peñuelas, and
3512 S. I. Seneviratne (2018). Quantifying soil moisture impacts on light use
3513 efficiency across biomes. *New Phytologist* 218(4), 1430–1449.
- 3514 Sulman, B. N., D. T. Roman, K. Yi, L. Wang, R. P. Phillips, and K. A.
3515 Novick (2016). High atmospheric demand for water can limit forest car-
3516 bon uptake and transpiration as severely as dry soil. *Geophysical Research
3517 Letters* 43(18), 9686–9695.
- 3518 Sulman, B. N., E. Shevliakova, E. R. Brzostek, S. N. Kivlin, S. L. Malyshev,
3519 D. N. L. Menge, and X. Zhang (2019). Diverse mycorrhizal associations
3520 enhance terrestrial C storage in a global model. *Global Biogeochemical Cy-
3521 cles* 33(4), 501–523.
- 3522 Sweet, S. K., D. W. Wolfe, A. DeGaetano, and R. Benner (2017). Anatomy
3523 of the 2016 drought in the Northeastern United States: Implications for
3524 agriculture and water resources in humid climates. *Agricultural and Forest
3525 Meteorology* 247, 571–581.
- 3526 Taylor, B. N. and D. N. L. Menge (2018). Light regulates tropical symbiotic
3527 nitrogen fixation more strongly than soil nitrogen. *Nature Plants* 4(9), 655–
3528 661.
- 3529 Terrer, C., S. Vicca, B. A. Hungate, R. P. Phillips, and I. C. Prentice (2016).
3530 Mycorrhizal association as a primary control of the CO₂ fertilization effect.
3531 *Science* 353(6294), 72–74.
- 3532 Terrer, C., S. Vicca, B. D. Stocker, B. A. Hungate, R. P. Phillips, P. B. Reich,
3533 A. C. Finzi, and I. C. Prentice (2018). Ecosystem responses to elevated CO₂
3534 governed by plant–soil interactions and the cost of nitrogen acquisition. *New*

- 3535 *Phytologist* 217(2), 507–522.
- 3536 Thieurmel, B. and A. Elmarhraoui (2019). suncalc: Compute sun position,
- 3537 sunlight phases, moon position, and lunar phase.
- 3538 Thomas, R. Q., E. N. J. Brookshire, and S. Gerber (2015). Nitrogen limita-
- 3539 tion on land: how can it occur in Earth system models? *Global Change*
- 3540 *Biology* 21(5), 1777–1793.
- 3541 Thomas, R. Q., S. Zaehle, P. H. Templer, and C. L. Goodale (2013). Global pat-
- 3542 terns of nitrogen limitation: confronting two global biogeochemical models
- 3543 with observations. *Global Change Biology* 19(10), 2986–2998.
- 3544 Thornton, P. E., J.-F. Lamarque, N. A. Rosenbloom, and N. M. Mahowald
- 3545 (2007). Influence of carbon-nitrogen cycle coupling on land model response
- 3546 to CO₂ fertilization and climate variability. *Global Biogeochemical Cy-*
- 3547 *cles* 21(4), GB4018.
- 3548 Tingey, D. T., D. L. Phillips, and M. G. Johnson (2000). Elevated CO₂ and
- 3549 conifer roots: effects on growth, life span and turnover. *New Phytolo-*
- 3550 *gist* 147(1), 87–103.
- 3551 Udvardi, M. and P. S. Poole (2013). Transport and metabolism in legume-
- 3552 rhizobia symbioses. *Annual Review of Plant Biology* 64, 781–805.
- 3553 USDA NRCS (2022). The PLANTS Database.
- 3554 Uselman, S. M., R. G. Qualls, and R. B. Thomas (2000). Effects of increased
- 3555 atmospheric CO₂, temperature, and soil N availability on root exudation
- 3556 of dissolved organic carbon by an N-fixing tree (*Robinia pseudoacacia* L.).
- 3557 *Plant and Soil* 222, 191–202.

- 3558 van Diepen, L. T. A., E. A. Lilleskov, K. S. Pregitzer, and R. M. Miller (2007).
- 3559 Decline of arbuscular mycorrhizal fungi in northern hardwood forests ex-
- 3560 posed to chronic nitrogen additions. *New Phytologist* 176(1), 175–183.
- 3561 Vance, C. P. and G. H. Heichel (1991). Carbon in N₂ fixation: Limitation or
- 3562 exquisite adaptation. *Annual Review of Plant Physiology and Plant Molec-*
- 3563 *ular Biology* 42(1), 373–392.
- 3564 Viet, H. D., J.-H. Kwak, K.-S. Lee, S.-S. Lim, M. Matsushima, S. X. Chang,
- 3565 K.-H. Lee, and W.-J. Choi (2013). Foliar chemistry and tree ring δ¹³C of
- 3566 *Pinus densiflora* in relation to tree growth along a soil pH gradient. *Plant*
- 3567 *and Soil* 363(1-2), 101–112.
- 3568 Vitousek, P. M., K. Cassman, C. C. Cleveland, T. Crews, C. B. Field, N. B.
- 3569 Grimm, R. W. Howarth, R. Marino, L. Martinelli, E. B. Rastetter, and
- 3570 J. I. Sprent (2002). Towards an ecological understanding of biological nitro-
- 3571 gen fixation. In *The Nitrogen Cycle at Regional to Global Scales*, pp. 1–45.
- 3572 Springer Netherlands.
- 3573 Vitousek, P. M. and R. W. Howarth (1991). Nitrogen limitation on land and in
- 3574 the sea: How can it occur? *Biogeochemistry* 13(2), 87–115.
- 3575 Vitousek, P. M., S. Porder, B. Z. Houlton, and O. A. Chadwick (2010).
- 3576 Terrestrial phosphorus limitation: mechanisms, implications, and nitro-
- 3577 gen–phosphorus interactions. *Ecological Applications* 20(1), 5–15.
- 3578 Walker, A. P., A. P. Beckerman, L. Gu, J. Kattge, L. A. Cernusak, T. F.
- 3579 Domingues, J. C. Scales, G. Wohlfahrt, S. D. Wullschleger, and F. I. Wood-
- 3580 ward (2014). The relationship of leaf photosynthetic traits - V_{cmax} and J_{max}
- 3581 - to leaf nitrogen, leaf phosphorus, and specific leaf area: a meta-analysis

- 3582 and modeling study. *Ecology and Evolution* 4(16), 3218–3235.
- 3583 Walker, A. P., A. L. Johnson, A. Rogers, J. Anderson, R. A. Bridges, R. A.
- 3584 Fisher, D. Lu, D. M. Ricciuto, S. P. Serbin, and M. Ye (2021). Multi-
- 3585 hypothesis comparison of Farquhar and Collatz photosynthesis models re-
- 3586 veals the unexpected influence of empirical assumptions at leaf and global
- 3587 scales. *Global Change Biology* 27(4), 804–822.
- 3588 Wang, H., I. C. Prentice, T. F. Keenan, T. W. Davis, I. J. Wright, W. K.
- 3589 Cornwell, B. J. Evans, and C. Peng (2017). Towards a universal model for
- 3590 carbon dioxide uptake by plants. *Nature Plants* 3(9), 734–741.
- 3591 Wang, H., I. C. Prentice, I. J. Wright, D. I. Warton, S. Qiao, X. Xu, J. Zhou,
- 3592 Kikuzawa, and N. C. Stenseth (2023). Leaf economics fundamentals ex-
- 3593 plained by optimality principles. *Science Advances* 9(3), eadd566.
- 3594 Wang, J., J. M. Knops, C. E. Brassil, and C. Mu (2017). Increased productivity
- 3595 in wet years drives a decline in ecosystem stability with nitrogen additions
- 3596 in arid grasslands. *Ecology* 98(7), 1779–1786.
- 3597 Wang, W., Y. Wang, G. Hoch, Z. Wang, and J. Gu (2018). Linkage of root mor-
- 3598 phology to anatomy with increasing nitrogen availability in six temperate
- 3599 tree species. *Plant and Soil* 425(1-2), 189–200.
- 3600 Weatherburn, M. W. (1967). Phenol-hypochlorite reaction for determination of
- 3601 ammonia. *Analytical Chemistry* 39(8), 971–974.
- 3602 Wellburn, A. R. (1994). The spectral determination of chlorophylls a and b, as
- 3603 well as total carotenoids, using various solvents with spectrophotometers of
- 3604 different resolution. *Journal of Plant Physiology* 144(3), 307–313.

- 3605 Wen, Z., P. J. White, J. Shen, and H. Lambers (2022). Linking root exuda-
3606 tion to belowground economic traits for resource acquisition. *New Phytolo-*
3607 *gist* 233(4), 1620–1635.
- 3608 Westerband, A. C., I. J. Wright, V. Maire, J. Paillassa, I. C. Prentice, O. K.
3609 Atkin, K. J. Bloomfield, L. A. Cernusak, N. Dong, S. M. Gleason, C. Guil-
3610 herme Pereira, H. Lambers, M. R. Leishman, Y. Malhi, and R. H. Nolan
3611 (2023). Coordination of photosynthetic traits across soil and climate gradi-
3612 ents. *Global Change Biology* 29(3), 1–29.
- 3613 Wieder, W. R., C. C. Cleveland, W. K. Smith, and K. Todd-Brown (2015).
3614 Future productivity and carbon storage limited by terrestrial nutrient avail-
3615 ability. *Nature Geoscience* 8(6), 441–444.
- 3616 Wieder, W. R., D. M. Lawrence, R. A. Fisher, G. B. Bonan, S. J. Cheng, C. L.
3617 Goodale, A. S. Grandy, C. D. Koven, D. L. Lombardozzi, K. W. Oleson,
3618 and R. Q. Thomas (2019). Beyond static benchmarking: using experimental
3619 manipulations to evaluate land model assumptions. *Global Biogeochemical*
3620 *Cycles* 33(10), 1289–1309.
- 3621 Wright, I. J., P. B. Reich, and M. Westoby (2003). Least-cost input mixtures
3622 of water and nitrogen for photosynthesis. *The American Naturalist* 161(1),
3623 98–111.
- 3624 Wright, I. J., P. B. Reich, M. Westoby, D. D. Ackerly, Z. Baruch, F. Bongers,
3625 J. Cavender-Bares, T. Chapin, J. H. C. Cornelissen, M. Diemer, J. Flexas,
3626 E. Garnier, P. K. Groom, J. Gulias, K. Hikosaka, B. B. Lamont, T. Lee,
3627 W. Lee, C. Lusk, J. J. Midgley, M.-L. Navas, Ü. Niinemets, J. Oleksyn,
3628 N. Osada, H. Poorter, P. Poot, L. Prior, V. I. Pyankov, C. Roumet, S. C.

- 3629** Thomas, M. G. Tjoelker, E. J. Veneklaas, and R. Villar (2004). The world-wide leaf economics spectrum. *Nature* 428(6985), 821–827.
- 3630**
- 3631** Xu-Ri and I. C. Prentice (2017). Modelling the demand for new nitrogen fixation by terrestrial ecosystems. *Biogeosciences* 14(7), 2003–2017.
- 3632**
- 3633** Yahdjian, L., L. A. Gherardi, and O. E. Sala (2011). Nitrogen limitation in arid-subhumid ecosystems: A meta-analysis of fertilization studies. *Journal of Arid Environments* 75(8), 675–680.
- 3634**
- 3635**
- 3636** Zaehle, S., B. E. Medlyn, M. G. De Kauwe, A. P. Walker, M. C. Dietze, T. Hickler, Y. Luo, Y. P. Wang, B. El-Masri, P. Thornton, A. Jain, S. Wang,
- 3637**
- 3638** D. Warlind, E. Weng, W. Parton, C. M. Iversen, A. Gallet-Budynek, H. McCarthy, A. C. Finzi, P. J. Hanson, I. C. Prentice, R. Oren, and R. J. Norby
- 3639**
- 3640** (2014). Evaluation of 11 terrestrial carbon-nitrogen cycle models against observations from two temperate Free-Air CO₂ Enrichment studies. *New Phytologist* 202(3), 803–822.
- 3641**
- 3642**
- 3643** Zaehle, S., S. Sitch, B. Smith, and F. Hatterman (2005). Effects of parameter uncertainties on the modeling of terrestrial biosphere dynamics. *Global Biogeochemical Cycles* 19(3), GB3020.
- 3644**
- 3645**
- 3646** Zhu, Q., W. J. Riley, J. Tang, N. Collier, F. M. Hoffman, X. Yang, and G. Bisht
- 3647**
- 3648** (2019). Representing nitrogen, phosphorus, and carbon interactions in the E3SM land model: development and global benchmarking. *Journal of Advances in Modeling Earth Systems* 11(7), 2238–2258.
- 3649**
- 3650** Ziegler, C., M. E. Dusenge, B. Nyirambangutse, E. Zibera, G. Wallin, and
- 3651**
- 3652** J. Uddling (2020). Contrasting dependencies of photosynthetic capacity on leaf nitrogen in early- and late-successional tropical montane tree species.

- 3653** *Frontiers in Plant Science* 11, 1–12.
- 3654** Ziehn, T., J. Kattge, W. Knorr, and M. Scholze (2011). Improving the pre-
3655 dictability of global CO₂ assimilation rates under climate change. *Geophys-
3656 ical Research Letters* 38(10), L10404.

3657 Appendix A: Supplemental material for "Structural carbon costs to
3658 acquire nitrogen are determined by nitrogen and light availability in
3659 two species with different nitrogen acquisition strategies"

Table A1. Summary table containing volumes of compounds used to create modified Hoagland's solutions for each soil nitrogen fertilization treatment. All volumes are expressed as milliliters per liter (mL/L)

Compound	0 ppm N	70 ppm N	210 ppm N	630 ppm N
1 M NH ₄ H ₂ PO ₄	0	0.33	1	1
2 M KNO ₃	0	0.67	2	2
2 M Ca(NO ₃) ₂	0	0.67	2	2
1 M NH ₄ NO ₃	0	0.33	1	0
8 M NH ₄ NO ₃	0	0	0	2
1 M KH ₂ PO ₄	1	0.67	0	0
1 M KCl	4	1.33	0	0
1 M CaCO ₃	4	3	0	0
2 M MgSO ₄	1	1	1	1
10% Fe-EDTA	1	1	1	1
Trace Elements	1	1	1	1

Table A2. Analysis of variance results exploring species-specific effects of light availability, nitrogen fertilization, and their interactions on the ratio of whole plant biomass to pot volume

	df	Biomass:pot volume		
		Coefficient	χ^2	p
<i>G. hirsutum</i>				
Intercept		0.740	-	-
Light (L)	1	-4.23E-03	189.581	<0.001
Nitrogen (N)	1	7.86E-04	17.927	<0.001
L*N	1	-6.61E-06	4.709	0.030
<i>G. max</i>				
Intercept		-0.233	-	-
Light (L)	1	-1.12E-02	69.500	<0.001
Nitrogen (N)	1	8.29E-04	40.297	<0.001
L*N	1	-8.51E-06	5.548	0.019

3660 *Significance determined using Wald's χ^2 tests ($P = 0.05$). P -values < 0.05 are
3661 in bold and p -values between 0.05 and 0.1 are italicized. Negative coefficients
3662 for light treatments indicate a positive effect of increasing light availability on
3663 all response variables, as light availability is treated as percent shade cover in all
3664 linear mixed-effects models.

Table A3. Slopes of the regression line describing the relationship between each dependent variable and nitrogen fertilization at each light level*

Shade cover	Slope
<i>G. hirsutum</i>	
0%	8.29E-04^a
30%	5.74E-04^a
50%	4.03E-04^a
80%	1.48E-04 ^a
<i>G. max</i>	
0%	7.86E-04
30%	5.87E-04
50%	4.55E-04
80%	<i>2.57E-05</i>

3665 *Slopes represent estimated marginal mean slopes from linear mixed-effects models described in the Methods. Slopes
3666 were calculated using the ‘emmeans’ R package (Lenth 2019). Superscripts indicate slopes fit to natural-log (^a) or
3667 square root (^b) transformed data. Slopes statistically different from zero (Tukey: $p < 0.05$) are indicated in bold.
3668 Marginally significant slopes (Tukey: $0.05 < p < 0.1$) are italicized.

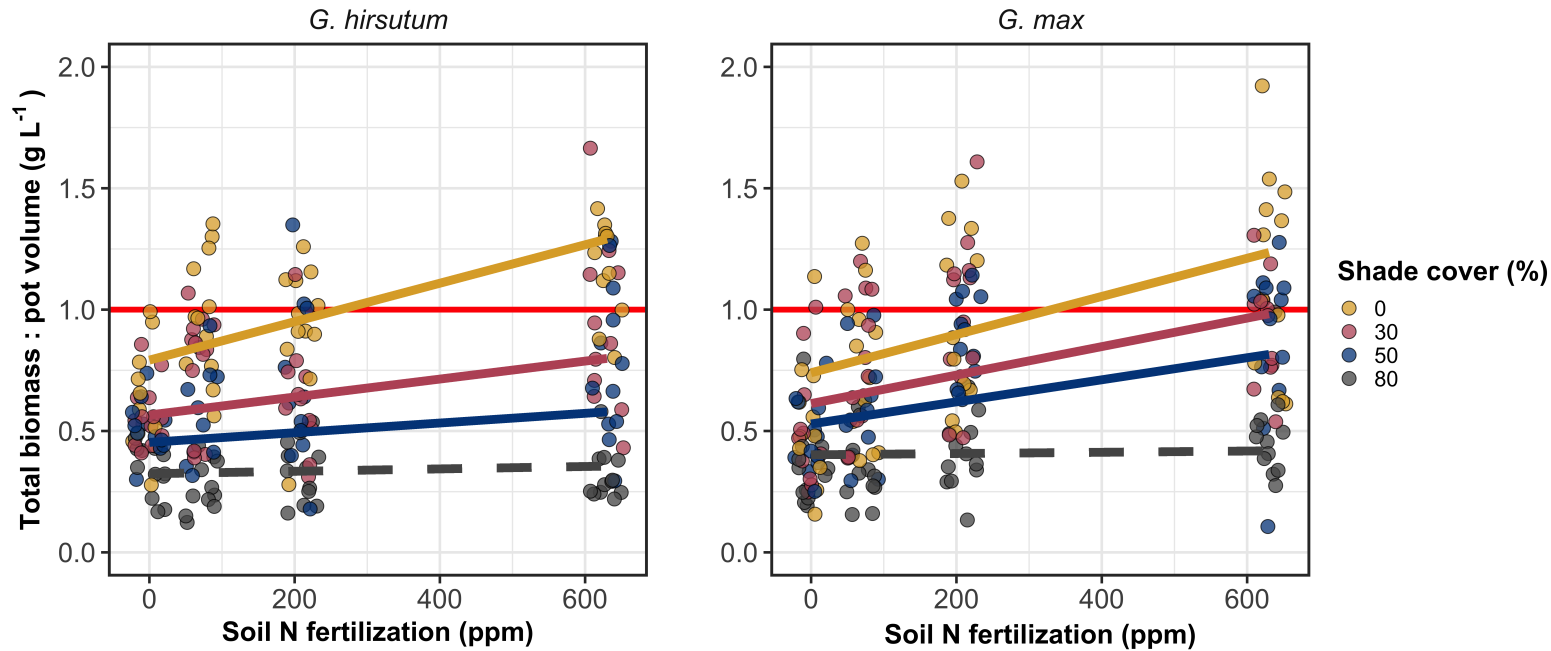


Figure A1. Effects of shade cover and nitrogen fertilization on the ratio of plant biomass to rooting volume in *G. hirsutum* (left panel) and *G. max* (right panel). The red horizontal line indicates the recommended 1 g L^{-1} threshold for BVR recommended by Poorter et al. (2012) to avoid pot size-induced growth limitation. Nitrogen fertilization treatments are represented on the x-axis. Shade cover treatments are represented through colored points and trendlines. Trendlines were created by back-transforming marginal mean slopes and intercepts from species-specific linear mixed-effects models. These values were calculated using the 'emtrends' and 'emmmeans' functions in the 'emmmeans' R package (Lenth 2019). Points are jittered for visibility. Yellow points and trendlines represent the 0% shade cover treatment, blue points and trendlines represent the 30% shade cover treatment, green points and trendlines represent the 50% shade cover treatment, and purple points and trendlines represent the 80% shade cover treatment. Solid trendlines indicate slopes that are significantly different from zero (Tukey: $p < 0.05$), while dashed trendlines indicate slopes that are not statistically different from zero.

3669 Appendix B: Supplemental material for "Soil nitrogen availability
3670 modifies leaf nitrogen economies in mature temperate deciduous
3671 forests: a direct test of photosynthetic least-cost theory"

Table B1. Sample sizes of each species, abbreviated by their USDA NRCS PLANTS database code, within each plot at each site

	ACRU	ACSA	FAGR	FRAM	QURU	N_{plot}
Bald Hill						
+N; +S	0	6	1	0	1	8
+N; -S	1	2	2	0	1	6
-N; +S	2	2	0	0	2	6
-N; -S	2	3	3	0	2	10
Carter Creek						
+N; +S	0	6	1	2	0	9
+N; -S	0	4	0	2	0	6
-N; +S	0	5	1	4	0	10
-N; -S	0	7	0	0	0	7
Mount Pleasant						
+N; +S	3	2	1	0	3	9
+N; -S	0	5	4	1	0	10
-N; +S	1	2	4	0	0	7
-N; -S	3	3	1	2	1	10
N_{spp}	12	47	18	11	10	98

3672 *Plots within each site are represented based on nitrogen and sulfur addition
3673 status. The final column on the right depicts total sample size per plot in each
3674 site (N_{plot}) and the final row on the bottom represents cumulative species sample
3675 size across all plots and all sites (N_{spp}). Key: ACRU = *A. rubrum*; ACSA = *A.*
3676 *saccharum*; FAGR = *F. grandifolia*; FRAM = *F. americana*; QURU = *Q. rubra*

Table B2. Analysis of variance results exploring the linear effect of leaf temperature on net photosynthesis rate and stomatal conductance measured at 400 $\mu\text{mol mol}^{-1}$ CO₂

		A_{net}		g_s	
	df	χ^2	p	χ^2	p
Leaf temperature	1	1.287	0.257	1.716	0.190

3677 Results detail linear mixed effects model where temperature was regressed against
3678 net photosynthesis or stomatal conductance, with site and species designated as
3679 random intercept terms. Significance was determined using Type II Wald χ^2
3680 tests ($\alpha = 0.05$). Key: A_{net} = net photosynthesis rate at 400 $\mu\text{mol mol}^{-1}$ CO₂;
3681 g_s =stomatal conductance measured at 400 $\mu\text{mol mol}^{-1}$ CO₂

Table B3. Second order log-polynomial regression coefficients that described the effect of leaf temperature on net photosynthesis and stomatal conductance measured at 400 $\mu\text{mol mol}^{-1}$ CO₂

	a	b	c
A_{net}	9.422	-0.573	0.010
g_s	-0.170	-0.186	0.003

3682 Net photosynthesis and stomatal conductance values were fit to the log-polynomial
3683 equation $\log(y) = a + bx + cx^2$, where x is leaf temperature. Key: A_{net} = net
3684 photosynthesis rate at 400 $\mu\text{mol mol}^{-1}$ CO₂; g_s = stomatal conductance measured
3685 at 400 $\mu\text{mol mol}^{-1}$ CO₂

Table B4. Mean, standard error, and 95% confidence interval ranges of soil nitrogen availability estimates across all measured plots. All units are expressed as $\mu\text{g N g}^{-1}$ resin d^{-1}

Site	Treatment	Mean	SE	Lower 95% CI	Upper 95% CI
Bald Hill	Ammonium sulfate	27.11	6.14	15.08	39.13
Bald Hill	Control	14.41	5.02	4.56	24.26
Bald Hill	Sodium nitrate	20.65	3.15	14.46	26.83
Bald Hill	Sulfur	6.33	2.19	2.04	10.62
Carter Creek	Ammonium sulfate	26.94	5.36	16.43	37.44
Carter Creek	Control	19.87	1.92	16.10	23.64
Carter Creek	Sodium nitrate	15.51	4.16	7.36	23.65
Carter Creek	Sulfur	5.50	1.40	2.75	8.25
Mount Pleasant	Ammonium sulfate	8.02	2.31	3.49	12.56
Mount Pleasant	Control	2.00	0.57	0.89	3.11
Mount Pleasant	Sodium nitrate	2.52	0.68	1.19	3.85
Mount Pleasant	Sulfur	2.42	0.39	1.66	3.17

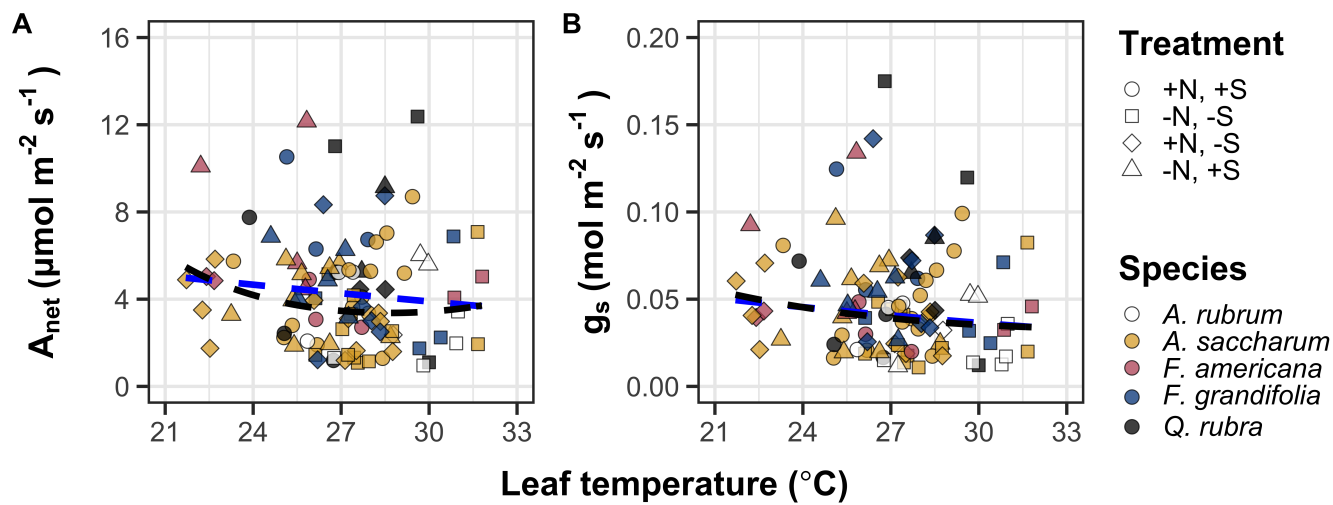


Figure B1. Effects of leaf temperature on net photosynthesis rate (panel A) and stomatal conductance (panel B) values when measured at $400 \mu\text{mol mol}^{-1} \text{CO}_2$. Leaf temperature is represented continuously on the x-axis, while species are represented as colored points. Colored points and shapes are as explained in Figure 3.1. The dashed blue trendline describes the linear relationship between leaf temperature and each response variable, while the dashed black trendline describes the same relationship with a log-polynomial regression equation.

**3686 Appendix C: Supplemental material for "The relative cost of resource
3687 use for photosynthesis drives variance in leaf nitrogen content across a
3688 climate and soil resource availability gradient"**

3689 C.1 Calculations for soil water holding capacity

3690 Water holding capacity (θ_{WHC} ; mm) was calculated as a function of the
3691 volumetric soil water storage at field capacity (W_{FC} ; m³ m⁻³), and the volumetric
3692 soil water storage at wilting point (W_{PWP} ; m³ m⁻³):

$$\theta_{WHC} = (W_{FC} - W_{PWP})(1 - f_{gravel}) * \min(z_{bedrock}, z_{max}) \quad (\text{C4.1})$$

3693 where f_{gravel} (%) is the fraction of gravel content in soil, $z_{bedrock}$ (mm) is the
3694 distance to bedrock, and z_{max} (mm) is the maximum allowable distance to bedrock,
3695 set to 2000mm. W_{FC} is calculated as:

$$\theta_{FC} = k_{fc} + (1.283 * (k_{fc})^2 - 0.374 * k_{fc} - 0.015) \quad (\text{C4.2})$$

3696 where

$$\begin{aligned} k_{fc} = & -0.251 * f_{sand} + 0.195 * f_{clay} + 0.011 * f_{OM} \\ & + 0.006 * (f_{sand} * f_{OM}) - 0.027 * (f_{clay} \\ & * f_{OM}) + 0.452 * (f_{sand} * f_{clay}) + 0.299 \end{aligned} \quad (\text{C4.3})$$

3697 W_{PWP} is calculated as:

$$W_{PWP} = k_{pwp} + (0.14 * k_{pwp} - 0.02) \quad (\text{C4.4})$$

3698 where

$$\begin{aligned} k_{pwp} = & -0.024 * f_{sand} + 0.487 * f_{clay} + 0.006 * f_{OM} \\ & + 0.005 * (f_{sand} * f_{OM}) - 0.013 * (f_{clay} \\ & * f_{OM}) + 0.068 * (f_{sand} * f_{clay}) + 0.031 \end{aligned} \quad (\text{C4.5})$$

3699 In Equations C4.4 and C4.5, f_{sand} (%) is the fraction of sand content in soil (%),
3700 f_{clay} (%) is the fraction of clay content in soil (%), and f_{OM} is the fraction of
3701 organic matter in soil (%). Organic matter in the soil was calculated in this study
3702 by converting soil organic carbon data extracted from SoilGrids 2.0 to soil organic
3703 matter using the van Bemmelen factor (1.724 conversion factor).

Table C1. List of sampled species and their plant functional group assignment

Symbol	Species	Photo. pathway	Growth duration	Growth habit	N-fixer?	Plant functional group	Number sampled
ACAN11	<i>Acaciella angustissima</i>	c3	perennial	forb	yes	c3_legume	3
AMAR2	<i>Ambrosia artemisiifolia</i>	c3	annual	forb	no	c3_nonlegume	25
AMPS	<i>Ambrosia psilostachya</i>	c3	perennial	forb	no	c3_nonlegume	32
ARAL3	<i>Argemone albiflora</i>	c3	annual	forb	no	c3_nonlegume	3
ARPU9	<i>Aristida purpurea</i>	c4	perennial	graminoid	no	c4_nonlegume	2
ASAS	<i>Asclepias asperula</i>	c3	perennial	forb	no	c3_nonlegume	3
ASLA4	<i>Asclepias latifolia</i>	c3	perennial	forb	no	c3_nonlegume	3
ASSY	<i>Asclepias syriaca</i>	c3	perennial	forb	no	c3_nonlegume	18
BASA	<i>Baccharis salicina</i>	c3	perennial	shrub	no	c3_nonlegume	3
BOIS	<i>Bothriochloa ischaemum</i>	c4	perennial	graminoid	no	c4_nonlegume	6
BOSA	<i>Bothriochloa saccharoides</i>	c4	perennial	graminoid	no	c4_nonlegume	6
CAAM2	<i>Callicarpa americana</i>	c3	perennial	shrub	no	c3_nonlegume	3
CAPL3	<i>Carex planostachys</i>	c4	perennial	graminoid	no	c4_nonlegume	3
CAREX	<i>Carex</i> spp.	c4	perennial	graminoid	no	c4_nonlegume	16
CHFE3	<i>Chamaesyce fendleri</i>	c3	perennial	forb	no	c3_nonlegume	2
CHPI8	<i>Chrysopsis pilosa</i>	c3	annual	forb	no	c3_nonlegume	3
COCO13	<i>Conoclinium coelestinum</i>	c3	perennial	forb	no	c3_nonlegume	3
COER	<i>Commelina erecta</i>	c3	perennial	forb	no	c3_nonlegume	3
CRGLL	<i>Croton glandulosus</i>	c3	annual	forb	no	c3_nonlegume	22
CYDA	<i>Cynodon dactylon</i>	c4	perennial	graminoid	no	c4_nonlegume	15
DATE3	<i>Dasyllirion texanum</i>	c3	perennial	shrub	no	c3_nonlegume	3
DIAN	<i>Dichanthium annulatum</i>	c4	perennial	graminoid	no	c4_nonlegume	8
ENPE4	<i>Engelmannia peristenia</i>	c3	perennial	forb	no	c3_nonlegume	6
EUMA8	<i>Euphorbia marginata</i>	c3	annual	forb	no	c3_nonlegume	6
GAPU	<i>Gaillardia pulchella</i>	c3	annual	forb	no	c3_nonlegume	16
GLGO	<i>Glandularia gooddingii</i>	c3	perennial	forb	no	c3_nonlegume	2
HEAN3	<i>Helianthus annuus</i>	c3	annual	forb	no	c3_nonlegume	6

Table C2. List of sampled species and their plant functional group assignment (cont.)

Symbol	Species	Photo. pathway	Growth duration	Growth habit	N-fix?	Plant functional group	Number sampled
HECA8	<i>Heterotheca canescens</i>	c3	perennial	forb	no	c3_nonlegume	2
HETE3	<i>Heliotropium tenellum</i>	c3	annual	forb	no	c3_nonlegume	3
IVAX	<i>Iva axillaris</i>	c3	perennial	forb	no	c3_nonlegume	4
LIAT	<i>Lilaeopsis attenuata</i>	c3	perennial	forb	no	c3_nonlegume	3
LIPU	<i>Liatris punctata</i>	c3	perennial	forb	no	c3_nonlegume	3
LOPE	<i>Lolium perenne</i>	c3	perennial	graminoid	no	c3_nonlegume	9
MIQU2	<i>Mimosa quadrivalvis</i>	c3	perennial	forb	yes	c3_legume	15
NALE3	<i>Nassella leucotricha</i>	c3	perennial	graminoid	no	c3_nonlegume	19
OECU2	<i>Oenothera curtiflora</i>	c3	annual	forb	no	c3_nonlegume	3
OENOT	<i>Oenothera</i> spp.	c3	annual	forb	no	c3_nonlegume	1
PAVI2	<i>Panicum virgatum</i>	c4	perennial	graminoid	no	c4_nonlegume	12
PRGL2	<i>Prosopis glandulosa</i>	c3	perennial	shrub	yes	c3_legume	33
QUHA3	<i>Quercus harvardii</i>	c3	perennial	shrub	no	c3_nonlegume	3
QUMO	<i>Quercus mohriana</i>	c3	perennial	shrub	no	c3_nonlegume	1
RACO3	<i>Ratibida columnifera</i>	c3	perennial	forb	no	c3_nonlegume	40
RHAM	<i>Rhamnus</i> spp.	c3	perennial	shrub	yes	c3_legume	1
RHSET	<i>Rhynchosia senna</i>	c3	perennial	forb	yes	c3_legume	1
RUHI2	<i>Rudbeckia hirta</i>	c3	perennial	forb	no	c3_nonlegume	3
RUNU	<i>Ruellia nudiflora</i>	c3	perennial	forb	no	c3_nonlegume	15
RUTR	<i>Rubus trivialis</i>	c3	perennial	vine	no	c3_nonlegume	3
SAFA2	<i>Salvia farinacea</i>	c3	perennial	forb	no	c3_nonlegume	7
SCHIZ4	<i>Schizachyrium</i> spp.	c4	perennial	graminoid	no	c4_nonlegume	8
SCSC	<i>Schizachyrium scoparium</i>	c4	perennial	graminoid	no	c4_nonlegume	3
SODI	<i>Solanum dimidiatum</i>	c3	perennial	forb	no	c3_nonlegume	1
SOEL	<i>Solanum elaeagnifolium</i>	c3	perennial	forb	no	c3_nonlegume	53
SOHA	<i>Sorghum halapense</i>	c4	perennial	graminoid	no	c4_nonlegume	38
STTE3	<i>Stillingia texana</i>	c3	perennial	forb	no	c3_nonlegume	3

Table C3. List of sampled species and their plant functional group assignment (cont.)

Symbol	Species	Photo. pathway	Growth duration	Growth habit	N-fixer?	Plant functional group	Number sampled
VEOC	<i>Verbesina occidentalis</i>	c3	perennial	forb	no	c3_nonlegume	3
VEST	<i>Verbena stricta</i>	c3	perennial	forb	no	c3_nonlegume	3
WEAC	<i>Wedelia acapulcensis</i>	c3	perennial	shrub	no	c3_nonlegume	6

Table C4. Model selection results for soil moisture, air temperature, and vapor pressure deficit. Soil moisture was used in a bivariate regression against β , while vapor pressure deficit was used in bivariate regressions against leaf $C_i:C_a$ *

Day	Soil moisture		VPD	
	AICc	RMSE	AICc	RMSE
1	1431.77	0.8400	-772.71	0.0853
2	1431.76	0.8400	-775.47	0.0849
3	1431.78	0.8400	-770.86	0.0854
4	1431.79	0.8401	-793.49	0.0839
5	1431.79	0.8401	-771.66	0.0853
6	1431.78	0.8401	-771.66	0.0853
7	1431.78	0.8401	-771.05	0.0854
8	1431.76	0.8401	-770.94	0.0854
9	1431.75	0.8401	-770.11	0.0854
10	1431.74	0.8401	-770.08	0.0855
15	1431.54	0.8401	-768.64	0.0856
20	1431.40	0.8401	-769.77	0.0855
30	1431.23	0.8400	-772.18	0.0853
60	1429.84	0.8391	-779.06	0.0848
90	1429.14	0.8385	-773.99	0.0852

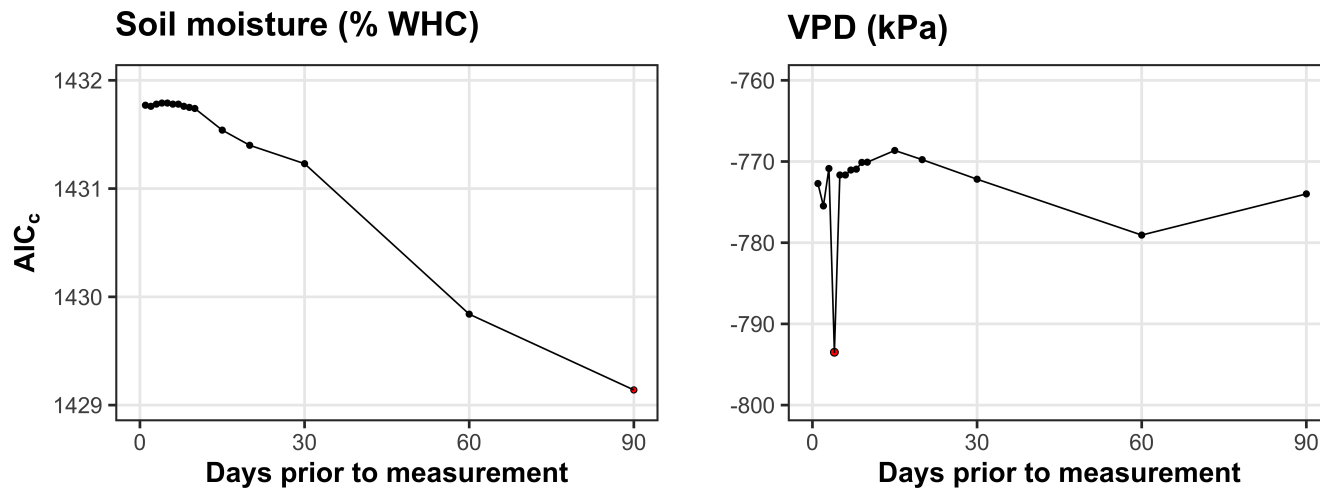


Figure C2. Model selection results exploring relevant timescales for soil moisture (left panel) and vapor pressure deficit (right panel). The x-axis indicates the number of days before each site visit and the y-axis notes the corrected Akaike Information Criterion value. The timescale with the lowest AIC_c value, and therefore most relevant timescale to include in statistical models, is noted as a red point.

**3704 Appendix D: Supplemental material for "Optimal resource investment
 3705 to photosynthetic capacity maximizes nutrient allocation to whole
 3706 plant growth under elevated CO₂"**

Table D1. Summary table containing volumes of compounds used to create modified Hoagland's solutions for each soil nitrogen fertilization treatment. All volumes are expressed as milliliters per liter (mL/L)

Compound	0 ppm N	35 ppm N	70 ppm N	105 ppm N	140 ppm N
1 M NH ₄ H ₂ PO ₄	0	0.165	0.33	0.5	0.67
2 M KNO ₃	0	0.335	0.67	1	1.33
2 M Ca(NO ₃) ₂	0	0.335	0.67	1	1.33
1 M NH ₄ NO ₃	0	0.165	0.33	0.5	0.67
8 M NH ₄ NO ₃	0	0	0	0	0
1 M KH ₂ PO ₄	1	0.85	0.67	0.5	0.33
1 M KCl	3	2.45	2	1.5	1
1 M CaCO ₃	4	3.33	2.67	2	1.33
2 M MgSO ₄	1	1	1	1	1
10% Fe-EDTA	1	1	1	1	1
Trace elements	1	1	1	1	1

Compound	210 ppm N	280 ppm N	350 ppm N	630 ppm N
1 M NH ₄ H ₂ PO ₄	1	1	1	1
2 M KNO ₃	2	2	2	2
2 M Ca(NO ₃) ₂	2	2	2	2
1 M NH ₄ NO ₃	1	3.5	0	0
8 M NH ₄ NO ₃	0	0	0.75	2
1 M KH ₂ PO ₄	0	0	0	0
1 M KCl	0	0	0	0
1 M CaCO ₃	0	0	0	0
2 M MgSO ₄	1	1	1	1
10% Fe-EDTA	1	1	1	1
Trace elements	1	1	1	1

Table D2. Summary of the daily growth chamber growing condition program

Time	Air temperature (°C)	Light (%)
09:00	21	25
09:45		50
10:30	25	75
11:15		100
22:45	21	75
23:30		50
00:15	17	25
01:00		0

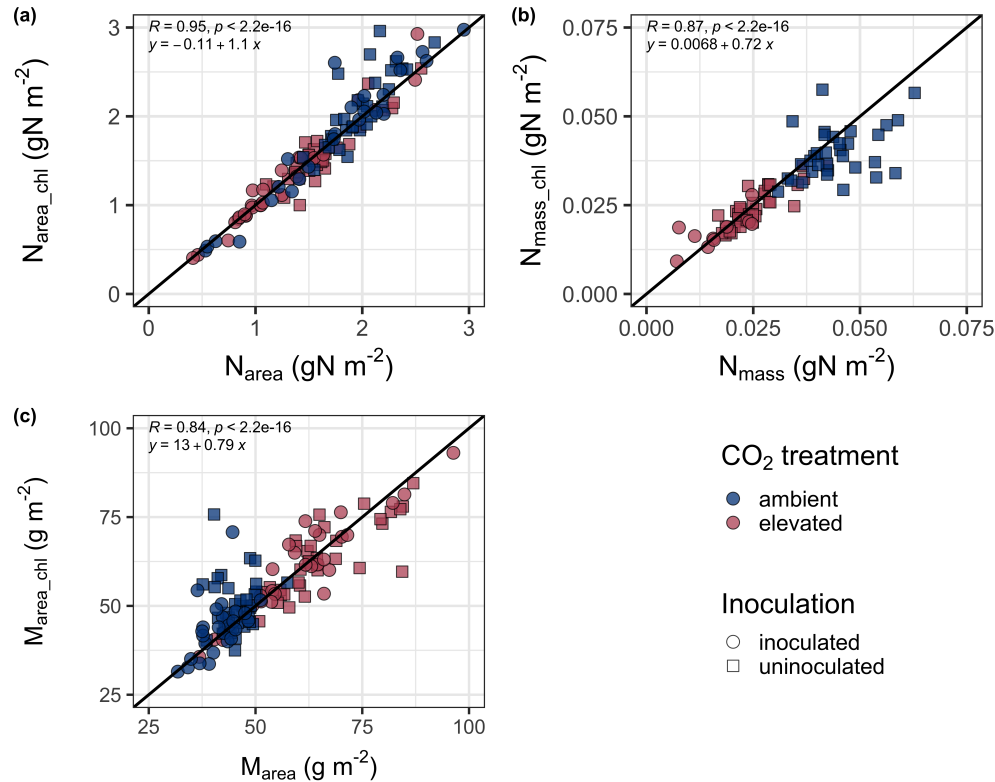


Figure D1. Relationships between area-based leaf nitrogen content (a), mass-based leaf nitrogen content (b), and leaf mass per unit leaf area (c) measured on the focal leaf used to generate A_{net}/C_i curves and leaf nitrogen content measured on the leaf used for chlorophyll extractions. Blue points refer to leaves grown under ambient CO₂ and red points refer leaves grown under elevated CO₂. Square points indicate uninoculated pots and circular points indicate inoculated pots. Pearson's correlation, associated p -values, and the line of the regression line that described each bivariate are included in the top left corner of each plot. The solid black line visualizes the trend given a 1:1 bivariate relationship.

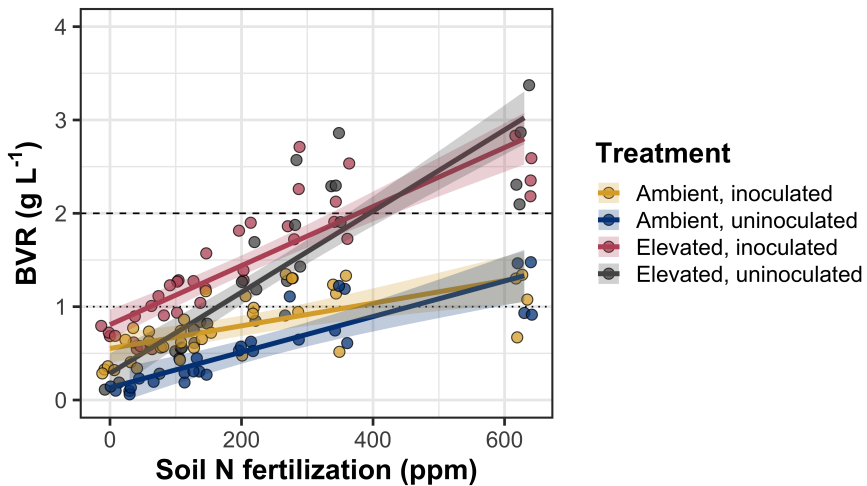


Figure D2. Effects of CO₂, fertilization, and inoculation on the ratio of whole plant biomass to pot volume. Soil nitrogen fertilization is represented on the x-axis in all panels. Yellow points and trendlines indicate inoculated individuals grown under ambient CO₂, blue points and trendlines indicate uninoculated individuals grown under ambient CO₂, red points and trendlines indicate inoculated individuals grown under elevated CO₂, and grey points indicate uninoculated individuals grown under elevated CO₂. Solid trendlines indicate regression slopes that are different from zero ($p < 0.05$), while dashed trendlines indicate slopes that are not distinguishable from zero ($p > 0.05$). The dotted horizontal line indicates the point where biomass:pot volume exceeds 1 g L⁻¹, and the dashed line indicates the point where biomass:pot volume exceeds 2 g L⁻¹.